University of South Carolina
Scholar Commons

Theses and Dissertations

2018

Cenozoic Tectono-Stratigraphic Evolution And Petroleum System Of The Eastern Cordillera Foothills And Adjacent Basins (Colombia)

Essam Saeid
University of South Carolina

Follow this and additional works at: https://scholarcommons.sc.edu/etd

 Part of the Geological Engineering Commons

Recommended Citation

Saeid, E.(2018). *Cenozoic Tectono-Stratigraphic Evolution And Petroleum System Of The Eastern Cordillera Foothills And Adjacent Basins (Colombia)*. (Doctoral dissertation). Retrieved from https://scholarcommons.sc.edu/etd/4964

This Open Access Dissertation is brought to you by Scholar Commons. It has been accepted for inclusion in Theses and Dissertations by an authorized administrator of Scholar Commons. For more information, please contact dillarda@mailbox.sc.edu.

CENOZOIC TECTONO-STRATIGRAPHIC EVOLUTION AND PETROLEUM SYSTEM OF THE EASTERN CORDILLERA FOOTHILLS AND ADJACENT BASINS (COLOMBIA)

By

Essam Saeid

Bachelor of Science
Benghazi University, 1998

Master of Science
Benghazi University, 2007

Submitted in Partial Fulfillment of the Requirements

For the Degree of Doctor of Philosophy in

Geological Sciences

College of Arts and Sciences

University of South Carolina

2018

Accepted by:

James Kellogg, Major Professor

Christopher Kendall, Major Professor

Camelia Knapp, Committee Member

Andrew Leier, Committee Member

Obi Egbue, Committee Member

Cheryl L. Addy, Vice Provost and Dean of the Graduate School

© Copyright by Essam Saeid, 2018
All Rights Reserved.

DEDICATION

This dissertation is dedicated to my family for their patience, love, and support throughout all years of my studies.

ACKNOWLEDGEMENTS

I would like to express my gratitude to my doctoral advisor, Dr. James Kellogg, for his support, guidance, encouragement, and mentorship throughout the course of the study. I am grateful to him for providing me the opportunity to work on such an interesting and comprehensive research projects. I would also like to thank my Co-Advisor Dr. Christopher Kendall for his help, support and guidance in the sequence stratigraphy part of this research. I am grateful to him for countless hours of discussion and guidance.

Special thanks must go to my doctoral committee members Drs. Camelia Knapp, Andrew Leier, Obi Egbue, whose comments and recommendation improved the quality of this dissertation. I would like to thank Dr. Thomas De Keyser, for sharing his experience in well logging. Dr. Brian Horton for his review and others anonymous reviewers improved the manuscript of Chapter II of this dissertation.

Pacific E&P Colombia (now Frontera Energy) provided the data set for this research. I am grateful to Jose Antonio Martinez for logistic support and for providing us with all the data, we requested during the course of this research in a timely manner. I would like to thank my colleague Baris Bakioglu for sharing his Master research results of Garzón area. The geophysical software's used for this research were provided by Schlumberger, Geosoft, Midland Valley, dGB Earth Sciences and GeoTeric. Finally, I would like to thank my sponsor the Minstry of High Edacation of Libya.

ABSTRACT

New gravity, magnetic, well and 3D seismic data provides a better understanding of regional structures and tectonic movement affecting the petroleum system and sedimentary history of an important region of oil production in the Foothills of the Eastern Cordillera of Colombia. To the south the Garzón fault was previously interpreted as a right-lateral strike-slip fault. New seismic, well, and gravity data demonstrate that this fault is also a low-angle (12–17 degrees) Andean fault that thrusts PreCambrian basement 10 to 17 km northwestward over Miocene rocks of the Upper Magdalena Valley (UMV) in a prospective footwall anticline. New geophysical data as well as previous field mapping were used to produce the first gravity and magnetic maps and retrodeformable structural cross section of the northern Garzón Massif. The new model distinguishes for the first time distinct episodes of "thin-skinned" and "thick-skinned" deformation in the Garzón Massif. To the north in the Foothills of the Eastern Cordillera spectral decomposition analysis of a 3D seismic volume and sequence stratigraphy of the Cenozoic sedimentary succession has developed new chronostratigraphic conceptual models and facies predictions. Earlier exploration in the Foothills was focused on structural traps that led to a number of significant discoveries, including the Cusiana and Cupiagua oil fields. However, more challenging stratigraphic play types have evolved from spectral decomposition (STFF, CWT, MP) analysis, enhancing our understanding of the fluvial reservoir architecture. Also this technique has helped improve our understanding of how regional structures and tectonic movements

affected local sedimentary history and produced regional geomorphologic features. Use of this technology can open new opportunities in hydrocarbon exploration in the eastern foothills of the northern Andes and adjacent basins.

TABLE OF CONTENTS

LIST OF FIGURES

CHAPTER I

CENOZOIC TECTONO-STRATIGRAPHIC EVOLUTION AND PETROLEUM SYSTEM OF THE EASTERN CORDILLERA FOOTHILLS AND ADJACENT BASINS (COLOMBIA)

1.0 INTRODUCTION

The Eastern Cordillera and Garzón Massif of Colombia form an intracontinental orogenic belt extending 750 km northeast from Ecuador to Venezuela (Figure. 1.1). They are located in the eastern part of the northern Andes, where they rise abruptly above the lowlands of the South American craton (Taboada et al., 2000)

The discovery of the Orito (1963), Caño Limón (1983), Cusiana (1988) and Cupiagua (1993) giant oil fields (Echeverry et al., 2008) helped fuel petroleum exploration on the eastern flank of the Eastern Cordillera and adjacent basins (Figure. 1.1). Recent medium-sized oil fields discovered include Moqurta-Costayaco and Cubaral (2017) along the eastern flank of the Andean foothills.

The largest foothills discovery, Cusiana and Cupiagua, followed earlier foreland exploration focused on easier plays. The idea of a prolific early migration of the oil should have occurred from the marine Cretaceous rocks or older shales in foredeep basin prior to Andean orogenic uplift (Miocene-Recent) of Eastern Cordillera seems reasonable with a widespread preamble sands in Cretaceous and Cenozoic rocks.

The largest discovery of Cusiana and Cupiagua on the foothills came lately since most of the explorations were focused on easier foreland basins. The idea of a prolific early migration of the oil should have occurred from the marine Cretaceous rocks or older shales.

The Upper Magdalena Valley (UMV) and Putumayo basins are two important oil - producing basins in southwestern Colombia (Figure. 1.1). The southern UMV, the Neiva Sub-basin, is an intermountain basin located between the Central Cordillera and Garzón Massif. The Putumayo is a foreland basin located to the east of the Garzón Massif. The Putumayo basin is a portion of a large geologic province formed by Marañon Basin in Peru, Oriente Basin in Ecuador and Putumayo Basin in Colombia (Higley, 2001).

However, Mora et al. (2010) proposed that during the Mesozoic and Paleogene, the UMV and Putumayo basin were part of the same extensive mega-basin, and they were later separated during the Andean orogeny when the Eastern Cordillera and Garzón Massif were uplifted.

The largest discovery in Putumayo basin was Orito oil field with an average production of 380 MMBO (ANH, 2012). To the east in the Putumayo foreland basin, the discoveries are relatively small in comparison with the giant oil field in the Oriente foreland in Ecuador.

The southern study area focuses on the Garzón Massif rising between the Upper Magdalena Valley (UMV) and the Putumayo/Caguan Basin of Colombia Figure (1.1).

The central Llanos foothills trend NE-SW and form the frontal thrust zone along the eastern flank of the Eastern Cordillera of Colombia. However, the Llanos foothills is divided into three main deformation zones that exhibit increasing structural complexity northeastward along the mountain front (Villamil et al., 2004; Martinez, 2006; Egbue,

2011) a frontal inverted normal fault zone (Cusiana), a transition bedding plane thrust zone (Cupiagua), and a triangle zone (Piedemonte).

The Cusiana giant oil field is bordered by the Yopal and Cusiana thrust fault systems, the Llanos foreland basin to the east, and by the Guaicaramo fault system and the Eastern Cordillera to the west.

The northern study area is located in the Llanos foothills. It is bordered by the Llanos foreland basin to the east and the Guaicaramo fault and Medina Basin to the west (Figure. 1.1). It is located 40 km southwest of the giant Cusiana oil field in Colombia. Most of the hydrocarbon exploration in the Llanos foothills has focused on structural traps in the hanging walls of thrust faults. There has been little exploration success in the footwall blocks, and most of the activity has been based on subtle structural traps. The Cusiana oil field is considered one of the most important structural traps that produce oil from the Eocene Mirador Formation. In the Llanos foreland basin the main reservoir is the Carbonera Formation (C-1, C-7) which is Oligocene to Lower Miocene in age Torrado et al., (2014).

The goal of this research is to understand the tectono-stratigraphic evolution and petroleum systems of the Eastern Cordillera Foothills and adjacent basins. The goal includes better understanding of how regional scale structures and tectonic movement have affected the petroleum system as well as the local sedimentary history and exploring the processes and mechanisms involved in producing the regional stratigraphic section. This study necessitated the use of seismic attribute analysis tied with a sequence stratigraphic framework for establishing chronostratigraphic concept models and facies prediction and

to find new stratigraphic traps. Do only structural plays exist along the eastern foothills of the Colombian Andes like Cusiana and Cupiagua, or are there promising stratigraphic traps that remain undiscovered?

In this research, geologic data, well logs, and seismic sections were interpreted with a multidisciplinary approach that involved structural interpretation and modeling, seismic attribute analysis (Spectral decomposition), potential field forward modelling, and tectono-stratigraphic and sequence stratigraphic modelling.

This dissertation comprises six chapters; Chapter I provides an introduction and the methodologies used in the dissertation. Chapter II deals with the mechanics and kinematics of basement tectonic uplifts, such as the Laramide Rocky Mountain orogeny, and their petroleum systems, which remain poorly understood and controversial. The Garzón Massif rising between the Upper Magdalena Valley (UMV) and the Putumayo/Caguan Basin of Colombia is an active basement uplift with well, seismic, gravity, and magnetic data available and presented here for the first time (Figure. 2.1). Chapter III describe how complex fluvial reservoir predication methods can be used southwest of the Cusiana giant oil field by applied continuous wavelet transform (CWT), spectral decomposition of a high-resolution seismic volume. Chapter IV proposed an exploration workflow to identify new potential reservoirs in the complex fluvial sediments of the Oligocene to Lower Miocene age Carbonera Formation (C-7 and C-5) south of the giant Eocene Mirador Formation Cusiana oil field. This study uses sequence stratigraphic framework ties for the first time with continuous wavelet transform (CWT) spectral decomposition to identify sequence boundaries and system tracts. Chapter V deals with techniques in sequence stratigraphy using log character, z plot and spectral decomposition in Paleogene fluvial and marginal

marine reservoir depositional systems of the Llanos Foothills. In connection with this chapter, a conceptual depositional environment model (Mirador Formation) and regional sequence stratigraphic framework were established using normalized well log character, spectrual decomposition and well logs cross plots. Finally, Chapter 6 is demonstrated how a regional scale structures and tectonic movement have affected the character of the local geomorhplogic features history. Matching Prusit spectral decomposition detect a changes in regional fluival pattern that reflect the regional tectonics of the Llanos foothills

1.1 DATA SET

The dissertation is based on the material obtained from the Forentiera Energy (Former Pacific Rubiales Energy Company) (Colombia). Geophysical data include 155 2D seismic line survey from 1987 to 2012 and migradted 42 km^2 3D-2008 Topoyaco in Putumayo Basin and 3D 246 km^2 3D-2008 Llanos-31 along the eastern foothills of the Eastern Corellidera. Petroseis Seismic Data Processing Services processed both 3D seismic for Pacific E&P Colombia (now Frontera Energy).

Also, 40 regional wells located along the Foothill of the Putumayo and Llanos basins as well as the southern part of Upper Magdalena Valley Basin (Neiva Sub-basin). Most of the wells with formation tops as well as wire-line logs include sonic, dip log, gamma ray, density, neutron porosity and spontaneous potential logs.

In addition, the Colombian National Hydrocarbon Agency (ANH) has provided surface geology, gravity and magnetic data. The surface geology maps include plate 431 with a scale of 1:100000 with booklet (2010). Plate 411, 412, 431, 448, and 465 with a scale of 1:200000 with booklets (2003).

1.2 METHODOLOGY

The methodology in the dissertation aimed at the integration of geophysical and geological aspects. Seismic reflection technique as well as available exploration wells are used to provide the basic tectonostratigraphic evolution and petroleum system of the Eastern Cordillera Foothills and adjacent basins.

However, the main steps conducted in this study:

- Seismic interpretation
- Structural interpretation and modeling
- Petroleum systems analysis
- Sequence stratigraphy framework

1.2.1 SEISMIC INTERPRETATION

The conventional interpretation of 3-D seismic data was carried out using Petrel interpretation software package. Seismic tie and regionally continuous seismic reflection were picked as chrono-stratigraphcally surface for this study. Time structure maps of significant seismic surfaces and isochore maps of seismic sequences were developed to highlight structural and deposional trends.

The quality of the seismic data varies, due to differences in acquisition parameters, sampling time, coordinate system, seismic processing and target between seismic surveys. The dataset acquired with different fold, between 1971 and 2012. It was necessary to build a database that uniforms all the seismic information. This includes re-projection of coordinates, datum correction by shift (between 0 and 400 ms).

Well information from exploration wells in the area; close to the 2D seismic lines have been used for reference under the seismic interpretation. In total 17 wells were selected to be tied to the seismic data. A variable suite of logs (gamma ray, resistivity and sonic logs), geological information (formation tops as well as rock description) together with geophysical information (check shot and velocity seismic profiles VSP) were used in well seismic-tie and determine geophysical properties of keys reflectors and to correlate the logs with the seismic character.

The interpretation includes the standard 3D seismic interpretation workflow such as 3D seismic volume, fracture analysis in 3D volume (Fault patch generation) seismic attributes (Variance ant tracking, Coherence attributes, reflection strength, and RMS attributes amplitude anomaly).

Spectral decomposition has been used to determine the marginal to fluvial systems of the potential reservoirs along Eastern Cordillera Foothills and adjacent basins. The spectral decomposition has been used to determine the layer thicknesses (Partyka, 1999, 2011), stratigraphic geometries (Marfurt and Kirlin, 2001), and direct hydrocarbon detection (e.g., Goloshubin et al., 2002; Castagna et al., 2003; Sinha et al., 2005; Welsh et al., 2008; Yu et al., 2011).

Our spectral decomposition workflow started with data conditioning (Spectral enhancement) and then investigated the three dominate frequencies for the horizon of interest then constructing a tuning map of the potential reservoirs to determine the stratigraphic features that could not be resolved in the time domain seismic cube. The frequency spectra volume separated to three dominant frequencies volumes (iso-frequency

volume) based on the three dominate frequencies. These volumes were manipulated and superimposed on generating bodies that matched geological features using the RGB/CMY Mixer application.

Spectral decompositions are short time Fourier transforms (STFT) and continuous wavelet transforms (CWT) and the matching Pursuit algorithm. Each of these has their advantages and disadvantages, and their selection depends on the objectives of the workflow. For instance, the STFT transformation depends on the time gate, a drawback for the transformation method (Sinha et. al., 2005). On the other hand, the CWT method is unlike the conventional SFFT method, which limits the time-frequency resolution by a predefined window width (Sinha et. al., 2005).

We found that CWT was better than STFT for spectral decomposition of the seismic volume to detect the stratigraphic features so all the analyses were based on the CWT approach. However, to a certain extent, CWT solves the dilemma of resolution if one can choose the mother wavelet which works best for the seismic data (Morlet, Gaussian, and Mexican Hat or Ricker). This choice depends on the 3D seismic interpretation package used.

The horizon probe is another useful technique for visualization of stratigraphic features in the time domain. The horizon probe is an irregular probe that follows one or two interpreted horizon surfaces, also referred to as "sculpting" in the industry (Schlumberger, 2017).

The application of seismic attribute in frequency volumes of CWT enhances the stratigraphic features such as river channel levees and point bars which are undetectable in time domain seismic data even with close scrutiny.

1.2.2 STRUCTURAL INTERPRETATION

In order to identify the structural style of the southern of Eastern Cordillera (Garzón Massif basement) and adjacent basins 2D, 3D seismic data and well data were integrated with the surface geology carried out using Structural interpretation software (MOVE Midland Vally2015). 2D seismic data include available well dip-logs and formation tops of Topoyaco in Putumayo basin and Iskana-1, Esnanga-1 wells in Upper Magdalena Valley Basin (Neiva Sub-basin) were converted from time to depth, using Time-Depth survey. In addition, DEM's data with the surface geologic maps were loaded on the workstation to draw regional cross sections and using volume-balancing technique in order to understand the geologic history of the southern of Eastern Cordillera (Garzón Massif basement) and adjacent basins.

1.2.3 PETROLEUM SYSTEMS ANALYSIS

1D petroleum system modeling was performed using 1D PetroMod 2014. The main input as following:

- Layers: there are five layers/formations, i.e., Pre-Cretaceous basement, Cretaceous Cabollos and Villeta Fm, Maastrichtian to Early Paleocene Rumiyaco Fm, Early Paleocene to Middle Eocene Pepino Fm, Middle Eocene to Middle Miocene Orito-Belen Gr and the Ospina Fm which were identified based on the generalized stratigraphic chart of Putumayo basin.
- Sub-layers : Top, Base, and Thickness (m) of each sub layer was defined based on cutting descriptions, and well logging data (final well reports),
- Duration of deposition to (Ma): geological age of a sub-layer was calculated, using the following equation:

$\mathbf{A}_{sbl,i} = A/H^* H_{sbl,i}$

Where: $\mathbf{A}_{sbl,i}$ = age calculated for the sub-layer i (Ma)

A = age of the layer/formation (Ma)

H = total thickness of the layer (m)

$H_{sbl,i}$= thickness of an individual sub-layer (m)

- Lithology: lithology of each sublayer obtained from the cutting description (final well reports). The rock type, however, should match with one in the database of PetroMod.
- Petroleum System Elements (PSE): Main types of PSE are source, reservoir, overburden, seal rocks according to the Petromod database. Type of PSE to be assigned for each sublayer was also made based on cutting description and well logging data analysis (final well reports).
- Erosion: thickness and age
- TOC and HI: Average TOC values have measured at 1.03% by weight with a maximum values 1.7% with average HI 120-180 mgHc/gTOC
- Kinetic model: Behar et.al (1997)_TII(PB), (Hantschel and Kauerauf, 2009)
- The boundary condition data for the heat flow analysis are temperature maps on the sediment–water interface and basal heat flow maps for the respective events:
    1. Paleo Water Depth (PWD) (0 m)
    2. Sediment Water Interface (SWIT) (20^{o} C)
    3. Heat Flow (HF) (45 ^{o}C)

The parameter of SWIT and HF were assumed as following.

$$q = \lambda_b \frac{T_b - T_{\text{swi}}}{h_l}, \qquad \frac{h_l}{\lambda_b} = \frac{h_m}{\lambda_m} + \frac{h_c}{\lambda_c} + \frac{h_s}{\lambda_s}$$

q = heat flow

λ_b = Average bulk thermal conductivity

λi = Bulk thermal conductivities

T_{swi} = Sediment water interface (20^o C)

λ_b = vertical thermal conductivity

h_l = thickness of the lithosphere and the corresponding properties of the upper mantle λ_m, h_m, the crust λ_c, h_c and sediments λ_s, h_s. (Hantschel and Kauerauf, 2009).

The result of 1D petroleum system modelling are burial history curves, source rock maturity (Vitrinite reflectance) and event chart.

The available data were used in the basin modelling software PetroMod 2014 in order to calculate the burial and thermal histories, source rock maturity %Ro (Calculated Vitrinite reflectance) Table1, and event chart with the critical moment. The figures discussed in the following section belong to the Topoyaco and San Gabriel pseudo-wells.

However, HI and TOC are excessive, but they were assumed in this study (using the average values for the remaining layers of source rocks). Also, the lacking of measured of $\%R_o$ causes the uncertainty on the calibration models and uncertainties in the basin modelling.

Vitrinite reflectance is the measurement of reflectance of vitrinite particles derived from higher plants. It is the most widely used indicator for source rock maturity. Vitrinite particles are calculated by 1D modeling. In basin analysis studies, it is used to calibrate the burial and thermal history models (Allen and Allen, 2005).

1.2.4 GRAVITY AND MAGNAETIC STUDY

The geophysical study of the northern Garzon Uplift included interpretation of the Garzon fault with two-dimensional gravity forward modeling constrained by seismic and well data by using Oasis Montaj Geosoft. A regional 2D model of the entire Garzon Massif based on surface geology, gravity and magnetic data was constructed and retrodeformed to 25 Ma to interpret the orogenic evolution of the mountain and petroleum system. The magnetic field was inverted with the Euler Deconvolution method to illuminate lateral variations in the Precambrian basement rocks of the Garzon Massif.

The airborne gravity survey data used in the project includes 2663 line kilometers gravimetry along 1 x5 and 1 x 4 km flight lines at elevations of 2564 and 4589 m above mean sea level. ArcGIS was used to create shapefiles and raster files from the database created in Oasis montaj. Moreover, the elevation and gravity raster gridded maps were converted to raster files in ArcGIS 10.1. The Bouguer gravity map was generated using a 0.5 x 0.5 km grid generated by the Geosoft Oasis Montaj graphic mapping system Fig. 26b is the complete (terrain corrected) Bouguer gravity map calculated for a reduction density of 2.80 g/cm3. The Bouguer map is constructed by upward continuing the low elevation data (2564 m above sea level) and merging it with the high elevation data (4589 m above sea level). The accuracy of the airborne gravity observations are confirmed by land gravity

observations collected along a north south profile east of the Iskana-1 well, in addition to land observations to the west of seismic line GAIT 99-21 (Fig. 2.6). Misfits between land and air gravity measurements are less than 3 mgal. The observed gravity was then extracted from the map data grid along the GAIT 99-21 profile line and exported to the 2-D profile. The range of the observed gravity is from _156 mgal to _84 mgal.

Figure 1.1 Location map of study area: Eastern Cordillera Foothills and adjacent basins (Colombia) with the giant oil files, Llanos Foothills, Upper Magdalena Valley, Garzón Massif, and Putumayo Oriente Marañon basin.

1.2.5 SEQUENCE STRATIGRAPHY FRAMEWORK

The best sequence stratigraphic models of the sedimentary fill of basins are provided by a combination of seismic data, well logs, and cores and outcrop studies in conjunction with biostratigraphy. The cores and well logs and outcrop studies provide access to a detailed vertical resolution of sedimentary sections while seismic and outcrop studies provide the lateral continuity to the sequence stratigraphic framework and the biostratigraphy provides the time constraints Kendell (2008).

In the use of sequence stratigraphy, the interpretations are best determined when well logs are tied to biostratigraphic markers. Using these two in combination one can:

Identify, match and tie sequence stratigraphic surfaces

Interpret the stacking patterns of the vertical sedimentary sequences

At the start of an interpretation of sequence stratigraphy using well logs one must first identify the predominant of sequence stratigraphic surfaces. The most important of these surfaces, and the first that should be identified when using logs, are maximum flooding surfaces (mfs) and transgressive surfaces (TS). These coincide and are correlated with radioactive shales (use of the gamma log) that are interpreted to have been deposited across relatively flat surfaces. Once the mfs and TS are established and tied, then the sequence boundaries (SB) of clastic sedimentary systems are identified. These will tend to lie directly beneath the sand sized sediment fill of depressions on eroded and incised surfaces and over the prograding clinoforms of high stand systems tracts (HST).

In clastics deposits the second and often co-incident step in the interpretation of well logs and cores is the use of parasequence stacking patterns (the vertical occurrence of

repeated cycles of coarsening or fining upwards sediment). This to identify the lowstand systems tracts (LST), parasequence cyclic stacking patterns which are commonly identified on the basis of variations in grain size. These fines upwards are indicated by triangles whose apex is up while those that coarsen upwards are indicated by inverted triangles whose apex is down (Kendell 2008).

However, we used a new Technique in sequence stratigraphy by using well logs character integrated with seismic attribute "Spectral Decomposition" for siliciclastics.

The techniques to better capture the sedimentological character and improve the interpretation of cyclicity and depositional settings in displays of well logs and cross-sections. We proposes a strategy to enhance the display and interpretation of borehole logs which first normalizes the gamma ray logs to remove systematic errors in well-to-well comparisons and displays them on a logarithmic scale to facilitate hierarchical cycle identification. Use of a logarithmic scale for gamma ray allows display of lithofacies with great variation in API counts and emphasizes cyclicity in very "clean" (low API counts) stratigraphic units. Detailed sedimentological core descriptions can be displayed with the logs and used to represent generalized lithology and petrophysical characteristics in uncored portions of the logs by providing a model for the color fill of the log curves. The gamma ray color fill is interactively adjusted to vary from red in the cleanest grain-supported fabrics to black in argillaceous or clay-rich fabrics. Neutron porosity (NPHI) is typically colored to vary from black at 0% to dark blue at 10% and higher. Bulk density (RHOB) is shaded red at densities above 2.80 gm/cc to illustrate anhydrite.

CHAPTER II

GARZÓN MASSIF BASEMENT TECTONICS: STRUCTURAL CONTROL ON EVOLUTION OF PETROLEUM SYSTEMS IN UPPER MAGDALENA AND PUTUMAYO BASINS, COLOMBIA[1]

[1]Saeid, E., K.B. Bakioglu, J. Kellogg, A. Leier, J.A. Martinez, E. Guerrero. 2017. *Marine and Petroleum Geology 88* (2017) 381-401.

Reprinted here with permission of publisher. Appendix B

2.0 OVERVIEW

The Garzón Massif, is an active Laramide style basement uplift flanked by the Upper Magdalena Valley (UMV) and the Putumayo Basin. In this paper, we use new gravity, magnetic, well and seismic data for the first geophysical interpretation of the Garzón Massif. The Garzón/Algeciras fault has been previously interpreted as a right-lateral strike-slip fault. The new seismic, well, and gravity data demonstrates that the Garzón fault is also a low-angle (12–17 degrees) Andean age fault thrusting PreCambrian basement 10 to 17 km northwestward over Miocene sediments of the UMV in a prospective footwall anticline.

The new geophysical data as well as previous field mapping were used to produce the first gravity and magnetic maps and retrodeformable structural cross section of the northern Garzón Massif. The new model distinguishes for the first time distinct episodes of "thin-skinned" and "thick-skinned" deformation in the Garzón Massif. The model indicates approximately 43 km of Early to Middle Miocene shortening by "thin-skinned" imbricate thrusting contemporaneous with the uplift of the nearby southern Central Cordillera (~9-16 Ma) and the main hydrocarbon expulsion event for the UMV and Putumayo Basin. This was followed by at least 22 km of Late Miocene (3-6 Ma) "thick-skinned" Andean shortening and 7 km of uplift on the symmetrical Garzón thrust and SE-verging basement thrust fault zone. The Andean uplift interrupted and exposed the hydrocarbon migration pathways to the Putumayo Basin.

3-D volume fracture analysis was used for the first time in this paper together with the first seismic and well data published for the Topoyaco and Miraflor structures to test

closure models for the Topoyaco foothills. Intense fracturing is observed in the Topoyaco basement monocline from the near-surface to depths of over 3.5 km. The high level of fracturing permitted freshwater flushing and oil biodegradation and hydrocarbon escape. In contrast, the Miraflor-1 well, located just southwest of the Topoyaco block, tested light gravity oil and is sealed from groundwater flushing and biodegradation by a backthrus.

2.1 INTRODUCTION

The mechanics and kinematics of basement tectonic uplifts, such as the Laramide Rocky Mountain orogeny, and the petroleum systems associated with these uplifts remain poorly understood and controversial. The Garzón Massif rising between the Upper Magdalena Valley (UMV) and the Putumayo/Caguan Basin of Colombia is an active basement uplift with well, seismic, gravity, and magnetic data available and presented here for the first time (Figure 2.1). In the past 10 Ma, Precambrian age granitic rocks of the Garzón Massif have been uplifted relative to Cretaceous and Tertiary sedimentary rocks of the UMV along the Garzón fault and uplifted to the southeast adjacent to the Putumayo Basin forming the Topoyaco monocline.

The Gigante oil field in the Neiva Sub-basin of the UMV (Figure 2.2a) contains 175 MMbbl of oil in situ in Monserrate Formation reservoirs in anticlinal traps (Sarmiento and Rangel, 2004). Just 3 km east of Gigante, PreCambrian crystalline basement rocks are in fault contact with Miocene sediments along the Garzón (also named Algeciras) fault. The Garzón/Algeciras fault has been previously interpreted as a right-lateral strike-slip fault based on remote sensing data (Chorowicz et al., 1996; Velandia et al., 2005; Bustamante et al., 2010). In 2002, 5 km southeast of the Garzón fault, Iskana-1 well was drilled by

HOCOL – TOTAL through 2743 meters of basement into the Miocene Honda Formation (DATALOG COLOMBIA, 2002, unpublished report). In this paper we present previously unpublished seismic, well, and gravity data demonstrating that the Garzón fault is also a low-angle fault (12–17 degrees) thrusting PreCambrian basement 10 to 17 km northwestward over Miocene sediments with reservoir potential.

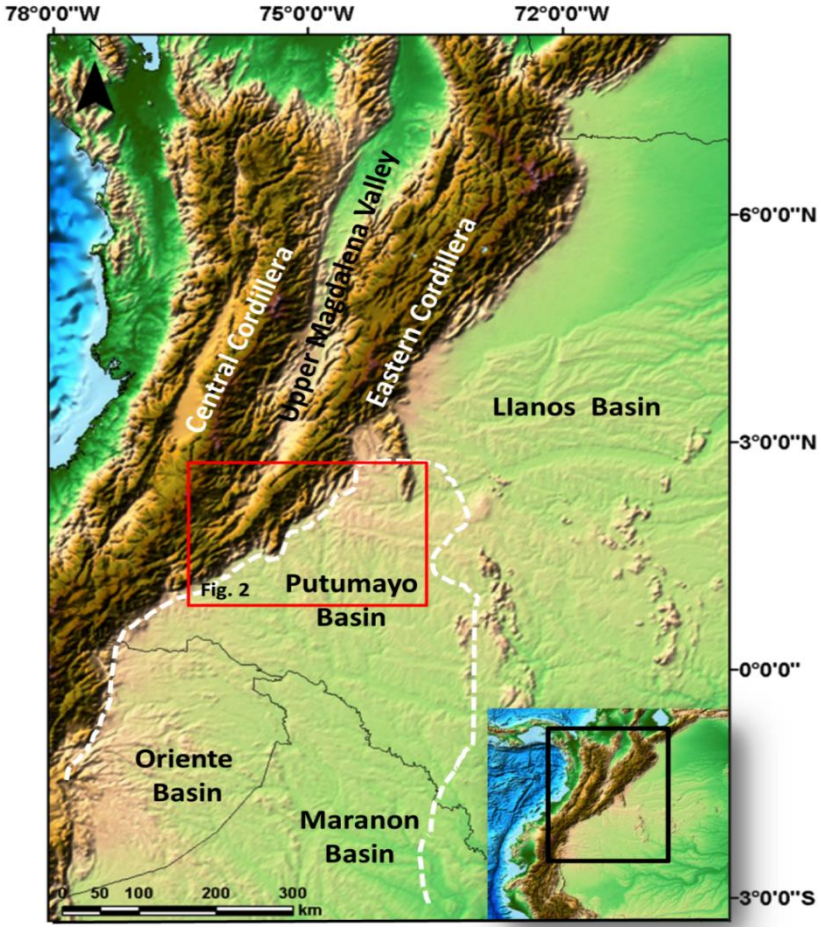

.Figure 2.1 Location map of study area: Upper Magdalena Valley, Garzón Massif, and Putumayo Oriente Marañon basin.

..

This study uses new subsurface wells, 2D, 3D seismic, aerogravimetric, aeromagnetic, and surface geologic data to generate an evolutionary model for the petroleum systems of the basins adjacent to the Garzón uplift. The data includes previously unpublished aerogravity and aeromagnetic surveys, wells, and new seismic reflection profiles.

Drilling and testing in all wells in or around the Topoyaco Block on the southeast flank of the Garzón uplift (Figure 2.2b) indicate the presence of fresh water (300 – 500 ppm) or heavy and extra-heavy and biodegraded oil (Wolaver et al., 2015). However, nearby Costayaco and Moqueta fields and Miraflor located to the southwest of Topoyaco (Figure 2.2b) have light gravity oil (Dueñas and Ramirez, 2012; Ramirez et al., 2012). Villegas et al. (1994), Ramón (1996), and Person et al. (2012) studied the importance of groundwater hydrodynamics in the evolution of the petroleum system and oil quality in the neighbouring Llanos foreland basin to the north (Figure 1.1). Wolaver et al. (2015) used 2-D numerical ground-water flow models to suggest that Putumayo reservoirs were water washed since Andean uplift and that four-way closure is essential to protect Putumayo reservoirs from groundwater influx and to trap oil. In this paper and in Kellogg et al. (2014) we present new interpreted seismic profiles for Topoyaco and Miraflor supporting the Wolaver et al. (2015) conclusions and illustrating the importance of four-way closure for oil quality and trapping.

New airborne gravity and magnetic data were used to produce potential field maps of the Garzón uplift and adjacent basins for this paper. Aerogravimetric data calibrated by well data and 2D seismic data constrain the possible geometry of the Garzón basement thrust fault and the top of basement. This study provides a well-documented example of crystalline basement actively overriding prospective hydrocarbon traps in footwall

sedimentary rocks along a low angle thrust fault. A new Euler deconvolution map of the magnetic field reveals rift graben structures in the basement rocks of the Garzón Massif.

1D basin modeling shows that no source rocks in the Putumayo Basin are presently buried deeply enough to produce the oil and gas observed in the basin's reservoirs (Gonçalves et al., 2002; Wolaver et al., 2015), except in the far southwest corner of the basin (Aguilera et al., 2010). Gonçalves et al. (2002) and Wolaver et al. (2015) therefore predicted that petroleum generation occurred more than 30 km to the west, under the present Central Cordillera or Upper Magdalena Valley (UMV). In this study we use 1-D models to map the present and paleo-petroleum systems to locate a potential hydrocarbon source pod and estimate the timing of hydrocarbon expulsion. Regional structural models and retrodeformed profiles predict migration pathways at the critical moment. A pseudo-van Kerevelen plot for samples from the Neiva Sub-basin, UMV, and the Putumayo Basin shows similar type II kerogen to mixed Type II and III oil families for both basins.

This study takes advantage of the new potential field, well, and seismic data as well as previous field mapping (Gómez Tapias et al., 2007), to produce the first retrodeformable volume-balanced structural cross section of the northern Garzón Massif. The new model presented here shows that the Garzón uplift and adjacent basins were deformed by previously unrecognized periods of distinct "thin-skinned" and "thick-skinned" deformation in the last 12 Ma. The timing of the two deformation events is critical for the evolution of the petroleum systems in the flanking UMV and Putumayo basins. The new regional profiles predict SE-verging (9-16 Ma) thin-skinned thrusting with 43 km minimum shortening, possibly synchronous with the main hydrocarbon expulsion event,

followed by symmetrical Andean (6 Ma – Present) uplift on basement thrust faults with 22 km shortening that interrupted and exposed the hydrocarbon migration pathways.

2.2 GEOLOGIC SETTING

2.2.1 PETROLEUM SYSTEMS AND STRATIGRAPHY

The Upper Magdalena Valley (UMV) and Putumayo basins are two important oil-producing basins in southwestern Colombia (Figure 2.1). The southern UMV, the Neiva Sub-basin, is an intermontane basin located between the Central Cordillera and Garzón Massif, the Putumayo is a foreland basin located to the east of the Garzón Massif. Mora et al. (2010) proposed that during the Mesozoic and Paleogene the UMV and Putumayo basins were part of the same extensive mega-basin, and they were later separated during the Andean orogeny when the Eastern Cordillera and Garzón Massif were uplifted.

The Putumayo Andean foreland basin in Colombia is the northern extension of the Oriente and Maranon basins of Ecuador and Peru (Figure 2.1; Higley, 2001). The Putumayo basin is relatively unexplored compared to the more mature Llanos basin to the north and the basins to the south, and offers prospective exploration opportunities. It covers about 50,000 km^2, between 0° - 3° N. Lat. and 74° - 77° W. Long. (Figure 2.1). The Putumayo basin has proved reserves of more than 365 million barrels of oil equivalent to date in 19 crude oil fields (Higley, 2001). In 1963 Texaco discovered the major Orito oil field with reserves on the order of 250 MMBO (Barrero et al., 2007). The hydrocarbons are sourced within three petroleum systems (Figure 2.3): (1) a nearshore marine clastic sequence of Lower Cretaceous Caballos Formation; (2) a proximal sequence of Upper

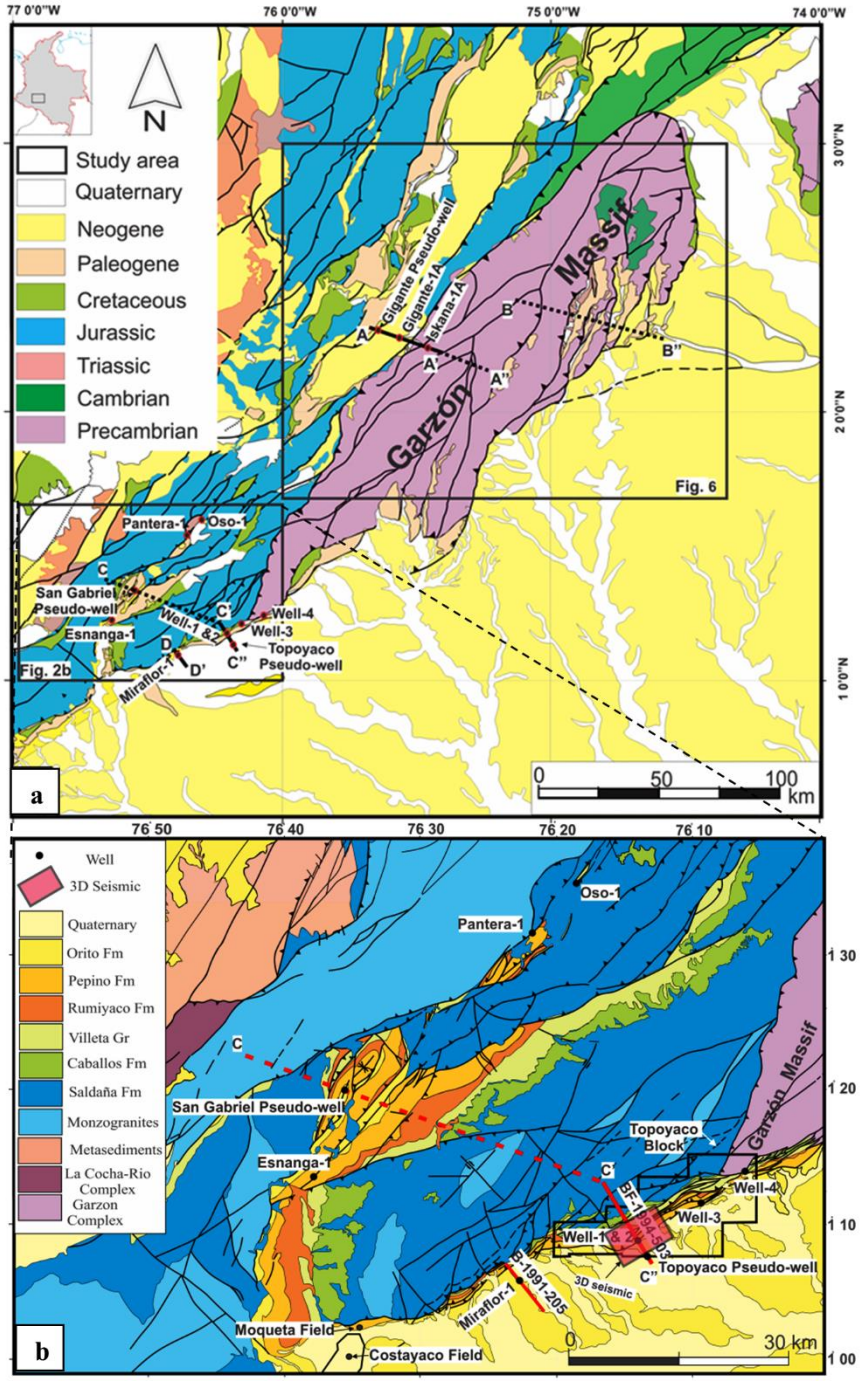

.Figure 2.2 a) Geologic location map of the northern and southern study areas, b) Geologic location map of the southern Putumayo/San Gabriel study area.

Cretaceous Villeta Formation; and (3) a distal marine carbonate sequence of the upper Villeta and Eocene Pepino (Gonçalves et al., 2002; Wolaver et al., 2015). The principal reservoir rocks are shallow-marine sandstones of the Caballos and Villeta Formations. Interbedded organic-rich source rocks and shales serve as source rocks and seals. The tectonic deformation in the Putumayo foreland basin has been variously described as being produced by dextral wrench faulting, rift basin inversion, "thin-skinned" thrust faults, and "thick-skinned" basement faults, e.g., Portilla (1991), Jimenez (1997) and Witte et.al (2013).

Between 1962 and 1982 several oil fields were discovered north of Neiva UMV in the Cretaceous Monserrate Formation In 1984 oil was discovered along the Dina-San Jacinto fault in the Aptian-Albian Caballos Fm (Sarmiento and Rangel, 2004). By 1994 542.1 MMbbl of recoverable oil and 91.9 BCF of gas had been discovered in more than 30 accumulations and 287.5 MMbbl of oil had been produced. A total of 191 exploration wells and more than 300 appraisal and development wells have been drilled in the UMV. Buitrago (1994) defined two petroleum systems in the southern Neiva sub-basin related to source rocks in the Villeta Group (Figure 2.3).

Vitrinite reflectance results for the Putumayo Cretaceous source rocks indicate thermal immaturity (Aguilera et al., 2010). Petroleum generation likely occurred to the west under the present Cordillera or within the UMV (Gonçalves et al., 2002; Wolaver et al., 2015). In the Neiva Sub-basin of the UMV Tmax pyrolysis data indicate intervals of early mature source rock in the lower part of the Villeta Group (Sarmiento and Rangel, 2004). Oil generation modelling indicate that the lower part of the Villeta Group reached the top of the main oil window at 3505 m during the beginning of the Miocene, and the bottom of the

late oil window at 4572 m at the end of Miocene (Sarmiento and Rangel, 2004). Basement for the Putumayo and Neiva UMV basins ranges from Grenville-age crystalline rocks to Triassic and Jurassic synrift siliciclastic and volcanic deposits of the Saldaña or Motema Formation (Figure 2.3, Mojica and Bayer, 1987; Ramos, 2010). Basement in the Putumayo and Neiva Sub-basins is overlain by two major megasequences separated by a regional unconformity.

The Aptian to Paleocene sedimentary rocks constitute a major marine megasequence (Figure 2.3). The source rocks and the main reservoir rocks are part of this megasequence. During Aptian to Maastrichtian times the sedimentation of the Caballos and Villeta Formations took place during regional thermal subsidence. The Villeta Formation which is the primary source rock in the basin with TOC 1.0-1.7%, has type II and III Kerogen and API 25-30 on the west side of the basin. Villeta sandstones have proven reservoir potential with average porosities of 12-18% and an average permeability 67 MD. From the Maastrichtian to Early Paleocene, the final accretion of the Western Cordillera caused the inversion of ancient normal faults, uplift of the Central Cordillera and a marked change of sedimentation from marine (Villeta Fm.) to continental (Rumiyaco Fm.) conditions (Montenegro and Baragan, 2011).

The second mainly continental megasequence extended from Eocene to Miocene (Figure 2.3), and records the sedimentary and tectonic burial responsible for petroleum generation and the deformation events that produced petroleum traps (Sarmiento and Rangel, 2004). During the Early Paleocene to Middle Eocene, increasing convergence rates between the Nazca and South America plates inverted normal faults, leading to the

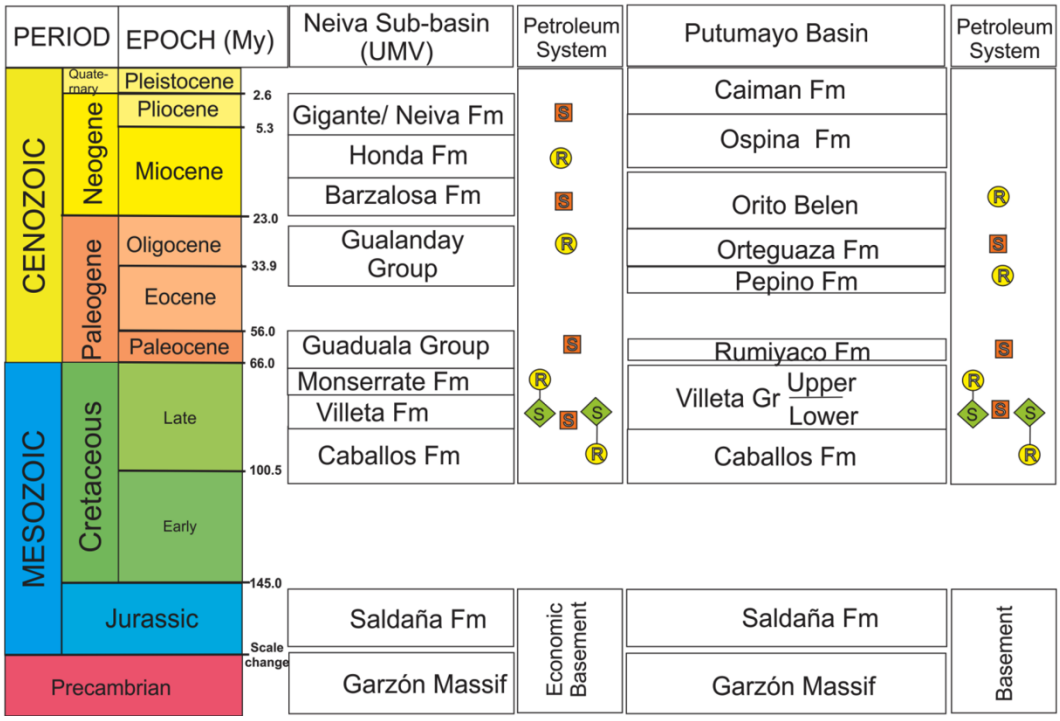

Figure 2.3 Stratigraphic columns and petroleum systems of Neiva Sub-basin (UMV) and Putumayo basins, (modified after Buitrago, 1994; Montenegro and Baragan, 2011).

development of thrust structures, and erosion and deposition of the coarse siliciclastics of the Pepino Formation. Uplift of the Central Cordillera during the Middle Eocene to Middle Miocene times induced flexural subsidence and the deposition of the Orito-Belen Group and the Ospina Formation in a foreland basin. Finally, the intense compression of the Andean Orogeny (Late Miocene to Recent) induced major uplift of the Eastern Cordillera and Garzón Massif, separating the Putumayo basin from the UMV which became an intermontane basin (Gonçalves et al., 2002).

2.2.2 LARAMIDE BASEMENT TECTONICS

One of the most controversial and least understood mountain forming styles is that of the Laramide orogeny (40-70 Ma) in the central and southern Rocky Mountains of the United States. The basement block, "germanotype", or "thick-skinned" tectonic style of the Laramide orogeny is characterized by broad zones of uniform strike and dip separated by narrow zones of steeper dips or high angle faults. The overlying sedimentary rocks may be folded or "draped" over the faulted basement blocks forming monoclines. Bouguer gravity anomalies directly reflect the movement of the basement blocks. The uplifts have Bouguer gravity anomaly highs indicating that dense basement rocks are involved and that the uplifts are "rootless", i.e., without crustal thickening. A controversial question has been whether the basement uplifts were formed by compressional tectonics or by vertical tectonics. Proponents of vertical tectonics believe that the magnitude of the vertical displacements exceeded the magnitude of horizontal displacements during the Laramide orogeny (e.g., Stearns, 1975). Subsequent seismic studies have revealed significant crustal shortening by brittle thrust faulting (e.g., Smithson et al., 1978; Erslev et al., 2016).

The common occurrence of overturned fault slivers of Mesozoic or Paleozoic sedimentary rocks beneath the Precambrian rock hanging-wall thrusts suggest a fault-related folding kinematic model for many of the Rocky Mountain basement uplifts. Low-temperature, basement-involved compressive folds are confined largely to the hanging walls of thrust faults and appear to be produced in response to both propagation and slip on non-planar faults. Kinematic models of three Laramide structures, including the Big Thompson anticline, Colorado (Narr and Suppe, 1994) involve thrust faults propagating through the brittle upper crust along non-planar paths (Figure 2.4). The stratified cover sequence in many cases forms a drape fold or monocline over the propagating basement fault. Other examples of basement fault monoclines are found throughout the Laramide US Rocky Mountains (e.g., Smithson et al., 1978; Miller and Mitra, 2011), the Venezuelan Merida Andes (DeToni and Kellogg, 1993), and the Sierras Pampeanas in Argentina (Jordan and Almendinger, 1986; Ramos et al., 2002). At least 16 wells have been drilled through Precambrian rocks for oil and gas prospecting in the sedimentary rocks that are concealed and virtually unexplored beneath the Rocky Mountain front thrusts (Gries, 1983). The wells set up potential footwall plays and helped define the structural geometry of the mountain-front thrusts, including the angle of the thrust, the amount of horizontal displacement, and the presence or absence of fault slivers containing overturned Mesozoic or Paleozoic rocks. Appendix A Table A.1 lists the well depths, dips of the fault angles at TD, and subthrust fault sliver thicknesses, if available. The mean dip angle from the ten wells is 22° with a large standard deviation. As Figure 2.5 shows, the measured dip angle distribution is bimodal, but the most common mode is low angle thrusting (5 to 30 degrees).

The measured Garzón thrust (Iskana-1) well dip angle (17°, this paper) lies near the average for the low angle basement thrust dip mode.

2.2.3 GARZÓN MASSIF GEOLOGIC BACKGROUND

The Garzón Massif is an uplifted basement block bounded by the UMV to the northwest and the Putumayo basin to the southeast (Fig 2.1). The Garzón Group basement, part of the Garzón-Santa Marta granulite belt, consists of 1.2 – 1.0 Ga old granulites, gneisses, amphibolites and minor ultramafic and calcsilicate rocks (Priem et al., 1989). Based on similar ages and rock types, Kroonenberg (1982) suggested that the Garzón-Santa Marta granulite belt and the Grenville Province at the southeastern edge of Laurentia were related and formed by the long-lived Grenville collision during the assembly of Rodinia. According to Van der Wiel's (1991) geochronological studies, the major uplift events in the Garzón Massif from 1.18 Ga to the present day are: 1) 1180 Ma: Relative rock uplift of 6 km, 2) 900 Ma: Orogeny, possibly also related to Grenville, resulting in at least 10 km rock uplift, 3) 12 Ma - Present: 6.5 km of rock uplift related to the Panama Arc-North Andes collision.

2.3 DATABASE AND METHODOLOGY

2.3.1 SEISMIC INTERPRETATION

Geophysical data provided for the southern part of this study (Figure 2.2b) included 155 (over 800 km) 2-D seismic lines acquired from 1987 to 2012, as well as 42 km2 of 3-D seismic data collected in 2008. 2-D and 3-D seismic spatial coverage was quite good, and 27 lines were reprocessed in 2012. Four regional 2-D lines run east-west and north-south and 12 regional wells are located along the foothills of the Putumayo Basin. Available borehole data included

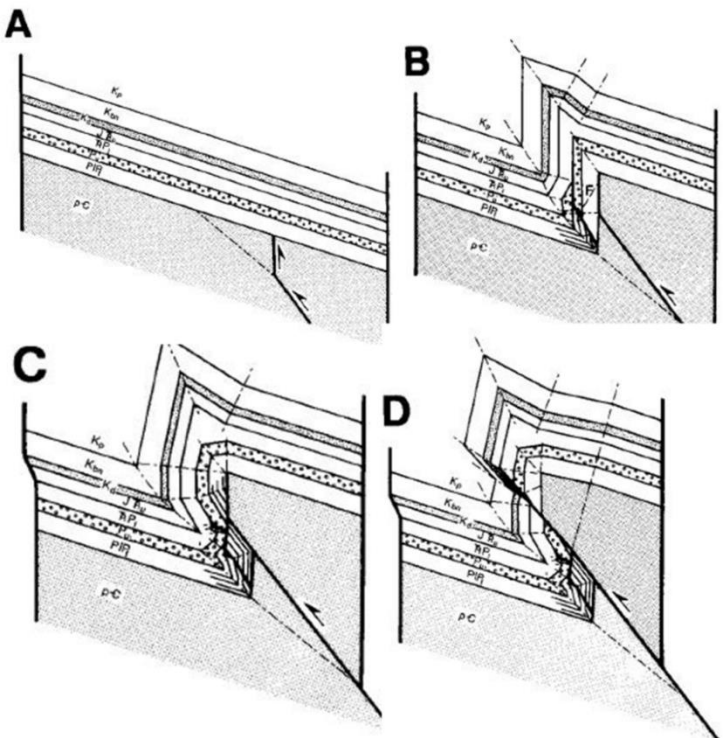

Figure 2.4 Kinematic sequence of development of Big Thompson anticline Colorado (Narr and Suppe, 1994)

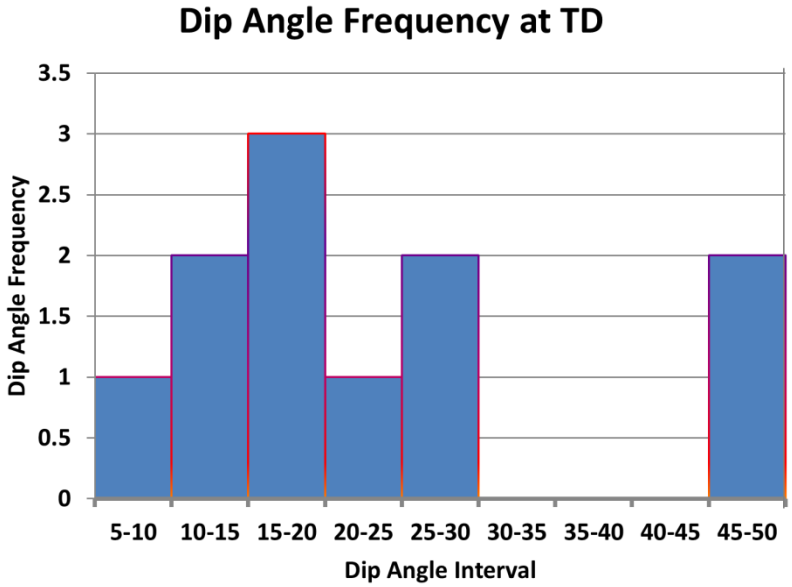

Figure 2.5 Frequency of dip angles at TD (Total Depth) from Table A.1 (Appendix A).

composite logs for 45 wells scattered around the study area with formation tops. Sonic, dip log, gamma ray and spontaneous potential logs were available for most of the wells.

The surface geology maps for the southern area (Figure 2.2b) were obtained from the Colombian Geological Survey, including plate 431 with a scale of 1:100,000 with report (Núñez and Gómez, 2010), and plates 411, 412, 431, 448, and 465 with a scale of 1:200,000 with reports (Núñez and Gómez, 2003).

This study is based on integration of geophysical and geological interpretation. Seismic reflection techniques provide the basic structural control of the subsurface geology constrained with available exploration wells. The research included seismic interpretation, structural modelling, 1D basin modeling, and data analyses.

Seismic interpretation was carried out using Petrel software, including regional seismic stratigraphy, structural maps, surface attributes (Fracture analysis in 3D volume) and time-depth conversion. PetroMod software was used to generate 1D basin models including burial history curves and source rock maturity.

The interpretation of the Topoyaco 3D survey included fracture analysis (Fault patch generation) Seismic Attribute (Variance ant tracking, Coherence attributes, and RMS attributes amplitude anomaly). Ant tracking is a Petrel process that identifies and utilizes discontinuities in 3D seismic data. The process can be applied to amplitude or other seismic attributes. These discontinuities may be associated with faults or fracture zones.

2.3.2 GRAVITY MAGNETIC STUDY OF THE GARZÓN BASEMENT UPLIFT

The geophysical study of the northern Garzón Uplift (Figure 2.2a) included interpretation of the Garzón fault with two dimensional gravity forward modeling constrained by seismic and well data. A regional 2D model of the entire Garzón Massif based on surface geology, gravity and magnetic data was constructed and retrodeformed to 25 Ma to interpret the orogenic evolution of the mountain and petroleum system. The magnetic field was inverted with the Euler Deconvolution method to illuminate lateral variations in the Precambrian basement rocks of the Garzón Massif.

The airborne gravity survey data used in the project includes 2,663 line kilometres gravimetry along 1 x 5 and 1 x 4 kilometre flight lines at elevations of 2564 and 4589 meters above mean sea level (Fig 2.6a). The data were obtained from the Agencia Nacional de Hidrocarburos Gravity Map of Colombia (2010). ArcGIS was used to create shape files and raster files from the database created in Oasis montaj. Moreover, the elevation and gravity raster gridded maps were converted to raster files in ArcGIS 10.1. The Bouguer gravity map was generated using a 0.5 x 0.5 kilometer grid generated by the Geosoft Oasis Montaj graphic mapping system (Fig 2.6b). Fig 1.6b is the complete (terrain corrected) Bouguer gravity map calculated for a reduction density of 2.80 g/cm^3. The Bouguer map is constructed by upward continuing the low elevation data (2564 meters above sea level) and merging it with the high elevation data (4589 meters above sea level). The accuracy of the airborne gravity observations are confirmed by land gravity observations collected along a north south profile east of the Iskana-1 well, in addition to land observations to the west of seismic line GAIT 99-21 (Figure 2.6). Misfits between land and air gravity measurements are less than 3 mgal. The observed gravity was then extracted from the map

data grid along the GAIT 99-21 profile line and exported to the 2-D profile. The range of the observed gravity is from -156 mgal to -84 mgal.

2.3.3 STRUCTURAL RESTORATION AND REGIONAL CROSS SECTIONS

Structural models were created in Move software, and were constrained by seismic and well data and surface geology. Digital elevation models (DEMs) were uploaded with the geologic maps to draw regional cross sections and retro-deform the sections using volume-balancing techniques (Suppe, 1983). To develop a model for the evolution of the northern Garzón Massif, the Garzón segment (western flank) of the regional profile was interpreted based on seismic and well control. This structural interpretation was then extended to a schematic regional geologic model constrained by surface geology, gravity and magnetic data.

On the southeast flank of the uplift, we interpret the Topoyaco and Miraflor structures (Figure 2.2b) using 2-D and 3-D seismic, well control, and surface geology. The Topoyaco interpretation is extended northwest to the San Gabriel fold belt, based on surface geology, to produce the southern regional cross-section.

2.4 RESULTS

2.4.1 TOPOYACO

We chose to model Topoyaco line BF1994-503 first (Figure 2.7a), because the line has well, 2-D and 3-D seismic, and surface geology control. The trend of the line coincides with the maximum dip direction at the mountain front and hence, accurately illustrates the

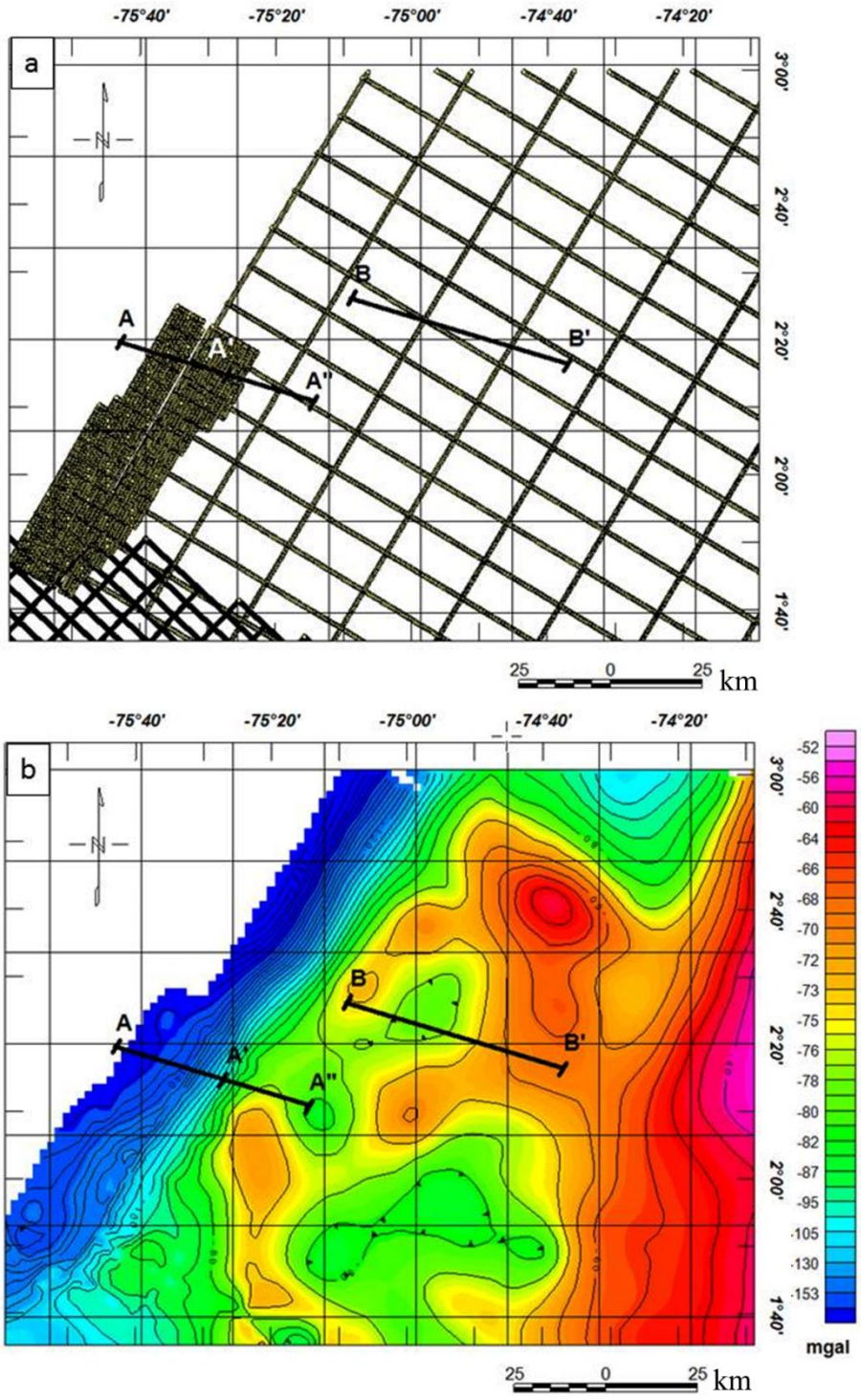

Figure 2.6 a) Location map for aerial gravity/magnetic surveys (northern Garzón Massif), b) Complete Bouguer gravity map (reduction density of 2.80 g/cm^3). For location see Figure 2.2. Data from Agencia Nacional de Hidrocarburos (2010).

major mountain front structure. The quality of the seismic data deteriorates at the mountain front, so that well and surface geology are valuable constraints on the geologic solution. Fortunately, an almost complete suite of dip log data is available for Well-2 (from near surface to 2.6 km depth). This dip data is critical because the 2-D and 3-D seismic data are incoherent over the key structural features of the mountain front. Our seismic interpretation is the first published interpretation to incorporate the complete Well-2 dip control. The 2-D seismic data from line BF1994-503 (Figure 2.7a) was imaged using Petrel® and Move® software. Average downhole velocities from the well check-shot survey were used to present the seismic data at approximately 1:1 scale (no vertical exaggeration). Surface geology from Colombian Geological Survey CGS mapping was projected onto the section (unit contacts, faults, and apparent dips). Figure 2.7a shows the well deviations and apparent bedding dips down hole. The dip data was degraded to make the output readable. The structural interpretation utilized Move® software. As a first approximation, unit thicknesses were conserved and fault-related folding was assumed (e.g., Narr and Suppe, 1994). The well dip log data reveals steep (~ 60°) basinward dipping beds, explaining why the seismic datasets could not image the structure.

The principal structure in line BF1994-503 is interpreted as a monocline produced by reverse faulting in the pre-Cretaceous basement rocks (Figure 2.7b). The monocline dips toward the basin at 25-45 ° near the surface, steepening to 60°, then shallowing to 25° at 2.6 km depth. Structural relief is > 4 km produced by a basement reverse fault dipping northwestward under the mountain at ~ 25° with ~ 6 km of slip. Timing of the monocline formation is certainly post- Miocene Ospina Fm and probably Andean (6 Ma – Present). The monocline is broken by 3 or 4 late stage break-through faults, but displacement on

these is limited to a maximum of ~ 700 meters. The monocline structure is very similar to basement fault monoclines discussed previously in this paper (Geologic setting 2.3. Laramide Basement Tectonics), such as in the Laramide US Rocky Mountains, the Venezuelan Merida Andes, and the Sierras Pampeanas in Argentina. Kinematic models of Laramide structures (Figure 1.5) by Narr and Suppe (1994) involve thrust faults propagating through the brittle upper crust along non-planar paths. The stratified cover sequence forms a drape fold or monocline over the propagating basement fault. Intense fracturing observed in the Topoyaco 3-D volume from the near-surface to depths of over 2000 msec (3.5 km) indicates that the highest level of fracturing permitted freshwater flushing and oil biodegradation in the Topoyaco block.

2.4.2 MIRAFLOR

We interpreted the MIRAFLOR-1 line B-1991-205 because, although the Miraflor-1 well is located just to the southwest of Topoyaco block, Miraflor-1 tested light gravity oil, while testing in all 7 Topoyaco wells indicates the presence of fresh water or heavy and extra-heavy and biodegraded oil. The interpretation of MIRAFLOR-1 line 205 was based on the 2-D seismic profile and formation-top picks from Miraflor-1 well. Unlike the Topoyaco line, the seismic resolution is high throughout the Miraflor structure (Figure 2.8a). Seismic reflectors are relatively coherent even in the basement. The structure is an asymmetric fault-bend fold with a pronounced monocline facing the basin and a low relief fold on the northwest side of the structure (Figure 2.8b). The fold was formed by a blind basement reverse fault dipping to the NW at ~ 25° with slip of 2 km. Structural relief on the monocline is about 1100 m but the back limb (NW) has only 100 m of relief thus limiting reservoir potential. Conformably folded bedding over the anticline indicates a

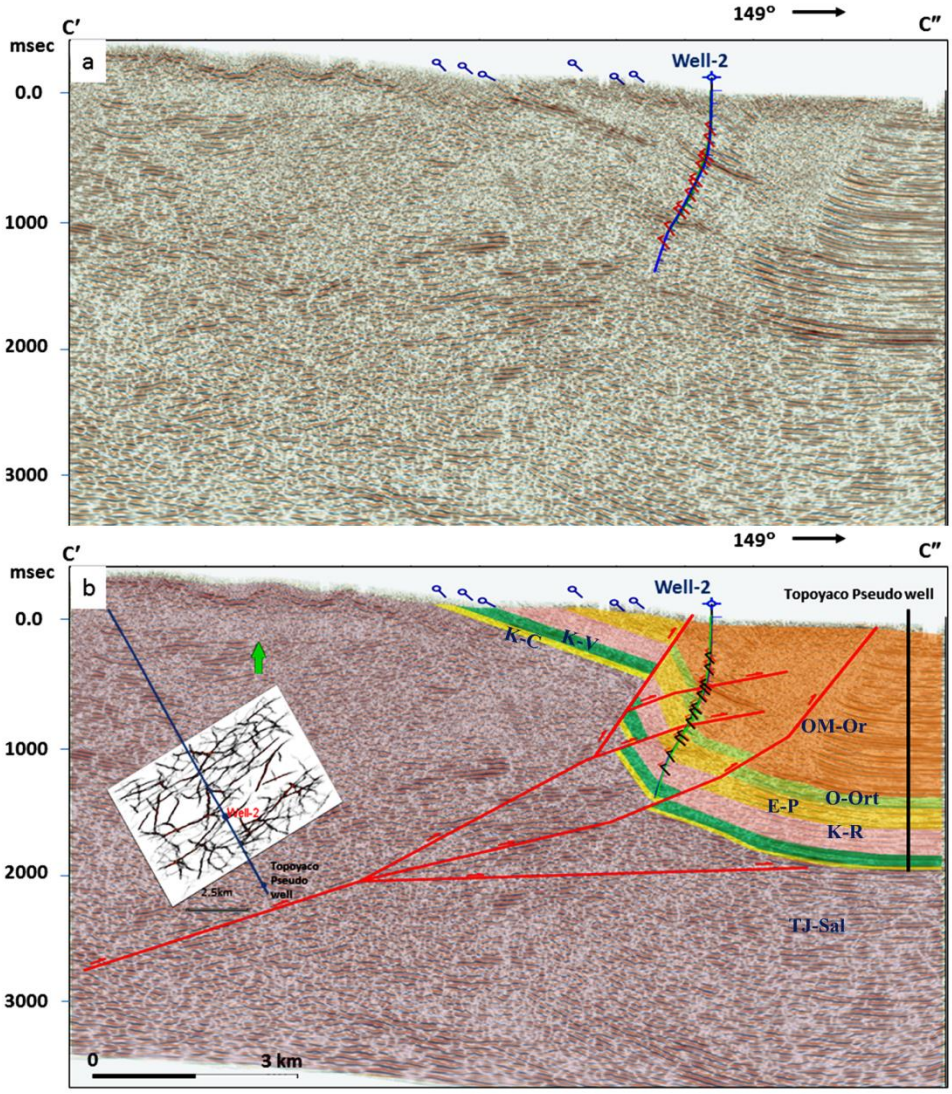

Figure 2.7 a) Uninterpreted 2-D Topoyaco seismic profile BF1994-503, b) interpreted seismic profile with seismic discontinuities attribute time slice (left inset) in 3D seismic at the reservoir level ~ 2000 ms. Orito Belen Fm (OM-Or), Orteguaza Fm (O-Or), Orteguaza Fm (O-Ort), Pepino Fm (E-P), Rumyaco Fm (K-R), Villeta Gr (K-V), Caballos Fm (K-C), Saldaña Fm (TJ-Sal). For locations, see Figure 2.2 b.

probable Andean age for the structure (6 Ma). The anticline was later fractured by a forelimb breakthrough fault with up to 400 m slip and a backthrust that may have produced the small NW limb of the anticline.

Although probably formed at the same time as the Topoyaco structure, the Miraflor anticline has apparent structural integrity, 4-way structural closure, and is relatively unfractured. The Miraflor anticline appears to be sealed from groundwater flushing and biodegradation by a backthrust on its northwest flank. The apparent structural integrity, 4-way trap closure, and lack of major fracturing also provided an effective seal for the hydrocarbons in the Miraflor anticline. The oil generation and migration may have occurred, either in the primary mid-Miocene expulsion event (14 ± 5 Ma) from a kitchen to the northwest into the incipient anticline or during the late Miocene-Pliocene (6 Ma-Present) "Andean" expulsion event from a kitchen in the present Putumayo mountain front depocenter to the southwest at or after the peak trap formation.

2.4.3 GRAVITY MAGNETIC STUDY OF THE GARZÓN BASEMENT UPLIFT

Complete Bouguer anomaly and Total field and Reduced to Pole magnetic anomaly maps for the northern Garzón Massif (Figs 2.6b, 2.9a and 2.9b) were generated with data from Agencia Nacional de Hidrocarburos, Colombia (2010). The gravity field of the northwestern flank of the Garzón Massif (Fig 2.6b) is characterized by a steep NNE-SSW trending gradient. Southeastward from the high peaks of the Massif the gravity field extends with low relief toward the Llanos. The magnetic field (Fig 2.9a) does not show a similar high correlation with the NW mountain front, and exhibits considerable relief over the basement rocks of the Massif. The magnetic field was inverted with Euler Deconvolution (Reid et al., 1990; Thomson, 1982, structural index = 0) in Fig 2.9b (See

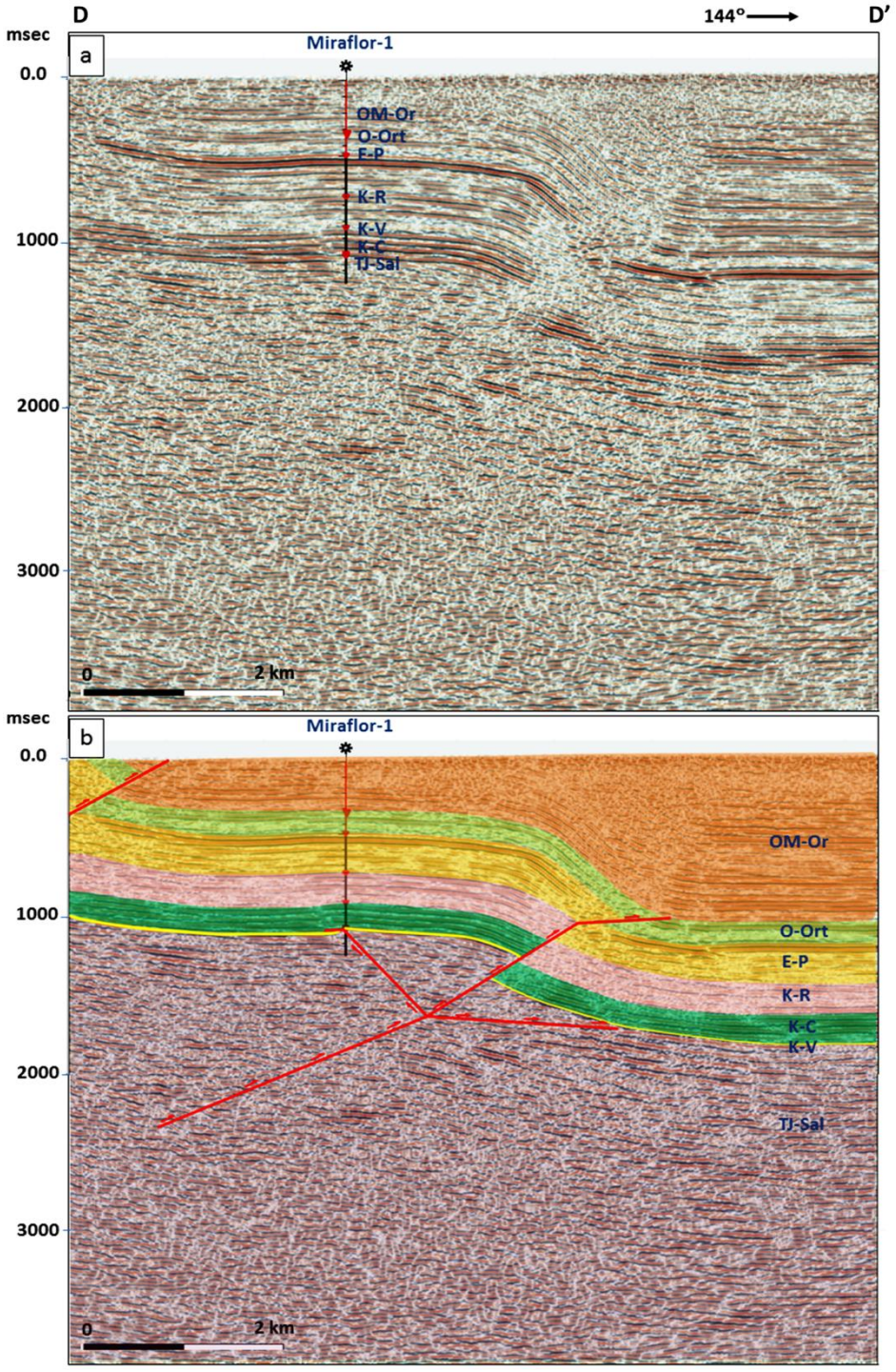

Figure 2.8 a) Uninterpreted 2-D Miraflor-1, seismic profile, b) interpreted profile. Symbols same as Figure 2.7. For location, see Figure 2.2 b.

Appindex A). The Euler solutions show several NNE-SSW trending patterns which are here interpreted as produced by faults bounding en-echelon grabens containing non-magnetic Precambrian sedimentary rocks.

2.4.4 GARZÓN THRUST FAULT

The Gigante oil field in the Neiva Sub-basin UMV (Figure 2.2a) contains 175 MMbbl of oil in situ in Monserrate Fm reservoirs in anticlinal traps (Sarmiento and Rangel, 2004). Just 3 km east of Gigante, Precambrian crystalline basement rocks at the surface are in contact with Miocene sediments along the Garzón fault. The Garzón/Algeciras fault has been previously mapped as a right-lateral strike-slip fault (Chorowicz et al., 1996; Velandia et al., 2005; Bustamante et al., 2010). However, in 2002, 5 km southeast of the Garzón fault, Iskana-1 well was drilled by HOCOL – TOTAL through 2743 meters of basement into the Miocene Honda Formation (DATALOG COLOMBIA, 2002, unpublished report). One original objective of this study was to use the gravity field to help constrain the dip on the Garzón thrust east of the Iskana-1 well and thereby estimate reservoir potential in the footwall anticline. The Garzón fault was located from surface geology (Gómez Tapias et al, 2007, referred to as Algeciras fault) and from the clear fault impedence contrast in the migrated seismic image (Fig 2.10). The fault is a listric thrust dipping 33 degrees (apparent) to the southeast near the surface. At a depth of 420 meters (1379 feet) below sea level, the apparent fault dip shallows to 19 degrees southeast until it is intersected by Iskana-1 well. Dipmeter and vertical seismic profile (VSP) independently suggest a fault dip of approximately 17 degrees. Taking into account the obliquity of the profile relative to the trace of the Garzón fault, the true dip of the fault is approximately 35 degrees southeast at the surface, shallowing to 21 degrees at a depth of 420 meters below sea level.

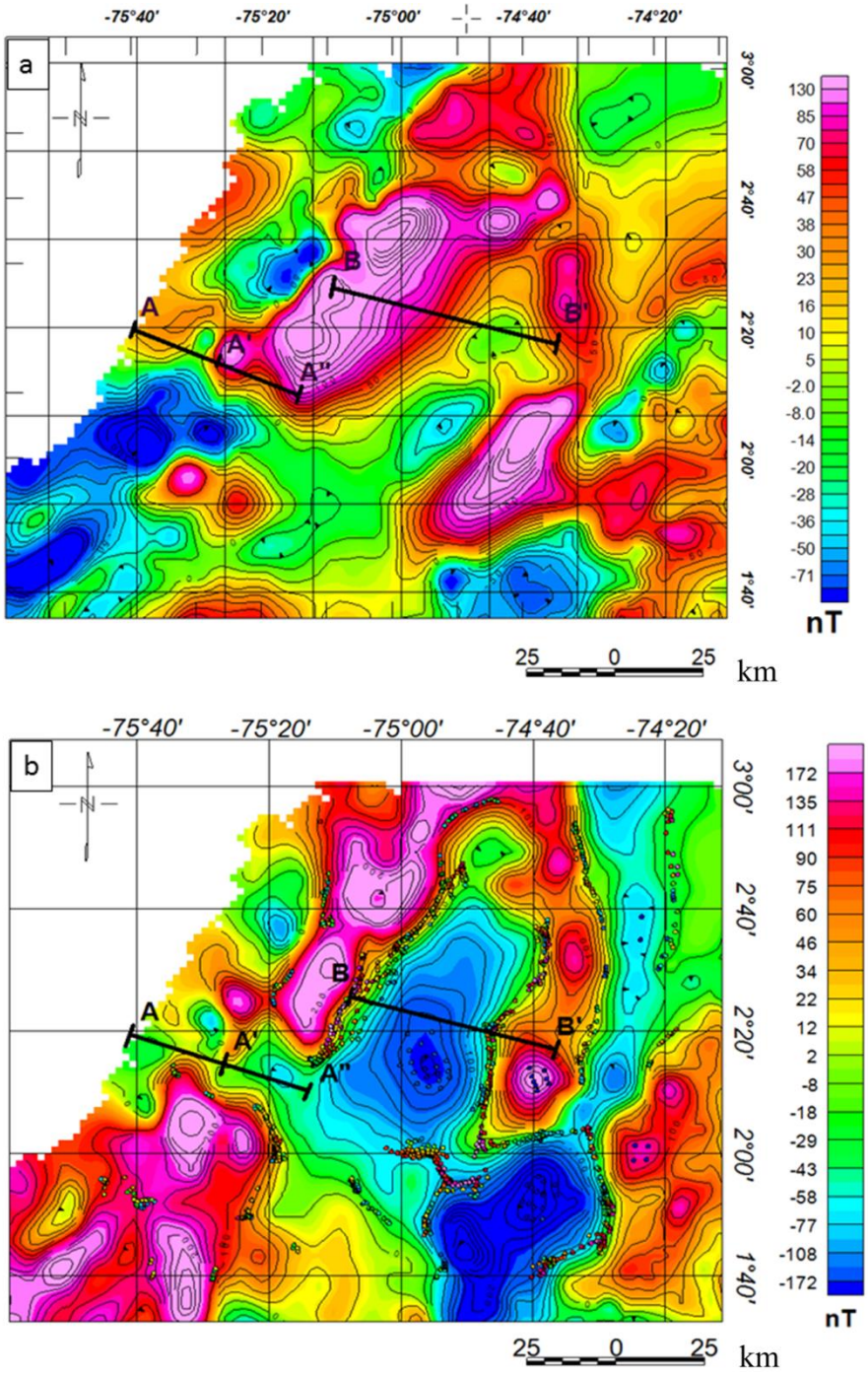

Figure 2.9 a) Total field magnetic anomaly map of northern Garzón Massif, b) Reduced to Pole magnetic anomaly map and Euler deconvolution map, tolerance 15%, structural index = 0 (Appendix A). For location, see Figure 2.2a

Initial rock densities for the 2D density model in Figure 2.11a were input from Table A.1, based on rock type, bulk density logs from Gigante-1 well, and seismic velocities. WNW-dipping dense basement polygons were included for the lower crust and the mantle to explain the regional gravity gradient linearly increasing to the east-southeast. The air polygon was given a density of 2.8 gr/cm^3, since this is the reduction density used to produce the complete Bouguer anomalies. The resulting calculated gravity field for the 10 degree dipping fault model (Figure 2.11a, solid line) agrees well with the observed gravity (dotted line).

Since the model fit varies with the density chosen for the Garzón Massif polygon, the misfit errors were calculated for densities ranging from 2.60 to 2.70 gr/cm^3 (Bakioglu, 2014). Higher densities for the thrust would indicate even shallower dips on the Garzón fault. The best-fit model solutions are 10 to 15 degrees (12 to 17) degrees after correction for apparent dip. This low angle thrust solution is supported by the measured 17 degree dip in the Iskana-1 well under the Garzón fault. It is also in agreement with the most common dip angles found for 10 exploration wells that drilled through Precambrian hanging wall blocks in the Laramide Rocky Mountains (Appendix A Table A.1; Gries, 1983). Our low-angle Garzón thrust fault solution predicts 10 to 17 km of thrusting, and that Cretaceous reservoir rocks in the Iskana footwall anticline may extend an additional 12 km east of the well (Figure 2.11).

2.4.5 REGIONAL CROSS SECTION NORTHERN GARZÓN MASSIF

A regional profile (Figure 2.11b) was selected in two segments, A – A`` and B – B`. The A – A`` profile extends the GAIT 99 -21 Garzón thrust fault profile to the southeast. The profile was offset to the B – B` profile in order to cross the imbricate thrust zone

mapped by Ingeominas and UPTC geologists (Rodriguez et al., 2003; Gomez Tapias et al., 2007; Rodriguez et al., 2009). The cross section contains Garzón Massif Complex units, fluvial/alluvial conglomerates of the Pepino Formation, and Orito Gp. sandstones. Rocks of the Pepino Formation and Orito Group are assumed to be Late Eocene to Middle Miocene in age (>14 Ma). The steep gravity gradient on the NW flank of the Garzón Massif is interpreted as produced by dense granitic basement rocks thrust over low density sediments of the UMV on the Garzón thrust fault (Figure 2.11). The low relief anomalies to the SE are interpreted to reflect uniformly shallow basement rocks and thin crust. The observed gravity does not require crustal thickening under the Garzón Massif. In the magnetic model (Figure 2.11b), the low magnetic anomalies over the SE flank of the massif are produced by non-magnetic (low susceptibility) Precambrian sediments.

2.4.6 TECTONIC EVOLUTION OF THE GARZÓN MASSIF (25 MA TO PRESENT)

To develop a model for the evolution of the Garzón Massif, a present-day structural interpretation was created and then retrodeformed. The GAIT 99-21 segment of the regional profile was interpreted based on seismic and well control (Figure 1.11b and 1.12a). This structural interpretation was then extended to a schematic regional geologic model constrained by surface geology, gravity and magnetic data (Figure 2.11b and 2.12a). The resulting retrodeformed profile highlights previously unrecognized distinct episodes of "thin-skinned" and "thick-skinned" deformation in the Garzón Massif. The timing of the deformation is critical for evolution of the UMV-Putumayo petroleum system.

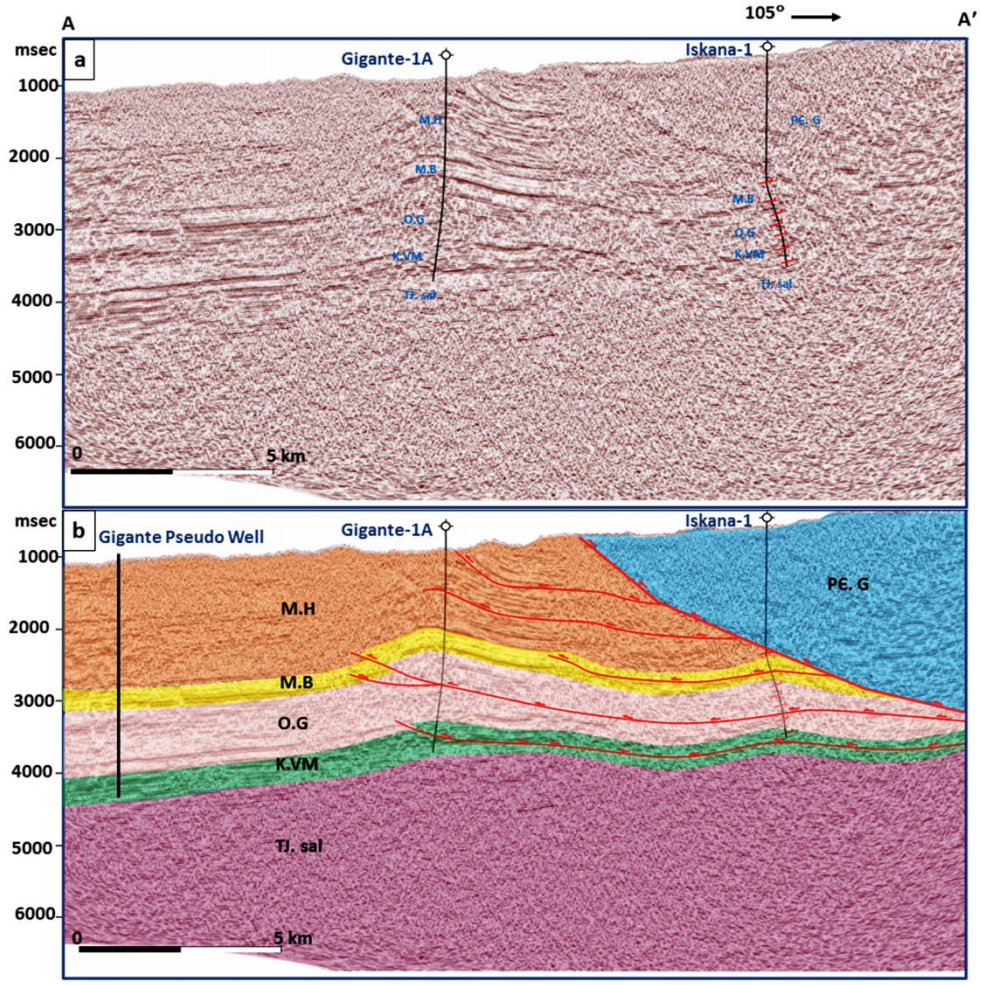

Figure 2.10 a) Migrated seismic profile GAIT-99-21, b) Interpreted seismic profile. Honda Fm (M.H), Barzalosa Fm (M-B), Gualanday Gp (O.G), Villeta Gp, Monserrate Fm (K.VM), Saldaña Fm (TJ. sal), Garzón Complex (PЄ. G), approximate vertical exaggeration: 1. See Figure 2.6 for location.

To retrodeform the Garzón uplift, first, the minimum displacement was removed from the Garzón basement thrust and the basement thrust on the SE flank of the massif (Fig 2.12b). Minimum slip on the Garzón thrust was 13 km and vertical structural relief was at least 7 km. The Garzón thrust is predicted to ramp up from a lower crustal detachment at a depth of about 15 km. Slip on the SE marginal basement thrust is estimated at 9 km, but this is poorly constrained. Upper Honda Formation sediments dated by K-Ar and fission-track ages (FTA) at over 9-10 Ma (Van der Wiel, 1991) underlie the Garzón thrust fault. Pebble and point counts show that sandstones of the Honda Formation and lower members of the Gigante Formation have a western provenance (Central Cordillera; Van der Wiel, 1991). The upper member of the Gigante Formation and the Las Vueltas Formation consist entirely of erosional products from the Garzón Massif, thus constraining the primary uplift of the Garzón Massif to 6.4 to 2.5 Ma (Van der Wiel, 1991). Apatite FTA from the Garzón Massif record an earlier uplift at 12 Ma, but the sedimentary record suggests that this event had little influence on the deposits in the UMV (Van der Wiel, 1991). Paleoprecipitation data indicate that a substantial orographic barrier was not fully established until 6–3 Ma, when >1 km/my. of material was exhumed (Anderson et al., 2016). Based on minimum exhumational ages provided by new apatite FTA data, as well as thermal history modeling, Anderson et al. (2016) suggest that thrust-induced rapid exhumation of the Garzón Massif was focused between 6.4 Ma and 3 Ma. Timing of the primary slip on the SE marginal basement thrust is therefore also assumed to be within the last 6 Ma. In the last 3 Ma strain partitioning may have resulted in diminished basement exhumation and right-lateral strike-slip motion along the Garzón/Algeciras fault system (Chorowicz et al., 1996; Velandia et al., 2005; Bustamante et al., 2010; Anderson et al., 2016).

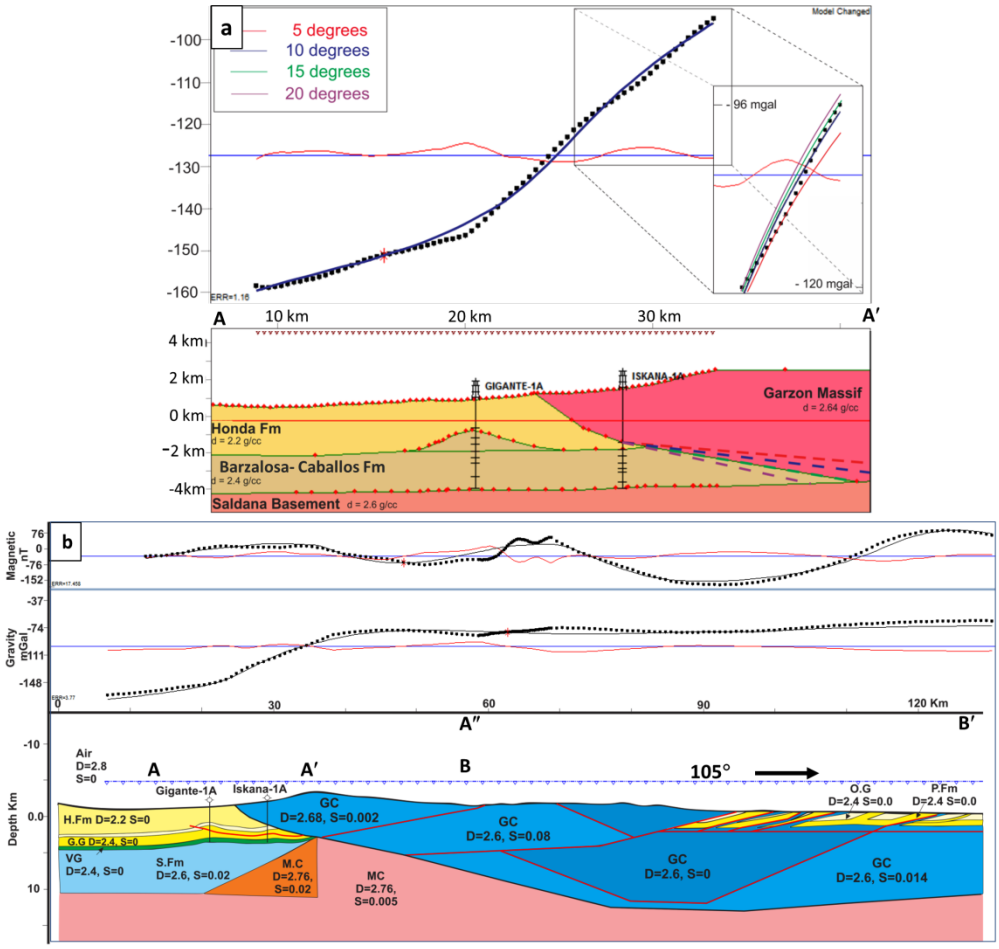

Figure 2.11 a) Density model for GAIT – 99 – 21. Model dips shown for Garzon thrust: 5, 10, 15, and 20 degrees. No vertical exaggeration. Calculated (solid lines), observed (dotted line), error (red line for 10 degree dip). b) Regional density and magnetic model. Calculated (solid lines, observed (dotted lines), error (red lines). Honda Fm (H. Fm), Orito Gp (O.G.), Gualanday Gp (G.G.), Pepino Fm (P.Fm), Villeta Gp. (V.G.), Saldaña Fm (S.Fm), Garzón Complex (G.C.), Middle Crust (M.C.). See figs. 2.6 and 2.9 for location.

The sediments of the Pepino Formation and Orito Group, exposed in imbricate thrusts on the SE flank of the Massif are dated as >14 Ma, Late Eocene to Middle Miocene (Rodriguez et al., 2003; Gomez Tapias et al., 2007). Rodriguez et al. (2009) mapped the thrust units as Pepino Formation and Orteguaza Formation, >25 Ma, Late Eocene to Oligocene. Thus, the southeastward verging "thin-skinned" thrusting must have been at least post Oligocene (< 25 Ma) and possibly post Early Miocene (or < 14 Ma) late and pre late Andean basement uplift (6 Ma).

The 'thin-skinned" thrusting may have coincided with the age of the Honda Fm and apatite fission-track ages for the Early to mid-Miocene uplift of the southern Central Cordillera (9 – 16 Ma) (Van der Wiel, 1991; Villagomez and Spikings, 2013). Minimum shortening by thin-skinned thrusting is estimated at 43 km. A retrodeformed model prior to the thrusting is shown in Fig 2.12c. It should be noted that the thin-skinned shortening estimate is very approximate and sensitive to the dips on the imbricate ramps. More accurate estimates will be derived through more detailed mapping of the dips in the imbricate thrust zone and a definitive age determination for the youngest unit in the thrusts.

2.4.7 REGIONAL CROSS-SECTION OF THE SOUTHERN GARZÓN UPLIFT

A regional structural model was needed to test source and migration pathway models relative to trap synchronization in the Miraflor and Topoyaco structures. As noted previously, the source rocks in the Putumayo Basin at present are either immature or marginally mature. Gonçalves et al. (2002) reported that vitrinite reflectance data together with modeling results showed that the source rock is practically immature in the Putumayo

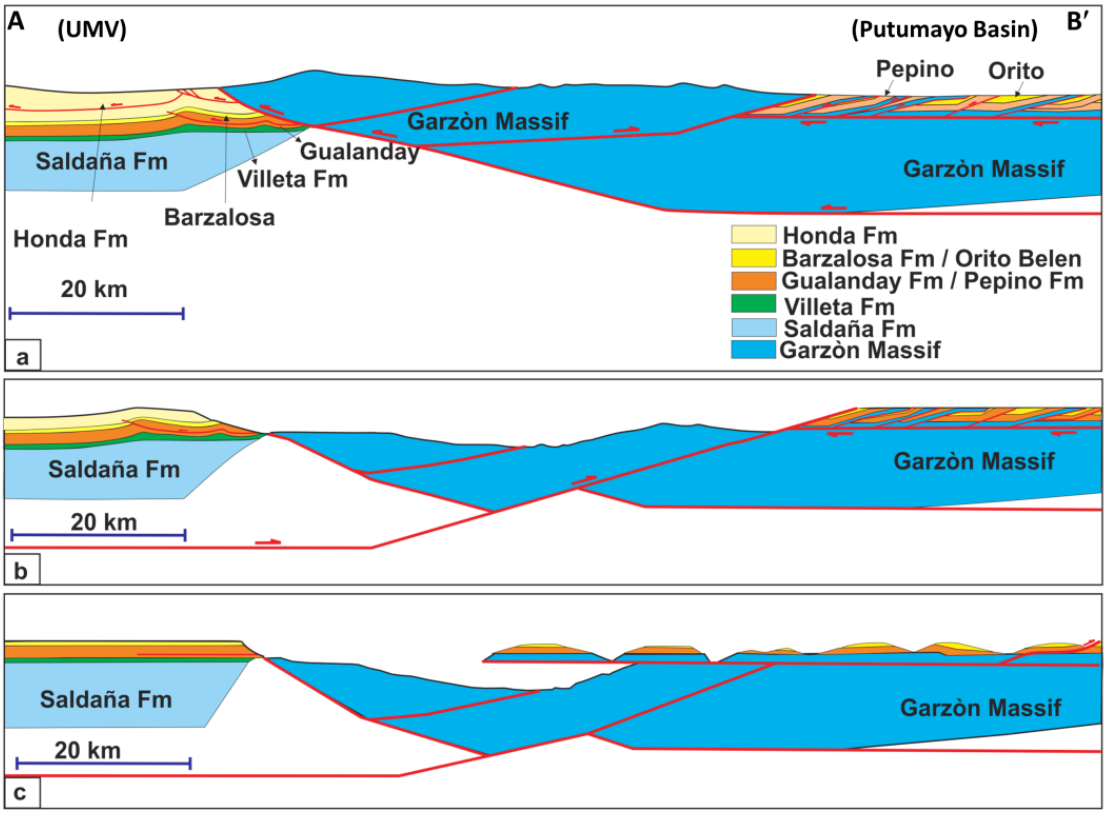

Figure 2.12 Evolution of the northern Garzón Massif (Profile A-B' in Figure 2.2a) a) Present Day, following symmetrical Andean (6 Ma – Present) uplift on NW-verging Garzón and SE-verging basement thrust faults, shortening ~ 22 km, b) 10 Ma, following SE-verging (~9-16 Ma) thin-skinned thrusting, shortening ~ 43 km. **c)** 25 Ma.

foothills, even in the footwall of large thrust faults. They proposed that Late Oligocene/Miocene petroleum generation and expulsion occurred from a location in the present cordillera area. To test this theory, our study utilized a number of wells that have been drilled in the inter-montane San Gabriel valley (Esnanga-1 near Mocoa, Pantera-1, and Oso-1, Figure 2.2b).

The southeastern end of the southern regional profile C-C" (Figure 2.13a) is Topoyaco line BF1994-503 C'-C". The rest of the profile C-C' is based on surface geology published by the INGEOMINAS, (2003). The line crosses the center of the San Gabriel fold belt. Thicknesses of the Caballos, Villeta, and Rumiyaco formations are taken from Esnanga-1 well. Thicknesses of the Pepino and Orteguaza formations are based on the mapped surface geology and Topoyaco well data. Surface geology from CGS mapping (unit contacts, faults, and apparent dips) and topography were projected onto the section (Figure 2.13a). The structural interpretation utilized Move software, unit thicknesses were conserved and fault-related folding was assumed (Figure 2.13b).

2.4.7.1 TOPOYACO UPLIFT

The Topoyaco uplift is interpreted as a mountain scale basement fault-propagation fold (Figure 2.13a). The forelimb is the steep Topoyaco monocline with break-through propagating faults. The backlimb dips gently to the northwest (13°) forming the southeast flank of the San Gabriel basin. The uplift was produced by a northwest-dipping midcrustal basement ramp to a blind thrust under the Topoyaco monocline resulting in ~ 15 km of shortening and 7 km of structural relief. The Topoyaco uplift is assumed to be Andean (6

Ma) in age based on the presence of conformably folded Miocene sediments in the monocline.

2.4.7.2 SAN GABRIEL FOLD BELT

The San Gabriel fold belt along the line of section (Figs. 2.2b, 2.13) consists of a basement fault-bend fold (ramp anticline) and two imbricate thrust faults. Both of the imbricate thrusts ramp to the surface in Rumiyaco bedding planes, indicating that the basement thrust must flatten on an upper flat in the Rumiyaco Formation Total shortening is 4.5 km and the structural relief is 3.5 km. The age of the San Gabriel folding is at least post-Oligocene based on conformably folded Orteguaza/Orito? Formation sediments and probably early to mid-Miocene (8-19 Ma) based on nearby apatite fission-track ages (Villagomez and Spikings, 2013). Note that this is similar to constraints on the timing of "thin-skinned" imbricate thrusting in the area of the present northern Garzón Massif (section 2.6.), i.e., post-Orteguaza/Orito Group (< 25 Ma) and pre late Andean basement uplift (6 Ma). The structural style is similar to that shown by a seismic profile intersecting Esnanga-1 well. Structural analogs for the San Gabriel anticline include the San Francisco anticline in the Middle Magdalena Valley and the Medina anticline in the Eastern Cordillera foothills.

2.4.7.3 RETRODEFORMED SAN GABRIEL TOPOYACO REGIONAL SECTION.

The regional profile was retrodeformed to 10 Ma by flattening on the top of the Orito Formation (Figs. 2.13b). We interpret the Orito Formation as representing syntectonic foredeep sedimentation associated with the Early to mid-Miocene uplift of the nearby

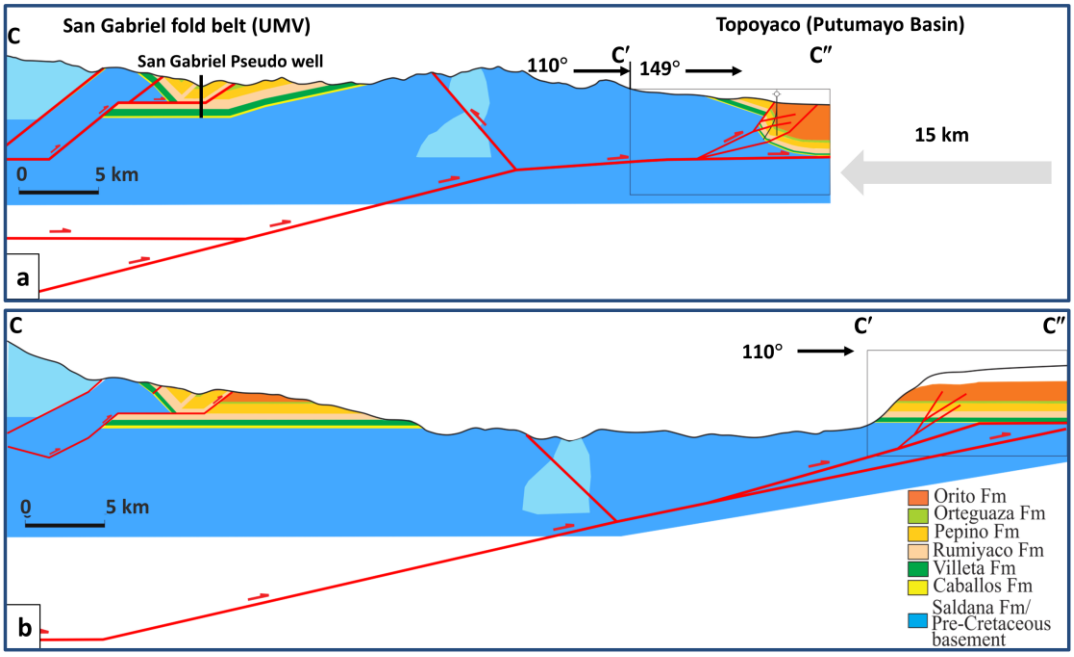

Figure 2.13 Evolution of the southern Garzón Massif (profile C-C' in Figure 2.2b) a) Present Day, b) 10 Ma.

southern Central Cordillera (8 -19 Ma: four apatite fission track ages for samples located within 30 km of the San Gabriel pseudo-well (Villagomez and Spikings, 2013). We estimated the original thickness of the Orito Formation in the San Gabriel fold belt by extrapolating the observed Present-day Orito Formation isopach gradient in the Putumayo foredeep (~1m/50m) 50 km northwestward into the present cordillera. The resulting thickness estimate is 3.5 km in the San Gabriel fold belt, almost all of which was exhumed during the Andean uplift (Figs. 2.13a and b).

Note that all reservoir rocks and migration pathways within the Topoyaco uplift were exposed to erosion during the Andean uplift (6 Ma).

2.4.8 HYDROCARBON MATURATION AND MIGRATION

Burial and thermal histories were constructed for Topoyaco, San Gabriel, and Gigante pseudo-wells using PetroMod thermal modeling software. The present-day heat flow was estimated from borehole-corrected downhole temperatures and from regional paleo heat-flow estimates (INGEOMINAS- ANH, 2008). The heat flow used for the foreland burial history was 35-45 mW/m2, typical for foreland basins worldwide. From these histories, timing of hydrocarbon charge may be inferred.

2.4.8.1 TOPOYACO PSEUDO-WELL

A Topoyaco pseudo-well was located in the deepest Villeta Formation rock in the Topoyaco footwall foredeep (Figure 2.14c) in order to estimate the maximum local potential source rock maturity up to the present. 1-D modelling based on the Topoyaco well would have underestimated the source rock burial depths by the > 1000 m thickness of Orito-Belen Formation rocks eroded during the Andean formation of the monocline. A

present-day depth of 3.5 km was estimated. Despite the tectonic complexity, a constant heat flow (40 mW/m^2) was assumed to best explain the measured vitrinite reflectance values in Well-1 well. Gonçalves et al. (2002) found that a similar constant heat flow equal to the present (36 – 38 mW/m^2) was the thermal history scenario that best accounted for the measured vitrinite reflectance values in two Putumayo wells modeled. Vásquez et al. (2009) noted that the oil-bearing source and reservoir succession in the Putumayo Basin was intruded by gabbroic dikes and sills. K/Ar dating indicated a Late Miocene to Pliocene "Andean" age (6.1 ± 0.7 Ma) for the igneous episode and suggested that magma chambers near the oil kitchens might have increased heat flow in the basin causing generation and expulsion of hydrocarbons and CO2 during the most recent expulsion event (Figure 2.15a).

The maximum calculated vitrinite reflectance value for the Topoyaco pseudo-well was 0.6-0.7 (immature to early mature). Assuming constant heat flow values of 40 mW/m^2 gave similar vitrinite reflectance values to those measured in the Esnanga-1 well (0.59-0.62). Note that the source rocks are immature even in the footwall of the Topoyaco monocline.

2.4.3.1 SAN GABRIEL PSEUDO-WELL

A pseudo-well was analyzed 50 km northwest of Topoyaco for the San Gabriel fold belt (Figure 2.14b) to test predictions by Gonçalves et al. (2002) and Wolaver et al. (2015) that the hydrocarbon kitchen for the main Putumayo expulsion event was located in the present cordillera. Burial history is based on our structural model (Figure 2.13b), and is calculated from the footwall to approximate maximum burial conditions. As discussed above, the original thickness of the Orito Formation in the San Gabriel fold belt was estimated by

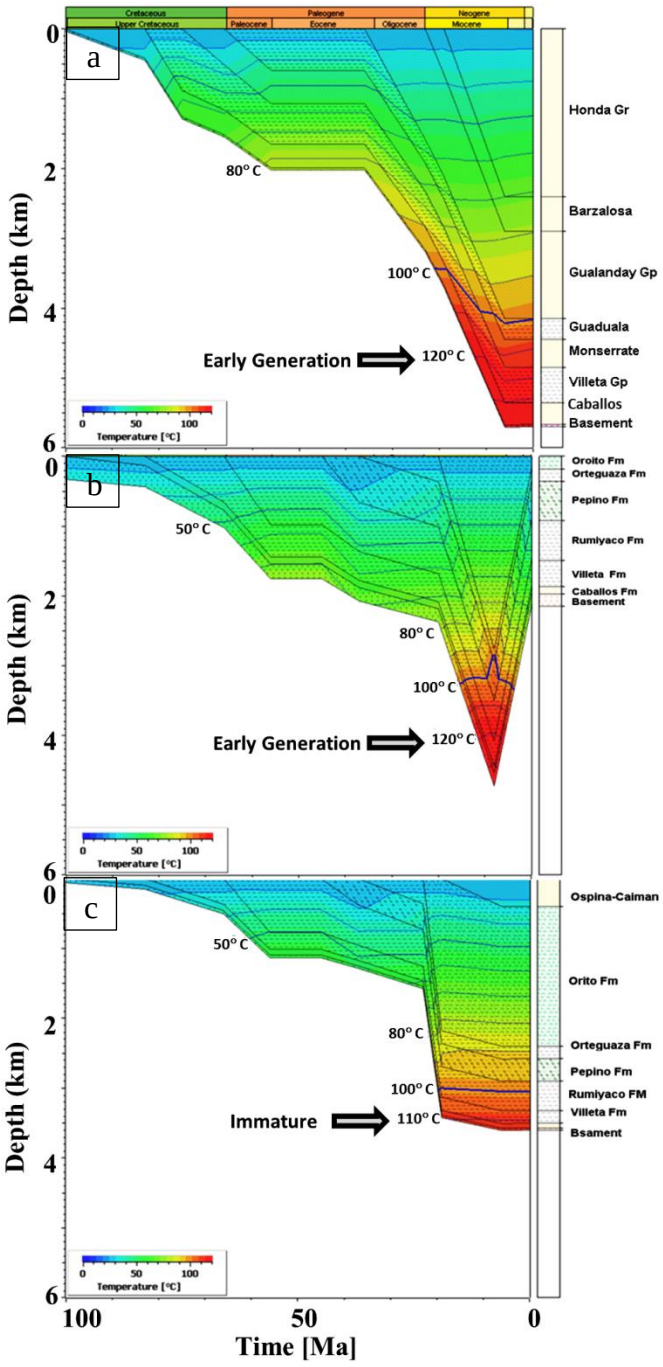

Figure 2.14 Burial histories assuming constant heat flow of 40 mW/m2 of a) Gigante pseudo-well b) San Gabriel pseudo-well and c) Topoyaco pseudo-well. For locations, see Figure 2.2.

extrapolating the observed present day Orito Formation isopach gradient in the Putumayo foredeep (~ 1m/50m) 50 km northwestward into the present cordillera. The resulting thickness estimate is 3.5 km in the San Gabriel fold belt, almost all of which was exhumed during the Andean uplift (Figure 2.13a).

We assume that the Villeta Formation in the San Gabriel fold belt reached its maximum depth in the Mid-Miocene (6-19 Ma), simultaneous with the uplift of the nearby southern Central Cordillera. Then, the belt was uplifted over 3 km during the Andean Topoyaco orogeny (3-6 Ma). At about 10 Ma in the mid-Miocene, the Villeta Formation source rocks reached a calculated vitrinite reflectance value of 0.7 - 0.85 or Peak Mature. Assuming constant heat flow values of 40 mW/m^2 gave "Early Oil" vitrinite reflectance values (0.62-0.67). This is consistent with measured vitrinite values in the Esnanga-1 well and a 1-D burial history model for Esnanga-1 well by Wolaver et al. (2015). Wolaver et al. (2015), however, predicted that Villeta source rocks entered the oil window from ~18 to 12 Ma, assuming that 12 Ma apatite fission track ages (van der Wiel, 1991) marked the Garzón Massif uplift. However, the sedimentary erosional record (van der Wiel, 1991), paleoprecipitation data, and minimum exhumation ages from new apatite FTA data (Anderson et al., 2016) suggest that rapid exhumation of the Garzón Massif was focused between 6.4 Ma and 3 Ma. Gonçalves et al. (2002) calculated a 1-D model for a hypothetical pseudo-well in the present Central Cordillera 80 km to the west of the mountain front. In his well, Gonçalves et al. (2002) predicted that Villeta Formation source rocks possibly started to generate petroleum during the Late Oligocene and reached a depth of 6,000 m by the beginning Miocene. In any case, our San Gabriel 1-D model supports the Gonçalves et al. (2002) and Wolaver et al. (2015) predictions of a source within the

present cordillera for the Early to mid-Miocene Putumayo oil expulsion thus providing the missing Putumayo kitchen.

2.4.3.2 GIGANTE PSEUDO-WELL

The Gigante pseudo-well is located several kilometres northwest of Gigante-1 (Figs. 2.2a, 2.14a) to approximate burial conditions in the Villeta source rocks with a full section of Honda Formation restored. A 1-D burial model based on the Gigante well would have underestimated the source rock burial depths by the 1100 m thickness of Honda Formation rocks eroded during Andean folding of the Gigante anticline. Assuming a heat flow of 40 mW/m2 in the Gigante pseudo-well, Villeta source rocks reached the oil window about 12 Ma (Figure 2.14a) and a depth of approximately 4 km by 10 Ma, and generation continues to the present (Figure 2.15b). This is in agreement with the oil generation models of Sarmiento and Rangel (2004) that Villeta source rocks in the Neiva Sub-basin of the UMV reached the top of the main oil window during the beginning of the Miocene and the bottom of the oil window at the end of the Miocene with maximum generation in Mid-Miocene.

The predicted Gigante pseudo-well critical moment may also be approximately coeval with the critical moment in the San Gabriel pseudo-well (9 – 16 Ma) and also be driven by foredeep subsidence associated with the rapidly rising southern Central Cordillera to the west. Earlier wide-spread slow uplift of the Central Cordillera from 45 to 30 Ma (Butler and Schamel, 1988; Villagómez and Spikings, 2013) may have provided earlier hydrocarbon kitchens to the west. However, Eocene migration pathways to the east might have been blocked by the Early/Middle Eocene uplift of the Garzón Massif.

Source rock maturity measurements on samples recovered from nearby Gigante-1A well where the Villeta Group is dominantly immature (pyrolysis Tmax less than 430° C) are consistent with our maximum calculated vitrinite reflectance value for the Gigante pseudo-well of 0.62-0.71 (immature to early mature).

2.4.8.4. OIL BIODEGRADATION IN TOPOYACO

Drilling and testing in all wells in or around the Topoyaco Block on the southeast flank of the Garzón uplift (Figure 2.2a) indicate the presence of fresh water (300-500 ppm) or heavy and extra-heavy and biodegraded oil (Wolaver et al., 2015). However, nearby Costayaco and Moqueta fields and Miraflor located to the southwest of Topoyaco (Figure 2.2b) have light gravity oil (Ramirez et al., 2012; Dueñas and Ramirez, 2012). Was the biodegradation the result of water flushing, burial at low temperatures, or stratigraphic variations in source and reservoir rocks? The geochemical analysis of the oil found in Topoyaco block suggested that the source rock is late Cretaceous anoxic shale (Talukdar, 2012). Gas chromatogram analysis indicated the presence of a mixture of highly biodegraded to moderately biodegraded oil. The biomarker maturity and estimated Ro maturity (0.75 and 0.80%) suggested that the original API of the oil in the reservoir was around 30° prior to migration and biodegradation of the oil, which is similar to the light oils found in the nearby field to the southwest (MIRAFLOR-1). Martinez et al. (2014) suggested that the only source rock in Putumayo Basin is Late Cretaceous or younger based on specific isotope analyses of biomarker and diamondoid of sixteen crude oil samples from the basin. The hydrogeochemical classification of the water sample obtained from Well-1 indicated alkali bicarbonate water type, with bicarbonate as the predominant ion. According to Piper (1944), the dominance of alkali bicarbonate water type could be

attributed to the infiltration of carbon dioxide rich rainwater derived from the atmosphere and input of alkali salts from anthropogenic sources.

Wolaver et al. (2015) used 2-D numerical ground-water flow models to suggest that Putumayo reservoirs were water washed since Andean uplift and that four-way closure is essential to protect Putumayo reservoirs from groundwater influx and to trap oil. Our 3-D volume fracture analysis and structural models for Topoyaco and Miraflor based on new seismic and well data (Figs 2.7 and 2.8), support the conclusions of Wolaver et al. (2015). Lack of four-way dip closure and intense fracturing observed in the Topoyaco 3-D volume from the near-surface to depths of over 2000 msec (3.5 km) indicates that the high levels of fracturing permitted freshwater flushing and oil biodegradation in the Topoyaco monocline (Figure 2.7b). However, in the Miraflor anticline, just south of Topoyaco (Figure 2.8b), structural integrity, four-way trap closure, and lack of major fracturing provided an effective seal for the hydrocarbons and prevented water flushing.

2.4.3.3 SOURCE ROCK CHARACTERIZATION AND DISTRIBUTION

A pseudo-van Kerevelen plot for samples of Villeta Formation from Gigante-1 (Neiva Sub-basin, UMV), Oso-1 and Esnanga-1 (San Gabriel Block, UMV), and Well-4 (Putumayo Basin) (Figure 2.16) shows type II kerogen to mixed Type II and III oil families for both basins. The San Gabriel Block (southern UMV) Oso-1 and Esnanga-1, and the Putumayo Well-4 well cluster particularly close together. Kerevelen plot determinations, however, need to be integrated with TOC, pyrolysis-gas chromatography and burial history diagrams to accurately interpret kerogen type (Dembicki, 2009). In Well-3, Putumayo Basin, source rock terpane and sterane biomarker data suggest a marine calcareous shale

source rock deposited in an anoxicmarine environment (Talukdar, 2012, unpublished report). This author proposed two phases of oil migration: a first phase of migration of high API oil in the reservoir rock, followed by intense biodegradation, then a second phase of oil migration, and finally moderate biodegradation. Based on kerogen and gas chromatography analyses of samples from Putumayo wells, Ramón (1996), Kairuz et al. (2000), and of samples from Putumayo wells, Ramón (1996), Kairuz et al. (2000), and Gonçalves et al. (2002), identified a proximal marine siliciclastic and a marine carbonate oil family. In the Neiva Sub-basin, UMV Sarmiento and Rangel (2004) also identified a calcareous Type II oil family, probably from the Villeta Formation. Thus, the oil families from the UMV, particularly the southernmost wells (San Gabriel), show similar characteristics to Putumayo Basin oil families.

Figure 17a shows the geographic extent of petroleum systems in the Neiva Sub-basin, UMV, and the Putumayo Basin. Depths to Villeta Formation source rocks and source pods are shown based on 3 new 1-D models of pseudo-wells presented in this paper, 1 from Gonçalves et al. (2002), and a new Putumayo Basin depth map based on 2D seismic data. The seismic profiles were acquired with different fold, between 1987 and 2012. It was necessary to reproject coordinates and apply datum shift corrections (between 0 and 400 ms). Well information from 17 exploration wells in the area, close to the 2D seismic lines, was tied to regionally continuous seismic reflectors. A variable suite of logs (gamma ray, resistivity and sonic logs), geological information (formation tops as well as rock descriptions) together with geophysical information (check shot and velocity seismic profiles VSP) were used to make the well seismic-ties.

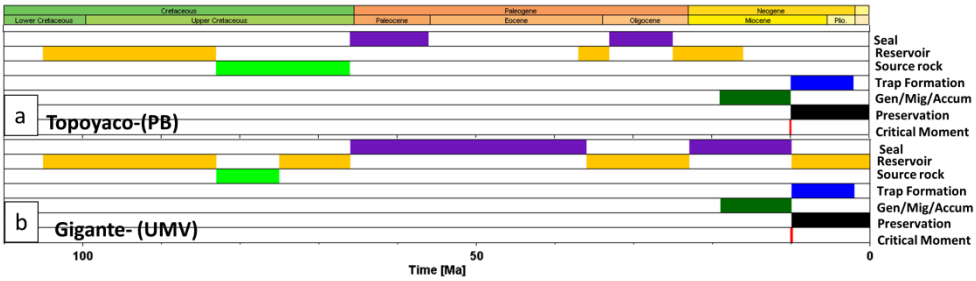

Figure 2.15 Event charts for a) Topoyaco – Putumayo Basin, b) Gigante – Neiva Sub-basin, Upper Magdalena Valley.

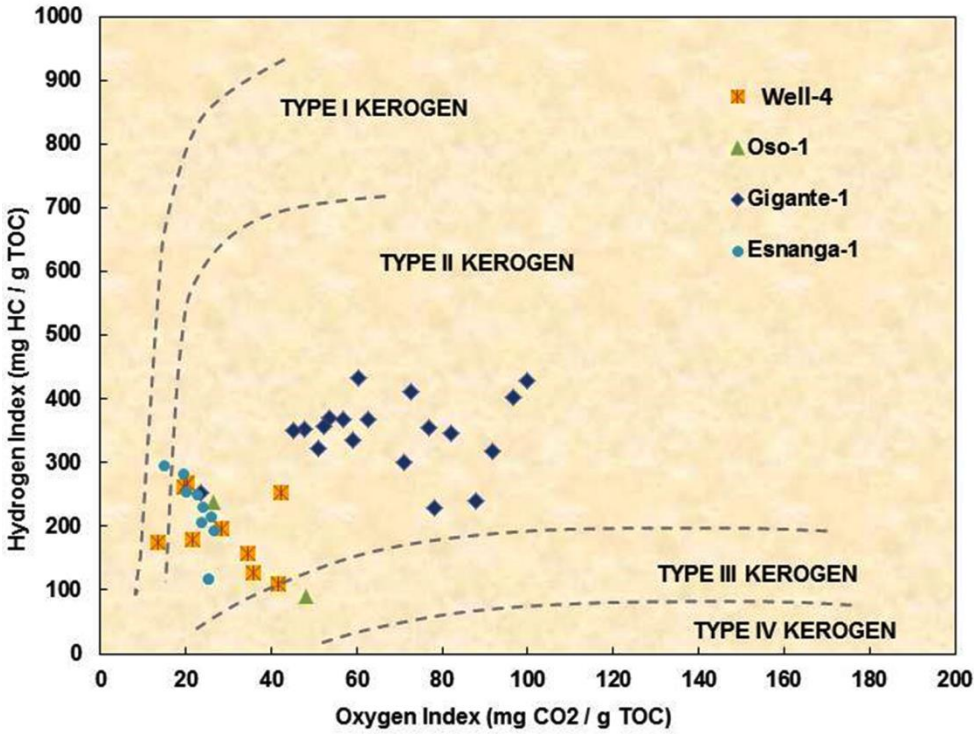

Figure 2.16 Van Krevelen diagram for samples of Villeta Formation from Gigante-1 (Neiva Sub-basin, UMV), Oso-1 and Esnanga-1 (San Gabriel Block, UMV), and Well-4 (Putumayo Basin) shows type II kerogen to mixed Type II and III oil families for both basins. For well locations, see Figure 2.2a and 2.2b.

Figure 2.17a shows our maximum estimated present-day depth to Villeta Formation source rocks in the Putumayo Basin as 4.0 km at a depocenter located approximately 100 km southwest of Well-1. This location could represent marginally mature source rocks at present, although certainly not the late stage high maturity hydrocarbons indicated by the geochemistry in Putumayo wells. Note that Gonçalves et al. (2002) made no present-day depth estimate for his pseudo well within the cordillera.

Figure 2.17b shows our estimates of depth to the Villeta Formation source rocks during the mid-Miocene (8-19 Ma) when the Villeta Formation source rocks reached the peak of oil generation prior to the Andean orogeny. At the Topoyaco pseudo well we estimated the paleo-depth of the Villeta Formation as 3.0 km. 1-D modeling for the San Gabriel pseudo well, located 50 km northwest of Well-1 in the cordillera, gave 4.5 km of burial for the Villeta Formation and peak mature. Our model for Gigante pseudo-well in the Neiva Sub-basin of the UMV predicted that the Villeta Formation reached the oil window at 4 km about 10 Ma. Tmax pyrolysis data indicate intervals of early mature source rock in the lower part of the Villeta Group (Sarmiento and Rangel, 2004), and their oil generation modelling indicates that the lower part of the Villeta Group reached the top of the main oil window at 3505 m during the beginning of the Miocene, and the bottom of the late oil window at 4572 m at the end of Miocene. 1-D modeling for Gonçalves et al. (2002) pseudo-well located in the Central Cordillera 80 km west of the present mountain front showed a maximum burial depth of 5.4 km at 10 Ma. Thus, the likely Villeta kitchen for peak Putumayo basin oil generation was located 50 – 80 km northwest of the present basin within the present cordillera or the UMV (Figure 2.17b).

In summary, during the Early-mid Miocene the main hydrocarbon expulsion event occurred from a kitchen located 50 to 80 km northwest of the present Topoyaco structure because the uplift of the nearby southern Central Cordillera at 8-19 Ma caused subsidence in the foreland basin, burying the source rocks in the oil window, and from which hydrocarbons migrated southeasterly toward Topoyaco (Figure 2.17b). Northward, in the area of the present Garzón Massif, Cretaceous migration pathways to the Putumayo foreland were eroded by an Early/Middle Eocene age uplift of the basement. Southeastward migration would have had to take advantage of permeable Late Eocene Pepino Formation reservoir sandstones. The later Andean age (3-6 Ma) orogeny uplifted the Topoyaco and Garzón basement and reservoir rocks exposing them to erosion. The apparent Andean age high maturity expulsion proposed by Gonçalves et al. (2002) may have also occurred from a kitchen under the cordillera early in the Andean uplift before the migration pathways were exhumed. A present day Putumayo Basin depocenter located 100 km southwest of Well-1 could represent marginally mature source rocks (Figure 2.17a).

2.5 DISCUSSION

2.5.1 SLAB DIP, INVERSION, REACTIVATION AND THICK-SKINNED BASEMENT TECTONICS

Thick-skinned basement deformation associated with convergent plate boundaries has been variously ascribed to inversion of pre-existing extensional basins (e.g., Perez et al., 2016), flat-slab subduction (e.g., Fan and Carrapa, 2014), transpression (e.g., Japas et al., 2016), and thin sedimentary sequences (e.g., DeCelles, 2004).

Prior to the basement Laramide orogeny in the U.S. Rocky Mountains, the region was the site of a Cordilleran foreland basin associated with thin-skinned deformation and flexural loading of a fold-and-thrust belt. Subsequent thick-skinned deformation (Laramide orogeny) partitioned the regional foreland basin and caused more than 4 km of localized exhumation of crystalline basement blocks, accompanied by localized subsidence of intermontane basins. It is generally accepted that the switch of deformation style from thin-skinned to thick-skinned was caused by the change from normal high-angle subduction to low-angle subduction of buoyant Farallon oceanic lithosphere beneath western North America (e.g., Saleeby, 2003; DeCelles, 2004; Liu et al., 2008; Fan and Carrapa, 2014). The thin Paleozoic-Mesozoic sedimentary sequence in Wyoming and its nearby area may have promoted the development of thick-skinned structures (DeCelles, 2004). Thick-skinned deformation in the Sierras Pampeanas in the southern Andes and the Eastern Cordillera of Colombia in the northern Andes were also preceded by thin-skinned deformation (e.g., Egbue et al., 2014; Japas et al., 2016). The thin-skinned to thick-skinned tectonic history of fold-thrust belts in Neuquén Basin, Argentina, had an impact on the evolution of the hydrocarbon systems. Locally, foreland hydrocarbon fields were charged prior to inversion of Mesozoic rift structures and the exhumation by basement uplift was highly destructive for existing hydrocarbon accumulations (Fuentes et al., 2016).

The rapid Andean (~6 Ma) uplift of the Eastern Cordillera of Colombia, north of the Garzón Massif, inverted a deep Mesozoic extensional basin (e.g., Mora et al., 2009; Egbue et al., 2014). However, on the east flank of the Garzón Massif, Eocene Pepino Formation rocks directly overlie basement (Figs. 2.2a, 2.12c). Farther east, small remnants of Cretaceous rocks are found beneath the Eocene unconformity. The Garzón Massif was

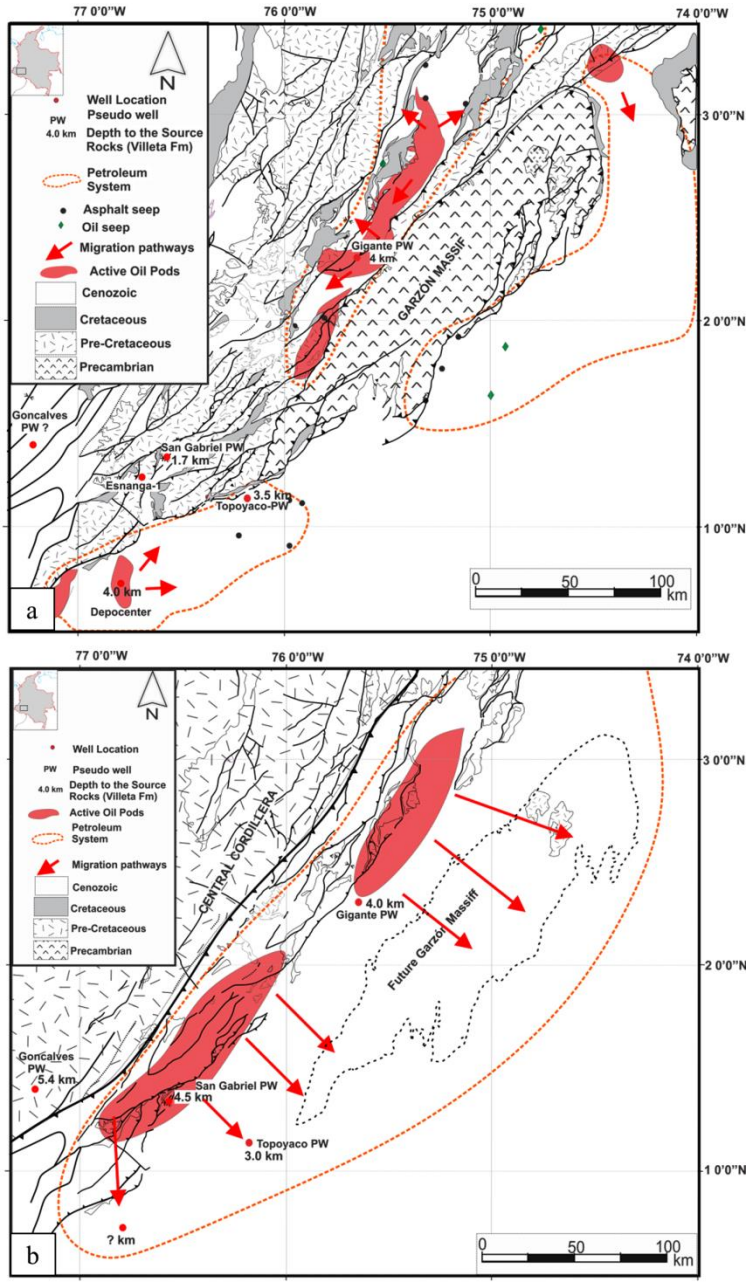

Figure 2.17 Petroleum systems in the Neiva Sub-basin UMV and Putumayo Basin showing estimated depths to source rocks (Villeta Fm) and migration pathways a) Present-Day, maximum estimated depth to Villeta Fm in the Putumayo Basin: 4.0 km. b) 8-19 Ma, Villeta Fm source rocks reached the peak of oil generation prior to the Andean orogeny in the Garzón Massif.

therefore uplifted after deposition of the Villeta Formation and prior to deposition of the Late Eocene Pepino Formation, most of the uplift probably occurring in the Early to Middle Eocene. The Andean-age Garzón thrust fault is therefore, not an inverted normal fault, but, most likely, a reactivated flanking reverse fault from an Early/Middle Eocene Garzón basement uplift. Like the Andean orogeny in the Eastern Cordillera, the Garzón uplift is aligned northeast-southwest with rapid uplift in the last 6 Ma. We speculate that both uplifts were driven in part by the Panama-Choco arc-North Andes collision (e.g., Kellogg and Vega, 1995). The Panama-Choco arc was the southwest boundary of the buoyant Caribbean plate which underthrust the North Andes at a shallow angle. Large remnants of the paleo-Caribbean slab (sometimes referred to as the Bucaramanga slab) still underlie northern Colombia, shutting off Central Cordillera volcanism north of 5° N latitude (e.g., Taboada et al., 2000).

The observed gravity does not require crustal thickening under the Garzón Massif, and the Garzón thrust is predicted to ramp up from a lower crustal detachment at a depth of about 15 km (Figs. 2.12-2.13). These predictions are compatible with seismic and gravity results for the Wind River thrust and recent passive source crustal imaging of the Bighorns Arch Seismic Experiment (BASE) that show no apparent crustal root or offset of the Moho under the uplifts (Smithson et al., 1978; Yeck et al., 2014). The lack of a crustal root under the Garzón Massif despite the 65 km of shortening estimated in this paper, may be explained by lower crustal removal during shortening, or pre-Cenozoic extensional thinning of the crust. We believe that Late Jurassic-Early Cretaceous extensional thinning is the most likely explanation as proposed for the nearby Eastern Cordillera (e.g.,

Sarmiento-Rojas et al., 2006; Mora et al., 2009; Horton et al., 2010a). Detachments are predicted in the lower crust (26 to 36 km) for the two Laramide uplifts.

2.5.2 BIODEGRADATION – LOW TEMPERATURES AND WATER WASHING

Biodegraded oils dominate the world petroleum inventory, with the largest oil reserves being found in super-giant tar sands on the flanks of foreland basins in the Americas (Head et al., 2003). Oxidation of oil during biodegradation leads to a decrease in saturated hydrocarbon content and API gravity, a measure that correlates with economic value, whereas oil density, sulphur content, acidity, viscosity and metal content increase. The probabilities of oil biodegradation increase with decreasing reservoir temperatures below about 80 °C and increase with water flow, which helps mineral dissolution and nutrient supply. Biodegradation is a slow process that takes around 1–2 Myr to compositionally perturb a 100 m oil column (Head et al., 2003).

Reservoirs throughout the Putumayo basin are in hydrologic connection with modern freshwater meteoric recharge. Water washing and biodegradation are favored in the study area by east-dipping structures, a strong topographically driven groundwater flow system, high precipitation, and reservoirs that lack the trap integrity provided by four-way closure with a robust top seal. Faulting also creates pathways for downward water flux and upward oil leakage. Evidence for water washing and biodegradation includes low API gravity oil, a groundwater flow system driven by elevated topography and high precipitation, relatively low-salinity formation water, depressed geothermal gradients, and reservoir temperatures <80°C (<176°F) (Wolaver et al., 2015). Formation water in the thrust belt along the Putumayo margin, and particularly in the study area, is consistently fresh (Cl^- <5‰).

Conversely, in the Llanos Basin to the north (Figure 2.1), Person et al. (2012) reported limited water washing in the proximal western Llanos basin and more extensive freshwater infiltration in the eastern foreland. In the Putumayo Basin, groundwater modeling by Wolaver et al., (2015) suggests reservoirs were water washed by 2–200 million pore volumes since Andean uplift. Finally, average reservoir temperatures are <80°C (<176°F), which further facilitated biodegradation.

2.6 CONCLUSIONS

The Early-mid Miocene main hydrocarbon expulsion event occurred from a petroleum kitchen located 50 to 80 km northwest of the present Putumayo Basin. Uplift of the southern Central Cordillera at 8 - 19 Ma loaded the foreland basin, burying the source rocks in the oil window, and provided migration pathways southeastward toward Topoyaco and the Putumayo Basin. Northward, in the area of the present Garzón Massif, Cretaceous migration pathways were already eroded during a Late Cretaceous/Paleocene uplift of the basement. Southeastward migration would have had to take advantage of Eocene Pepino Formation pathways.

The later Andean age (3-6 Ma) orogeny uplifted the Topoyaco and Garzón basement and reservoir rocks, exposing them to erosion. The apparent Andean age high maturity expulsion may have also occurred from a kitchen under the cordillera early in the Andean uplift before the migration pathways were exhumed. A present day Putumayo Basin depocenter located 100 km southwest of Well-1 could represent marginally mature source rocks.

3-D volume fracture analysis was used for the first time in this paper together with the first seismic and well data published for the Topoyaco and Miraflor structures to test closure models for the Topoyaco foothills. Intense fracturing is observed in the Topoyaco 3-D volume from the near-surface to depths of over 2000 msec (3.5 km). The high level of fracturing permitted freshwater flushing and oil biodegradation in the Topoyaco block. Lack of structural closure and fractures on Topoyaco block hanging-wall structural traps has permitted hydrocarbon escape as proposed by Wolaver et al. (2015). In contrast, Miraflor-1 well, located just southwest of Topoyaco block, tested light gravity oil. The Miraflor anticline is sealed from groundwater flushing and biodegradation by a backthrust on its northwest flank. Apparent structural integrity, 4-way trap closure, and lack of major fracturing provided an effective seal for hydrocarbons in the Miraflor anticline.

The Garzón Massif is an active Laramide style basement uplift. In this paper we use new gravity, magnetic, well and seismic data for the first geophysical interpretation of the Garzón Massif. The Garzón/Algeciras fault has been previously interpreted as a right-lateral strike-slip fault based on remote sensing data. The new seismic, well, and gravity data demonstrates that the Garzón fault is also a low-angle Andean age fault (12 – 17 degrees) thrusting PreCambrian basement 10 to 17 km northwestward over Miocene sediments in a prospective footwall anticline with reservoir potential. The Garzón fault is a reactivated flanking reverse fault from an Early/Middle Eocene basement uplift. The Garzón thrust dips 12 to 17 degrees to the southeast under the Massif, similar to thrust faults in the Laramide Rocky Mountains. Our low-angle Garzón thrust fault model predicts that Cretaceous reservoir rocks in the footwall anticline extend an additional 12 km east of the Iskana-1 well, the only well penetrating the Massif. In the last 3 Ma strain partitioning

may have resulted in diminished basement exhumation and right-lateral strike-slip motion along the Garzón/Algeciras fault system.

The Garzón Massif is asymmetric with a deep sedimentary basin (UMV) on its NW flank. New retrodeformed 2D regional models show distinct episodes of "thin-skinned" and "thick-skinned" deformation in the Garzón Massif, critical structural events for the UMV-Putumayo petroleum system. The models indicate at least 22 km of shortening and 7 km of uplift on NW-verging Garzón and SE-verging basement thrust faults in the last 6 Ma that interrupted the hydrocarbon migration pathways for the Putumayo Basin. This was preceded by approximately 43 km of shortening by thin-skinned imbricate thrusting to the southeast (~9-16 Ma) contemporaneously with uplift of the nearby southern Central Cordillera and the main hydrocarbon expulsion event for the Putumayo Basin and UMV. The Garzón thrust ramped up from a lower crustal detachment at a depth of about 15 km. Detailed structural studies of the northeastern flank of the Garzón uplift are needed to test the regional model proposed in this paper.

CHAPTER III

DETECTION OF FLUVIAL SYSTEMS USING SPECTRAL DECOMPOSITION (CONTINUOUS WAVELET TRANSFORMATION) AND SEISMIC MULTI-ATTRIBUTE ANALYSIS A NEW POTENTIAL STRATIGRAPHIC TRAP IN THE CARBONERA FORMATION, LlANOS FOOTHILLS, COLOMBIA[1].

[1]Saeid, E., J. Kellogg, C. Kendall, I. K. Hafiz, Z. Albesher, Extended Abstract AAPG ACE 2018, Salt Lake City, Utah.

3.0 OVERVIEW

Since the discovery of the giant Cusiana oil field in Colombia, hydrocarbon exploration in the Llanos foothills has focused on structural traps in the hanging walls of thrust faults. There has been little exploration success in the footwall blocks, and most of the activity has been based on subtle structural traps. Cusiana oil field is considered one of the most important structural traps that produce oil from the Eocene Mirador Formation. In the Llanos foreland basin the main reservoir is the Carbonera Formation (C-1, C-7) which is Oligocene to Lower Miocene in age. Using 3D high-resolution seismic data combined with well logs, we propose a set of prediction methods for complex fluvial reservoirs in the area south of the giant Cusiana oil field. The methods 1) use visualization and co-rendering of 3D seismic multi-attribute (including RMS, Coherence, reflection strength) to predict sedimentary sub-facies, 2) use time slices and horizon probes (Sculpture) to predict the configuration of the sandstone using 3D visualization techniques, 3) predict the fluvial structures using spectral decomposition (CWT) with different wavelet (Morlet, Gaussian and, Mexican hat) and (RGB) blending of the frequency cubes, 4) use continuous wavelet transformation for evaluation of hydrocarbon reservoirs, and 5) use multi-attribute analysis on the frequency cubes (frequency domain) to enhance stratigraphic features that are undetectable in time domain seismic data. From the perspective of potential plays CWT spectral decomposition interpretations apply to low frequency shadows that may be direct indicators of gas accumulations associated with overbank and channel fill.

3.1 INTRODUCTION

This paper describe how complex fluvial reservoir prediction methods can be used southwest of the Cusiana giant oil field to interpret seismic data with continuous wavelet transform (CWT) spectral decomposition of high resolution seismic volume and well log data. Seismic interpretation techniques used include 1) 3D seismic attribute technique (RMS, Coherence and reflection strength, etc.) to predict sedimentary sub-facies, 2) time slice and horizon probe (Sculpture) to predict the configuration of the sandstone using the 3D visualization technique, 3) continuous wavelet transformation (CWT) spectral decomposition and (RGB) blending of the frequency cubes to predict the fluvial structures. 4) CWT for evaluation of hydrocarbon reservoirs. Most of the techniques used here were based on 3D seismic interpretation in Brown (2011), Partyka et.al (2011), Lughlin et al., (2002), Sinha et al (2005), and Marfurt (2015).

The technique has been applied in the eastern part of the Llanos foothills 40 km southwest of the giant Cusiana oil field in Colombia and east of the Guaicaramo fault and Medina Basin (Figure 3.1). The Cusiana oil field is considered one of the most important structural traps producing oil from the Eocene Mirador Formation (De'Ath, 1995; Cooper et al., 1995). In the Llanos foreland basin, the main reservoir is the Carbonera Formation (C1, C7) that accumulated from the Oligocene to Lower Miocene (e.g. Cooper et al. 1995, Parra et al., 2009b). Since the large Cusiana discovery, hydrocarbon exploration in the foothills along the Cusiana fault has focused on structural traps in the hanging wall, while most exploration in the footwall targeted subtle structural traps.

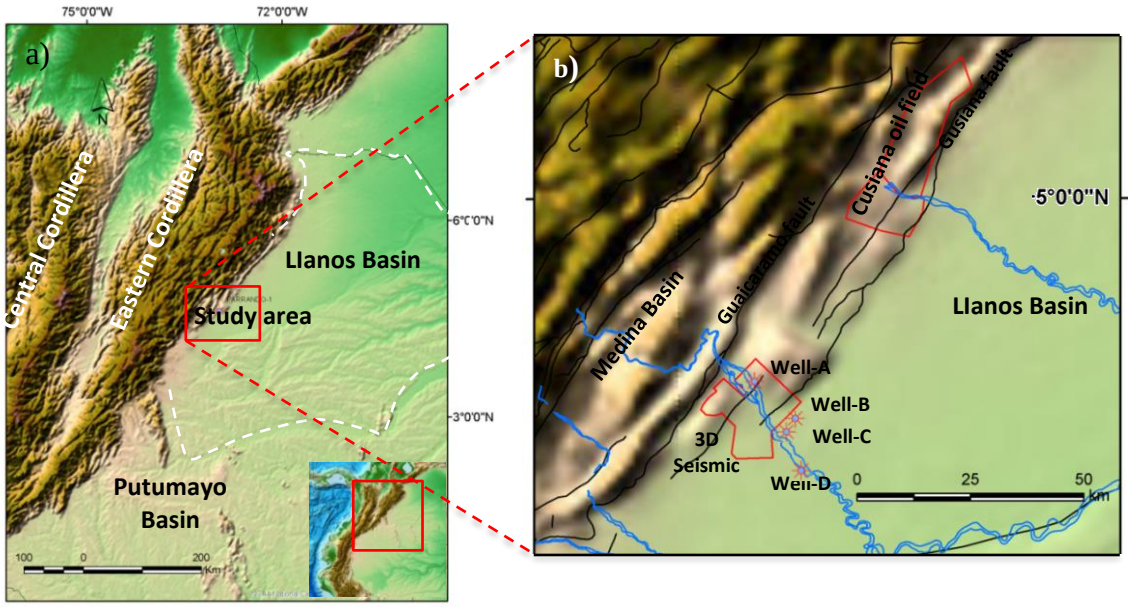

Figure 3.1 a) Location map of study area: Llanos Foothills, Llanos Basin, Eastern Cordillera of Colombia. b) Location of Cusiana oil Fields and the 3D seismic surveys.

3.2 PREVIOUS WORK

The accumulation of the Carbonera Formation of late Eocene to late Miocene age Fig (3.2) was discussed in several regional studies including Bogota-Ruiz, (1988), Cooper et al., (1995), Mora et al., (2006), Bayona et al., (2007), Jaramillo et al., (2009) and Parra et al. (2009b). All the studies have been analysed Carbonera Formation at a basin scale which does not predict the fluvial architecture and distribution of the sand bodies within the Carbonera Formation.

Cooper et al. (1995) described the Carbonera Formation as produced by four major cycles of marine-influenced lower coastal plain deposition that occurred in the Llanos basin and foothills and was bounded by widespread maximum flooding surfaces. Each cycle consists of a mud-dominated highstand systems tract followed by a thin, forced retrogradational systems tract, and ended with a sand-prone transgressive systems tract that culminates with the maximum flooding surface.

Bogota-Ruiz, (1988), Jaramillo et al., (2009) and Parra et al. (2009b) subdivided the Carbonera Formation into eight informal units (C8 to C1) with odd numbers assigned to sandstones and even numbers assigned to mudstones. Bayonaet et al., (2008), focused on Member C3, C2 and C1 of the Carbonera Formation in Saltarín-1 well drilled through the Miocene succession of the eastern Llanos basin. He argued that tectonic subsidence and climate were the controlling factors of the basin filling.

Based on lithology and sedimentary structures, Parra et al. (2009a) subdivided the lower Carbonera Formation C8-C6 into 15 lithofacies and four facies associations in the Medina Basin just west of the study area. Parra et al. (2010) recognized the same four facies associations for the Upper Carbonera Formation (C5-C1) that represent tidally influenced deltaic, lacustrine, alluvial plain and braided fluvial sedimentary settings. They considered the Lower Carbonera Formation C8-C6 as a syntectonic wedge, while the upper Carbonera Formation was syntectonic with growth-strata relationships that were rocks equivalent to C5-C2 west of the Medina Basin along Lengupa fault. This coincided with the progressive isolation of the Llanos Basin in the east from the Magdalena Basin in the west (Mora et al., 2013; Reyes-Harker et. al 2015). They proposed a new chronostratigraphic framework for

the C8-C6 members of Carbonera Formation based on palynological zonation (T-05 to Ca07) which are of early Eocene – early Miocene age.

Torrado et al. (2014) integrated 700 Km2 of 3D seismic with well data in the central Llanos Basin to characterize the Carbonera Formation (C1, C3, C5 and C7) from seismic attributes. Their interpretation of fluvial sands focused on identifying geoforms and channel filling material, characterizing them as prospective and non-prospective hydrocarbon plays. Also, they recommended advanced techniques that included spectral decomposition, RGB blending of frequency as well as seismic inversion to detect thinner channels within the wider channel belt complex.

3.3 RESEARCH METHODS

3.3.1 SYNTHETIC SEISMOGRAM

A synthetic seismogram was created from well-A logs in the 3D seismic volume (see Figure 3.1 for location). This synthetic seismic trace was tied to the seismic cross section using well check-shot survey data, and adjusting the T-D function through stretching and squeezing the wavelet accordingly, to match the data Fig (3.3a). The Carbonera Formation was defined as extending between 2350 to 3025 ms and including the Oligocene to Miocene fluvial sand reservoirs (Fig 3.3b).

3.4 DETECTION OF FLUVIAL SYSTEM USING SPECTRAL ANALYSIS, RGB BLENDING AND HORIZON PROBE (SCULPTURE) TECHNIQUES

Spectral decomposition has been used to determine layer thicknesses (Partyka, 1999, 2011), stratigraphic geometries (Marfurt and Kirlin, 2001), and direct hydrocarbon

detection (e.g., Goloshubin et al., 2002; Castagna et al., 2003; Sinha et al., 2005; Welsh et al., 2008; Yu et al., 2011). Additionally, spectral decomposition breaks the seismic signal into narrow frequency sub-bands or horizons (Partyka, 2011). This is achieved by transforming the seismic data from the time domain into frequency domain (Chopra and Marfurt, 2015). We used the recommended workflow by Partyka (2011) for the seismic volume, extracting more than 75 different bands in a frequency range 5-75 Hz. However, we modified this approach. Our spectral decomposition workflow started with data conditioning (Spectral enhancement) and then investigated the dominate frequency for the horizon of interest (Fig 4) constructing a tuning map of the Carbonera Formation to determine the stratigraphic features that could not be resolved in the time domain seismic cube.

The frequency spectra for the Carbonera Formation include the following dominant frequencies: 18-21, 25- 33, and 38-41 Hz (Fig 3.4). The seismic volume within the Carbonera Formation was thus separated into iso-frequency volumes based on these frequencies (Fig 3.5). These volumes were manipulated and superimposed generating bodies that matched geological features using the RGB/CMY Mixer application. Spectral decompositions are short time Fourier transforms (STFT) and continuous wavelet transforms (CWT) and the matching Pursuit algorithm. Each of these has their advantages and disadvantages, and their selection depends on the objectives of the workflow. For instance, the STFT transformation depends on the time gate, a drawback for the transformation method (Sinha et. al., 2005). On the other hand, the CWT method is unlike the conventional SFFT method, which limits the time-frequency resolution by a predefined

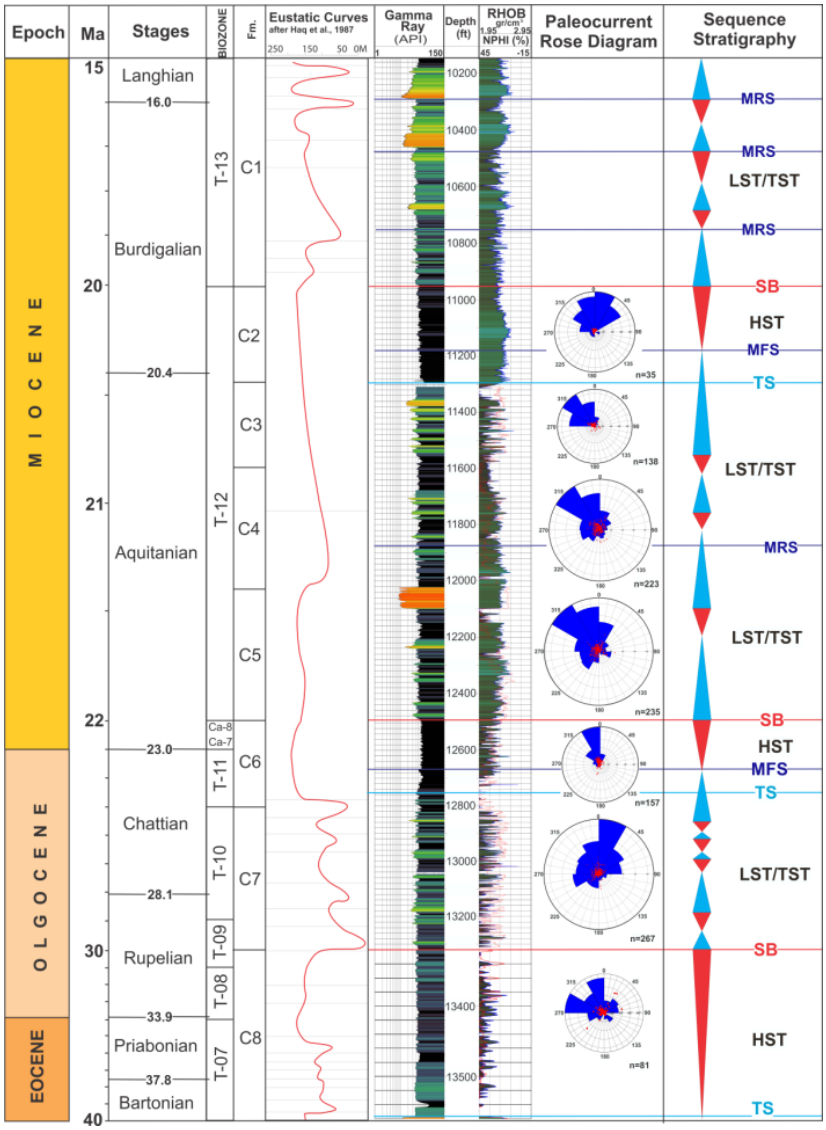

Figure 3.2 Stratigraphic column for the Carbonera Fm. showing biozones after Parra et al. (2009 & 2010), Eustatic curves after Haq et al. (1987), Gamma ray, density and neutron logs, palaeocurrent rose diagrams and sequence stratigraphy in Well (E). See Fig 3.1 for location.

window width (Sinha et. al., 2005). Narrow windows give good time resolution but poor frequency resolution, whereas wide windows give good frequency but poor time resolution. However, to a certain extent, CWT solves the dilemma of resolution if one can choose the mother wavelet which works best for the seismic data (Morlet, Gaussian, and Mexican Hat or Ricker). This choice depends on the 3D seismic interpretation package used.

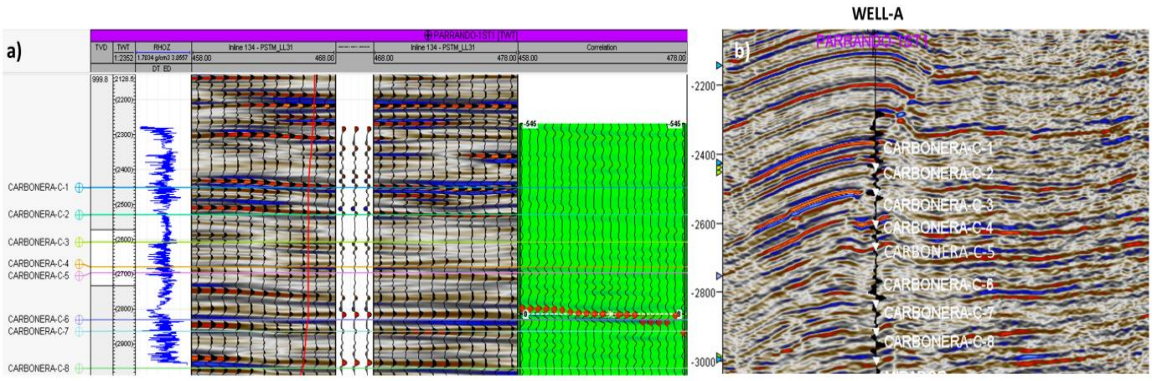

Figure 3.3 a) Synthetic seismogram along with sonic and density logs. b) Seismogram displayed on the seismic section showing the horizon of interest.

Some seismic interpretation workstations offer general spectral decomposition (GSD) as a hybrid of the STFT and CWT through a design wavelet using three parameters: frequency, number of cycles, and phase. The designed wavelet is eventually used to decompose (Correlation) or filter (Convolution) the input seismic data (Schlumberger, 2017). In this case after extracted the dominated frequencies you have to flatting each frequency volumes then flatting the horizon of the interses at the flatting frequency volumes to blend these volumes by RGB mixer in order to detect the channels. Other seismic interpretation workstations offer separate spectral decomposition as STFT and CWT through a design of the window width and design the wavelet (Morlet, Gaussian, and Mexican) respectively.

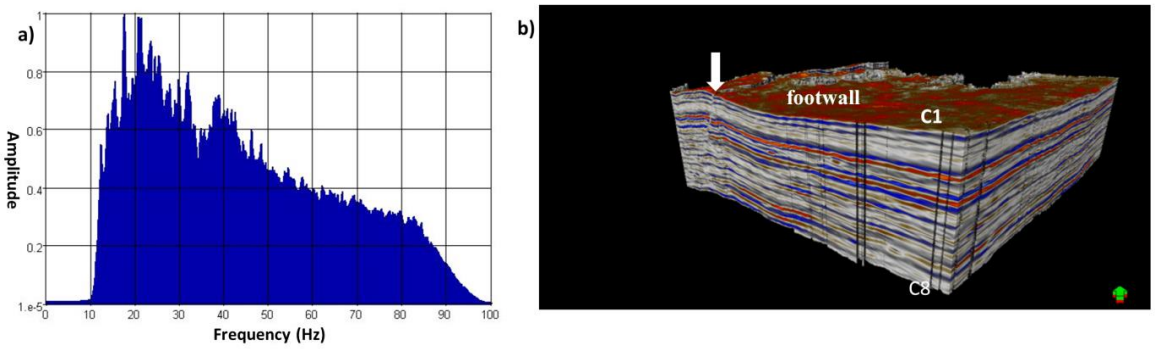

Figure 3.4 a) Frequency spectrum for the zone of interest. b) 3-D horizon probe of Carbonera Fm (C-1 to C-8) showing a reverse fault (white arrow) and the footwall study area.

We used the CWT algorithms of dGB OpendTect to achieve spectral decomposition and reveal fluvial channels throughout the Carbonera Formation. CWT and the calculated isofrequency seismic sections were based on all three wavelets; Morlet, Gaussian, and Mexican. When examining the frequencies of 18, 25, and 38 Hz using this refined approach the images seen in Figs. 3.6 and 3.7 were produced. Since we found CWT was better than STFT for spectral decomposition of the seismic volume to detect the stratigraphic features in the Carbonera Formation, the remaining analyses were based on the CWT approach.

3.5 USING CONTINUOUS WAVELET TRANSFORMATION (CWT) TO DETECT FLUVIAL SYSTEM CHANNELS

The continuous wavelet transform (CWT) is an alternative method for frequency distribution analysis and is achieved by increasing or decreasing time support (transit time defining seismic volume) in the CWT, causing the frequency support (frequency content of seismic volume) of the wavelets to shift towards the high frequencies or low frequencies

respectively. Thus, when the frequency resolution increases, the time resolution decreases and vice versa (Mallat, 2009). The CWT is focused on the spectral attributes of horizons rather than the entire stratigraphic interval as in the SFFT method (Sinha et al., 2005). The CWT method depends on the choice of the mother wavelets that include the Morlet, Gaussian, and Mexican hat.

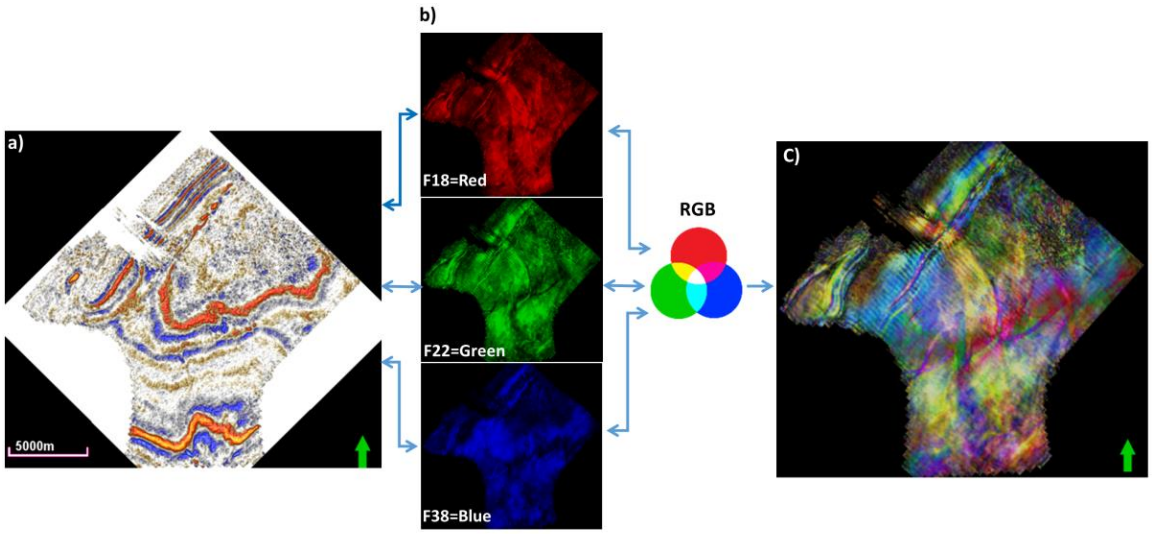

Figure 3.5 a) Amplitude time slice at 2424 ms. b) Frequency slice showing amplitude in narrow frequency bands around 38 Hz as blue, 22 Hz as green and 18 Hz as red. c) RGB blends of iso-frequencies F18, F22, and F38.

CWT were calculated as single frequency seismic sections based on the Morlet, Gaussian, and Mexican hat wavelets with frequencies of 18, 25, and 38 Hz. The results are shown in Figure 3.6 for a temporal depth of 2727 ms within the Carbonera Formation. At frequencies of 18 and 21 Hz (Figure 3.6), the Morlet wavelet provides better resolution when compared to Gaussian or Mexican hat. At 25 Hz a Gaussian wavelet provides better resolution than the frequency slice resolved by the Morlet wavelet. At 38 Hz, both Morlet

and Gaussian wavelets provide relatively good resolution, although the Morlet wavelet captures major fluvial channels and the thickness of sediment fill in the channel at high frequencies. The low frequency (18-21 Hz) tunes the thicker part of a fluvial reservoir, whereas the high frequency 38 Hz tunes the thinner sediment fill of the main channel as described by Laughlin et al. (2002).

At frequencies of 18 and 21 Hz (Figure 3.7), the Morlet wavelet provides poorer vertical resolution than the Gaussian and Mexican hat wavelets. The Mexican hat provides very good vertical resolution at low frequencies. By using different mother wavelets in the wavelet transform process, different results in terms of vertical and horizontal resolution are obtained. Since the Morlet wavelet is considered to be the best mother wavelet horizontally, it was selected for further use in seismic attribute analysis and for comparing the attributes based on time domain to the attributes in the time-frequency domain based on the CWT transform.

Li and Lu (2014) combined spectral decomposition and coherence attributes to provide a qualitative measure of geologic discontinuities such as channels, faults, and caves. Li et al. (2015) used the same workflow as proposed by Li and Lu (2014) and combined RGB images of 20, 35, and 50 Hz spectral decomposition with corresponding coherence images to map the various stages of incised valley fill of the Red Fork Formation in the Anadarko basin, Oklahoma. In this paper we combined spectral decomposition strata slices of C3, C5, and C7 with coherence (Figure 3.8) as proposed by Li and Lu (2014) to identify the various stages of the fluvial system with complex superimposed channel geometry.

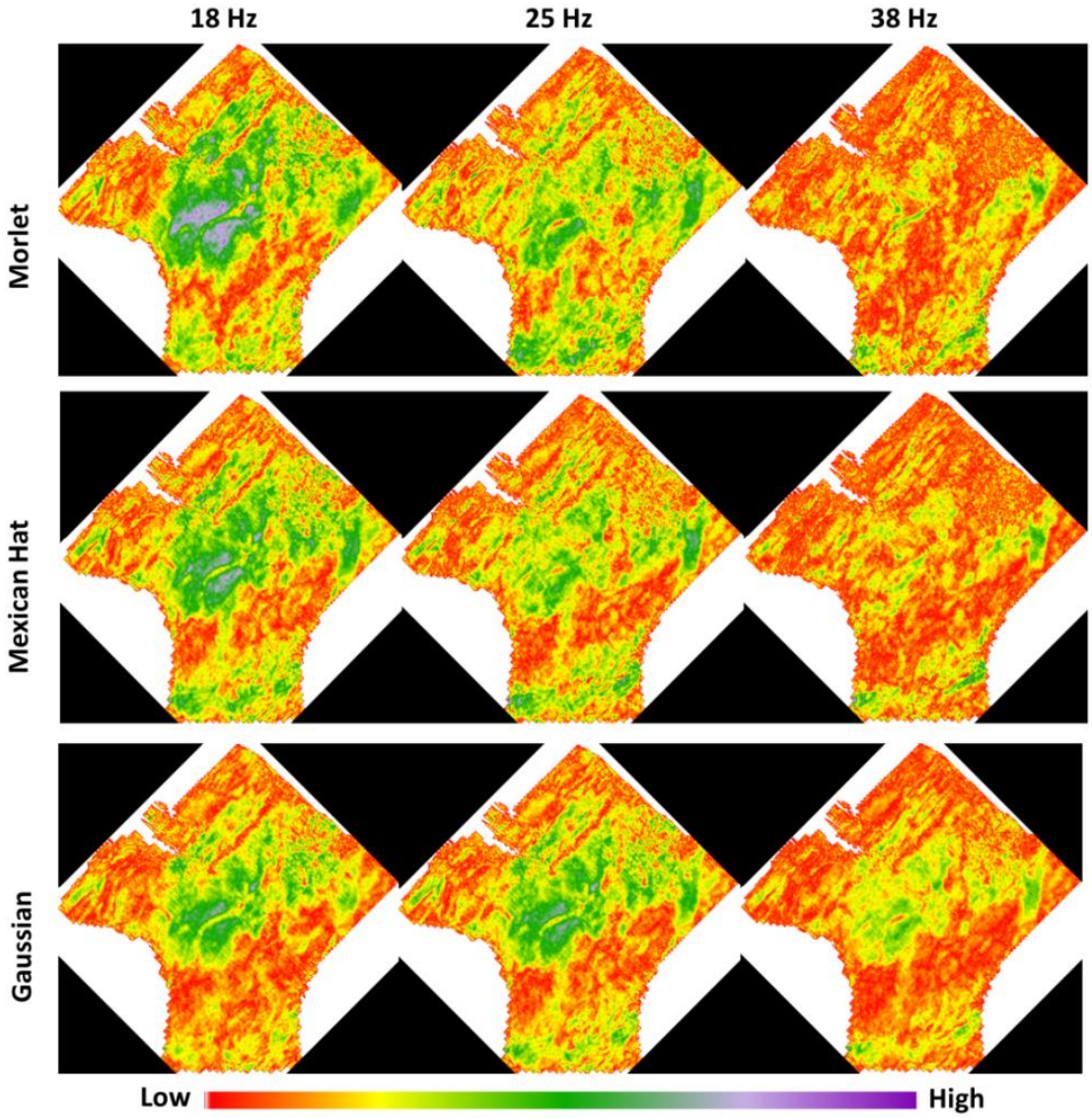

Figure 3.6 Time slices (2727ms) from 18 Hz (left), 25 Hz (middle), and 38 Hz (right) volumes showing CWT spectral decomposition carried out using Morlet (upper), Gaussian (middle), and Mexican (lower) wavelets.

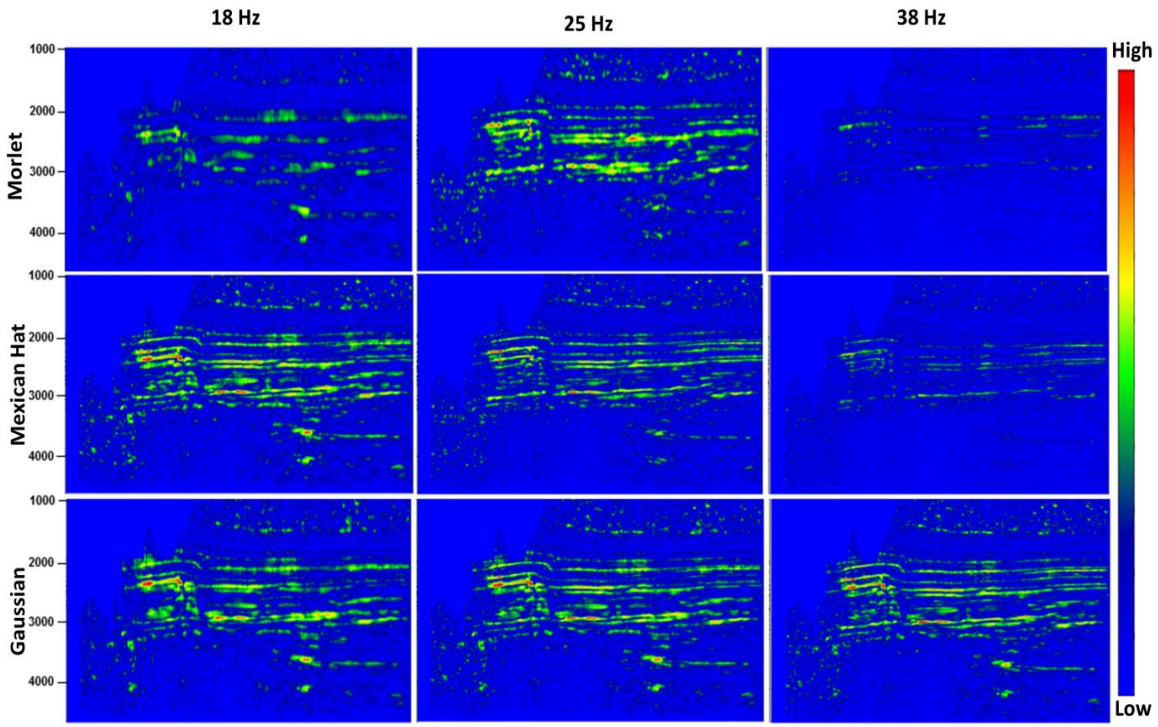

Figure 3.7 Seismic sections (inline 243) from 18 Hz (left), 25 Hz (middle), and 38 Hz (right) volumes showing CWT spectral decomposition carried out using Morlet (upper), Mexican Hat (middle), and Gaussian (lower) wavelets.

The horizon probe is another useful technique for visualization of stratigraphic features in the time domain. The horizon probe is an irregular probe that follows one or two interpreted horizon surfaces, also referred to as "sculpting" in the industry (Schlumberger, 2017). The use of the horizon probe alone may not be sufficient to detect fluvial systems, but when used with opacity, another powerful visualization technique (Roberts 2011); it allows the interpreter to examine a volume of seismic data using varying transparency revealing the morphology of high-amplitude channel features. Manipulating the transparency of a small cube of seismic data often reveals the morphology of high-amplitude channel features. Figure 3.8 shows a fluvial system with a complex superimposed channel geometry in C3, C5 and C7 including superimposed channels, point bars and crevasse splays.

Furthermore, we found that the horizon probe was useful for mapping of fluvial systems and identifying their various stages. The spectral decomposition of C7 strata shows a high-sinuosity channels oriented NE - SW with widths ranging from 400 ft to 750 ft. The two main channels developed parallel to the present Llanos foothills (Figs. 3.1 and 3.8). The paleoflow of C7, inferred from CWT spectral decomposition, is consistent with the paleocurrent pattern and compliments the dipmeter log of Figure 3.2. The consistent results of these two independent methods support the power of these methods for exploration and production.

The spectral decomposition of C-5 strata shows a low-sinuosity wide channel oriented NW-SE with widths ranging from 1400 to 2500 ft. (Figure 8). The channel cuts through the present foothills and the older fluvial system in C7. The channel lacks sharp edges, but is very clear in almost all the attributes, including Envelop and RMS. The paleoflow of C7

inferred from CWT spectral decomposition is consistent with the paleocurrent patterns in the dipmeter log Fig (3.2), again showing how powerful these tools are together. The C3 strata are characterized by high-sinuosity channels incised through the large channel in C5. The channels flow from NW to SE cutting through the edges of the earlier channel with widths ranging from 300 to 650 ft. (Figure 3.8). The paleoflow of C5 and C3 are inferred from CWT spectral decomposition and are again consistent with dipmeter log paleocurrent patterns Figure 3.2.

3.6 3D SEISMIC ATTRIBUTES IN FREQUENCY DOMAIN AND USING CONTINUOUS WAVELET TRANSFORMATION CWT FOR THE EVALUATION OF HYDROCARBON RESERVOIRS.

Many seismic attributes are very useful for detection of fluvial facies. For example, coherence (or Variance) may help detect sands associated with fluvial systems. Root Mean square (RMS) amplitude helps detect channels with density variations from surrounding units. Combinations of multiple attributes in the same image can provide increased geologic insight (Marfurt, 2015). Envelop attribute or reflection strength as described by Taner et al. (1979) is the amplitude derived from a complex trace by mean Hilbert transforms, that is used to transform a seismic trace to a complex trace. A complex seismic trace can be generated either by a Hilbert transform or a continuous wavelet transform. The Hilbert transform works in the time domain, whereas the continuous wavelet transform works in time-frequency domain to generate a complex trace. High-reflection strength is often associated with major lithologic changes between adjacent rock layers and with gas accumulations (Taner and Sheriff, 1977).

The application of reflection strength in CWT Morlet 18-21 Hz enhances the stratigraphic information (Figure 3.9) where sand bodies represent high reflection strength enclosed by shales with low strength. On the other hand, these significant details of stratigraphic features such as river channel levees and point bars are undetectable in time domain seismic data even with close scrutiny.

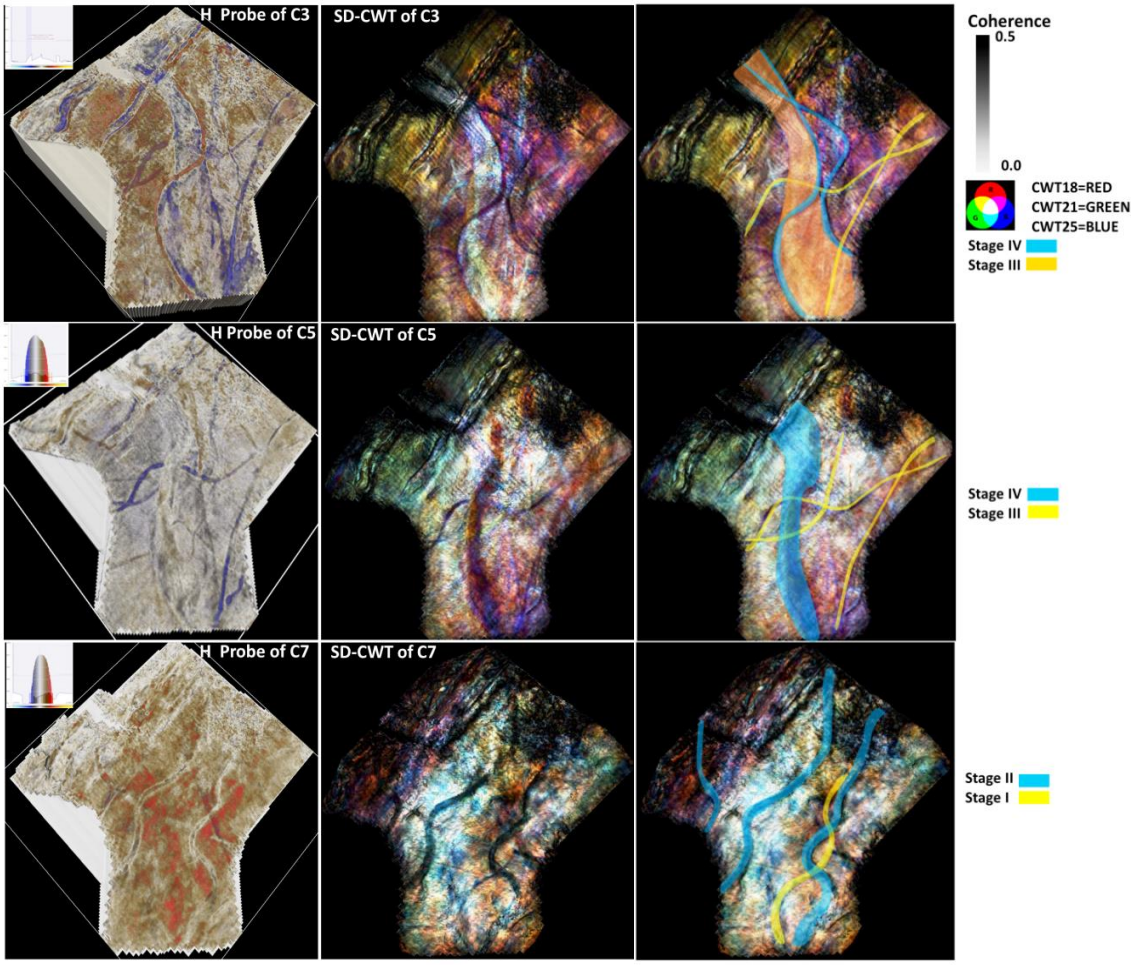

Figure 3.8 Horizon probe used manipulated transparency (left) versus CWT Spectral decomposition (middle) strata slices for C3 (upper), C5 (middle), and C7 (lower). The CWT spectral decomposition used a Morlet wavelet in narrow frequency bands around 38 Hz as blue, 22 Hz as green, and 18 Hz as red co-rendered with coherence attribute, with our fluvial interpretation stages (right).

One of the objectives of this study is to use the continuous wavelet spectral decomposition method for direct hydrocarbon detection through the frequency anomalies in a geologically and seismically challenging area such as the Llanos Foothills. Most of the tradition methods to detect hydrocarbons are based on the amplitudes of seismic reflections (bright spots) which are subject to variations of many parameters such as thickness, lithology, porosity, and fluid content (Avseth et al., 2005). The high resolution of the CWT method provides a good reservoir image (Figure 3.9) and detects low frequency shadows under the reservoir which have been linked to HC content in multiple cases study (e.g., Castagna et al., 2003; Goloshubin et al., 2006; Welsh et al., 2008; Tai et al., 2010).

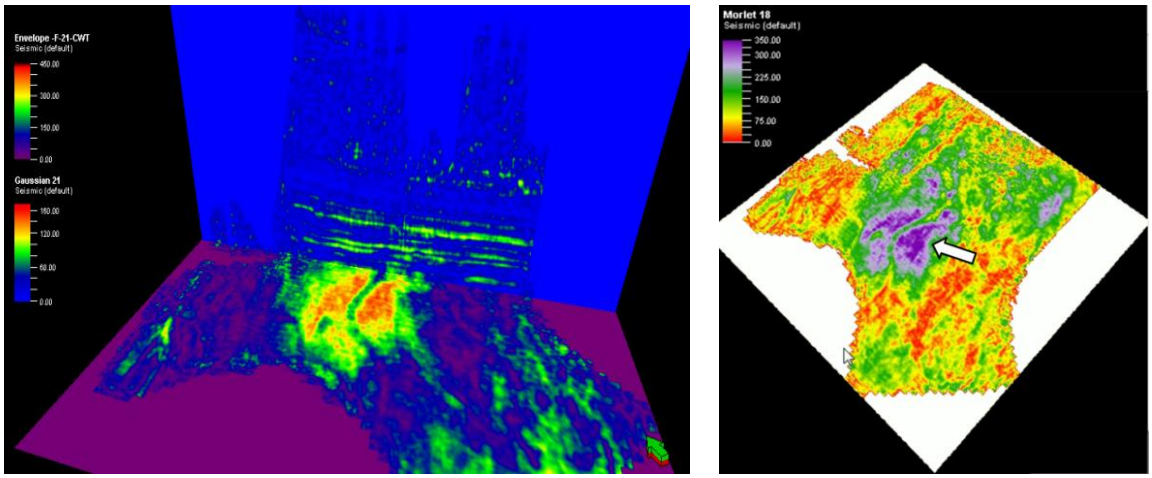

Figure 3.9 Application of attributes to CWT volumes and hydrocarbon indication, a) reflection strength (envelop) time slice (2727) from 21 Hz volume showing CWT Morlet with CWT-Morlet (inline-243) vertical cross section. b) Low frequency shadow within the C7 seismic frequency volume below a potential reservoir. Note the meandering channel fill (green) and the overbank sediments beside it (blue, white arrow).

3.7 CONCLUSION AND FUTURE APPLICATIONS

We conclude that CWT spectral decomposition techniques provide powerful tools to help resolve fluvial sediment distribution in the subsurface for exploration and production models. In particular, they can be applied to other subsurface data sets to study the fluvial systems.

In this study CWT spectral decomposition was used to detect and map fluvial systems in the frequency domain. CWT mapping of the fluvial system in Carbonera Formation captured the complicated paleocurrent orientations of the sandier horizons of C7, C5 and C3. The results of CWT spectral decomposition were found to depend upon the choice of wavelets, namely the Morlet, Gaussian and Mexican hat. Our results show that the CWT Morlet wavelet has good horizontal resolution, especially at low frequencies compared with the other wavelets. The Gaussian wavelet had relatively good resolution at low and medium frequencies but not as good as with a Morlet wavelet. On the other hand, the Morlet wavelet has poor vertical resolution compared with Gaussian and Mexican hat. The Mexican hat provides very good vertical resolution, especially at low frequencies, and the Gaussian wavelet has relatively good vertical resolution at medium to high frequencies.

The horizon probe is a powerful visualization technique useful for mapping of fluvial systems and identifying their various stages in time domain if used with opacity. Furthermore, by mapping the fluvial system using CWT spectral decomposition we were able to tie the variations in fluvial systems to the regional tectonics of the Eastern Cordillera. The C7 horizon fluvial facies were mainly high sinuosity channels consistent with the well log paleo-currents flowing with the regional drainage of the Oligocene Proto-

Orinoco river system as described by Villamil (1999). Within the thick fluvial system of the C5-C3 horizons the drainage switched from low sinuosity to high sinuosity channels with the channel directions consistent with the paleo-currents obtained from well logs. A key observation related to the C5 horizon is a change in spectral strata suggesting an evolution from braided fluvial accumulation to the overlying C3 horizon that captured a meandering fluvial system.

These changes in geometric character document a change in slope gradient, sediment sources and tectonic activity of the present day Eastern Cordillera. The application of continuous wavelet transforms provides a better understanding of how regional scale structures and tectonic movement affected the local sedimentary history and helps explain the processes and mechanisms involved in producing the regional stratigraphic section. It is the contention of this paper that the use of these techniques can help explorationists to better resolve, identify and interpret the style of channel fill from braided to meandering systems, point bar fill, stranded ox-bows and abandoned channel fill, crevasse splays and other over bank phenomena.

In conclusion, the application of attribute analysis in frequency volumes enhances the stratigraphic features that are undetectable in time domain seismic volumes. It is hoped that this study will be expanded to a more detailed multi-attribute analysis in frequency domain for reservoir characterization and sand connectivity of the Carbonera Formation and other formations in the region and beyond. By using CWT spectral decomposition new potential reservoirs plays were recognized southwest Cusiana giant oil field in the footwall of the Cusiana fault and this could open a new exploration era along the eastern flank of the Eastern Cordillera.

CHAPTER IV

SEQUENCE STRATIGRAPHIC FRAMEWORK, SPECTRAL DECOMPOSITION AND WELL LOG CHARACTER DETERMINE DEPOSITIONAL MODELS FOR THE CARBONERA FORMATION, LlANOS FOOTHILLS, COLOMBIA[1]

[1]Saied, E., C. Kendall, C., Kellogg, J, De Keyser, T., I. K. Hafiz, Z. Albesher Submitted to AAPG bulletin, January 24, 2018.

4.0 OVERVIEW

An exploration workflow is proposed which identifies potential reservoirs in the complex fluvial sediments of the Oligocene to Lower Miocene aged Carbonera Formation (C-7 and C-5) area south of the giant Eocene Mirador Formation Cusiana oil field of the Llanos Foothills of Columbia. The workflow involves the use of well log character integrated with spectral decomposition of 3D seismic data. Gamma ray well logs are normalized to capture the sedimentological character and improve the interpretation of cyclicity and depositional settings of well log displays and cross-sections while spectral decomposition detects the subtle stratigraphic features undetectable in the time domain seismic data. Continuous wavelet transforms (CWT) applied to the spectral decomposition analysis techniques identify and map the complex fluvial potential reservoirs along the footwall blocks of thrust faults. The observed changes in fluvial systems geometry in Carbonera Formation revolutionises depositional models that predict changes in slope gradient, sediments source, and tectonics activity of the present day Eastern Cordillera.

By integrated Well-log character and CWT spectral decomposition, we were able to detect and map the character of fluvial systems of the Carbonaera Formation including complicated paleocurrent orientations of sand prone horizons that are match the dipmeter of palaeoflow patterns. From the perspective of potential plays CWT spectral decomposition interpretations apply to low frequency shadows that may be direct indicators of gas accumulations associated with overbank and channel fill.

4.1 INTRODUCTION

This paper describes how exploration of complex fluvial depositional systems and their potential reservoir character is significantly enhanced by the display and interpretation of borehole logs integrated with spectral decomposition techniques. These techniques have been used in the geological section with hydrocarbon potential in the eastern part of the Llanos foothills, 40 km southwest of the giant Cusiana oil field in Colombia, and east of the Guaicaramo fault and Medina Basin (Figure 4.1).

The significant structural trap confining the Cusiana oil field produces oil from the Eocene Mirador Formation (De'Ath, 1995; Cooper et al., 1995). To the south west in the Llanos foreland basin, the main reservoir facies are in the Carbonera Formation (C1, C7) which accumulated from the Oligocene to Lower Miocene (e.g. Cooper et al. 1995, Parra et al., 2009b). The Cusiana Field discovery is trapped in tidal channel sandstones overlapping fluvial channel sandstones of the Mirador Formation (Linares, et al., 2009). This spurred hydrocarbon exploration in the foothills parallel to the Cusiana fault focusing on fluvial depositional systems within the larger structural traps of the hanging-wall rather than exploration targeted on the fluvial sediments of the subtle structural traps of the footwall.

The workflow (Figure 4.2) described below can be replicated in other areas establishing powerful interpretive techniques for the generation of exploration and production depositional models.

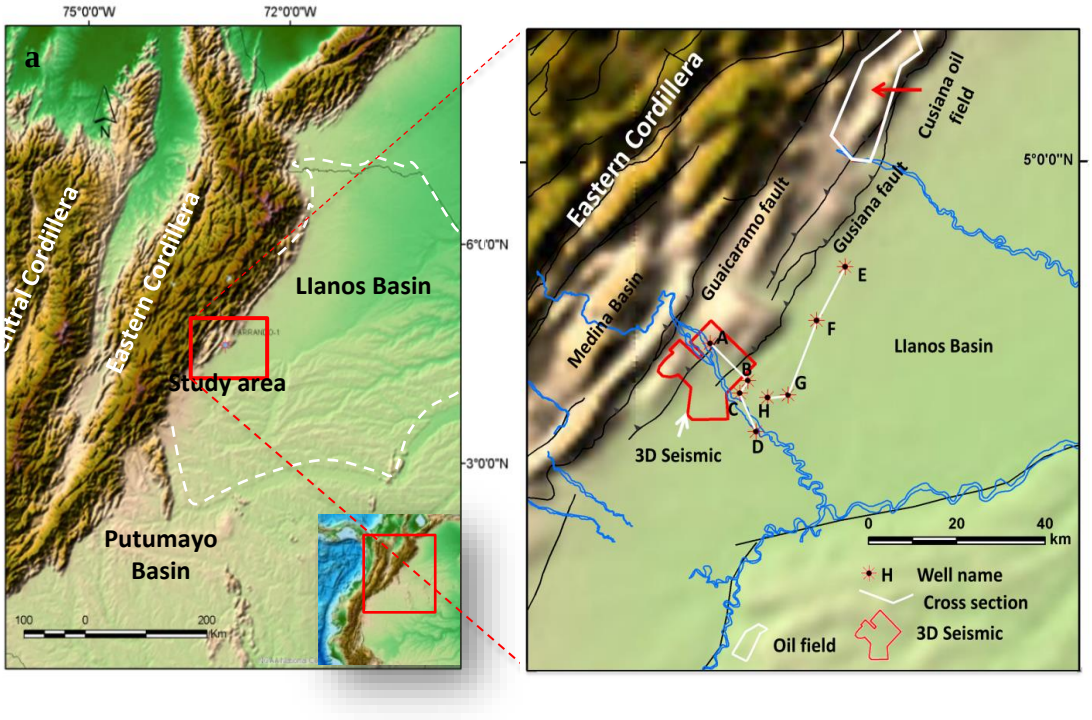

Figure 4.1 a) Location map of study area: Llanos Foothill, Llanos Basin, Eastern Cordillera in Colombia. b) Location of Cusiana oil Fields and the 3D seismic surveys.

1. The gamma ray logs displayed at a logarithmic scale are individually normalized to remove systematic errors from well-to-well comparisons. The resulting display of log character captures hierarchical depositional cycles and their subdividing framework of SBs (sequence boundaries). This coupled with uniformly scaled neutron and density well logs help interpret the penetrated lithologies. This depositional stratigraphic interpretation uses the character of well logs (gamma ray, density, neutron, and resistivity) and the normalized GR as a proxy of the grain size (see Rider, 1999; Miall, 1996; Catuneanu, 2002; Kendall, 2008; Maill, 2014).
2. An interpretation of the seismic data follows using continuous wavelet transform (CWT) spectral decomposition of high resolution seismic volumes establishing the geometries of the sediment filling the fluvial channels. This interpretative technique includes:
    a. 3D seismic attribute technique combining RMS, Coherence and reflection strength to predict sedimentary sub-facies,
    b. Time slice and horizon probe (Sculpture) to predict the configuration of the sandstone using the 3D visualization technique
    c. Continuous wavelet transformation (CWT) spectral decomposition and (RGB) blending of the frequency cubes to predict the fluvial structures.
    d. Continuous wavelet transformation to evaluate potential hydrocarbon reservoirs using low frequency shadows.

Most of the 3D seismic interpretations techniques listed are based on the work of Brown (2011), Partyka et.al (2011), Lughlin et al., (2002), Sinha et al (2005), and Marfurt (2015).

The main objective of this paper was to demonstrate the utility of CWT spectral decomposition to detect and explore the sequence stratigraphy of complex fluvial depositional systems. The result is a description of how the reservoir character of the complex fluvial can be predicted to the southwest of the Cusiana giant oil field.

4.2 GEOLOGICAL HISTORY

4.2.1 PETROLEUM SYSTEMS AND STRATIGRAPHY

The Eastern Cordillera represents a Late Jurassic - Early Cretaceous extensional basin system inverted during the Cenozoic Andean orogeny (Colletta et al., 1990; Cooper et al., 1995 Mora et al., 2006; Sarmiento-Rojas et al., 2006).

By the Early Cretaceous, considerable accommodation space was created in the Eastern Cordillera. Late Jurassic to Early Cretaceous as rifting generated basaltic intrusions, thinning of the lithosphere, and shallowing of the mantle (Ojeda, 1996). Throughout the Cretaceous period this rifting phase was followed by thermal subsidence (Pindell and Tabbutt, 1995; Ojeda, 1996).

From the Early Cretaceous to Late Cretaceous period, accumulation of sediments in the Eastern Cordillera area was almost entirely in a marine setting. The synrift Une Formation (Figure 4.3) accumulated from the Early Cretaceous until the Cenomanian and is composed of sandstones deposited in shallow marine conditions (Linares, et al., 2009).

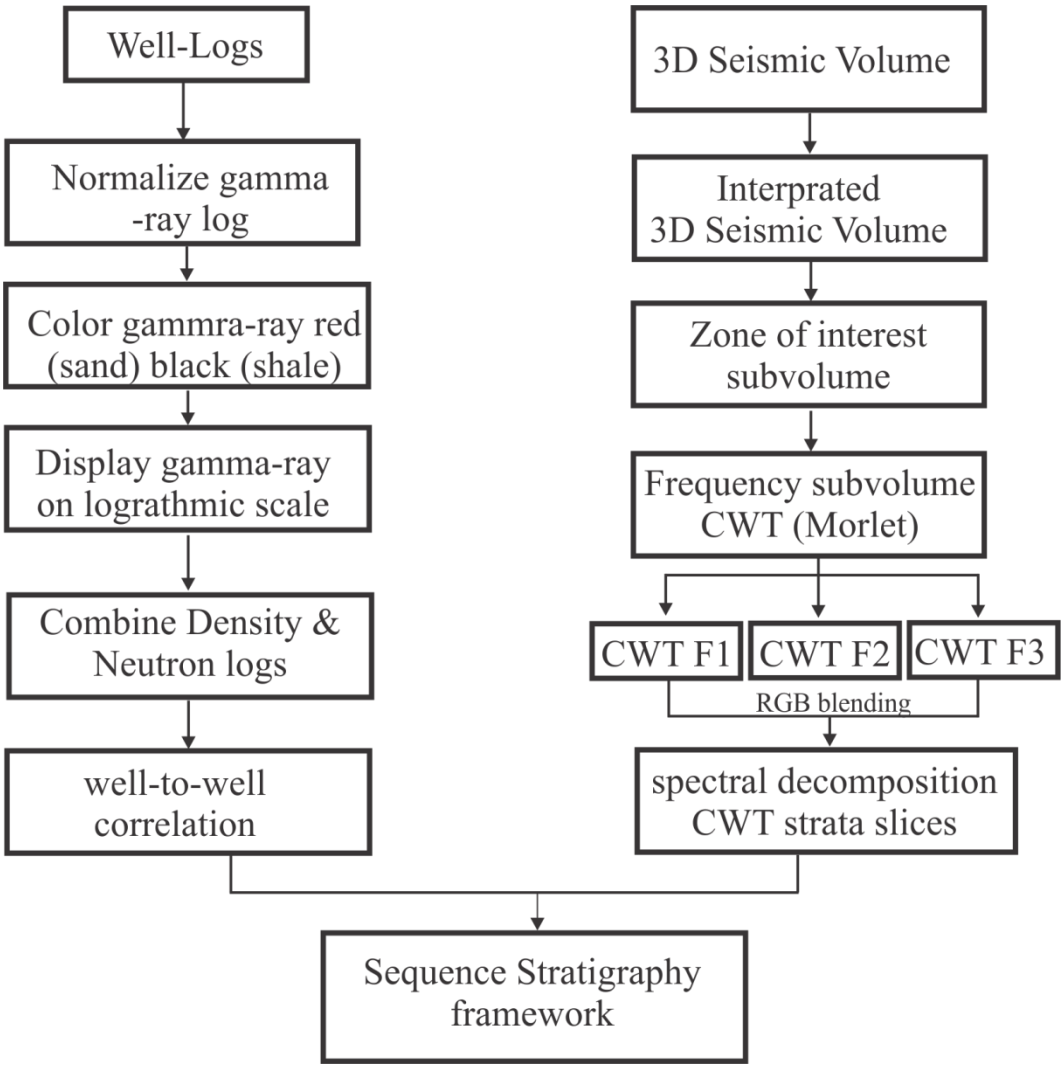

Figure 4.2 The Proposed workflow of sequence stratigraphic framework of Carbonera Formation, Llanos Foothills.

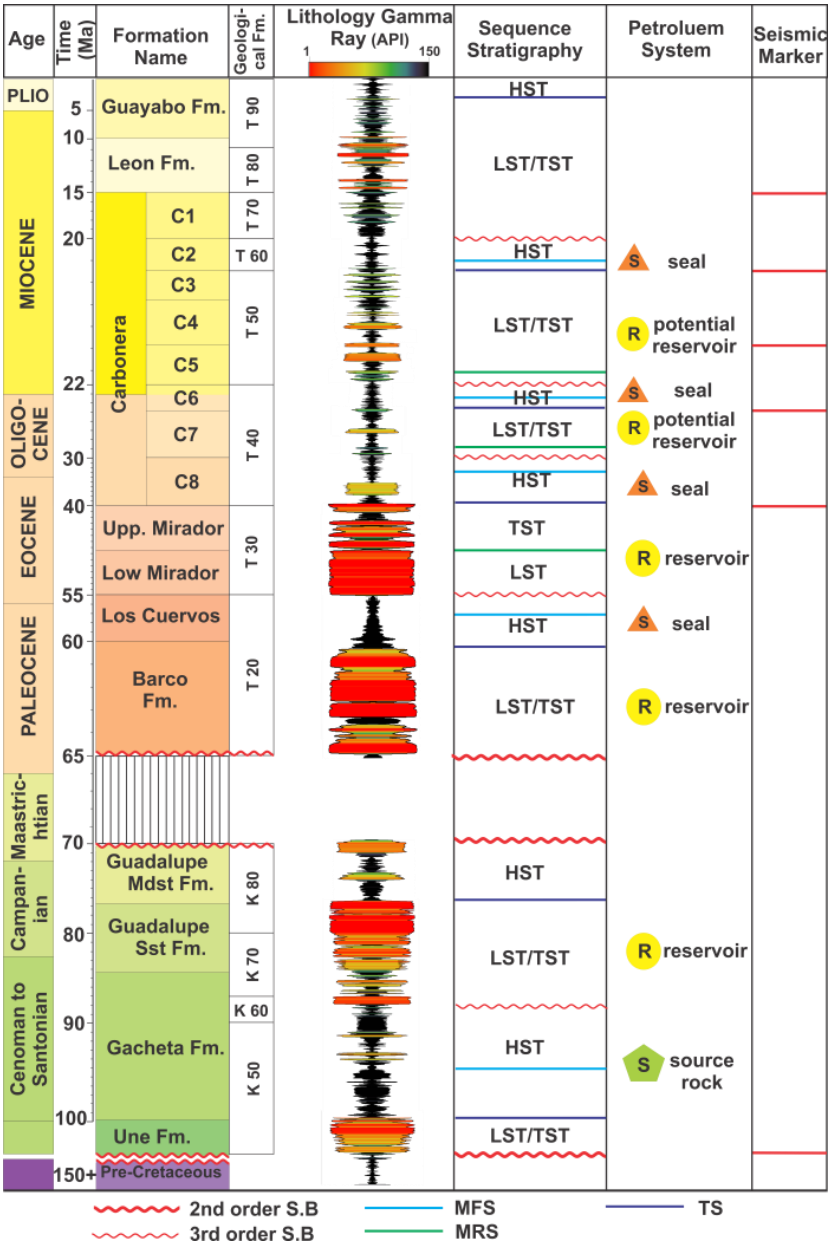

Figure 4.3 Generalized Stratigraphic column, sequence stratigraphy and petroleum systems of Llanos Foothills.

In the Late Cretaceous, an inferred global sea level rise (Haq et al., 1987) was combined with postrift thermal subsidence, and accommodated marine mudstones of the Gacheta Formation (Figure 4.3); a prolific source rock that is contemporaneous with La Luna Formation (Pindell and Tabbutt, 1995).

A drop in sea level during the Campanian-Maastrichtian accompanied the accumulation of the Guadalupe Group on a shallow marine shelf (Linares, et al., 2009). The Guadalupe Group is predominantly a progradational sandstone unit that progressively thins toward the east. Late Cretaceous subsidence in the Eastern Cordillera area accompanied lithospheric cooling, water loading, and horizontal compressional stresses caused by the collision of oceanic terranes in western Colombia (Sarmiento-Rojas et al., 2006).

Deformation resulting from the accretion of oceanic terranes of the Western Cordillera to western Colombia from Late Cretaceous to early Palaeocene marked a significant change from a shallow marine to continental setting in the incipient foreland basin (Sarmiento-Rojas et al., 2006). This foreland basin likely resulted from the topographic load of the Central Cordillera, a volcanic arc that formed as part of the Farallon plate subduction complex along the west coast of Colombia (Cooper et al., 1995). Starting in the middle Palaeocene, the basal transgressive Barco Formation, accumulated as a fluvial to distributary channel sandstone that was interbedded with shales that accumulated during marine flooding events. In the late Paleocene, a relative high stand in sea level initiated the accumulation of the Los Cuervos Formation composed mostly of shale intercalated with sandstones, siltstones, and coal beds (Linares, et al., 2009).

In the Eocene, the Mirador Formation accumulated during a transgression which originated in the foreland basins to the west and north. The Mirador Formation

accumulated in two phases interrupted by a regional unconformity (Martinez, 2006). The depositional setting was expressed by tidal channel sandstones overlapping fluvial channel sandstones (Linares, et al., 2009). The base of the Mirador Formation was dated as ca. 55 Ma and is based on palynological data (Jaramillo et al., 2009). The Mirador Formation is the main reservoir of the Cusiana and Cupiagua areas, and the thickness of the Mirador sequence decreases eastward from the Llanos foothills to the Llanos Basin (Cooper et al 1995).

The accumulation history of the Carbonera Group of late Eocene to late Miocene age is the focus of several regional studies including those of Bogota-Ruiz, (1988), Cooper et al., (1995), Mora et al., (2006), Bayona et al., (2007), Jaramillo et al., (2009) and Parra et al. (2009b). All the studies have analysed the Carbonera Formation at a basin scale but did not predict the fluvial architecture and distribution of the sand bodies within the Carbonera Formation.

Cooper et al. (1995) described the Carbonera Formation as subdivide by widespread maximum flooding surfaces, accumulating as four major cycles of marine-influenced lower coastal plain deposition in the Llanos basin and foothills. Each cycle consists of a mud-dominated highstand systems tract followed by a thin, forced retrogradational systems tract, and ended with a sand-prone transgressive systems tract that culminates with a maximum flooding surface.

Bogota-Ruiz, (1988), Jaramillo et al., (2009) and Parra et al. (2009b) subdivided the Carbonera Formation into eight informal units (C8 to C1) with odd numbers assigned to sandstones and even numbers assigned to mudstones. Bayona et al., (2008), focused on Member C3, C2 and C1 of the Carbonera Formation in Saltarín-1 well drilled through the

Miocene succession of the eastern Llanos basin. He argued that tectonic subsidence and climate were the controlling factors of the basin filling.

Based on lithology and sedimentary structures, Parra et al. (2009a) subdivided the lower Carbonera Formation C8-C6 into 15 lithofacies and four facies associations in the Medina Basin just west of the study area. Parra et al. (2010) recognized the same four facies associations for the Lower Carbonera Formation (C5-C1) that represent tidally influenced deltaic, lacustrine, alluvial plain and braided fluvial sedimentary settings. They considered the Lower Carbonera Formation C8-C6 as a syntectonic wedge, while the upper Carbonera Formation was syntectonic with growth-strata relationships that were rocks equivalent to C5-C2 west of the Medina Basin along Lengupa fault. This coincided with the progressive isolation of the Llanos Basin in the east from the Magdalena Basin in the west (Mora et al., 2013; Reyes-Harker et. al 2015). They proposed a new chronostratigraphic framework for the C8-C6 members of Carbonera Formation based on palynological zonation (T-05 to Ca07) which are of early Eocene – early Miocene age.

Torrado et al. (2014) integrated 700 Km^2 of 3D seismic with well data in the central Llanos Basin. They characterized the Carbonera Formation as cycles C1, C3, C5 and C7 on the basis of seismic attributes. Their interpretation of fluvial sands focused on identifying geoforms and channel filling material, characterizing these as prospective and non-prospective hydrocarbon plays. Also, they recommended using advanced interpretive techniques that included spectral decomposition, RGB blending of frequency, as well as seismic inversion to detect thinner channels within the wider channel belt complex.

A global rise in sea level followed the deposition of the Carbonera Group in the middle Miocene (Haq et al., 1987) leading to the accumulation of the Leon Formation shales over

the Llanos basin. It should be noted that the Leon Formation is shaly and thicker (~1000m) in Llanos basin whereas it is relatively thinner and sandier toward the Llanos Foothills.

4.3 RESEARCH METHODS

4.3.1 SYNTHETIC SEISMOGRAM

A synthetic seismogram was created with from the logs of Well A in the 3D seismic volume (Figure 4.1). This synthetic seismic trace was tied to the seismic cross section using well check-shot survey data, and adjusting the T-D function through stretching and squeezing the data Fig (4.4a). The Carbonera Fm was defined as extending between (2350) to (3025) ms and includes the Oligocene to Miocene fluvial sand reservoirs (Fig 4.4b).

4.3.1 INTERPRETATION OF WELL LOGS AND SEISMIC SECTIONS

A regional reconnaissance of the Carbonera Formation used the available gamma ray (GR), resistivity, density and neutron logs. The logs and cross-sections all use the same header, scales, and color-fill settings so facilitating well-to-well correlation. The GR logs were normalized, displayed at a logarithmic scale to reveal any cyclicity in grain size, and their color fill was adjusted so red represented sand sized fabrics while black argillaceous fabrics (Kadar, et al, 2015, De Keyser et al in press). The resulting GR log displays were used as a proxy for sediment grain size. The neutron porosity (NPHI) is colored to vary from black at 0% to dark blue at 10% and higher. The bulk density (RHOB) is shaded red at densities above 2.80 gm/cc.

Following procedures established by Rider (1999) a combination of neutron and density well logs were used to identify the lithology of the strata penetrated by the wells. Two cross sections of the stratigraphic interval of the Carbonera Formation were constructed which displayed the distribution of the sand prone horizons of the Carbonera Formation (C1, C3,

C4, C5 and C7). These sand rich stratigraphic horizons are enclosed within two regional low GR log events for each of the Carbonera Formation cycles between C2 and C6 Fig (4.5a, 4.5b) and Fig (4.6a, 4.6b).

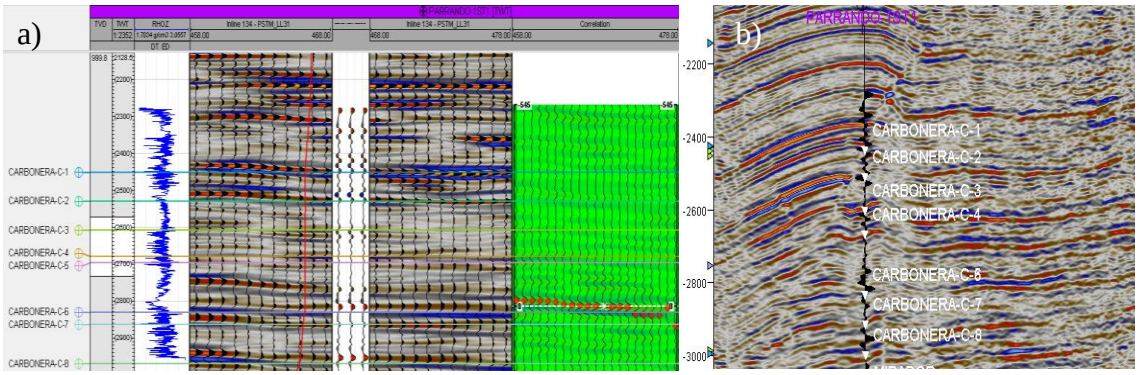

Figure 4.4 a) Synthetic seismogram along with sonic and density logs. b) Seismogram displayed on the seismic section showing the horizon of interest.

Miall, (2014) established that from the perspective of reservoir character the most important control on fluvial reservoir performance is the connective architecture of fluvial sand bodies (the "sand fairway"). Our study recognizes the complexity of the fluvial depositional systems and their potential reservoir character of the Carbonera Formation. It has thus focused on defining local fluvial systems recognizing that even with dense well control, potential associated reservoirs are likely to be highly discontinuous and difficult to correlate and map (Miall 2006; Tye 1991; Bridge and Tye 2000; and Miall 2014). It is hoped that the study reported in this paper be later expanded to a more detailed statistical study of the local fluvial sandstone dimensions, orientation, shape, and stratigraphic

distribution and so further evaluate static reservoir connectivity of the Carbonera Formation.

Having established a sequence stratigraphic framework, we connected the sand units between the wells penetrating the Carbonera Formation using two basic characteristics: channels normally have flat bases, and the major sand bodies had blocky-shaped, low-value gamma ray signatures (Miall 2014). This vertical change shape of the amplitude the signals of well-logs was used to interpret of depositional facies successions (Selley, 1978; Cant 1992; Emery and Myers, 1996; Rider, 1999, Coe et al., 2002; and Kendall 2008; sepmstrata.org). Three types of log pattern were identified from the gamma ray and resistivity signature seen in 28 wells penetrating the Carbonera Formation. 1- Coarsening upward patterns (C-U), 2- fining upward patterns (F-U), and 3- Cylindrical patterns (CY). Electro-facies were compared and matched (Rider, 1999; Coe et al., 2002'; and Miall, 2014) and used to interpret the facies tracts and characterize the reservoirs components of the Carbonera Fm. Based on neutron and density logs combined with gamma ray and sonic logs two condensed sections were identified in the Carbonera Fm. The first associated with C6 and the second associated with C2 with high gamma ray, neutron and low density, resistivity log response respectively, especially the lower part of C6. Fluvial sequences accumulated during the low stand system tract of C7 which was followed by the condensed section seen in C6 and also in C5 to C-3 followed by the marine event of C2. Both the C6 and C2 units contain maximum flooding surfaces which coincide with a global rise in sea level (Haq et al., 1987) of the Late Oligocene and the middle Miocene Fig (4.7).

Sequence boundaries are picked at a sudden decrease in gamma ray, resistivity logs. However, on the logs after SB-2 (Top of C6) show three coarsening upward cycles followed by two fining upward cycles (C5). The same trend is repeated in C3 with five coarsening upward cycles followed by cylindrical to fining upward cycles Figs (4.5a, 4.5b) and Figs (4.6a, 4.6b).

Filtered HDT logs (High Resolution Dipmeter Tool) are plotted with Gamma ray in Carbonera Formation as paleocurrent indicators Fig (4.7). The azimuth rose of the Carbonera shows the vector mean of C7 to the NE, whereas the vector mean of C5, C4 and C3 are to the NW. As suggested by (Miall, 1984) minor variation in the vectors may be attributed to the different orientations of the meander belts cut by wells, or the rejuvenation of local minor source area as a result of minor tectonics and/ or climatic events during the evolution of the river system.

4.3.2 DETECTION OF FLUVIAL SYSTEM USING SPECTRAL ANALYSIS, RGB BLENDING AND HORIZON PROBE (SCULPTURE) TECHNIQUES

Spectral decomposition has been used to determine layer thicknesses (Partyka, 1999, 2011), stratigraphic geometries (Marfurt and Kirlin, 2001), and direct hydrocarbon detection (e.g., Goloshubin et al., 2002; Castagna et al., 2003; Sinha et al., 2005; Welsh et al., 2008; Yu et al., 2011). Additionally, spectral decomposition breaks the seismic signal into narrow frequency sub-bands or horizons (Partyka, 2011). This is achieved by transforming the seismic data from the time domain into frequency domain (Chopra and Marfurt, 2015).

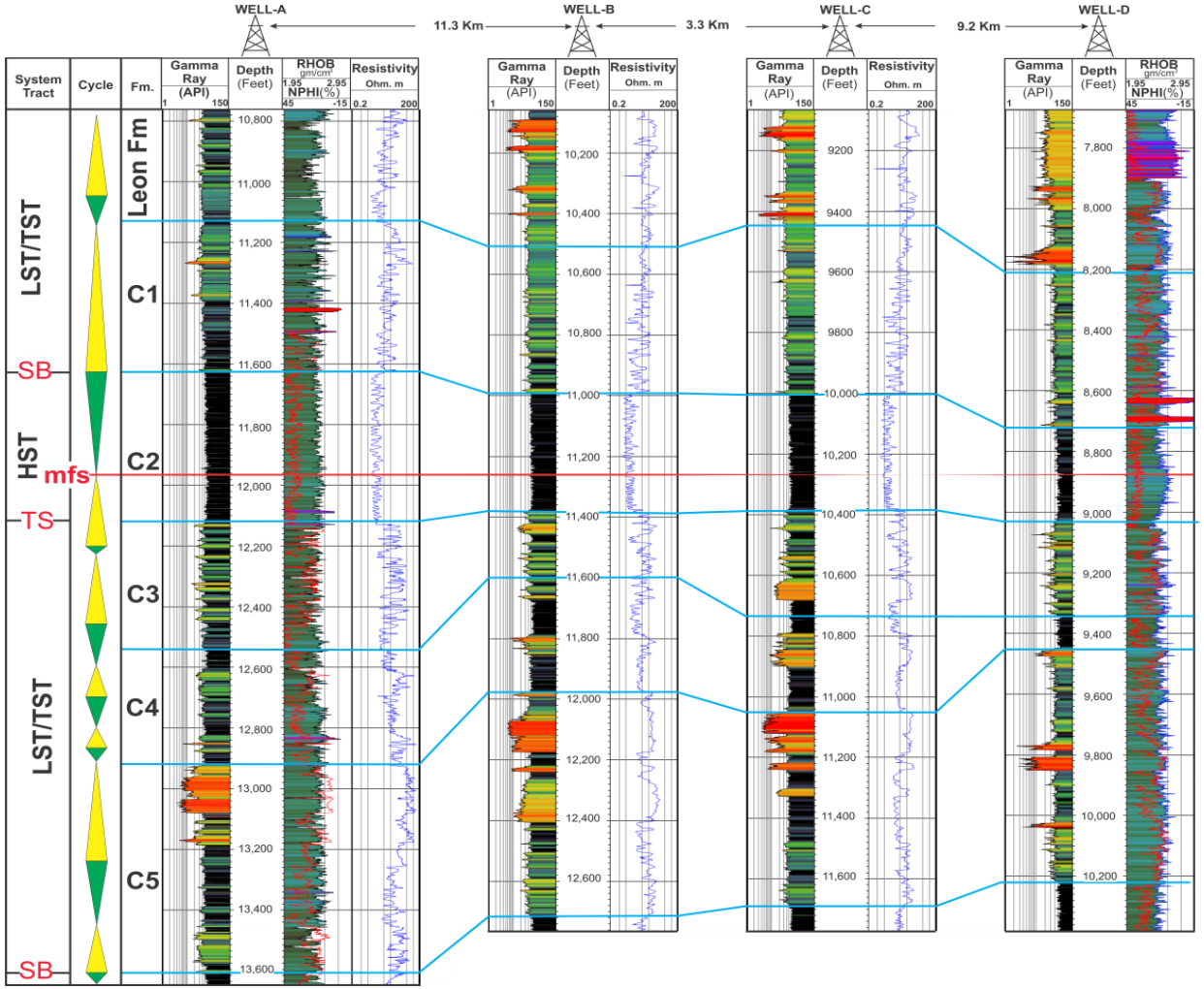

Figure 4.5 a) Well correlation of Carbonera Fm (C5 to C1) and Leon Fm. The correlation is based on gamma-ray logs, resistivity, and neutron density logs. The datum is msf in C2. For location see Figure 1.

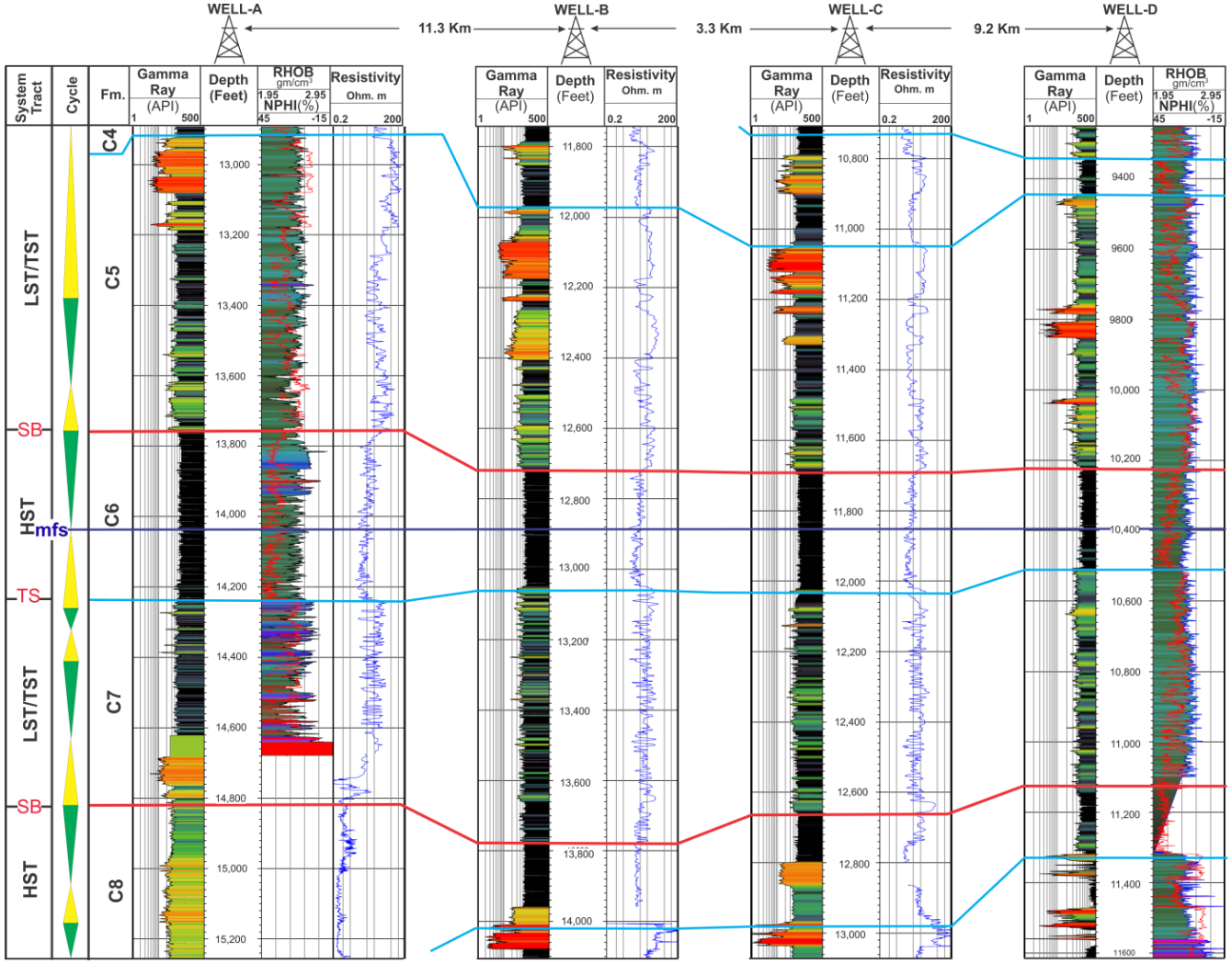

Figure 4.5 b) Well correlation of Carbonera Fm (C8 to C4). The correlation is based on gamma-ray logs, resistivity, and neutron density logs. The datum is msf in C6. For location, see Figure 1.

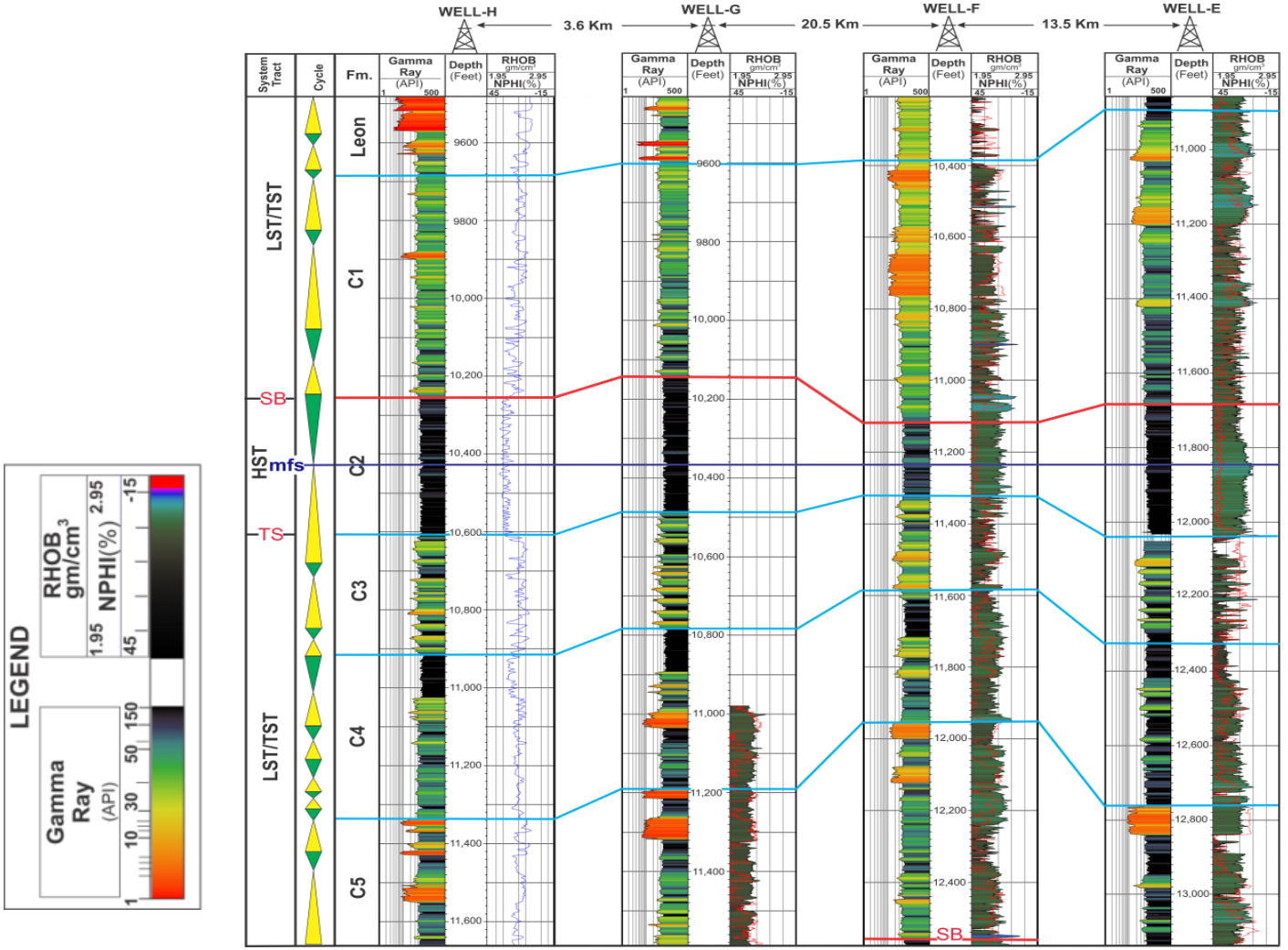

Figure 4.6 a) Well correlation of Carbonera Fm (C5 to C1) and Leon Fm. The correlation is based on gamma-ray logs, resistivity, and neutron density logs. The datum is msf in C2. For location see Figure 1.

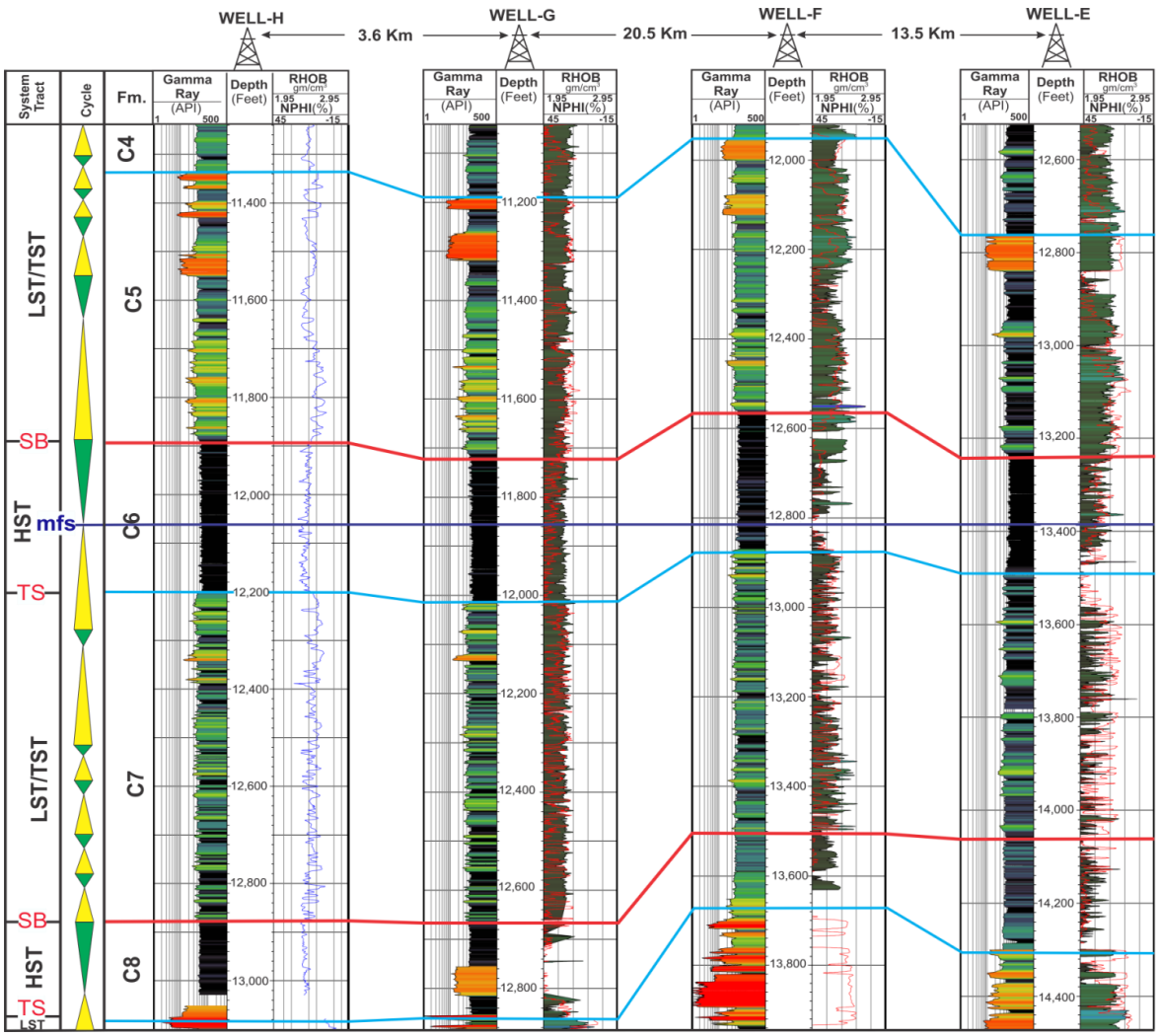

Figure 4.6 b) Well correlation of Carbonera Fm (C8 to C4). The correlation is based on gamma-ray logs, resistivity, and neutron density logs. The datum is msf in C6. For location see Figure 1.

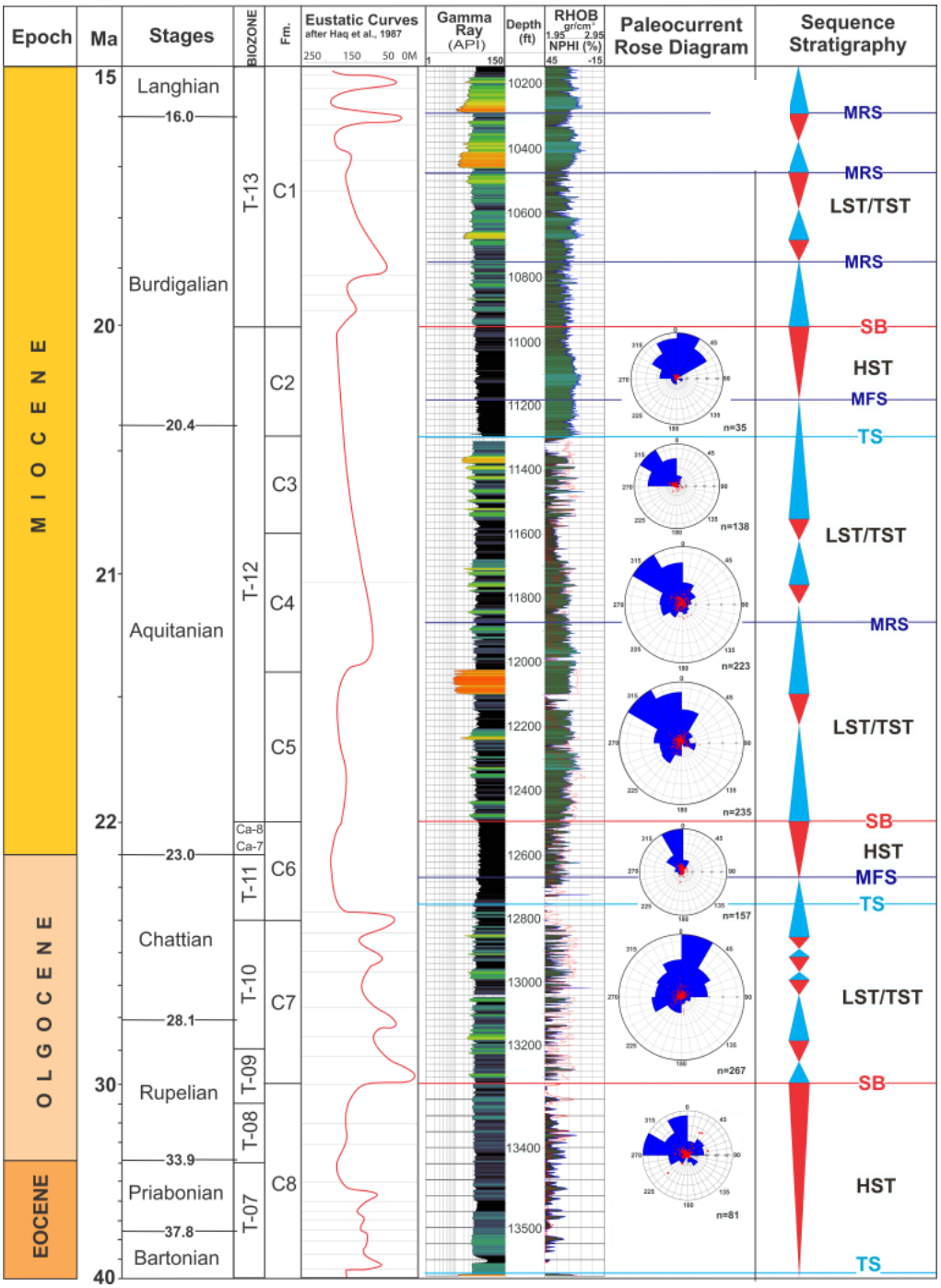

Figure 4.7 Stratigraphic column of Carbonera Fm. showing Biozone after Parra et al., (2009 & 2010), Eustatic curves after Haq et al., (1987), Gamma ray, density and neutron logs, palaeocurrent rose diagram and sequence stratigraphy in Well (E).

We used Partyka's (2011) recommended workflow to analyse the seismic volume, extracting more than 75 different bands with a frequency range ~ 5 - 75 Hz. We modified our spectral decomposition workflow by starting with data conditioning (spectral enhancement) and then investigated the dominant frequency for the horizon of interest (Fig 4.8), constructing a tuning map of the Carbonera Formation to determine the stratigraphic features that could not be resolved in the time domain seismic cube.

The frequency spectra of the Carbonera Formation include the following dominant frequencies: 18-21, 25-33, 38-41 Hz (Fig 4.8). Using these the seismic volumes within the Carbonera Formation these separated into iso-frequency volumes based on these frequencies (Fig 4.9). These volumes were manipulated and superimposed generating bodies that matched geological features using the RGB/CMY Mixer application.

Spectral decompositions are short time Fourier transforms (STFT) and continuous wavelet transforms (CWT) and the matching Pursuit algorithm. Each of these has their advantages and disadvantages, and their selection depends on the objectives of the workflow. For instance, the STFT transformation depends on the time gate, a drawback for the transformation method (Sinha et.al 2005). On the other hand, the CWT method is unlike the conventional SFFT method, which limits the time-frequency resolution by a predefined window length (Sinha et. al., 2005). Narrow windows give good time resolution but poor frequency resolution, whereas wide windows give good frequency but poor time resolution. However, to a certain extent, CWT solves the dilemma of resolution if one can choose the mother wavelet which works best for the seismic data (Morelet, Gaussian, and Mexican Hat or Ricker). This choice depends on the 3D seismic interpretation package used.

Some seismic interpretation workstations offer general spectral decomposition (GSD) as a hybrid of the STFT and CWT through a design wavelet using three parameters: frequency, number of cycles, and phase. The designed wavelet is eventually used to decompose (Correlation) or filter (Convolution) the input seismic data (Schlumberger, 2017).

We used the CWT algorithms of dGB OpendTect to achieve spectral decomposition and reveal fluvial channels throughout the Carbonera Fm. CWT and the calculated isofrequency seismic sections were based on all three wavelets; Morelet, Gaussian, and Mexican. When examining the frequencies of 18, 25, and 38 Hz using this refined approach the images seen in Figs. 4.9, 4.10, & 4.11) were produced. Since we found CWT was better than STFT for spectral decomposition of the seismic volume to detect the stratigraphic features in the Carbonera Formation, the remaining analysis were based on the CWT approach.

4.4 CONTINUOUS WAVELET TRANSFORMATION (CWT) DETECTION OF FLUVIAL SYSTEM CHANNELS AND EVALUATION OF THE HYDROCARBON RESERVOIRS.

The continuous wavelet transform (CWT) is an alternative method for frequency distribution analysis and is achieved by increasing or decreasing time support (transit time defining seismic volume) in the CWT, the frequency support (frequency content of seismic volume) of the wavelets shifted towards the high frequencies and low frequencies respectively. Thus when the frequency resolution increases, the time resolution decreases and vice versa (Mallat, 1999 and 2009). The CWT is focused on the spectral attributes of horizons rather than the entire stratigraphic interval as in SFFT method (Sinha et al., 2005).

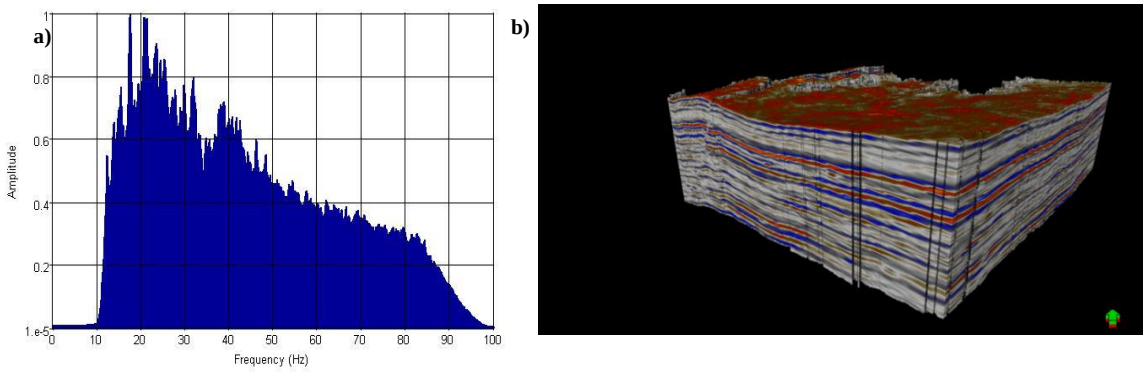

Figure 4.8 a) Frequency spectrum of the interested zone. b) Horizon probe of Carbonera Fm (C-1-C-8) showing the Causian fault and the footwall area of the investigation.

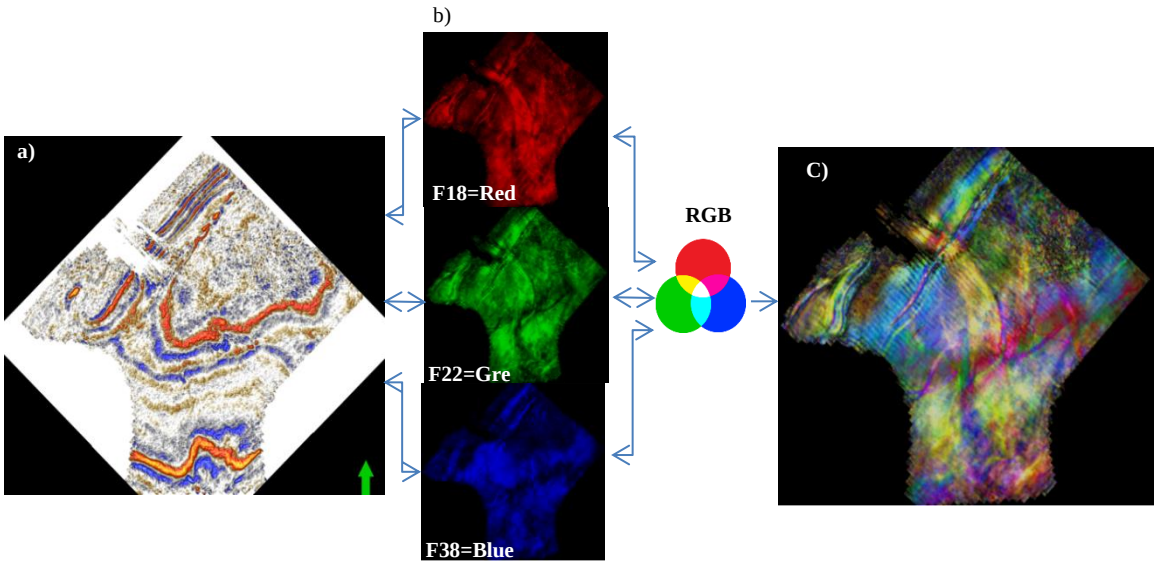

Figure 4.9 a) Amplitude time slice at =2424 ms b) Frequency slice showing amplitude in narrow frequency bands around 38 Hz as blue, 22 Hz as green and 18 Hz as red, c) RGB blend of iso-frequencies F18, F22, and F38.

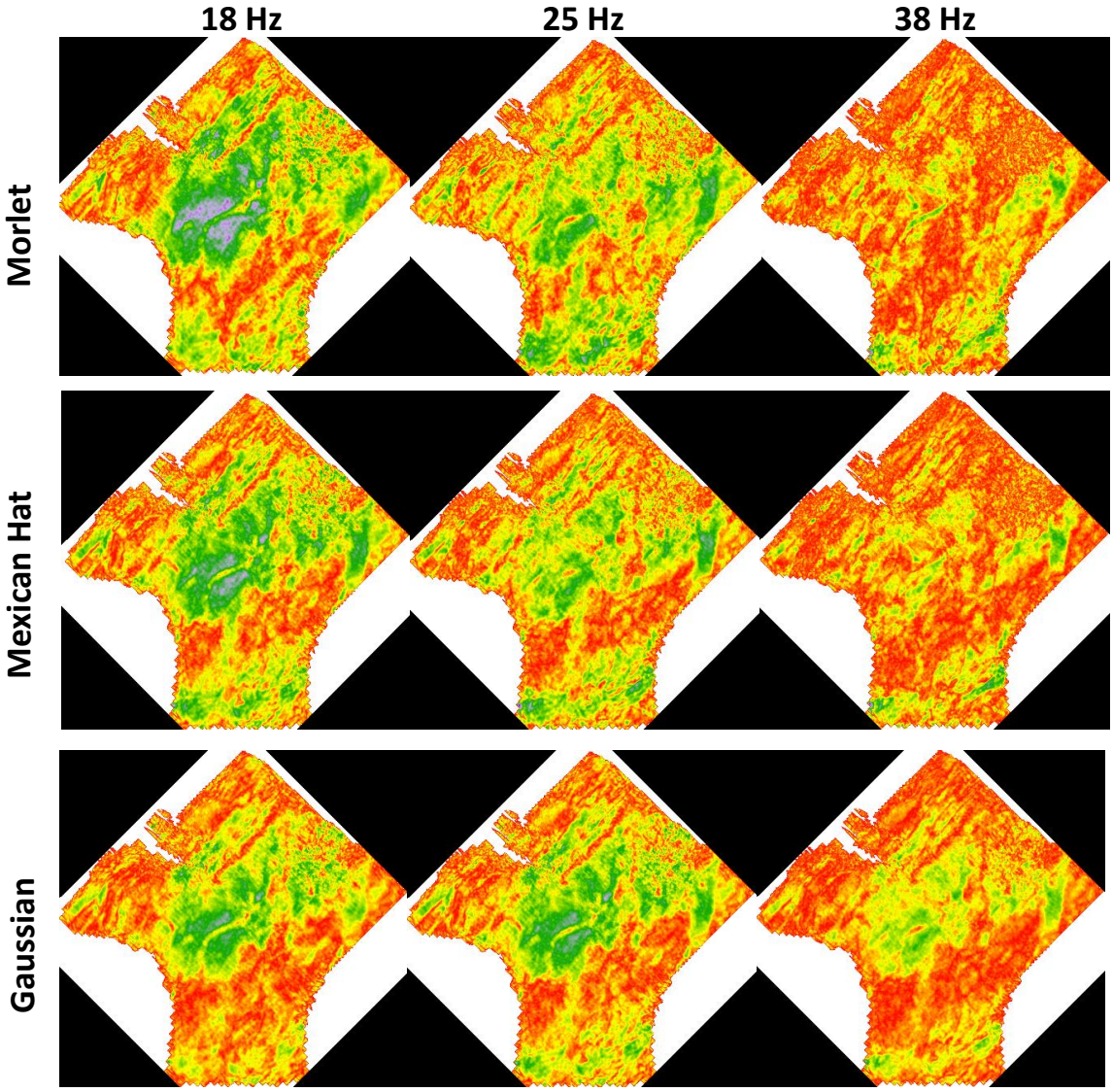

Figure 4.10 Time slices (2727ms) from 18 Hz (left), 25 Hz (middle), and 38 Hz (right) volumes showing CWT spectral decomposition carried out using Morlet (upper), Gaussian (middle), and Mexican (lower) wavelets.

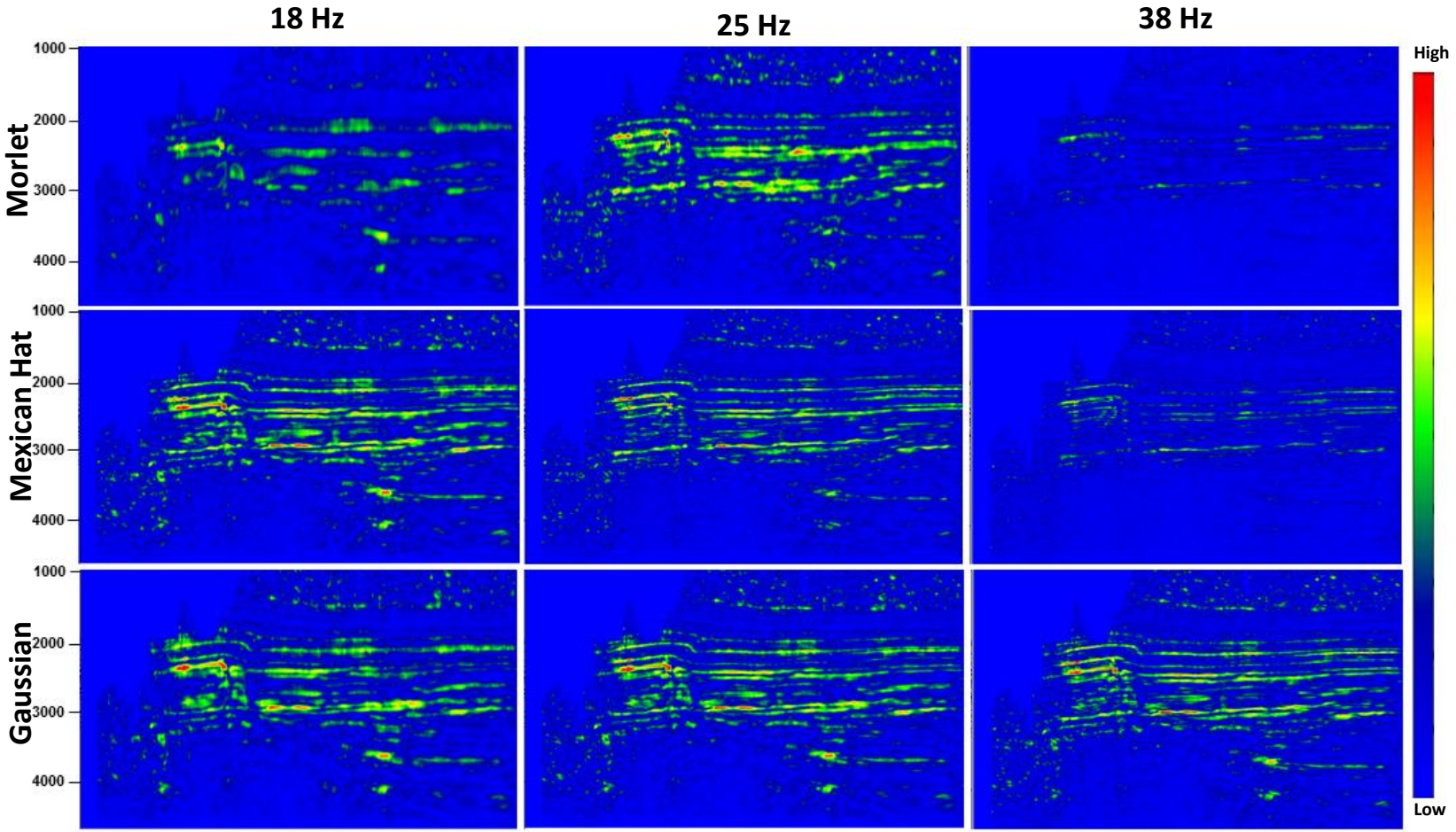

Figure 4.11 Seismic sections (inline 243) from 18 Hz (left), 25 Hz (middle), and 38 Hz (right) volumes showing CWT spectral decomposition carried out using Morlet (upper), Mexican Hat (middle), and Gaussian (lower) wavelets.

The CWT method depends on the choice of the mother wavelets that include the Morlet, Gaussian, and Mexican hat. CWT is calculated as a single frequency seismic sections based on the Morlet, Gaussian, and Mexican hat wavelets with frequencies of 18, 25, and 38 Hz. The results are shown in (Figure 4.10) for a temporal depth of 2727 ms within the Carbonera Formation.

At frequencies of 18 and 21 Hz (Figure 4.10), the Morlet wavelet provides better resolution when compared to Gaussian or Mexican hat. At 25 Hz frequency a Gaussian wavelet provides better resolution than the frequency slice resolved by the Morlet wavelet. At 38 Hz frequency, both Morlet and Gaussian wavelets provide relatively good resolution, although the Morlet wavelet captures major fluvial channels and the thickness of sediment fill in the channel at high frequency. The low frequency (18-21 Hz) tunes the thicker part of a fluvial reservoir, whereas the high frequency 38 Hz tunes the thinner sediment fill of the main channel as described by Laughlin et al. (2002).

Vertically, as frequencies of 18 and 21 Hz vary (Figure 4.11), the Morlet wavelet provides poorer vertical resolution when the results are compared to the products of the Gaussian and Mexican hat wavelets. The Mexican hat provides very good vertical resolution at low frequencies. By using different mother wavelets in the wavelet transform process, different results in terms of vertical and horizontal resolution are obtained.

Since the Morlet wavelet is considered to be the best mother wavelet horizontally, it was selected for further use in seismic attribute analysis and for comparing the attributes based on time domain to the attributes in the time-frequency domain based on the CWT transform.

Li and Lu (2014) combined spectral decomposition and coherence attributes to provide a qualitative measure of the geologic discontinuities such as channels, faults, and caves. Li et al. (2015) used the same workflow as proposed by Li and Lu (2014) and combined RGB images of 20, 35, and 50 Hz spectral decomposition with corresponding coherence images to map the various stages of incised valley fill of the Red Fork Formation in the Anadarko basin, Oklahoma. In the study of this paper, we combined spectral decomposition strata slices of C3, C5, and C7 with coherence (Figure 4.12) as proposed by Li and Lu (2014) to identify the various stages of the fluvial system with a complex superimposed geometry of channels.

Another useful technique used for visualization of the stratigraphic features in the time domain is to use the horizon probe. The horizon probe is an irregular probe that follows one or two interpreted horizon surfaces. It is also referred to as "sculpting" in the industry (Schlumberger, 2017). The use of horizon probe may not be enough alone to detect fluvial systems, but when used with opacity, another powerful visualization technique (Roberts 2011), it allows the interpreter to examine a volume of seismic data using varying transparency and reveal the morphology of high-amplitude channel features.

Using the manipulation of transparency of a small cube of seismic data often reveals the morphology of the high-amplitude channel features. Figure 4.11 shows a fluvial system with a complex superimposed geometry of channels in C3, C5 and C7. It enables the visualization of fluvial systems including the superimposed geometry of channels, point bars and crevasse splays. Furthermore, we find the horizon probe is very useful for the mapping of these fluvial systems and identifying their various stages. The base of C7 is characterized by high-sinuosity channels oriented NE to SW with widths ranging from 400

ft to 750 ft. The two main channels were developed parallel to the present Llanos foothills (Figs. 4.12 and 4.13). The palaeoflow of the C7, inferred from CWT spectral decomposition, is consistent with the palaeocurrent pattern and compliments the dipmeter log of Figure (4.7). Together these two tools confirm the power of this approach to exploration and production.

The spectral decomposition of C-5 strata shows a low-sinuosity wide channel oriented NW-SE with widths ranging from 1400 to 2500 ft. (Figs. 4.12 and 4.13). The channel cuts through the present foothills and the older fluvial system in C7. The channel lacks sharp edges, but is very clear in almost of all the attributes including Envelop and RMS. The palaeoflow of the C7 inferred from CWT spectral decomposition is consistence with palaeocurrent pattern of the dipmeter log Fig (4.7). Again showing how powerful both these tools are together. The C3 strata are characterized by high-sinuosity channels incised through the large channel in C5. The channels are oriented as flowing from NW to SE cutting through the edges of the main earlier channel with widths ranging from 300 to 650 ft (Figs. 4.12 and 4.13). The palaeoflow of the C5 and C3 are inferred from CWT spectral decomposition and are consistent with dipmeter log palaeocurrent patterns Fig (7). Again powerful confirmation of both approaches.

The high resolution images using CWT method identifies seismic volumes that may indicate a direct detection of potential reservoirs and also capture a low frequency shadow beneath the potential reservoirs that have been linked to hydrocarbon content in multiple cases study (Castagna et al 2003; Goloshubin et al., 2006; Welsh et al., 2008; Tai et al., 2010). A preferentially illuminated isofrequency section at 18 Hz from CWT (Morlet,

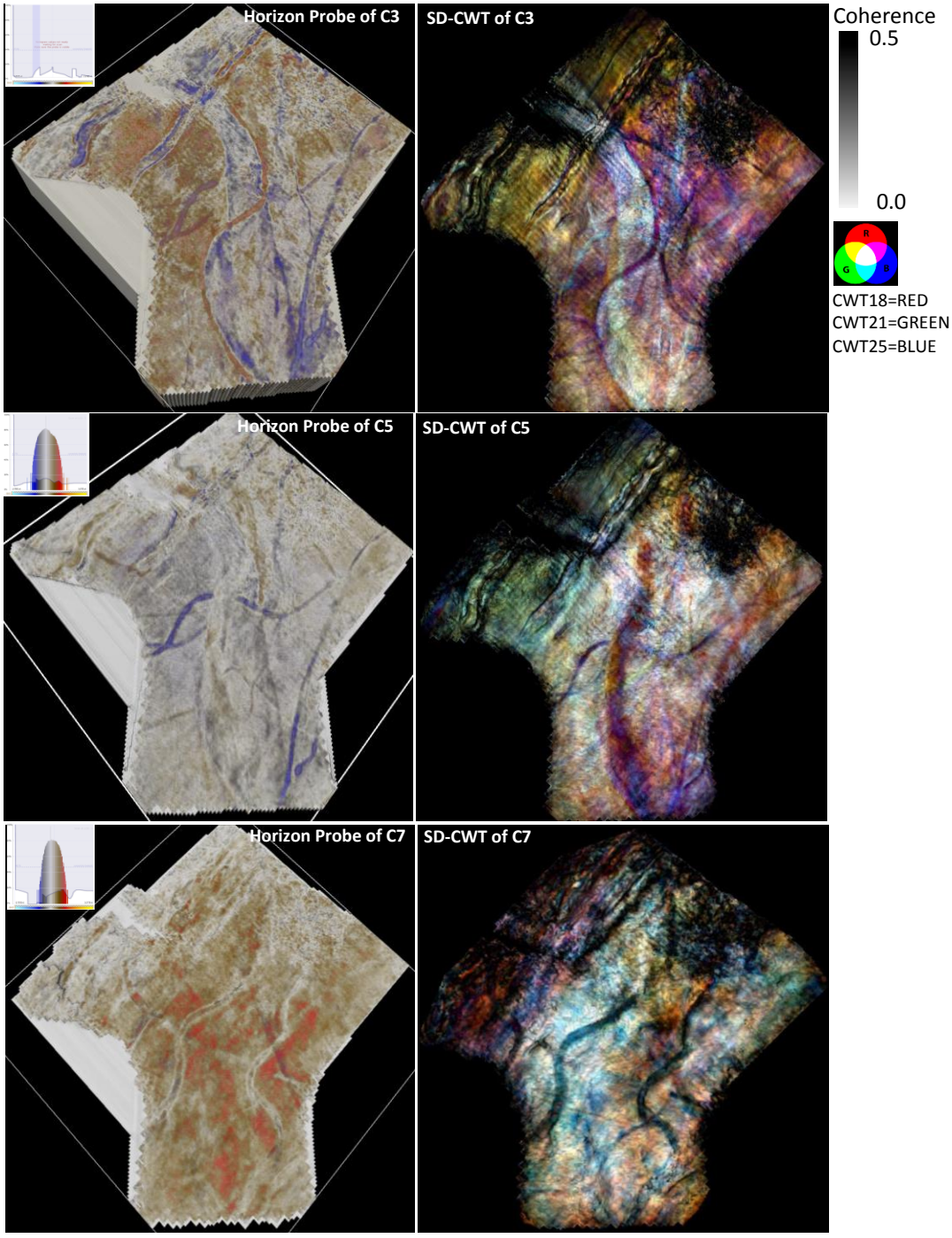

Figure 4.12 Horizon probe versus CWT Spectral decomposition strata slices of C3 (upper), C5 (middle), and C7 (lower). The horizon probe carried out using manipulated transparency (upper left). The CWT spectral decomposition carried out using Morlet wave of amplitude in narrow frequency bands around 38 Hz as blue, 22 Hz as green and 18 Hz as red co-rendering with coherence attribute.

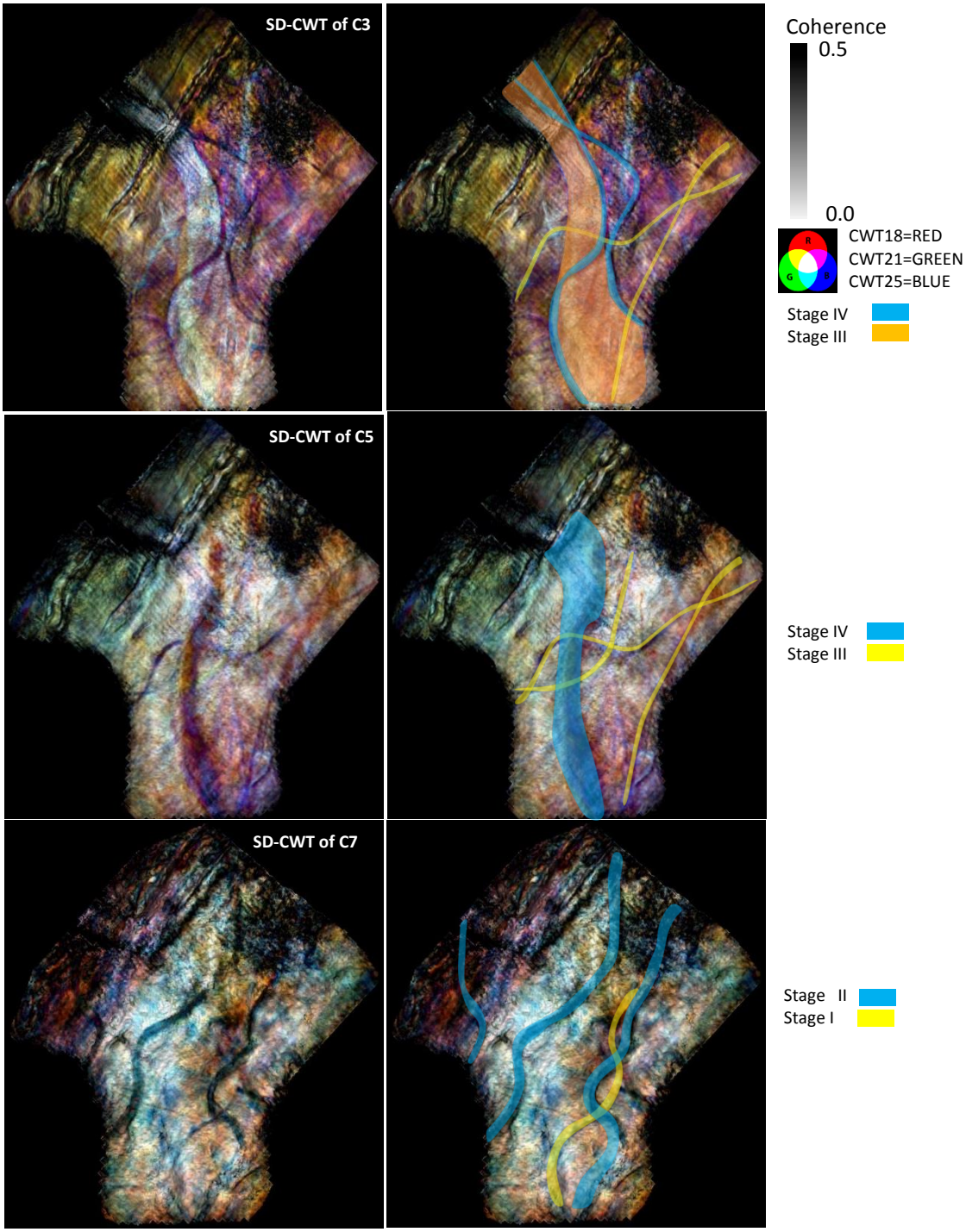

Figure 4.13 CWT Spectral decomposition strata slices of C3 (upper), C5 (middle), and C7 (lower). The CWT spectral decomposition carried out using Morlet wavelet of amplitude in narrow frequency bands around 38 Hz as blue, 22 Hz as green and 18 Hz as red co-rendering with coherence attribute (left column), with fluvial interpretation stages (right column).

Gaussian, and Mexican hat) data volume shows high amplitude low frequency anomalies (white arrow) in Fig (4.14).

4.5 RESULTS AND DISCUSSION

CWT spectral decomposition is a powerful tool that in this study was used to detect and map fluvial systems in the frequency domain. CWT mapping of the fluvial system in Carbonera Formation captures the complicated paleocurrent orientations of the sandier horizons of C7, C5 and C3 which are consistence with the palaeoflow pattern inferred from the dipmeter log.

The result of CWT spectral decomposition depends upon the choice of wavelets, namely the Morlet, Gaussian and Mexican hat. Our results show that the CWT Morlet wavelet has good horizontal resolution, especially at low frequencies when compared with the other wavelets. The Gaussian wavelet has relatively good resolution at low and medium frequencies but is not as good as a Morlet wavelet. On the other hand, the Morlet wavelet has poor vertical resolution when compared with the Gaussian and Mexican hat wavelets. The Mexican hat wavelet provides very good vertical resolution, especially at low frequencies, and the Gaussian wavelet has relatively good vertical resolution at medium to high frequencies.

However, the spectral decomposition method does not always work as expected, since each seismic dataset may react in a differently to these techniques. It’s up to the interpreter to experiment to find the best wavelet for a particular seismic volume. This iterative approach to this technique should be followed for different seismic volumes to evaluate

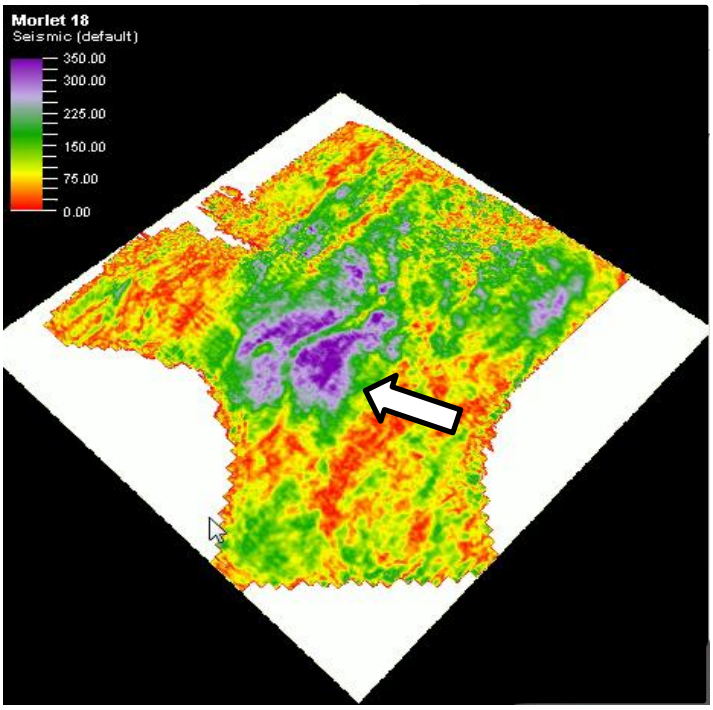

Figure 4.14 Low frequency shadow within the C7 seismic frequency volume below a potential reservoir. Note the meandering channel filled by green and the overbank sediments beside it colored high frequency blue, Note the white arrow indicating the zone of interest.

CWT by trying different wavelets. Later, detailed frequency attribute studies of CWT, STFT and MPD (Matching pursuit decomposition) should be made to evaluate the best decomposition type for subtle stratigraphic features.

The sequence stratigraphic model that evolved from this study was determined from a mix of well-log character and CWT spectral decomposition interpretations provides a stratigraphic framework. Using electro-stratigraphic techniques tied to log response (e.g.

Rider, 1999; e.g. Maill, 1996; e.g. Kendall, 2008; e.g. Maill, 2014) it was possible to analyse the variations of the vertical grain size character and determine the style of fluvial fill expressed by the Carbonera Fm. Identifying the style of sediment fill to CWT technique has enabled the explanation of all of the major features expressed by the Carbonera Fm fluvial systems defined within the three stratigraphic sequences.

The palaeontological zonation of the Carbonera Formation in the eastern foothills of the Eastern Cordillera (Jaramillo and Dilcher, 2000, 2001; Parra, 2008; Parra et al., 2009; and Parra et al., 2010) suggests that the formation accumulated within bio-zones T-07 to T-13 that range in age from 40-15 Ma.

The C8 horizon accumulated within the Late Eocene T-07 bio-zone (~ 40-30 Ma), the C7-C6 horizons accumulated within the Oligocene T-10-Ca-7 bio-zones (~30-22 Ma), corresponding to, and the C5-C2 horizons accumulated in Early Miocene (22-20 Ma).

The Oligocene epoch marks a time of major changes in the paleogeography of Colombia. In the Early Oligocene period tectonic subsidence occurred in large areas of Colombia enabling marginal marine systems to transgress over the Llanos Basin, Llanos foothills, Middel Magdalena Valley and Lower Magdalena Valley (Villamil 1999). This coincided with the upper C8, which is accumulated during a high stand system tract.

Based on detrital zircon ages from the Carbonera Group in the eastern foothills of the Eastern Cordillera, Horton et al. (2010b) concluded that uplift-induced recycling of basin fill which was well under way by the latest Oligocene to early Miocene (26-23 Ma). This coincided with our observation of C7 which is the first fluvial signal of the uplift of eastern flank of the Eastern Cordillera and marked the change from a marine setting C8 to fluvial setting C7.

This Late Oligocene Early Miocene uplift generated a new drainage parallel to the eastern flank of Eastern Cordillera, the "Proto-Orinoco river system" that received sediments from the Guayana Shield to the east and Eastern Cordillera to the west (Villamil, 1999).

Evidence of intra-Oligocene uplift events are recorded in the stratigraphic record as local to regional unconformities (Villamil 1999).

The C7 horizon is interpreted to be comprised of a stack of incised valley sequences that accumulated within a low stand system tract (LST). The fluvial facies of this stage were mainly high sinuosity channels flowing with the regional drainage of the Oligocene Proto-Orinoco river system (Villamil, 1999)

The logs and seismic reflections of this sequence are capped by mud dominated marine deposits. The C6 interval is interpreted to have accumulated during a maximum flooding event. As described by Parra (2008) and Parra et al., (2009) the top of this sequence is marked by a horizon rich in bivalves which is interpreted to coincide with a sequence boundary.

The C6 horizon marine deposits are followed by a thick sequence of interbedded sand and shale units. Key observations derived from the CWT start with the C5 horizon slice characterized by low sinuosity channels with a flow direction perpendicular to that of the C7 horizon which cuts through the present mountain front of the Eastern Cordillera. This change in direction of channel drainage suggests a change of the gradient slope and uplift of Eastern Cordillera matching the top of C6 as sequence boundary.

The drainage switches from low sinuosity to high sinuosity channels within the thick fluvial system of the C5-C3 horizons. A key observation related to the C5 horizon is that

there is a change in spectral strata that suggests an evolution from braided fluvial accumulation to the overlying C3 horizon that captures a meandering fluvial system. These changes in geometric character document a change in slope gradient, sediments source and tectonics activity of the present day Eastern Cordillera. These changes occur across sharp surfaces which can be mapped over tens of kilometres and are interpreted to coincide with maximum regressive surfaces.

The thick fluvial system of the C5-C3 horizon is followed by mud dominated marine deposits. The C2 interval is interpreted to represent a maximum flooding event. The C2 horizon is followed by another fluvial event expressed within the C1 horizon as meandering streams.

The modern fluvial analog of the Carbonera Formation is Ucayali River system of Peru, which shows a complicated fluvial system which shifts enormously in less than 30 yr. as displayed in YouTube films capturing shifts during 5 km/year intervals (Ucayali River Peru, 1985-2013) (https://www.youtube.com/watch?v=izgc3vFimP8). In contrast, the Carbonera Formation accumulated during 35 Ma and by integration of well logs and the spectral decomposition technique we were able to show some of the complicated fluvial systems formed within the Andes.

Undoubtedly, the project area would have been affected by Late Cenozoic global climate changes. However, with the given data availability, there is no way to apply the response of the fluvial systems to changes in discharge, sediment yield and vegetation cover to the seismic data represented in this paper. Therefore, the climate-change-stratigraphic model has not been proposed and is being considered for a future study.

4.6 CONCLUSIONS

Well-log character and CWT spectral decomposition interpretations can be used to develop a sequence stratigraphic framework and depositional model for fluvial sections. Exploration and production geologist should iteratively apply varying seismic volumes and wavelet CWT spectral decomposition in the frequency domain to detect and map the character of fluvial systems including complicated paleocurrent orientations of sand prone horizons matching dipmeter of palaeoflow patterns. From the perspective of potential plays CWT spectral decomposition interpretations apply to low frequency shadows that may provide direct indicators of gas accumulation.

This approach established a series of clastic depositional models for the Carbonera Formation, Llanos Foothills, Colombia that prior to the application of the CWT technology were next to impossible to resolve but only speculate to exist. For instance, the paper demonstrates that vertical variations grain size character and style of fluvial fill and be detected. Distinction can be made between high sinuosity channels, low sinuosity channels, meandering streams, braided fluvial accumulation and marginal marine systems that transgress the fluvial domain

CHAPTER V

TECHNIQUES IN SEQUENCE STRATIGRAPHIC ANALYSIS: LOG CHARACTER & SPECTRAL DECOMPOSITION USED TO DISPLAY PALEOGENE FLUVIAL & MARGINAL MARINE RESERVOIRS OF LlANOS FOOTHILLS, COLOMBIA[1]

[1]Saied, E., Kendall, C., Kellogg, J, De Keyser, T. Submitted to South American Earth Sciences, October 20, 2018

5.0 OVERVIEW

The exploration technique used in this study displays old geophysical logs and integrates these with the seismic attributes of spectral decomposition to provide a sequence stratigraphic framework. This technique was used to map the complex Paleogene sedimentary fluvial reservoir depositional systems of the Llanos Foothills southwest of the giant Cusiana oil field of Colombia. The limited lateral continuity and facies changes in the sand prone units of non-marine and marginal marine reservoirs were enhanced in a sequence stratigraphic framework. Normalized and color-filled logarithmic gamma ray (GR) logs, singly or in cross-sections, had their color fill interactively adjusted. This better identifies the lithofacies character and improves the interpretation of the cyclicity of depositional facies. Z plots of well logs were used to identify Paleogene sequence boundaries, system tracts and parasequences. With well log ties, seismic spectral decomposition was used to identify the sedimentary geometries of channel facies and their overbank equivalents in the eastern part of the Llanos Foothills in a sequence stratigraphic framework providing a Paleogene depositional model.

5.1 INTRODUCTION

The main objective of this paper is to describe how to integrate seismic attributes of spectral decomposition with better displays of old geophysical logs within a sequence stratigraphy framework to map complex sedimentary fluvial reservoir depositional systems. This approach was used on a geological section with hydrocarbon potential in the eastern part of the Llanos Foothills, 40 km southwest of the giant Cusiana oil field of Colombia, and east of the Guaicaramo fault and Medina Basin (Figure 5.1). The main

reservoirs in Cusiana are estuarine sandstones of the Eocene Mirador Formation and deeper estuarine sandstones of the Paleocene Barco Formation and shallow marine sandstones of the Santonian-Campanian Upper Guadalupe Formation (Cazier et al., 1995; Cooper et al., 1995). In this study we focus on the Paleogene fluvial to marginal marine reservoirs, particularly in the Mirador Formation.

It is difficult to predict the siliciclastic geometries of fluvial and marginal marine sediments in the stratigraphic record, although these sedimentary systems contain sizeable hydrocarbon reserves. Much of the oil in the giant fields of Prudhoe Bay (Alaska), Statjord and Brent (North Sea), Daqing, La Cira-Infantas and Mirador (Colombia) is contained in fluvial reservoirs (Dickey, 1992; Cooper et al., 1995; Miall, 1996). These reservoirs typically show vertical and lateral heterogeneity and so have low recovery efficiency (Tyler and Finley, 1991). Similarly well data, including cores and logs which are used to determine the internal architecture, can be poor tools for the evaluation of the reservoir bodies of fluvial systems. In fact, many researchers suggest that vertical profiles are not reliably diagnostic of fluvial style. Even with closely spaced wells and detailed core records it may be difficult to impossible to determine whether a particular vertical profile relates to a single channel-fill record or to superimposed fragments of several or many channel and bar deposits (Miall, 1980; Collinson,1986; Tye, 1991; Breage and Tye, 2001, Lunt et al., 2004; and Miall, 2014). As there is limited lateral continuity and facies change in the sand prone units, establishing a sequence framework of non-marine and marginal marine reservoirs is challenging relative to that found in marine sequences.

The integration of well logs and 3D seismic sections provides a powerful tool to image the geometry of the fluvial deposits, and even to accurately define reservoir heterogeneities

(Miall, 1991, 1996; Selley, 1996). North (1996) emphasized the complexity and variability of fluvial successions and the difficulties in predicting fluvial architecture in the subsurface. He demonstrated that limits of vertical seismic resolution and the limits imposed by a borehole network, even within a mature basin, might limit the ability of the geologist to accurately define and predict fluvial architecture. Now new techniques tied to spectral decomposition can enhance seismic resolution and predict the reservoir geometry even with thin fluvial reservoirs (Partyka et.al 2011, Lughlin et al., 2002).

5.2 GEOLOGIC SETTING

5.2.1 PETROLEUM SYSTEMS AND STRATIGRAPHY

The Eastern Cordillera is a Cretaceous extensional basin system that was inverted during the Cenozoic Andean orogeny (Colletta et al., 1990; Cooper et al., 1995; Mora et al., 2006; Sarmiento-Rojas et al., 2006). By the Early Cretaceous, considerable accommodation space had been generated in the Eastern Cordillera by Late Jurassic to Early Cretaceous rifting, extrusion and intrusion of basaltic magma, thinning of the lithosphere, and shallowing of the mantle (Ojeda, 1996). Throughout the Cretaceous period, thermal subsidence followed the rifting phase (Pindell and Tabbutt, 1995; Ojeda, 1996).

From the Early Cretaceous to Late Cretaceous period, accumulation of sediments in the Eastern Cordillera area was almost entirely in a marine setting. The synrift Une Formation (Figure 2) accumulated from the Early Cretaceous to the Cenomanian and is composed of sandstones that accumulated in shallow marine settings (Linares, et al., 2009). In the Late Cretaceous, eustatic sea level rise (Haq et al., 1987) combined with postrift thermal subsidence accommodated the marine mudstones of the Gacheta Formation (Figure 5.2), a

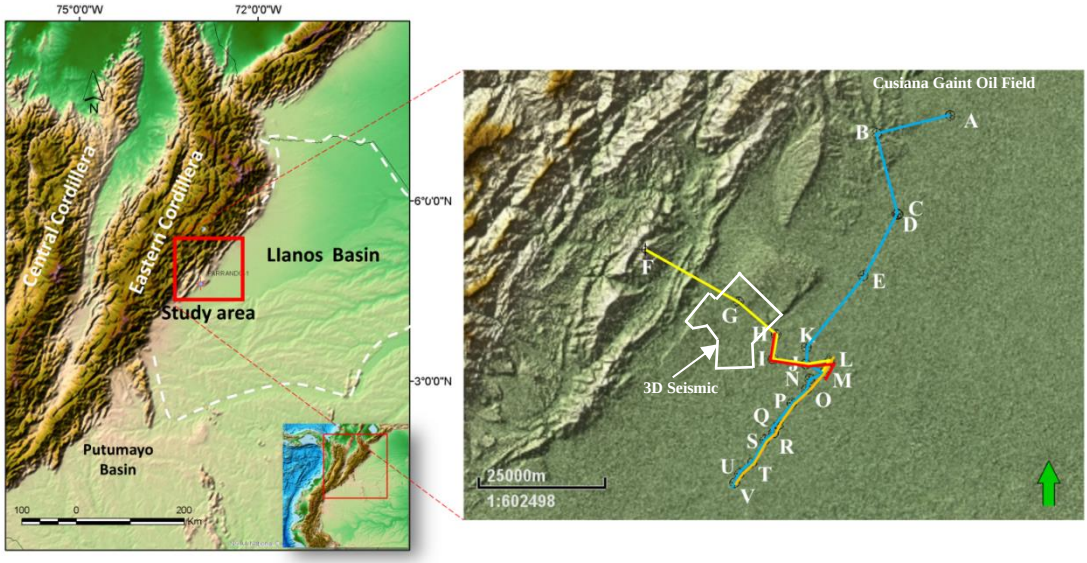

Figure 5.1 Location map of study area: Llanos Foothill, Llanos Basin, Eastern Cordillera in Colombia. b) Location of starigarphic cross sections and the 3D seismic surveys.

prolific source rock that is contemporaneous with the La Luna Formation (Pindell and Tabbutt, 1995).

A drop in sea level during the Campanian-Maastrichtian accompanied the accumulation of the Guadalupe Group on a shallow marine shelf (Linares, et al., 2009). This Guadalupe Group is predominantly a progradational sandstone unit that progressively thins toward the east and is considered one of the deep reservoir units in the Foothills (Cazier et al., 1995). Late Cretaceous subsidence in the Eastern Cordillera area was mostly driven by lithospheric cooling, water loading, and horizontal compressional stresses resulting from the collision of oceanic terranes in western Colombia (Sarmiento-Rojas et al., 2006).

Deformation resulting from the accretion of oceanic terranes of the Western Cordillera to western Colombia from the Late Cretaceous to early Palaeocene marked a significant change from a shallow marine to a continental depositional setting in an incipient foreland basin (Sarmiento-Rojas et al., 2006). This foreland basin likely developed as a result of the topographic load of the Central Cordillera, a volcanic arc that formed as part of the Farallon plate subduction complex along the west coast of Colombia (Cooper et al., 1995). Starting in the middle Palaeocene, the basal transgressive Barco Formation, accumulated as a fluvial to distributary channel sandstone that was interbedded with shales that were deposited during marine flooding events (Linares, et al., 2009). In the late Paleocene, a relative high stand in sea level initiated the deposition of the Los Cuervos Formation, which is composed mostly of shale intercalated with sandstones, siltstones, and coal beds (Linares, et al., 2009). Cooper et al., (1995) indicated that the Los Cuervos Formation accumulated in a regressive, mud-dominated coastal plain system. A major drop in relative sea level at approximately 54 Ma ended Los Cuervos Formation accumulation and created

a hiatus in the Cusiana area that lasted approximately 16 m.y (Cazier et al., 1995). Ramon and Fajardo (2006) interpret the Los Cuervos Formation as consisting of aggradational flood plain deposits and an isolated single story channel belt. Bayona et al. (2008) subdivided the Los Cuervos Formation into lower coastal plain and tidal flats, consisting of coals, meandering fluvial sandstone and local estuarine to isolated lakes with shale fill and upper fine grained alluvial plain sediments that accumulated under well oxygenated conditions.

Martinez (2006) reported that the Mirador Formation accumulated in two stages, namely tidal channel sandstones overlapped by fluvial channel sandstones, and Linares, et al. (2009) identified a regional unconformity between these sandstones. Based on palynological data, Jaramillo et al. (2009) dated the base of the Mirador Formation in the Llanos Foothills as ca. 55 Ma, whereas in the Llanos Basin, the base was dated as 42 Ma to 29 Ma, but they found no unconformity surface at the contact between the Eocene Los Cuervos and Mirador Formations. They believed that the Mirador Formation accumulated during a transgression, which originated in the foreland basins to the west and north. The Mirador Formation is the main reservoir of the Cusiana and Cupiagua areas and the thickness of this sequence decreases eastward from Llanos Foothills to the Llanos Basin (Cooper et al., 1995).

Jaramillo et al., (2009) believed that accumulation of the Mirador Formation sediments in the Llanos Basin and the Llanos Foothills was diachronous, but as will be seen later in this paper, this is a misconception probably related to miscorrelation of the fluvial stratigraphy and the awkward nomenclature of the Mirador Formation.

From the research results of this study the Eocene Mirador Formation accumulated only in the Llanos Foothills area and the younger Oligocene sand in the Llanos Basin is more likely to be the lower part of the lower Carbonera Formation (C8). Based on ties between the local sequence stratigraphic framework and spectral decomposition attribute analysis, C8 was assumed to a high stand system tract in an upper part of the Mirador Formation sequence.

Ramon and Fajardo (2006) identified short, intermediate and long-term scale cycles in the Mirador Formation. Short-term (high-frequency) cycles correspond to progradational-aggradational units. Six intermediate-term cycles were identified from the stacking patterns of their component short-term cycles and the general trend of facies successions. Two long-term cycles were defined from the stacking patterns of the intermediate term cycles and by the general trend of facies successions. The lower half of the Mirador Formation consists of coastal-plain facies tracts and is composed of channel, crevasse splay, and swamp and flood-plain facies successions. A bay facies tract occurs in the upper half of the Mirador Formation and is composed of bay-fill, bay-head delta, and channel facies successions.

The Carbonera Group accumulated during the Late Eocene (~ 40 Ma) to Early Miocene (15 Ma) (Jaramillo and Dilcher, 2000, 2001; Parra, 2008; Parra et al., 2009; and Parra et al., 2010). Cooper et al. (1995) described the Carbonera Formation as composed of four major cycles of marine-influenced lower coastal plain deposition that accumulated in the Llanos Basin and foothills bound by widespread maximum flooding surfaces. Each cycle consists of a mud-dominated highstand systems tract followed by a thin, forced retrogradational systems tract, and ending with a sand-prone transgressive systems tract that culminates with the maximum flooding surface.

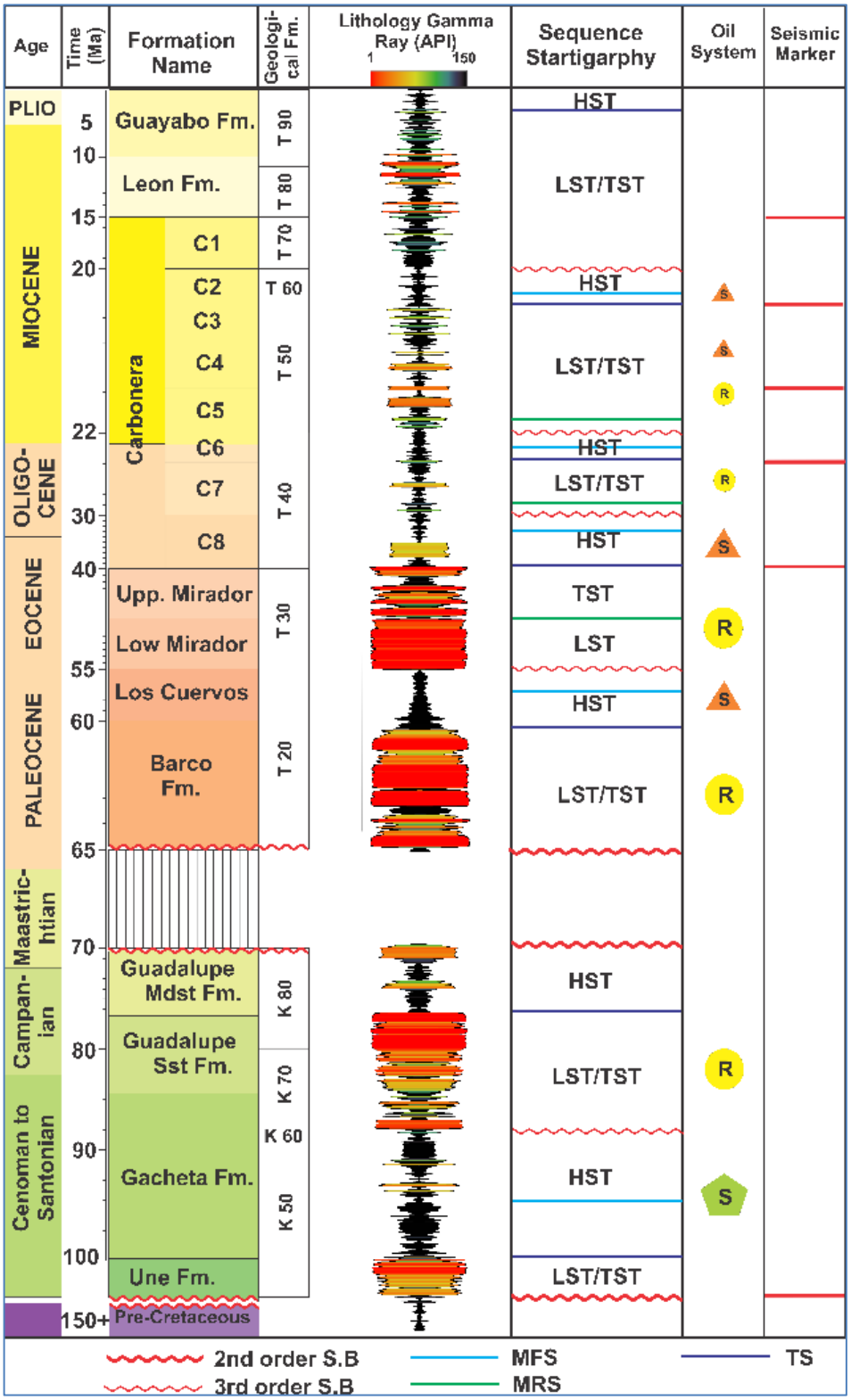

Figure 5.2 Generalized Stratigraphic column, sequence stratigraphy and petroleum systems of Llanos Foothills.

A global rise in sea level followed the accumulation of the Carbonera Group in the middle Miocene (Haq et al., 1987), creating the accommodation space for the accumulation of the Leon Formation shales in the Llanos Basin. This coincided with the isolation of the Llanos Basin in the east from the Magdelena Basin in the west according to Cooper et al. (1995), Villamil (1999), and Ramon and Fajardo (2006). Recent studies based on new data, however, conclude that the progressive isolation of the Llanos Basin in the east from the Magdalena Basin in the west occurred in Early Miocene (Mora et al., 2013; Reyes-Harker et. al 2015). However, it should be noted that the Leon Formation is shaley and thicker (~1000m) in the Llanos Basin, whereas it is relatively thinner and more sandy toward the Llanos Foothills.

5.3 THE MAIN RESEARCH METHODS

Well logs and the seismic attributes used to determine spectral decomposition were integrated to explore the complex fluvial reservoir depositional systems, and enhance the capture of the sedimentological character while improving the interpretation of cyclicity and depositional settings in the Llanos Foothills. The workflow used in this study (Figure.5.3) and described below can be replicated in other areas establishing powerful interpretive techniques for the generation of exploration and production depositional models.

5.3.1 WELL LOGS

The gamma ray logs were normalized to remove systematic errors in well-to-well comparisons and displayed at a logarithmic scale to facilitate hierarchical cycle identification and interpretation. Interactive cross-plots and Zplots, especially gamma ray/neutron and density/neutron and spectroscopy gamma ray (Gamma ray Uranium, Potassium and Thorium), and photoelectric logs, were used to identify the reservoir petrophysical character as well as sequence stratigraphic surfaces. Detailed sedimentological core descriptions accompanied by lithology data, acquired from acid-etched cores and carefully depth-corrected for display with the logs, added precise interpretation of lithofacies, depositional settings, and sequence hierarchy.

5.3.1.1 CHOOSING A COLOR SCALE

This study followed some of the methodology set out by Kader et al. (2015) and De Keyser et al. (in press) using Petrel to build color templates to display the mineralogy and lithology of sedimentary sequences identifiable with Gamma Ray (GR), density (RHOB), and neutron porosity (NPHI) logs. For the Gamma Ray (GR) the color fill template was adjusted to vary so the GR curve display could be used as a proxy for grain size. The red color was selected to represent a clean sand or "grain-supported" fabric, evaporites and coal beds; the yellow–green color represents a "mud-supported" fabric; while the dark color fill represents shale or fine sediments (Figure 5.4). The neutron porosity (NPHI) is colored to vary from black for 0% to dark blue for 10% and higher porosity lithologies. The bulk density (RHOB) logs are shaded red for high densities that range from (2.8-2.95 g/cm^3) to illustrate anhydrite. The log curves shaded magenta-dark blue were intended to

identify the presence of dolomite (2.68-2.87 g/cm^3), and the dark blue to light blue indicate densities from 2.54 to 2.71 g/cm^3. The (RHOB) colored blue-dark green indicate densities ranging from 2.32 to 2.65 g/cm^3 for quartz and dark to capture the clays (Figure 5.4). By themselves, both the neutron and the density log are difficult to use for gross lithology identification, but when combined, they become better indicators of lithology (Rider 1999). If high-resolution RHOB, NPHI and GR were combined and the resistivity and water saturation logs were available these were added. In any case, the color filled templates for GR, RHOB, and NPHI together enhanced the vertical and lateral resolution of the well correlation, making visualization of depositional units and lithofacies changes easier to see and quicker to use.

5.3.1.2 LINEAR VS. LOGARITHMIC SCALE

Gamma Ray well logs are traditional proxies for the sediment grain size (Rider, 1999; Emery and Myers, 1996; Kendall, 2008). Wentworth (1922) tracked grain sizes from 0.98 μm (clay) to 4-8 mm (fine gravel), using the Gamma Ray log displayed at logarithmic scale, making potential grain size variations easier to see and improving the interpretation of cyclicity and depositional settings. In this paper the Gamma Ray logs of siliciclastic sequences are displayed on a logarithmic rather than linear scale in Figure 5, allowing the interpreter to see the same level of detail at the coarse and fine ends of the scale. In this paper, for both siliciclastic and carbonate sediments the minimum value of 1 API unit was

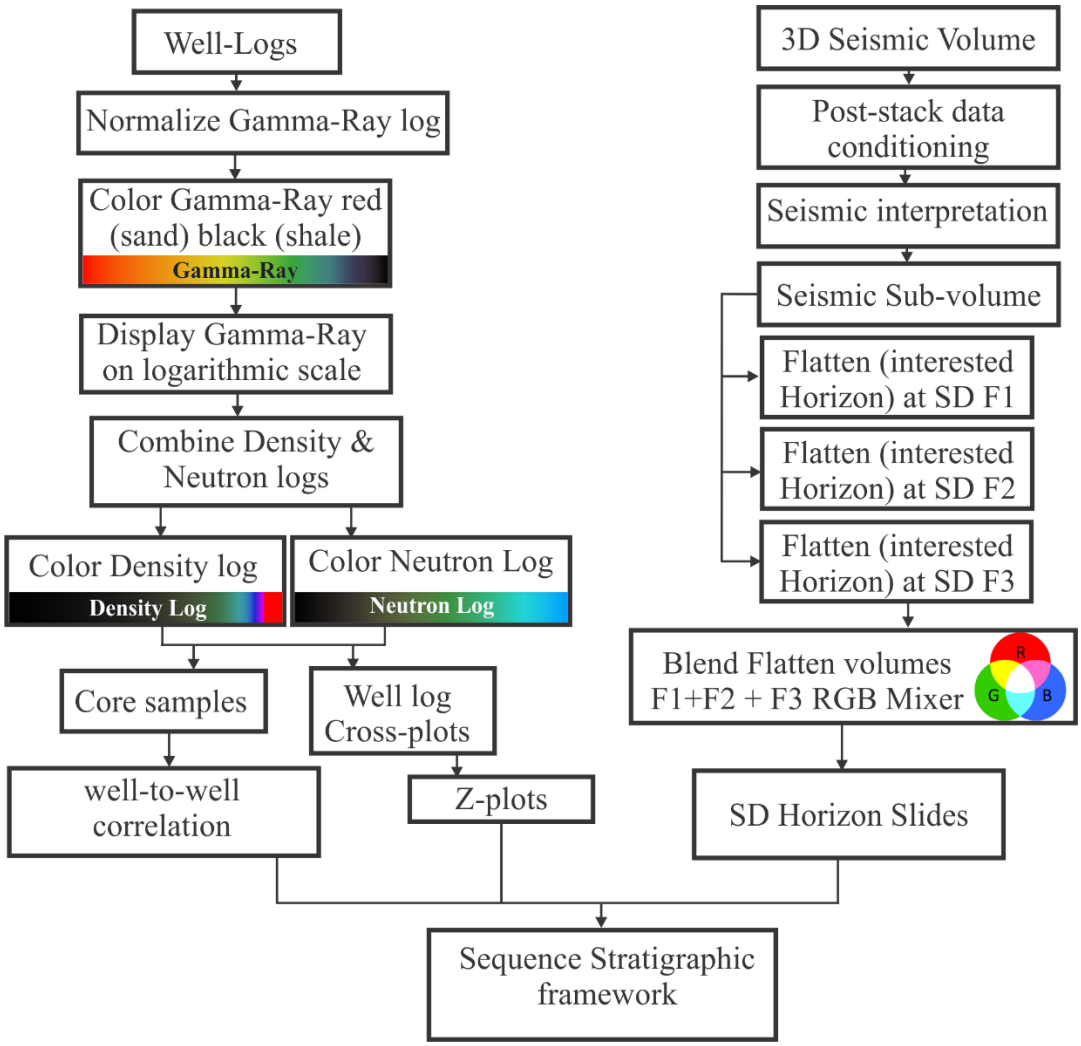

Figure 5.3 The workflow of new techniques to display old geophysical well logs and seismic attribute in sequence stratigraphy and reservoir characterization.

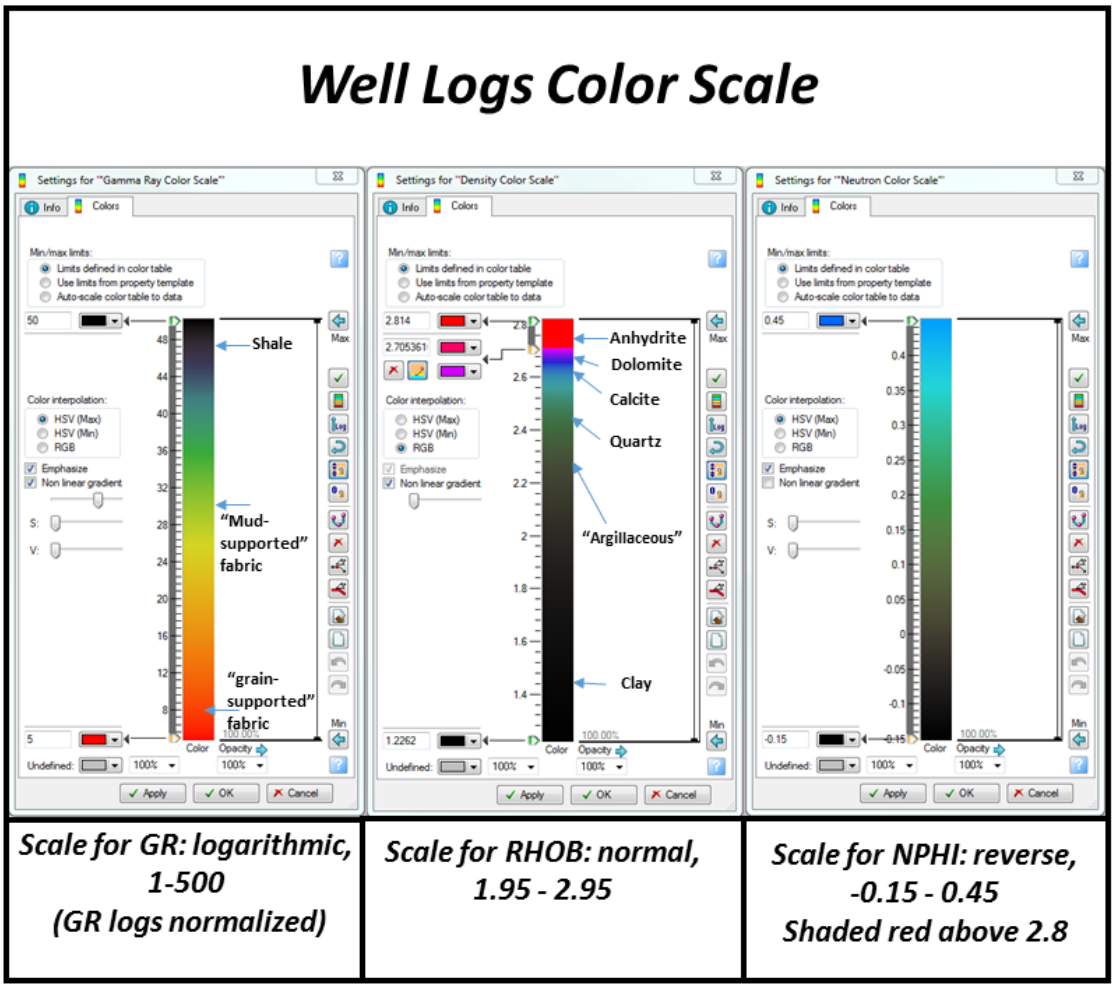

Figure 5.4 Modified color fill of Gamma-Ray (GR), Density (RHOB) and Neutron (NPHI) logs shown in this study.

5. 3.1.3 NORMALIZATION OF GR LOGS

chosen and the maximum value of the logarithmic scale was generally chosen to be greater than the maximum observed API count (Figure 5.5).

Any well log curve may be considered as a sum of the signals of actual rock properties, including random noise and systematic errors. Well log normalization represents a process for eliminating systematic errors from well logs (Shire, 2004). Conforming to the underlying physics of the tool, gamma ray logs are acquired under different drilling conditions and borehole environments, so the logs must be normalized to be quantitatively comparable (Neinast and Knox, 1974).

Gamma ray logs are normalized statistically so that a particular clean sand in all wells will have the same GR value or within shale zones all wells have the same GR value. The GR normalization technique is based on minimum and maximum values of the GR for each individual well. It is a statistical analysis run over the same geological interval in each individual well as follows:

$$GR\text{-}_{Normalization} = (1\text{-}*(GR._{log} - GR._{min}) / (GR._{max} - GR._{min})) + 1$$

$$GR\text{-}_{Normal\text{-}Rev} = 1 - GR\text{-}_{Normal}$$

$$GR\text{-}_{Normalized} = GR._{max} * GR\text{-}_{Normal\text{-}Rev}$$

The best way to evaluate the normalized curve is by comparing the new GR curve to known lithologies, including those from cores, gamma ray core or by density neutron combinations (Figures 5.5 and 5.6) or distinctive intervals of known uniform lithology

(Figure 5.6). When all logs in a cross-section have been carefully statistically normalized, the result

provides a clear visual identification of laterally extensive lithologic bodies, making visualization of depositional units, sequence boundaries, and lithofacies changes quicker and more intuitive.

5.3.3 SEISMIC INTERPRETATION

The seismic workflow of the study began with Post-stack Data Conditioning, followed by seismic well tie, and seismic attribute analysis using spectral decomposition.

5.3.3.1 POST-STACK DATA CONDITIONING

The hybrid frequency decomposition used for the data conditioning workflow depended on data quality and the vertical resolution or frequency resolution required for the study (Figure 5.7). A hybrid method integrating STFT (Short time Fourier transform) and CWT (Continuous wavelet transform) spectral decomposition using Petrel (Schlumberger, 2017) provided the best resolution vertically and the frequency content needed. Petrel's convolution general spectral decomposition algorithm was used which works as a band-pass filter. In this algorithm, the subset of the signal correlated with the wavelet is passed to the output, and all other frequencies are attenuated. The convolution algorithm was chosen with a frequency that works best for the seismic data, which is 54 Hz in this study. The number of cycles chosen defined the oscillations of the wavelet. Increasing the number of cycles increased the frequency resolution. In contrast, if this number was decreased it

Linear Vs. Logarithmic Scaling of Gamma ray log, and Normalized Vs. un-normalized Gamma ray at Logarithmic Scaling

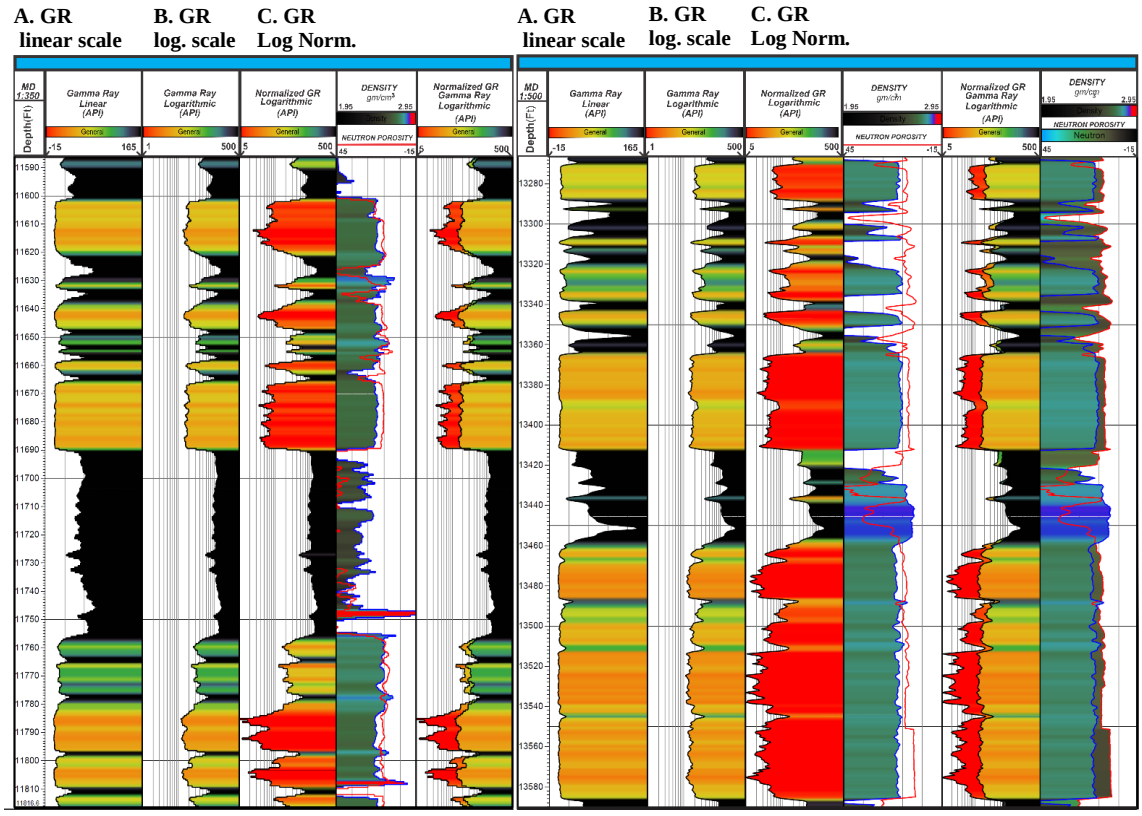

Figure 5.5 Comparison of 3 displays of Gamma ray logs at linear vs. logarithmic scale and un-normalized at logarithmic scale vs normalized at logarithmic scale, accompanied by density-neutron logs, A. linear scale, -15-165; B. logarithmic scale, 1-500, C. normalized GR at logarithmic scale, 1-500.

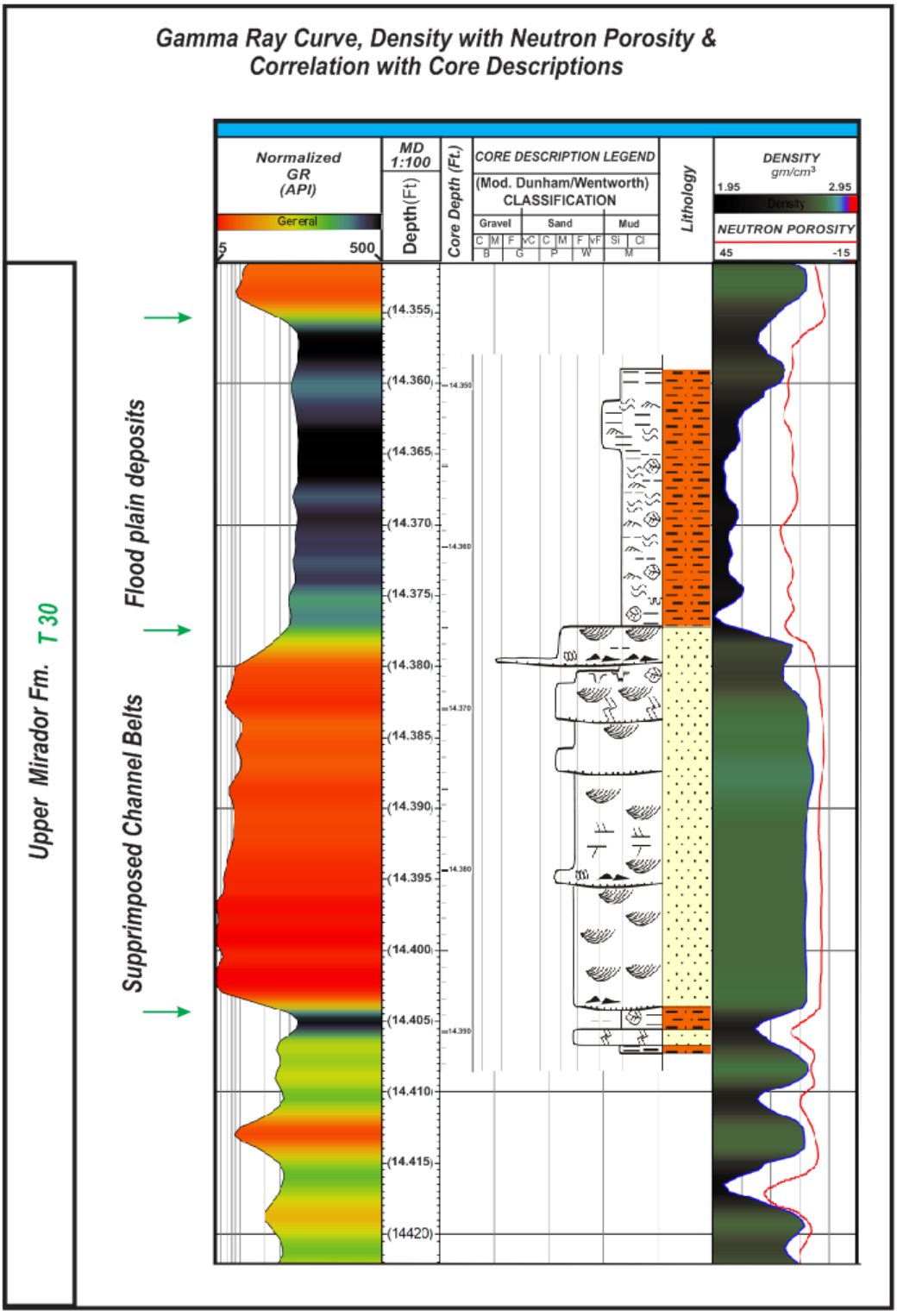

Figure 5.6 Well display for U. Miradir in a well with normalized GR curve and a detailed sedimentological core description. Depth shift for the core is a best fit of lithologies to GR, density and neutron curves and that providing an excellent tie of lithology to the GR curve.

provided better vertical resolution. The phase chosen (min: -180, max: 180) was a 90 degree phase providing a positive correlation with a peak for the top layer and through to the basal layer.

Also the method of "sample by sample calculation" or "Full trace calculation" was used. Both methods produced the same output with the only difference being in the time to perform the algorithm. When working in an in-line/x-line direction, the full trace calculation was preferentially faster. The application of these processes improved the vertical resolution of the seismic (Figure 5.8), improving the seismic well tie and the seismic attribute analysis.

5.3.3.2 SYNTHETIC SEISMOGRAM

Well G located in the 3D seismic volume was used to make a synthetic seismogram for the well to seismic tie. The well check-shot survey was used and established a correlation between the seismic and synthetic seismograms adjusting the T-D function through stretch and squeeze

(Figure 5.8a). The Paleogene Formations are defined by a thin sequence from 3100 to 3250 ms, which includes the Paleocene to Eocene fluvial sand reservoirs of the Mirador and Barco formations. Seismic well ties in the time domain sometimes have errors related to matching the high-resolution well logs (synthetic seismograms) to lower frequency seismic sections (Figure 5.8a). It was determined that the best fit between synthetic seismogram signals and the seismic sections was in the frequency domain rather than in the time domain (Figure 5.8b).

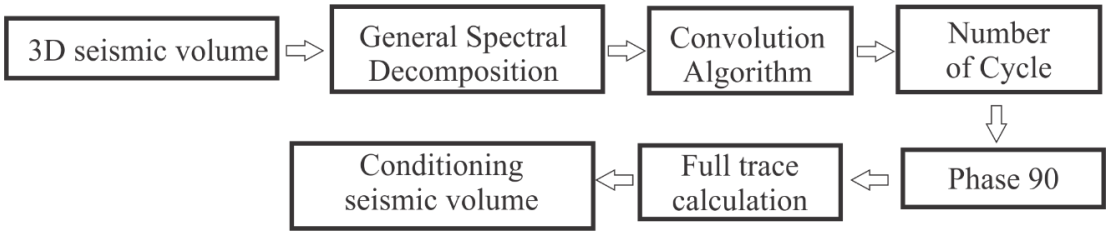

Figure 5.7 Post-Stack Data Conditioning workflow to enhance the vertical resolution.

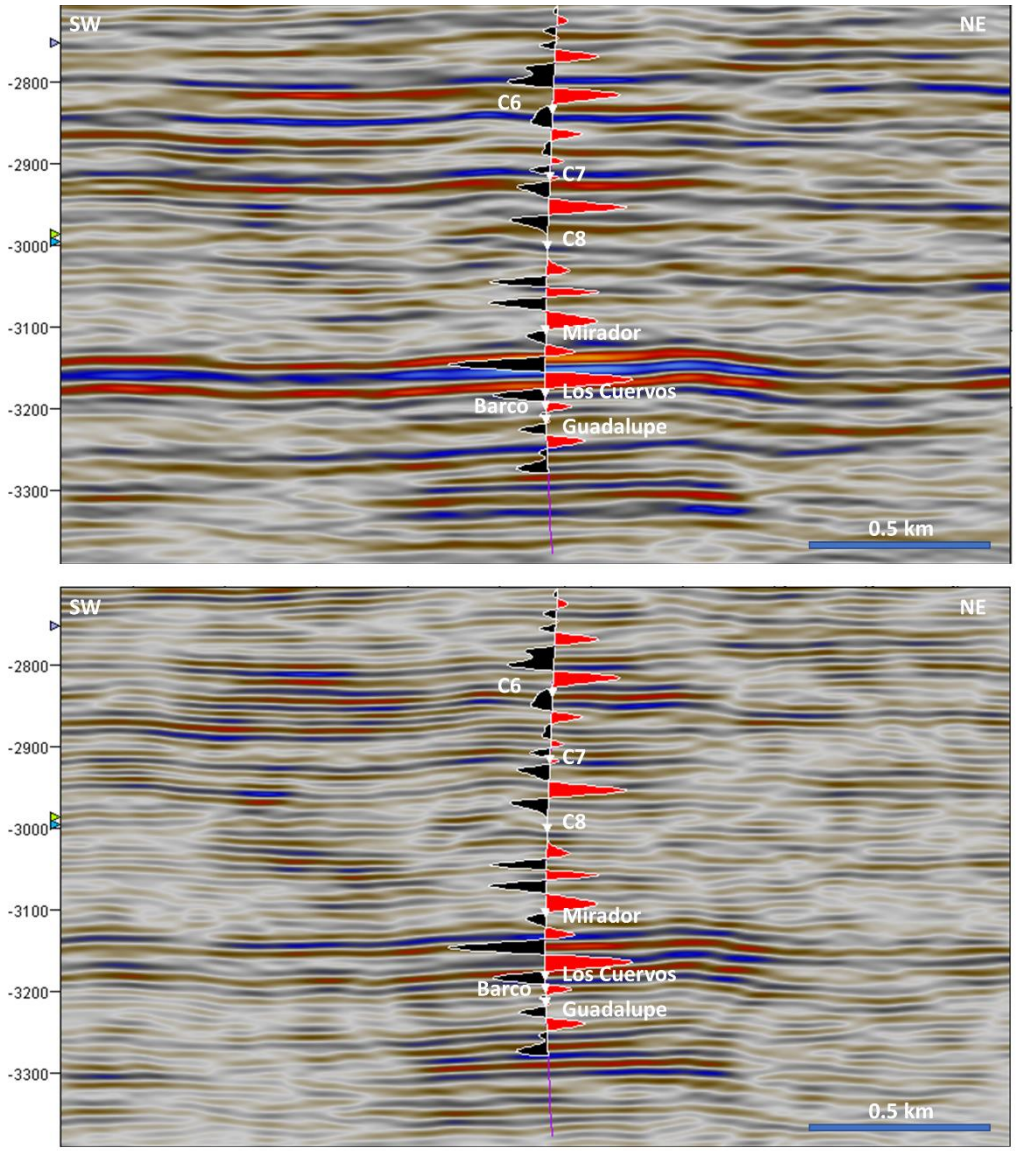

Figure 5.8 a) Original seismic with well tie b) Seismic data conditioning with well tie by using GSD (General Spectral decomposition) with frequency of 54 Hz . Notes the improvement of vertical seismic resolution and the best fit of the synthetic seismogram with conditioning seismic.

5.3.3.3 SEISMIC ATTRIBUTEES

Seismic attributes that help detect fluvial facies include: coherence (or variance) helps detect sands associated with fluvial systems; root mean square (RMS) amplitude detects channels where density variations exist with surrounding sediments; and combinations of multiple attributes can provide increased geologic insight (Marfurt, 2015). The horizon probe is another useful technique for visualization of stratigraphic features in the time domain. The horizon probe is an irregular probe that follows one or two interpreted horizon surfaces, also referred to as "sculpting" in the industry (Schlumberger, 2017). The use of the horizon probe alone may not be sufficient to detect fluvial systems, but when used with opacity, another powerful visualization technique (Roberts, 2011), it allows the interpreter to examine a seismic volume using varying transparency to reveal the morphology of high-amplitude channel features. Figure 5.9 shows a fluvial system with a complex meandering channel geometry in C8.

5.3.2.3.1 SPECTRAL DECOMPOSITION

Spectral decomposition breaks the seismic signal into narrow frequency sub-bands or horizons (Partyka, 2011) which are linked to stratigraphic surfaces identified on synthetic logs. During this process the seismic data is transformed from time domain to frequency domain (Chopra and Marfurt, 2015). Spectral decomposition has been used to determine layer thicknesses (Partyka, 1999, 2011), stratigraphic geometries (Marfurt and Kirlin, 2001), and direct hydrocarbon detection (e.g., Goloshubin et al., 2002; Castagna et al., 2003; Sinha et al., 2005; Welsh et al., 2008; Yu et al., 2011).

The techniques reported on here use a mix of well logs and spectral decomposition of seismic volumes to identify the sedimentary geometries of channel facies and their overbank equivalents in the eastern part of the Llanos Foothills. This spectral decomposition includes short time Fourier transforms (STFT), continuous wavelet transforms (CWT), and the Matching Pursuit algorithm. Each of these has its advantages and disadvantages, and selection depends on the objectives of the workflow. For instance, the STFT transformation depends on the time gate, a drawback for the transformation method (Sinha et. al., 2005). On the other hand, the CWT method is unlike the conventional SFFT method, which limits the time-frequency resolution by a predefined window length (Sinha et. al., 2005). Narrow windows give good time resolution but poor frequency resolution, whereas wide windows give good frequency but poor time resolution. However, to a certain extent, CWT solves the dilemma of resolution if one can choose the mother wavelet which works best for the seismic data (Morlet, Gaussian, and Mexican Hat or Ricker). This choice depends on the 3D seismic interpretation package used. High definition frequency decomposition (HDFD) using the Matching Pursuit algorithm is the best technique at the reservoir scale to solve the vertical resolution problem. However, short time Fourier transforms (STFT), also known as constant bandwidth, has the most frequency separation, but the lowest vertical resolution, whereas high definition frequency decomposition (HDFD) has the greatest vertical localization but does not show the same frequency separation through its RGB interference pattern (McArdle and Ackers, 2012). There is always a trade-off between vertical resolution and frequency resolution, so the choice of method depends on the purpose of the study. The workflow of this paper determines and assesses variations in the fluvial marginal marine lithofacies to build

conceptual depositional models for channel fill and overbank deposits. These models are achieved by integration of well logs character and frequency spectral decomposition.

HDFD Matching Pursuit algorithm and CWT Exponential Constant Q spectral decomposition strata slices reveal a braided fluvial channel in the Lower Mirador (Figure 9). The braided channel contains a potential thick reservoir to the northeast and southwest corresponding to the low frequency 18 Hz, the red color of the GRB color blend (Figure 5.9) based on thin-bed tuning and the amplitude of spectral components in thin reservoirs (Laughlin et al., 2003). In thin reservoirs, seismic data with higher dominant frequencies highlight the thinner portions of the reservoir on amplitude maps, lower dominant frequencies highlight the thicker portions on an amplitude map. In contrast, HDFD Matching Pursuit algorithm and the CWT Exponential Constant Q spectral decompositions strata slice of the Upper Mirador shows a complex meandering fluvial channel systems (Figure 10). These fluvial features are undetectable in the time domain seismic data, whereas spectral decomposition detects subtle stratigraphic events in the Mirador Formation that match the events in the well logs. Using these techniques also permits the detection of minor meandering fluvial channel systems in the lower Carbonera C8. The meandering fluvial channels are clearer when the horizon probe (sculpture) is used with the HDFD spectral strata slice of C8 (Figure 11). Despite the above interpretation of the lithofacies, the Carbonera C8 is considered to be a regional seal, especially over the Cusiana oil field (e.g. Cooper et al., 1995; Sanchez et al., 2015).

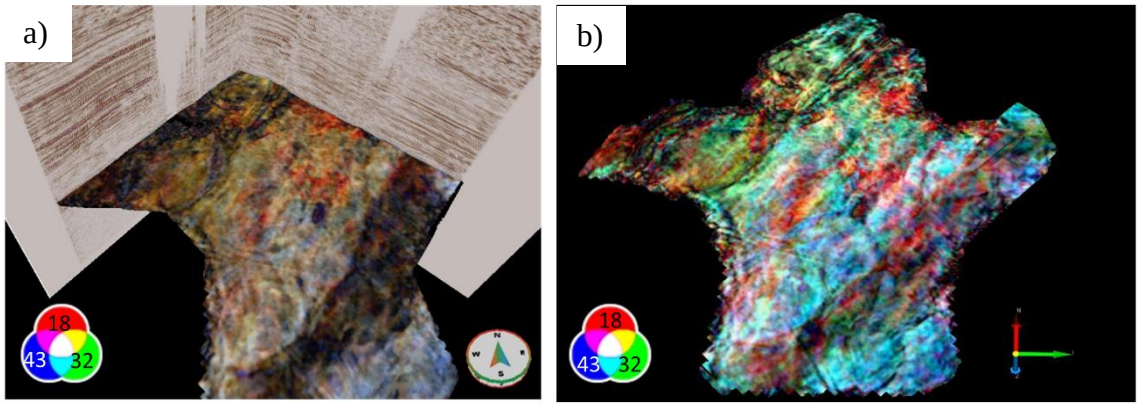

Figure 5.9 a) HDFD Spectral decomposition carried out using Matching Pursuit algorithm of Lower Mirador Fm. in narrow frequency bands around 43 Hz as blue, 32 Hz as green and 18 Hz as red. b) CWT Spectral decomposition (Exponential Constant Q) of Upper Mirador Fm. in narrow frequency bands around 43 Hz as blue, 32 Hz as green and 18 Hz as red co-rendered with similarity attribute showing a braided channel system.

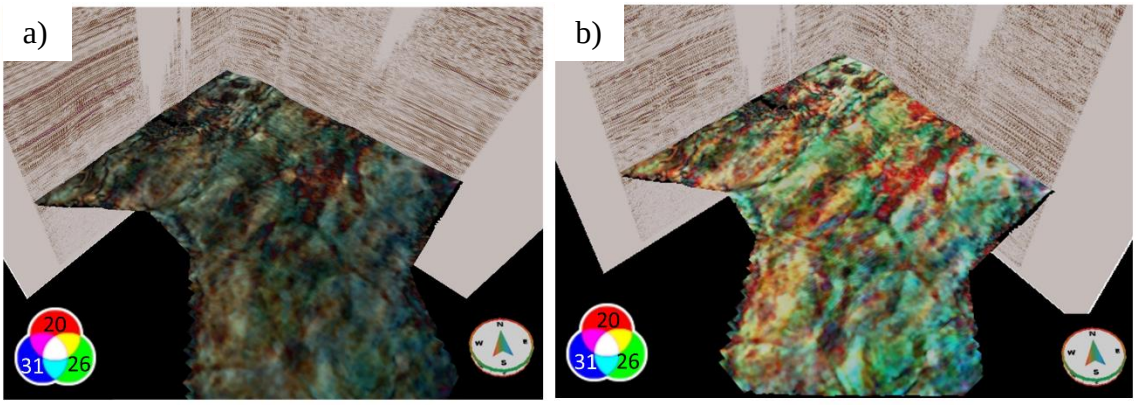

Figure 5.10 a) HDFD Spectral decomposition carried out using Matching Pursuit algorithm of Upper Mirador Fm.in narrow frequency bands around 31 Hz as blue, 26 Hz as green and 20 Hz as red. b) CWT Spectral decomposition (Exponential Constant Q) of Upper Mirador Fm. in narrow frequency bands around 31 Hz as blue, 26 Hz as green and 20 Hz as red showing a complex meandering fluvial channels.

.

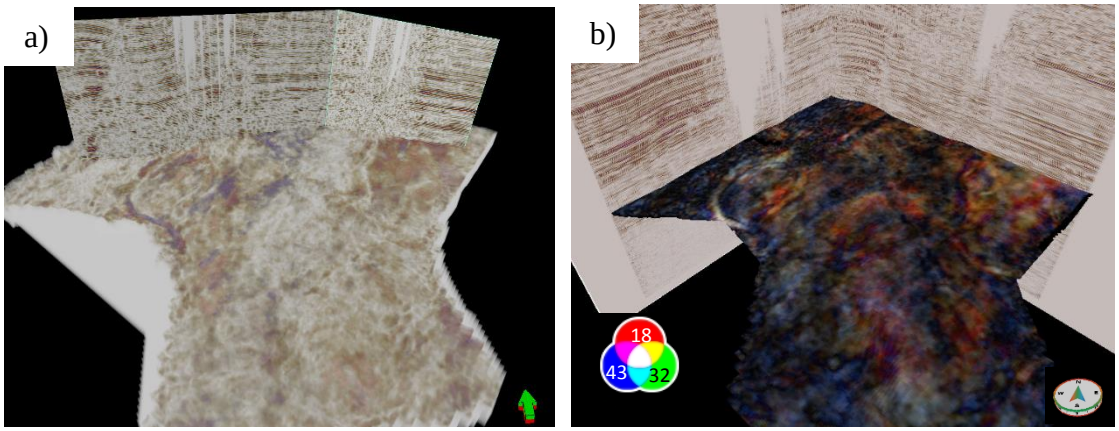

Figure 5.11 a) Horizon probe of C8 carried out using manipulated transparency (upper left). b) HDFD Spectral decomposition carried out using Matching Pursuit algorithm in narrow frequency bands around 43 Hz as blue, 32 Hz as green and 18 Hz as red, showing a minor meandering fluival channels.

5.4 INTERPRETATION OF THE CHARACTERISTIC OF THE WELL LOGGING CURVES

In this study, a regional reconnaissance of the Paleogene formations used the available gamma ray (GR), density and neutron logs (figures 12 through 15). The logs and cross-sections had the same header, scales, and color-fill settings thus facilitating well-to-well correlation. Following procedures established by Rider (1999) a combination of neutron and density well logs were used to identify the lithology of the strata penetrated by the wells. Four cross sections of the stratigraphic intervals of the Paleogene formations were constructed which displayed the sequence stratigraphic framework of the C8 Carbonera, Mirador, Los Cuervos and Barco formations. The vertical change of the amplitude signals of the well-logs was used to interpret depositional facies successions (Selley, 1978; Cant 1992; Emery and Myers, 1996; Rider, 1999, Coe et al., 2002; and Kendall 2008; sepmstrata.org). Three types of log patterns were identified from the gamma ray and resistivity signature seen in 28 wells penetrating the Paleogene formations. 1- Coarsening upward patterns (C-U), 2- fining upward patterns (F-U), and 3- Cylindrical patterns (CY). Electro-facies were compared and matched (Rider, 1999; Coe et al., 2002'; and Miall, 2014) and used to interpret the facies tracts and characterize the reservoir components of the Paleogene formations.

Based on neutron and density logs combined with gamma ray and resistivity logs, the lower condensed section in the K80 Guadalupe mudstone was identified at the base of the Barco Formation. The other two condensed sections were identified in the Paleogene formations. The first is associated with the Los Cuervo Formation and the second is

associated with the C8 Carbonera Formation, each with high gamma ray, neutron and low density, resistivity log response respectively.

Sequence boundaries were picked at abrupt changes in gamma ray, spectroscopy gamma ray as well as neutron density combinations. Miall (2014) established that from the perspective of reservoir character, the most important control on fluvial reservoir performance is the connective architecture of fluvial sand bodies, or "sand fairway". The study reported here recognizes the complexity of the fluvial depositional systems and the potential reservoir character of the Paleogene formations. It has been focused on defining local fluvial systems, recognizing that even with dense well control, potential associated reservoirs are likely to be highly discontinuous and difficult to correlate and map (Tye, 1991; Bridge and Tye, 2000; Miall, 2006 and 2014). However, integration of well logs with seismic volumes is invaluable and plays an important role in predicting reservoir heterogeneities. Vertical seismic resolution can be improved using techniques of spectral decomposition described in this study to predict the reservoir geometry even with thin fluvial reservoirs. It is hoped that the study reported in this paper will be later expanded to a large seismic volume spectral decomposition study of fluvial sandstone dimensions, orientation, shape, and stratigraphic distribution to evaluate static reservoir connectivity in the Paleogene formations.

5.5 INTERPRETATION OF THE WELL LOG CROSSPLOT TO ESTABLISH SEQUENCE STRATIGRAPHY SURFACE AND SYATEMS TRACTS

The cross plots of well logging have been used to identify mineralogy, lithology, porosity and fluid content (e.g., Schlumberger, 1992; Rider, 1996; Schlumberger, 2013; Schön, 2015). This study used well logging and cross plots to establish the sequence

stratigraphic boundaries and system tracts following an often ignored concept expressed by Ridder (1996). All the available well logs were used, including Gamma ray (GR), spectroscopy gamma ray (U, Th, and K), and electrical resistivity (RT), Neutron porosity (NPHI), density (RHOB), acoustic log (DT), photoelectric absorption coefficient (Pe) and well as compound parameters M & N, to identify sequence boundaries and system tracts. Clear cluster patterns were used in the most frequently used cross plots, including Neutron porosity (NPHI), density (RHOB) with Normalized GR as a third dimension (known as Z-plot) (Figure 18). Most of the well log Z plots of the Paleogene sequence show clear cluster patterns that tie with sequence stratigraphic boundaries and system tracts. Obvious condensed sections coincide with a 3th order sequence boundary between upper Cretaceous Guadalupe mudstone and lower Paleocene Barco Formation (Figure 18). Shale clusters represent HST and TST of Los Cuervos, C8, and the Barco and Mirador formations. There is clear clustering of sands in both LST and TST of the Barco and Mirador reservoirs.

The spectroscopy gamma ray consists of Potassium (K) Thorium (Th) and Uranium (U), which were used as shale indicators with caution. According to Rider (1996) "…as shale indicators, Thorium may be used in most cases, Potassium may be used in many cases, but Uranium should not be used at all". Radiation of sedimentary rocks is important for reservoir characterization, as well as for the distinction between clay and sand layers, determination of the clay content, and characterization of "clay type" (Schön 2015). Thorium and Potassium are the "mineral significant" radioactive components of clay minerals and are characterized by different ratios of the two elements (Schön 2015). The condensed section appears as a few points on low Gamma ray values, high density and

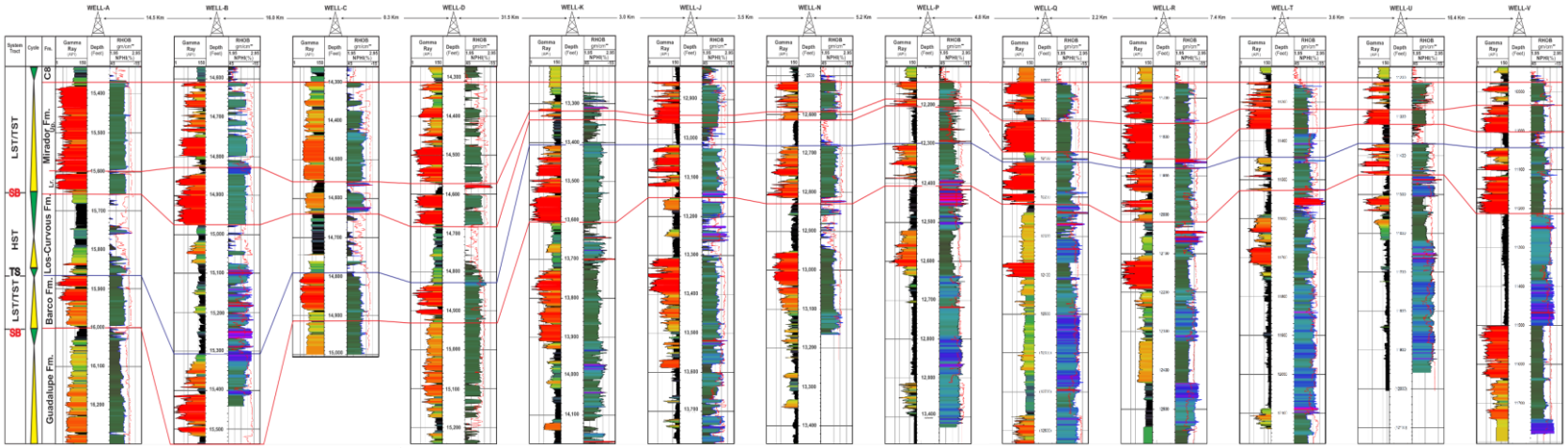

Figure 5.12 Regional well correlation of Paleogene Formations (Barco, Los Curvous, Maridor and Carbonera C8). The correlation is based on Normalized gamma - ray logs, and combination of neutron-density logs. The datum is the top of Maridor Formation. For location, see Figure 1.

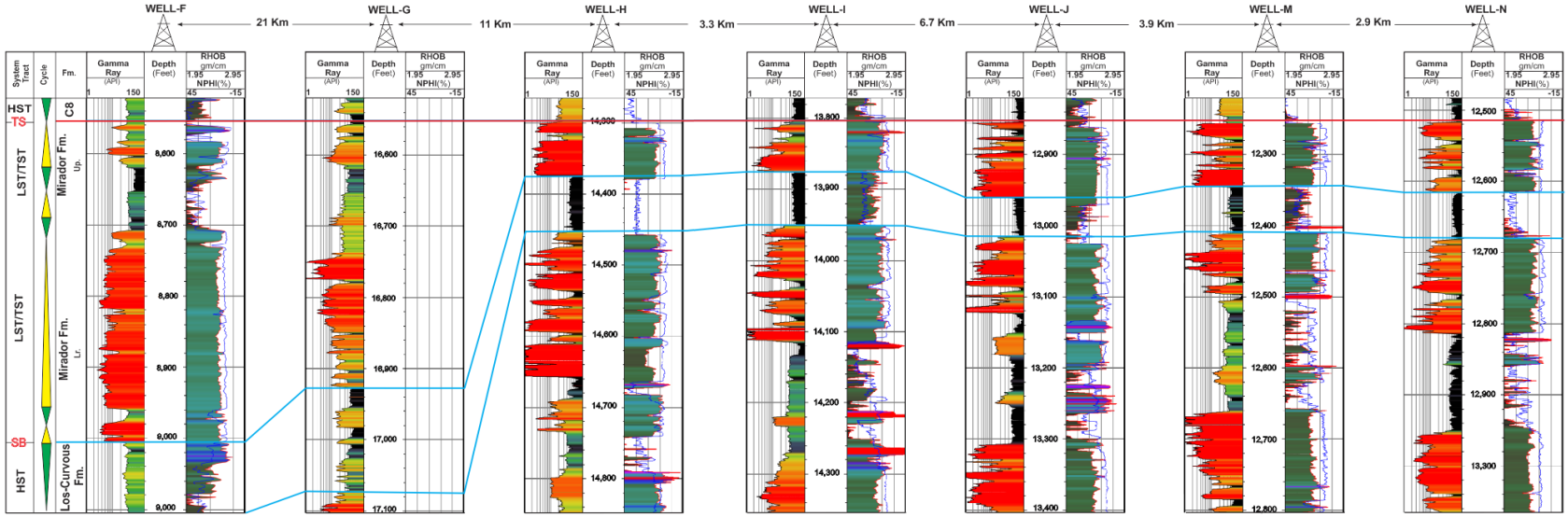

Figure 5.13 Well correlation of Paleogene Formations (Los Curvous, Maridor and Carbonera C8). The correlation is based on Normalized gamma - ray logs, and combination of neutron-density logs. The datum is the top of Maridor Formation. For location, see Figure 1

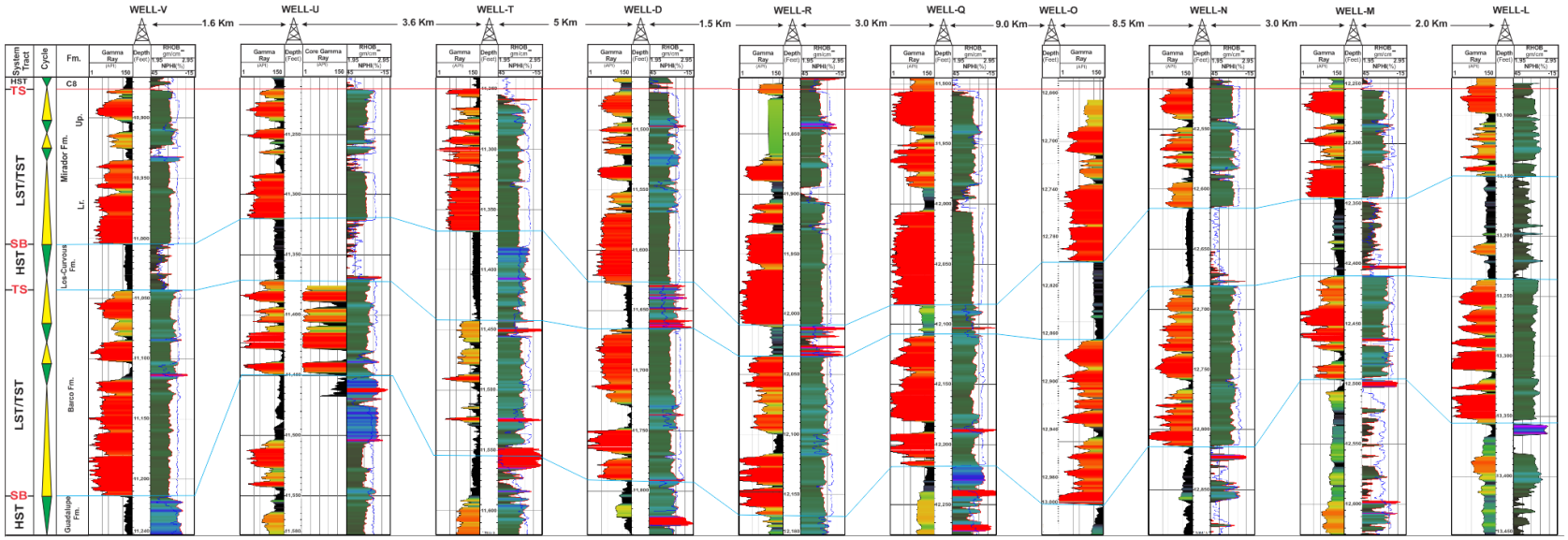

Figure 5.14 Well correlation of Paleogene Formations (Barco, Los Curvous, Maridor and Carbonera C8). The correlation is based on Normalized gamma - ray logs, and combination of neutron-density logs. The datum is the top of Maridor Formation. For location, see Figure 1.

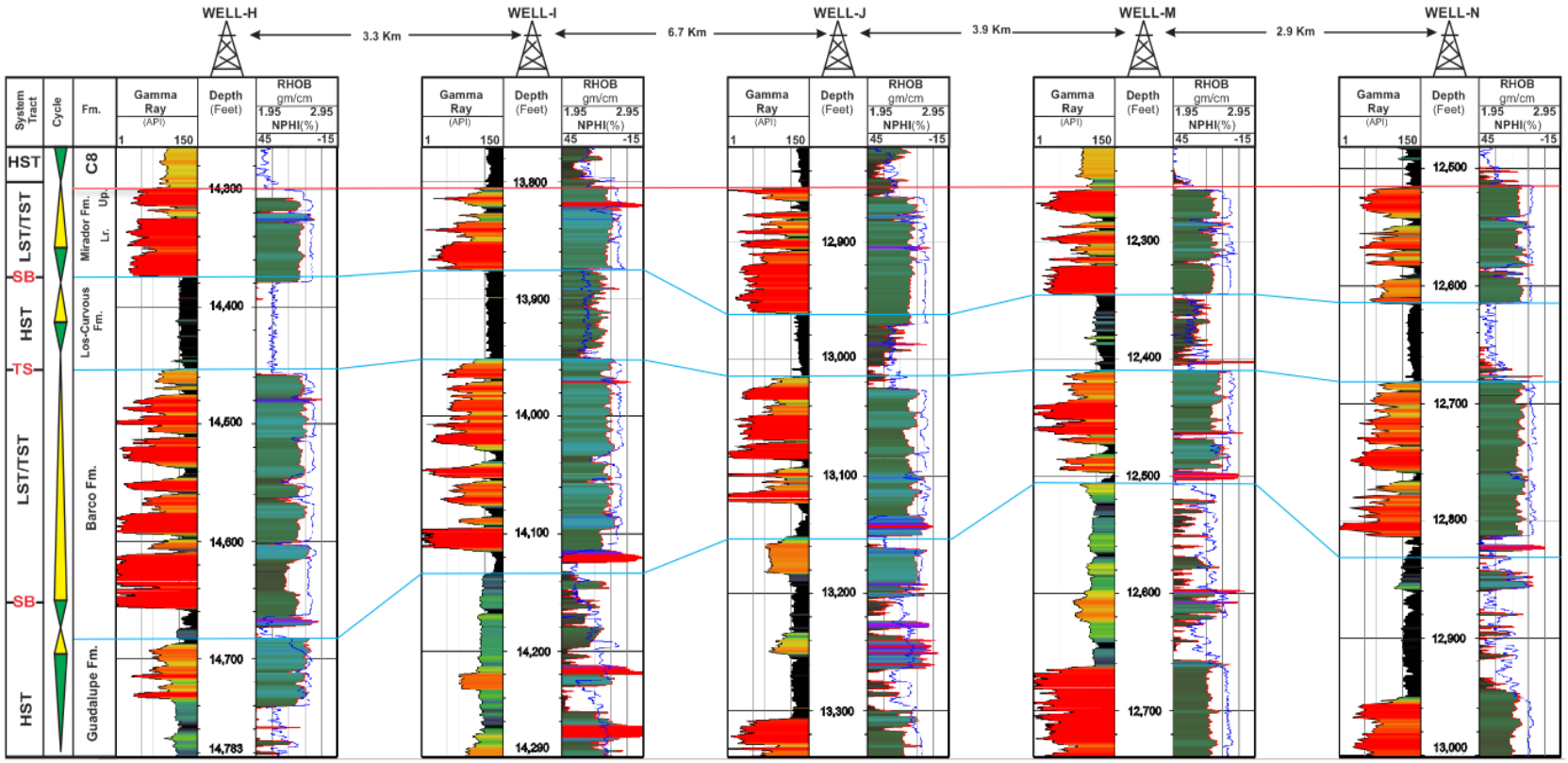

Figure 5.15 Well correlation of Paleogene Formations (Barco, Los Curvous, Maridor and Carbonera C8). The correlation is based on Normalized gamma - ray logs, and combination of neutron-density logs. The datum is the top of Maridor Formation. For location, see Figure 1

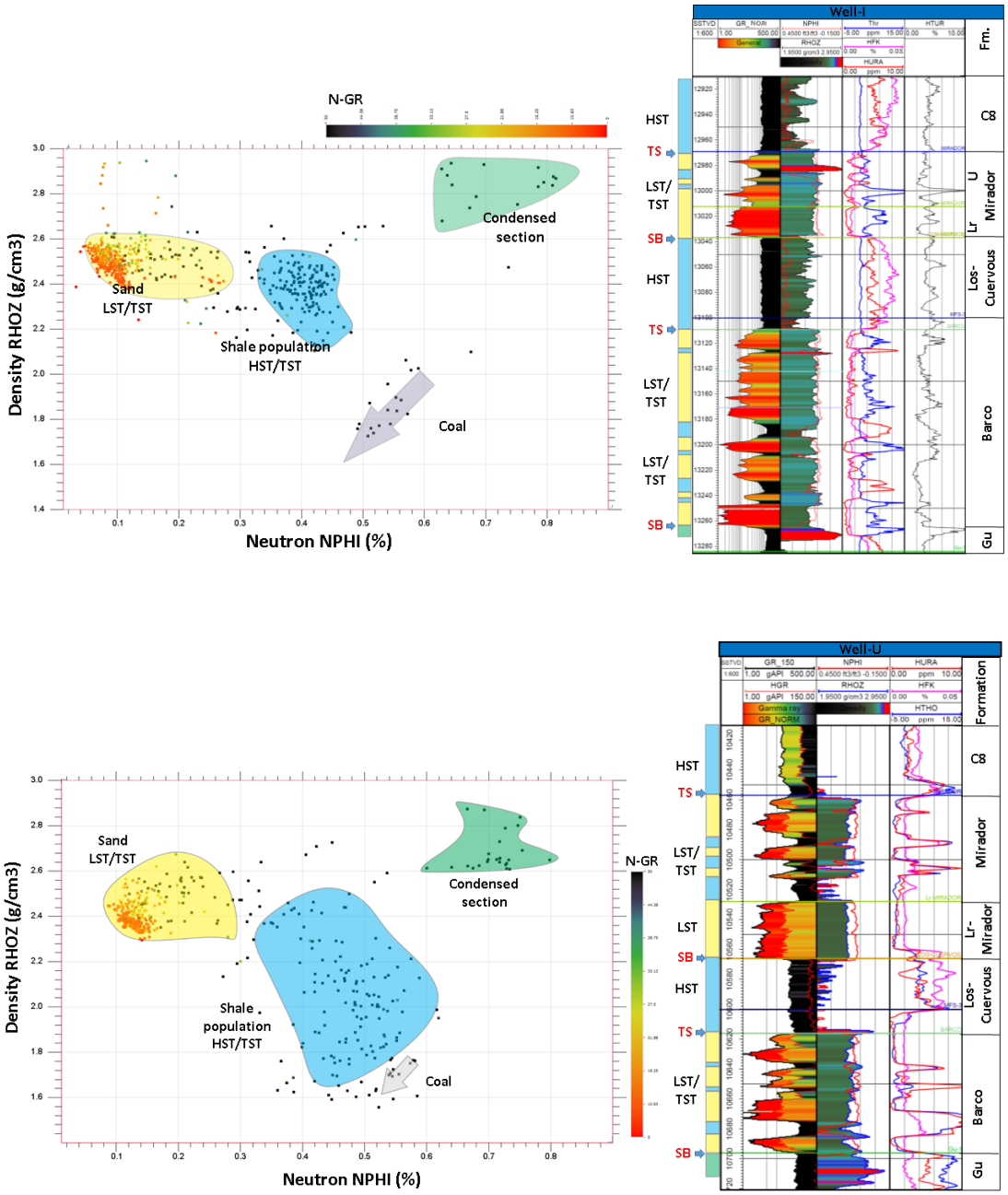

Figure 5.16 Z-plot of Paleogene sequence stratigraphy of Barco, Los Curves and Mirador Formations with the well logs. The logs are Normalized GR, Computed GR, Combination of Density (RHOZ) and Neutron (NPHI), Spectroscopy GR, Potassium (HFK) Thorium (HTHO) and Uranium (HURA). The Z-plot (Density vs Neutron vs GR) shows the clear cluster pattern coincided with sequence boundaries and systems tracts.

high neutron values. The shale composition changes from high to low radioactive (K and Th) in most of the wells and coincides with maximum flooding surfaces (MFS) as in Figure 18.

Very often pure clean sandstones, orthoquartzite, exhibit very low radioactivity since their thorium, uranium and potassium contents are very low too. This is generally assumed to be reworked sand and consequently a high chemically and texturally mature detrital deposit, with probably a medium to coarse grain size, and very well sorted (Schlumberger 1983). That coincides, to some extent, with Mirador Formation with very low radioactivity, with the exception of the lower part of the Lower Mirador Formation where there is high radioactivity thought to be a good indication of a sequence boundary.

5.6 CONCEPTUAL MODELS OF PALEOGENE FLUVIAL AND MARGINAL MARINE DEPOSITIONAL SYSTEM OF LLANOS FOOTHILLS, COLOMBIA

One of the main objectives of this paper was to build a conceptual depositional model of Paleogene reservoirs of the Barco and Mirador formations and predict the geometries of these reservoirs, reservoir heterogeneity and the upside potential stratigraphic traps in the study area. There is a diversity of opinions concerning the impact of changes in sea level on the sediments of continental settings (Shanley and McCabe, 1994). For fluvial systems there is an interrelationship between sediment grain-size distribution, and depositional models including braided or meandering systems and geometries. These geometries are functions of climate, varying sediment sources, presence of vegetation, and accommodation space controlled by tectonics and eustasy. Variations of accommodation space as a function of relative sea level change is the only factor common to all subaerial

settings at any given time (Posamentier and Vail, 1988). Within coastal plain settings, the concept of a graded stream profile plays a common role. The Shanley and McCabe (1993) model proposes that changes in fluvial sedimentology and geometry correlate with changes in marine and nearshore strata as a function of base level change. A similar model has been proposed by Wright and Marriott (1993) and modified later by Catuneanu et al. (2011). Local factors related to climate and tectonics complicate the application of sequence stratigraphy to fluvial strata if eustasy is assumed to be the dominant control on accommodation; for instance, further inland a fluvial system will be affected by relative sea level change more closely allied to tectonics (Posameniter and Weimer, 1993). Schumm (1993) suggested that base level changes tied to local tectonics affect the vertical position of a river to perhaps as much as 300 km inland using as an example the Mississippi valley. Koss et al., (1994) show that the base level changes are significantly linked to the fluvial deposition pattern and their proximity to the source area. These non-marine sequences are affected by the interaction between sediment supply, local tectonics and climate changes. Shanley and McCabe (1993) suggested that the fluvial systems within perhaps 100-150 km of the sea may be greatly changed by base level or relative sea level changes (i.e. the combined product of eustasy and tectonic movement)

In the Foothills of the Llanos Basin the vertical depositional architecture of the Paleogene Mirador, and Barco formation sedimentary reservoirs match many of the marginal marine fluvial deposits described in sedimentological literature. The most direct and relevant analogs are those found in mixed fluvial coastal marine strata of the Cretaceous western interior basin of Utah, USA proposed by Shanley and McCabe (1991, 1993 and 1995) and Blum and Tornqvist (2000). Shanley and McCabe (1995) also

extended the sequence stratigraphic model to the interpretation of the marine to fluvial sections of the Kaiparowits Plateau of South Utah. Starting at the base they noted the following pattern of deposition from stratigraphic bottom to stratigraphic top after each of their proposed sequence boundaries:

1) Deposition of coarse-grained, vertically and laterally amalgamated braided fluvial channels accompany a slow base level rise (the equivalent of a marine lowstand);
2) Deposition of tidally influenced fluvial channels accompanying a marine transgression;
3) Deposition of fine-grained, isolated, meandering fluvial channels encased in thick floodplain alluvium during a high rate of base level rise. This is the equivalent of an early marine highstand with accommodation that includes both eustatic and tectonic controls.

The Barco Formation (T20) accumulated over a condensed section of marine mudstone (Upper Guadalupe Mudstone Formation K90). The boundary between the Barco Formation (T20) and the Guadalupe Mudstone Formation is a third order sequence boundary (Figure 5.2) as indicated by the Z plots technique (Figure 18). The Barco Formation is composed (LST/TST) of a stack of incised valley deposits that collected during a slow base level rise equivalent to a marine LST (figures 12 through 15 and Figure 17). No significant tidal influence has been detected in the Barco Formation since usually the recognition of tidal influence would be more obvious in a down dip transition to an estuarine system However, a base level rise would be expected to promote the preservation of a complete fining upward channel unit associated with more rapid flood plain aggradation. This period of

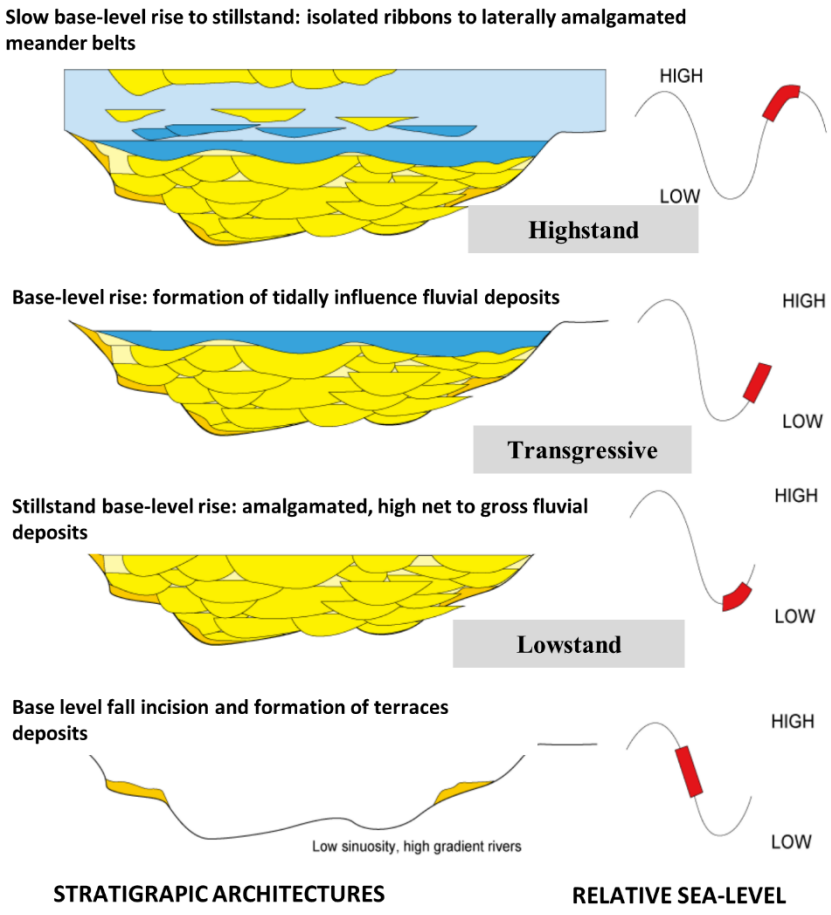

Figure 5.17 The general architecture of alluvial strata and the related systems tracts that develop over a base-level cycle (modified from Shanley and McCabe, 1993).

TST was associated with soils and flood plain peats (Emery and Myers, 1996) of a fluvial Lowstand systems tract.

The top of the Barco Formation is marked by a transgressive surface overlain by the progradation of an early highstand systems tract of the Los Cuervos Formation marine shale seen on the well logs and well log cross plots. This period of sediment accumulation is associated with increased rates of sediment supply and progressive reduction in accommodation space. The top of the Los Cuervos Formation accumulated as floodplain alluvium with minor channels in the upper portion of the section that collected during a high rate of base level rise equivalent to an early marine highstand. The Lower Mirador Formation (T30) overlies the Los Cuervos Formation and is composed of stacked incised valley deposits that collected during a slow base level rise equivalent to a marine LST (figures 17-19). As seen on well logs and a CWT spectral decomposition strata slice (Figure 11) the Lower Mirador Formation is composed of amalgamated braided fluvial channels. The limited accommodation space is interpreted to have promoted floodplain reworking during a slow rate of base level rise. This reworking by low and high sinuosity channel systems produced amalgamated channel sandstone stories similar to those of a fluvial lowstand systems tract (Emery and Myers, 1996). The Lower Mirador Formation was followed by a tidally influenced fluvial sediment package that accumulated during a marine transgression. Low gamma ray signal, density neutron logs, and well cross plots indicate carbonate minerals. The depositional setting of the Upper Mirador Formation (T30) is interpreted as the accumulation of a transgressive systems tract punctuated by high frequency lowstand events (Figure 10). In contrast, the lower Carbonera C8 suggests the accumulation of floodplain alluvium enclosing minor channels in the upper part of the

section that collected during a high rate of base level rise equivalent to an early marine highstand systems tract (Figure 9).

As seen in Figure 17, the Paleogene Llanos Foothills sequences have few similarities between the local accommodation and the eustatic sea level chart of Haq et al. (1987). This observation strengthens the interpretation that variations in the character of the Paleogene sequences in the Llanos Foothills are related to base level fluctuations predominantly caused by changes in the local rates of tectonic subsidence and only partially caused by eustatic sea level changes (e.g., Catuneanu et al., 2011 and Csato et al., 2012). As indicated earlier in the geologic setting of this paper, most previous authors have related variations in the Paleogene sequences to fluctuations in eustatic sea level (e.g., Cooper et al., 1995; Cazier et al., 1995) which this study suggests is mistaken. The top of Guadalupe Mudstone Formation is a third order sequence boundary followed by the LST/TST of the Barco Formation that accumulated during a slow base level rise equivalent to a marine lowstand systems tract.

The Barco Formation is overlain by the HST of the Los Cuervos Formation parasequence that was partially deposited as a marine shale. The upper part of the section accumulated as floodplain alluvium enclosing minor channels that formed during the high rate of base level rise equivalent to an early marine highstand. The top of Los Cuervos Formation and the base of the lower Mirador Formation is a fourth order sequence boundary. The Mirador Formation is a LST/TST parasequence deposited during a slow base level rise equivalent to a marine lowstand system tract. The upper Mirador Formation was followed by HST of the C8 Carbonera Formation parasequence that accumulated as

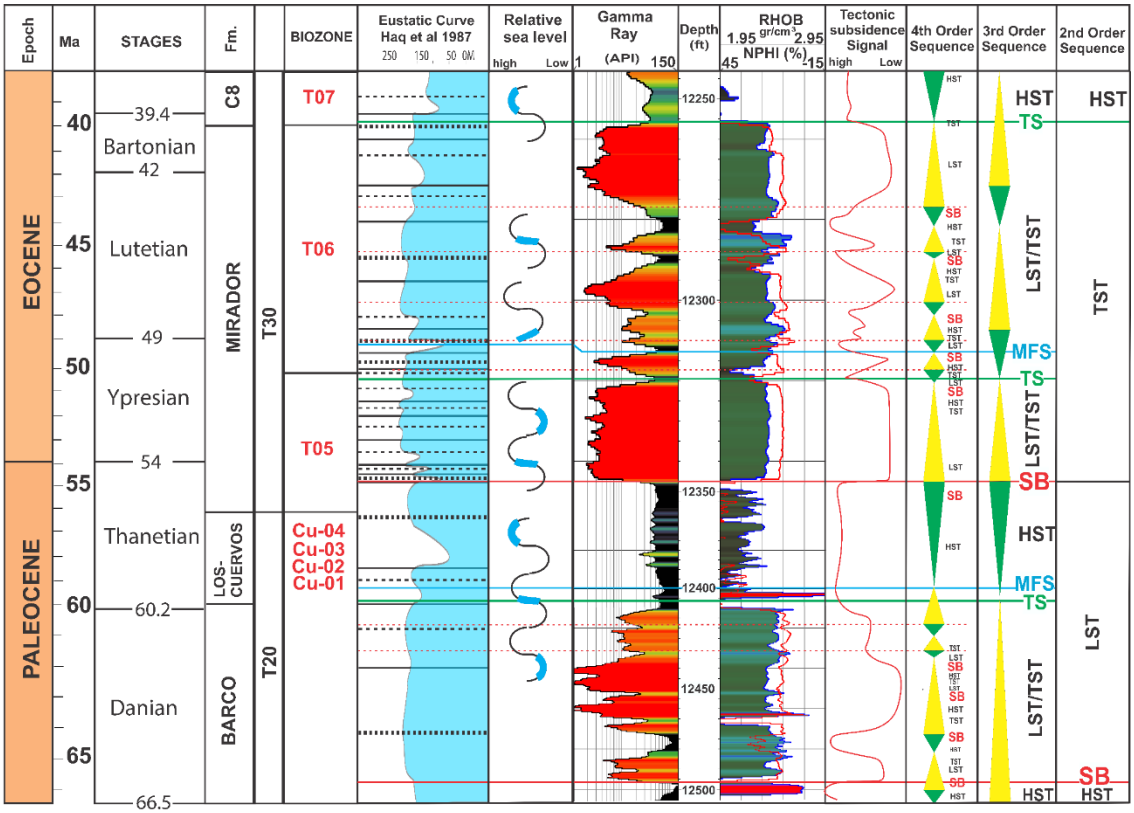

Figure 5.18 Llanos Foolhills Paleogene sequence stratigraphy of Barco, Los Curves and Mirador Formations. Biozon's after Jaramillo et al (2005) and Jaramillo et al (2015). Eustatic curve after Haq et al (1987).

floodplain alluvium enclosing minor channels in the upper part of the section that collected during the high rate of base level rise equivalent to an early marine highstand.

5.7 CONCLUSION

The integration of well-log character, seismic spectral decomposition and Z plots techniques to develop a sequence stratigraphic framework and depositional model for the Paleogene sequence of the Llanos Foothills demonstrates the power of these techniques for exploration. These include displaying logarithmic GR logs, singly or in cross-sections while interactively adjusting color fill to better identify lithofacies character and improve the interpretation of cyclicity and depositional settings.

Z plot techniques provide a means to establish the sequence stratigraphic boundaries and system tracts.

Attribute analysis using spectral decomposition permits distinction between meandering streams, braided fluvial accumulation, and marginal marine systems that transgress the fluvial domain.

The above techniques established a series of clastic depositional models for the Paleogene Formations, Llanos Foothills, Colombia that prior to the integration of the well-log character, seismic spectral decomposition and Z plots techniques were next to impossible to resolve.

The Barco Formation accumulated over a condensed section of marine mudstone (Upper Guadalupe Mudstone Formation). The boundary between the Barco Formation and the Guadalupe Mudstone Formation is a third order sequence boundary. The Barco Formation is composed of a stack of incised valley deposits during a slow base level rise equivalent

to a marine lowstand systems tract. The top of the Barco Formation is marked by a transgressive surface overlain by the progradation of a highstand systems tract of the Los Cuervos shale. The Lower Mirador Formation overlies the Los Cuervos shale and is composed of stacked incised valley deposits that collected during a slow base level rise equivalent to a marine lowstand systems tract. The Lower Mirador Formation was followed by a tidally influenced fluvial sediment package that accumulated during a marine transgression. The interpretation of the depositional setting of the Upper Mirador Formation suggests the accumulation of a transgressive systems tract punctuated by high frequency lowstand events. In contrast, the lower Carbonera C8 suggests the accumulation of floodplain alluvium enclosing minor channels in the upper part of the section that collected during a high rate of base level rise equivalent to an early marine highstand systems tract.

Exploration and production geologists should iteratively apply varying seismic volumes and spectral decomposition in the frequency domain to detect and map the character of fluvial systems. This approach established a series of fluvial depositional models for the Paleogene sequence of the Llanos Foothills, Colombia. The paper demonstrates that the integration of well log character and spectral decomposition is useful to detect and distinguish between meandering streams, braided fluvial accumulation, and marginal marine systems that transgress the fluvial domain.

The Paleogene Foothills of the Llanos Basin sequences shows few similarities in the local accommodation to the eustatic sea level chart of Haq et al. (1987). This observation

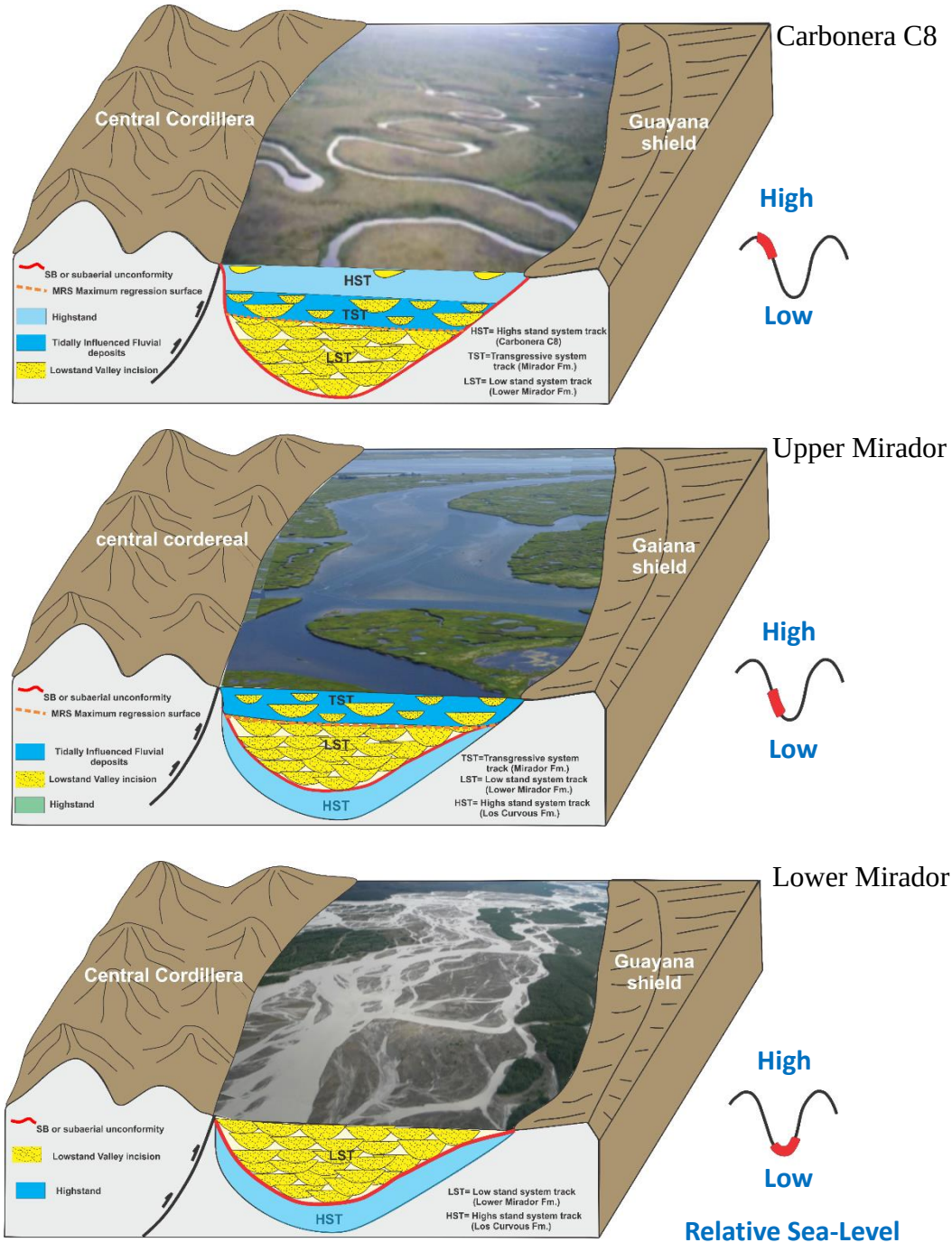

Figure 5.19 Conceptual Model of Paleogene Fluvial and Marginal Marine Depositional System of Llanos Foothills.

indicates that variations in the character of the Paleogene sequences in the Llanos Basin Foothills are related to base level fluctuations predominantly caused by changes in the local rates of tectonic subsidence and only partially caused by eustatic sea level changes.

CHAPTER VI

APPLICATION OF SEISMIC MATCHING PURSUIT DECOMPOSITION FOR ANALYSIS OF CENOZOIC TECTONIC HISTORY OF LIANOS FOOTHILLS, COLOMBIA.

6.0 OVERVIEW

This paper demonstrated how regional scale structures and tectonic movement have affected the character of the local sedimentary history and to explore the processes involved in producing the regional geomorphologic features. The workflow involves the use of Matching Pursuit decomposition of 3D seismic data to detect the subtle stratigraphic features undetectable in the time domain and tie these features with the regional geology of the eastern flank of the Eastern Cordillera. By using frequency decomposition techniques, we detect the first post-Eocene fluvial signal in Carbonera C7, which indicated the Late Oligocene uplift of the eastern flank of the Eastern Cordillera and marked the change from a marine setting for Carbonera C8 to a fluvial setting for Carbonera C7. An exploration workflow is proposed to use the spectral decomposition technique to identify potential reservoirs in the complex fluvial sediments of the Carbonera (C-7 and C-5, and C3), and Mirador formations south of the giant Cusiana oil field of the Llanos foothills.

6.1 INTRODUCTION

The Eastern Cordillera is a well-known example of a Cenozoic inverted orogeny (Colleta et al., 1990; Cooper et al., 1995; Mora et al., 2006). The timing of the Cenozoic uplift of the Eastern Cordillera is still controversial. The timing varies from the western to eastern foothills as well as along strike from north south to the Garzón Massif. There is clear agreement that the most rapid deformation of the Eastern Cordillera occurred during the Late Miocene, but studies suggest several deformation phases in the Eastern Cordillera throughout the Cenozoic (e.g., Parra et al 2009a, b; Mora et al., 2010b; Horton et al., 2010; Mora et al., 2013; and Reyes-Harkeret al., 2015). However, timing of the Cenozoic uplift of the Eastern Cordillera ranges from Paleogene to Neogene according to some authors. Coarse facies deposition was directly attributed to Andean orogenesis in late Miocene (Cooper et al., 1995), Oligocene according to Bande et al. (2012), and Paleocene by Bayona et al. (2008). Based on detrital zircon ages from the Carbonera Group in the eastern foothills of the Eastern Cordillera, Horton et al. (2010b) concluded that uplift-induced recycling of basin fill was well under way by the latest Oligocene to early Miocene (26-23 Ma).

This paper focuses on the Cenozoic fluvial depositional systems of the Eastern Foothills of the Eastern Cordillera south of the Cusiana oil field (Figure 1) using HDSF spectral decomposition techniques in order to date the activation of several thrust systems.

The workflow involves the use of Matching Pursuit decomposition of 3D seismic data to detect the subtle stratigraphic features undetectable in the time domain and tie these features with the regional geology of the eastern flank of the Eastern Cordillera. The goals

of this paper have been to better understand how regional scale structures and tectonic movement have affected the local sedimentary history. The workflow in this paper will determine a Cenozoic tectonic model for the eastern flank of the Llanos foothills suggesting possible targets to drill and test, using Frequency spectrum and acoustic signals to predict hydrocarbon distribution.

6.2 CENOZOIC STRATIGRAPHY

The Eastern Cordillera represents a Cretaceous extensional basin system that was inverted during the Cenozoic Andean orogeny (Colletta et al., 1990; Cooper et al., 1995 Mora et al., 2006; Sarmiento-Rojas et al., 2006).

By the Early Cretaceous, considerable accommodation space was created in the Eastern Cordillera. Late Jurassic to Early Cretaceous rifting generated basaltic intrusions, thinning of the lithosphere, and shallowing of the mantle (Ojeda, 1996). Throughout the Cretaceous period the rifting phase was followed by thermal subsidence (Pindell and Tabbutt, 1995; Ojeda, 1996).

From the Early Cretaceous to Late Cretaceous period, deposition of sediments in the Eastern Cordillera area was almost entirely in a marine setting. The synrift Une Formation (Figure 6.2) accumulated from the Early Cretaceous until the Cenomanian and is composed of sandstones deposited in shallow marine conditions (Linares, et al., 2009).

In the Late Cretaceous, a global sea level rise (Haq et al., 1987) combined with postrift thermal subsidence accommodated the marine mudstones of the Gacheta Formation

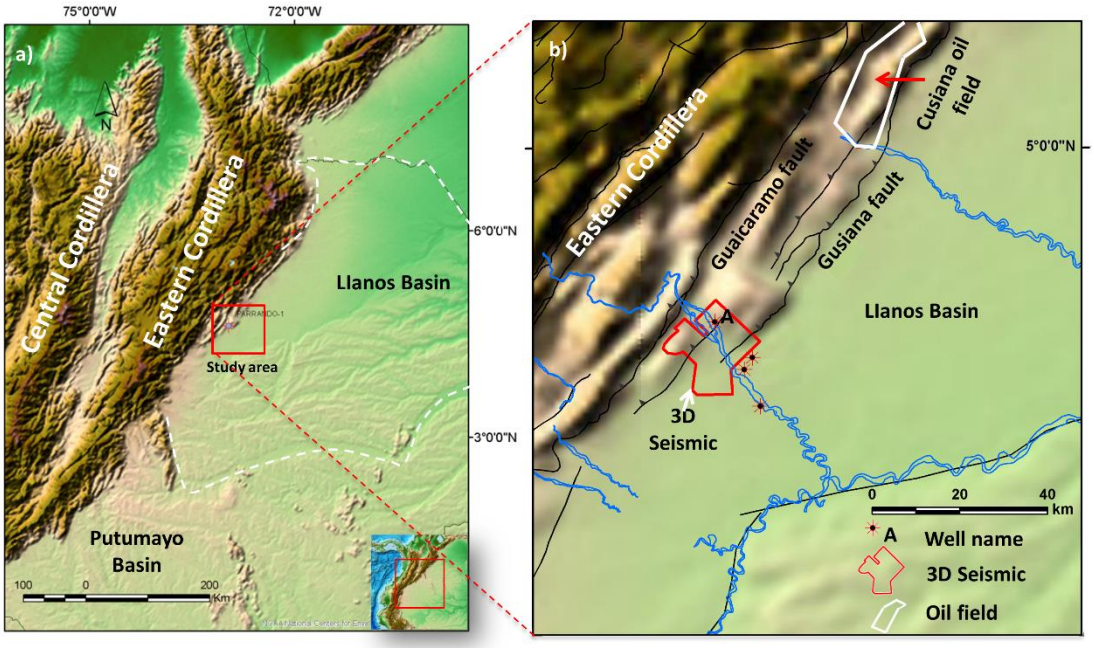

Figure 6.1 Location map of study area: Eastern Cordillera, Llanos Basin, Guaicaramo and Cusiana faults and the location of the 3D seismic volume.

(Figure 6.2), a prolific source rock that is contemporaneous with the La Luna Formation (Pindell and Tabbutt, 1995).

A drop in sea level during the Campanian-Maastrichtian accompanied the accumulation of the Guadalupe Group on a shallow marine shelf (Linares, et al., 2009). The Guadalupe Group is predominantly a progradational sandstone unit that progressively thins toward the east and is considered one of the deep reservoir units in the Foothills (Cazier et al., 1995). Late Cretaceous subsidence in the Eastern Cordillera area was mostly driven by lithospheric cooling, water loading, and horizontal compressional stresses resulting from the collision of oceanic terranes in western Colombia (Sarmiento-Rojas et al., 2006).

Deformation resulting from the accretion of the oceanic terranes of the Western Cordillera from Late Cretaceous to early Palaeocene marked a significant change from a shallow marine to continental setting in an incipient foreland basin (Sarmiento-Rojas et al., 2006). This foreland basin likely developed as a result of the topographic load of the Central Cordillera, a volcanic arc that formed as part of the Farallon plate subduction complex along the west coast of Colombia (Cooper et al., 1995). Starting in the middle Paleocene, the basal transgressive Barco Formation accumulated as a fluvial to distributary channel sandstone that was interbedded with shales that accumulated during marine flooding events (Linares, et al., 2009). In the late Paleocene, a relative high stand in sea level initiated with the deposition of Los Cuervos Formation, which is composed mostly of shale intercalated with sandstones, siltstones, and coal beds (Linares, et al., 2009). Cooper et al., (1995) indicated that the Los Cuervos Formation accumulated in a regressive, mud-dominated coastal plain system. A major drop in relative sea level at approximately 54 Ma ended Los Cuervos Formation deposition and created a hiatus in the Cusiana area

that lasted approximately 16 m.y. (Cazier et al., 1995). However, according to a palynological study by Jaramillo et al. (2009) there is no unconformity surface at the contact between Los Cuervos and Mirador formations.

In the Eocene, the Mirador Formation accumulated during a transgression which originated in the foreland basins to the west and north. The Mirador Formation was deposited in two stages interrupted by a regional unconformity (Martinez, 2006). Tidal channel sandstones overlap fluvial channel sandstones (Linares, et al., 2009). The base of the Mirador Formation in the Llanos Foothills was dated with an age of ca. 55 Ma, whereas in the Llanos Basin the Mirador Formation was dated as 42 Ma to 29 based on palynological data (Jaramillo et al., 2009). The Mirador Formation is the main reservoir for the Cusiana and Cupiagua areas, and the thickness of the Mirador sequence decreases eastward from the Llanos Foothills to the Llanos Basin (Cooper et al 1995).

The Mirador Formation in the Llanos basin and Llanos Foothills is very diachronous and not continuous across the Llanos Basin (Jaramillo et al., 2009). This is due to the fluvial stratigraphic miscorrelation and awkward nomenclature of the Mirador Formation. It looks like the Mirador Formation (Eocene) existed only in the Llanos Foothills area and the younger (Oligocene) sand in Llanos basin is more likely a lower Carbonera Formation (C8). However, based on sequence stratigraphy framework ties with spectral decomposition attribute analysis we consider C8 as high stand system tract as a upper part of the Mirador sequence.

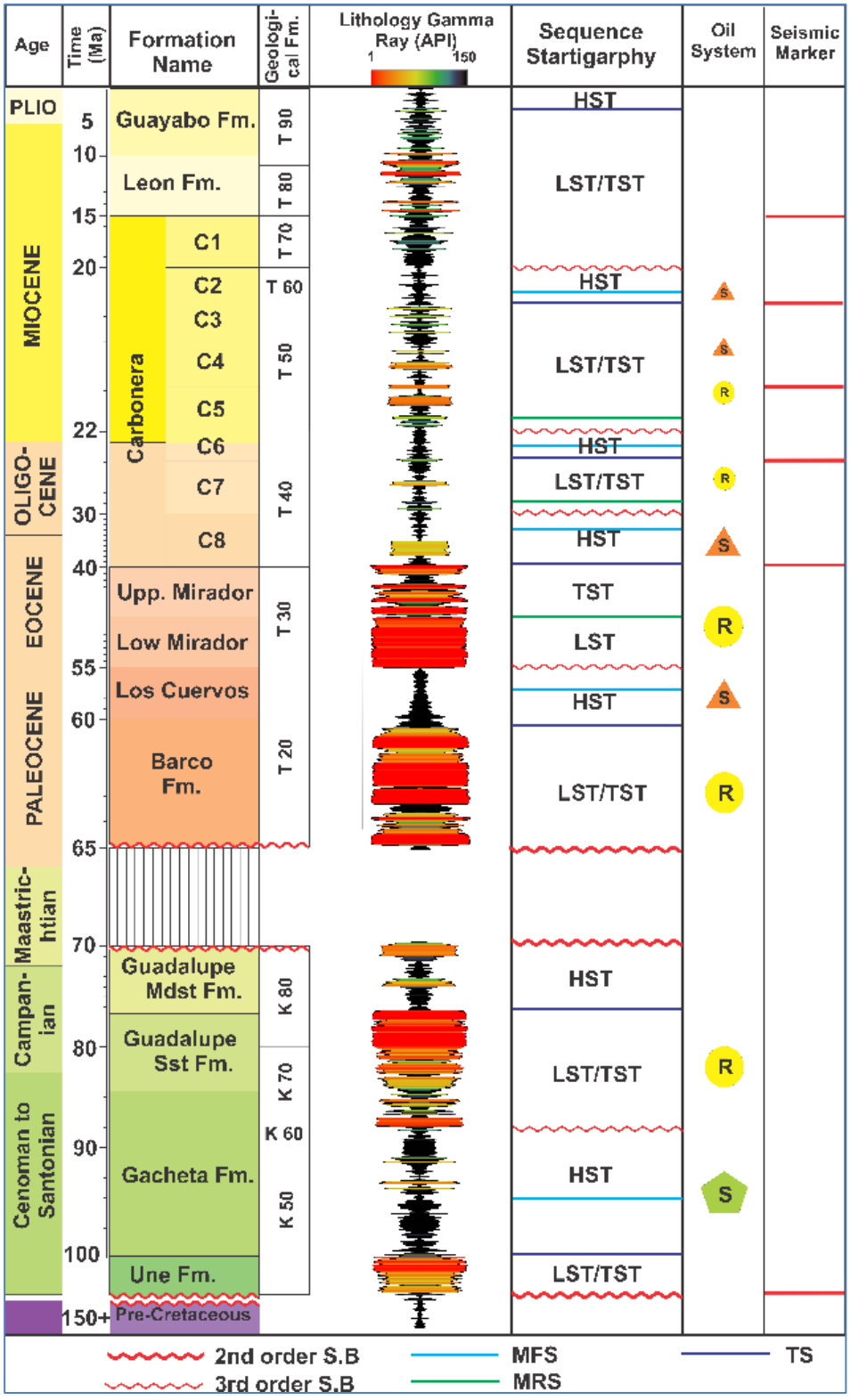

Figure 6.2 Generalized stratigraphic column, sequence stratigraphy and petroleum systems of the Llanos Foothills.

Ramon and Fajardo (2006) identified short, intermediate and long-term cycles in the Mirador Formation. Short-term (high-frequency) cycles correspond to progradational-aggradational units. Six intermediate-term cycles were identified by the stacking patterns of their component short-term cycles and by the general trend of facies successions. Two long-term cycles were defined from the stacking patterns of the intermediate term cycles and by the general trend of facies successions. The lower half of the Mirador Formation consists of coastal-plain facies tracts and is composed of channel, crevasse splay, and swamp and flood-plain facies successions. A bay facies tract occurs in the upper half of the Mirador Formation and is composed of bay-fill, bay-head delta, and channel facies successions.

The Carbonera Group accumulated within the Late Eocene (~ 40Ma) to Early Miocene (15 Ma) (Jaramillo and Dilcher, 2000, 2001; Parra, 2008; Parra et al., 2009; and Parra et al., 2010). The C8 horizon accumulated within the Late Eocene T-07 bio-zone (~ 40-30 Ma), the C7-C6 horizons accumulated within the Oligocene T-10-Ca-7 bio-zones (~30-22 Ma), and the C5-C2 horizons accumulated in Early Miocene (22-20 Ma).

Cooper et al. (1995) described the Carbonera Formation as produced by four major cycles of marine-influenced lower coastal plain deposition that occurred in the Llanos basin and foothills and was bounded by widespread maximum flooding surfaces. Each cycle consists of a mud-dominated highstand systems tract followed by a thin, forced retrogradational systems tract, and ended with a sand-prone transgressive systems tract that culminates with the maximum flooding surface.

Based on lithology and sedimentary structures, Parra et al. (2009a) subdivided the lower Carbonera Formation C8-C6 into 15 lithofacies and four facies associations in the Medina

Basin just west of the study area. Parra et al. (2010) recognized the same four facies associations for the Lower Carbonera Formation (C5-C1) that represent tidally influenced deltaic, lacustrine, alluvial plain and braided fluvial sedimentary settings. They considered the Lower Carbonera Formation C8-C6 as a syntectonic wedge, while the upper Carbonera Formation was syntectonic with growth-strata relationships that were rocks equivalent to C5-C2 west of the Medina Basin along the Lengupa fault. This coincided with the progressive isolation of the Llanos Basin in the east from the Magdalena Basin in the west (Mora et al., 2013; Reyes-Harker et. al 2015). They proposed a new chronostratigraphic framework for the C8-C6 members of Carbonera Formation based on palynological zonation (T-05 to Ca07) which are of early Eocene – early Miocene age.

A global rise in sea level followed the deposition of the Carbonera Group in the middle Miocene (Haq et al., 1987), leading to accumulation of the Leon Formation shales over the Llanos basin. It should be noted that the Leon Formation is shaly and thicker (~1000m) in the Llanos basin, whereas it is relatively thinner and more sandy toward the Llanos Foothills.

6.3 RESEARCH METHODS

6.3.1 POST-STACK DATA CONDITIONING

Noise is often a problem in post stack seismic data that makes the interpretation task harder and slower. Applying post stack data conditioning can improve data quality and make the interpretation easier and quicker. However, the GeoTeric seismic interpretation package has three different filters all structurally oriented that follow the regional dip. These filters works in different ways that more effective with different types of noise

(random, coherent and aggressive noise) with three-filter sizes (small, medium and large). The post stack data conditioning improves reflector continuity for a more complete interpretation and increases signal to noise ratio for better attribute responses. Figure (6.3) shows the seismic before and after post-stack noise cancelation.

6.3.2 SPECTRAL ENHANCEMENT (POST-STACK SPECTRAL ENHANCEMENT)

Post-stack data spectral enhancement improves reflector continuity for a more complete interpretation, increases signal to noise ratio for better attribute responses, and enhances seismic resolution to better image thin-bed events (Figure 6.4). It does not apply a band pass filter but rather a minimum distance algorithm to match the data to the target curve. Post-stack data spectral enhancement provides a statistical table with the relevant information required to understand what effects spectral shaping is having on your data (Figure 6.5). Post-stack data spectral enhancement will reveal distinct layers that tie with Gamma Ray log response where the original data does not separate these out. However, in areas where we have a thick well preserved low frequency zone and the thin layers fit with the Gamma Ray log response, using post-stack data spectral enhancement enhanced the high frequency thin bed information and maintained the low frequency information. Figure 6.6 shows the seismic before and after post-stack data spectral enhancement and how the spectral enhancement improved thin bed resolution.

6.3.3 FREQUENCY DECOMPOSITION AND RGB BLENDING TECHNIQUES

Spectral decomposition has been used to determine layer thicknesses (Partyka, 1999, 2011), stratigraphic geometries (Marfurt and Kirlin, 2001), and direct hydrocarbon

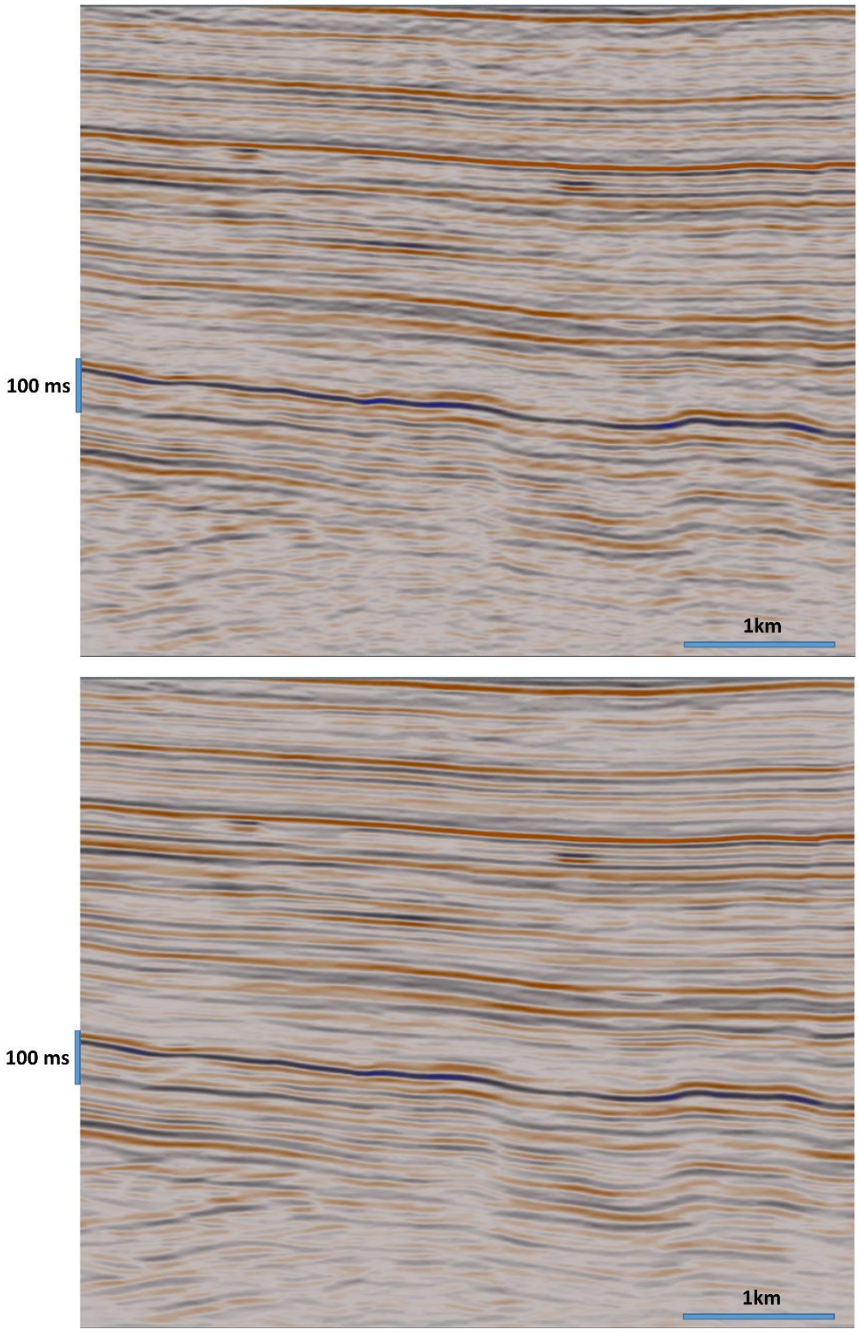

Figure 6.3 Post stack noise cancelation, a) before b) after structurally oriented coherence noise cancelation (Filter size 9)

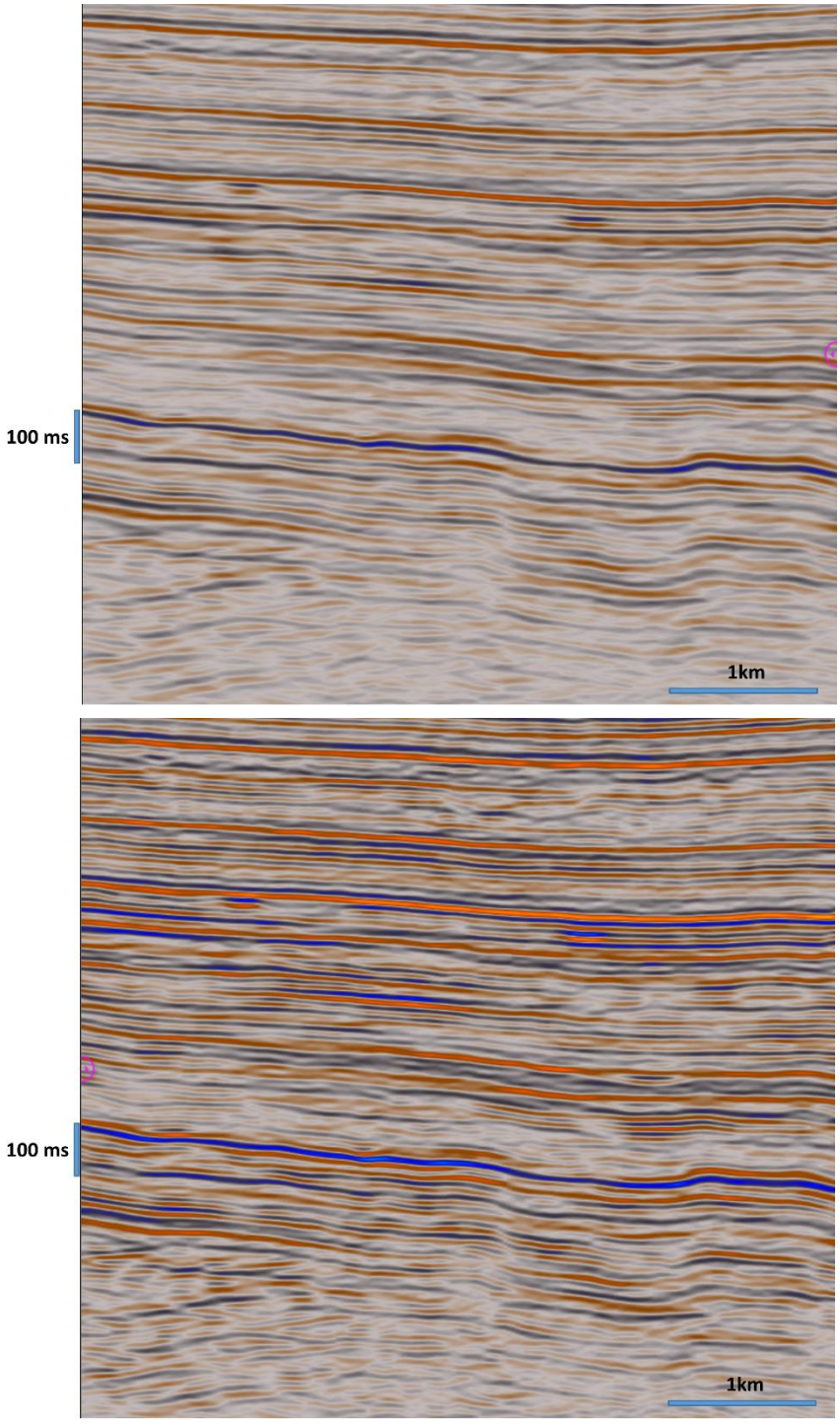

Figure 6.4 . Post-stack data spectral enhancement, a) before b) after

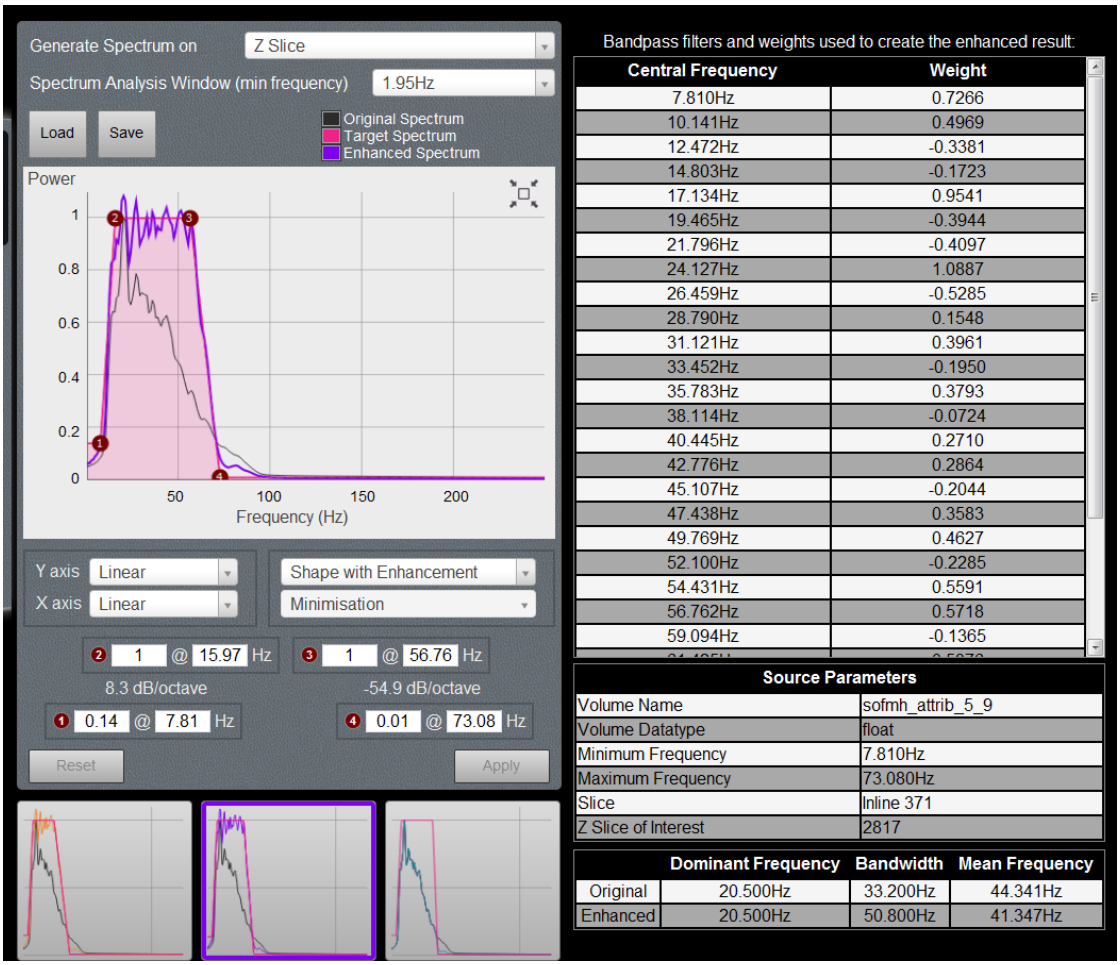

Figure 6.5. Post-stack spectral enhancement statistical table with the relevant spectral enhancement information.

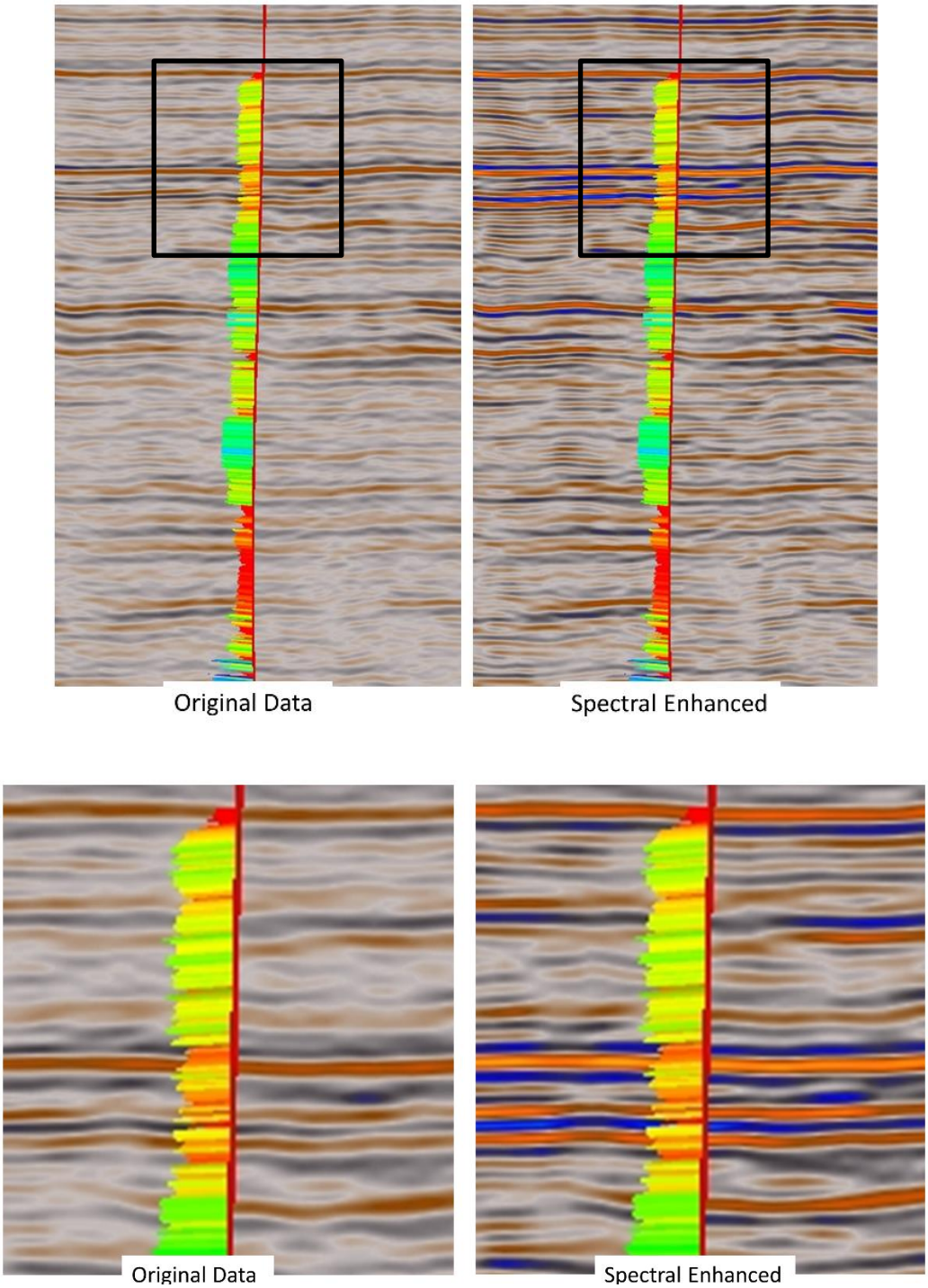

Figure 6.6 Original (left) vs Spectral Enhanced (right) seismic data shows how the post-stack data spectral enhancement reveals distinct layers that tie with Gamma Ray log response where the original data does not separate these out.

indicators (e.g., Goloshubin et al., 2002; Castagna et al., 2003; Sinha et al., 2005; Welsh et al., 2008; Yu et al., 2011). Additionally, spectral decomposition breaks the seismic signal into narrow frequency sub-bands or horizons (Partyka, 2011). This is achieved by transforming the seismic data from the time domain into frequency domain (Chopra and Marfurt, 2015).

Spectral decomposition includes short time Fourier transforms (STFT) and continuous wavelet transforms (CWT) and the Matching Pursuit algorithm. Each of these has its advantages and disadvantages, and selection depends on the objectives of the workflow. For instance, the STFT transformation depends on the time gate, a drawback for the transformation method (Sinha et. al., 2005). On the other hand, the CWT method is unlike the conventional SFFT method, which limits the time-frequency resolution by a predefined window length (Sinha et. al., 2005). Narrow windows give good time resolution but poor frequency resolution, whereas wide windows give good frequency but poor time resolution. However, to a certain extent, CWT solves the dilemma of resolution if one can choose the mother wavelet which works best for the seismic data (Morlet, Gaussian, and Mexican Hat or Ricker). This choice depends on the 3D seismic interpretation package used. High definition frequency decomposition (HDFD) using Matching Pursuit algorithm is the best technique at the reservoir scale to solve the vertical resolution problem. However, short time Fourier transforms (STFT), also known as constant bandwidth, show the most separation of frequency, but with the lowest vertical resolution, whereas high definition frequency decomposition (HDFD) has the greatest vertical localization but does not show

the same frequency separation through its RGB interference pattern (McArdle and Ackers, 2012).

There is always a trade-off between vertical resolution and frequency resolution, which is governed by the uncertainty principle, so there is a time when you would choose one method over the other depending on the purpose of the study. Figure 6.7 shows the different vertical and frequency resolution for the STFT, CWT and MP spectral decomposition methods.

Spectral decomposition and RGB blending can be used on the enhanced data to reveal more geologic information and understand fluvial reservoir heterogeneity and thickness variations. According to Laughlin et al. (2003), typical amplitude maps are dominated by the frequency content of seismic data and best image stratigraphy with thickness related to the dominant frequencies processed. Figure 6.8 shows the interrelationship between thin-bed tuning and the amplitude of spectral components through an idealized channel. In thin reservoirs with varying thickness, seismic data with a higher dominant frequency would highlight the thinner parts of the reservoir on amplitude maps, while seismic with a lower dominant frequency would highlight the thicker parts on an amplitude map.

Conventional analysis through animation of spectral components and generation of many output volumes at 1 Hz increments between 15 and 75 Hz (Partyka et al., 1999) quickly fills the available disk space. Even after reducing sampling to every 10 Hz, it is still awkward to simultaneously deal with 7 common frequency volumes. However, after

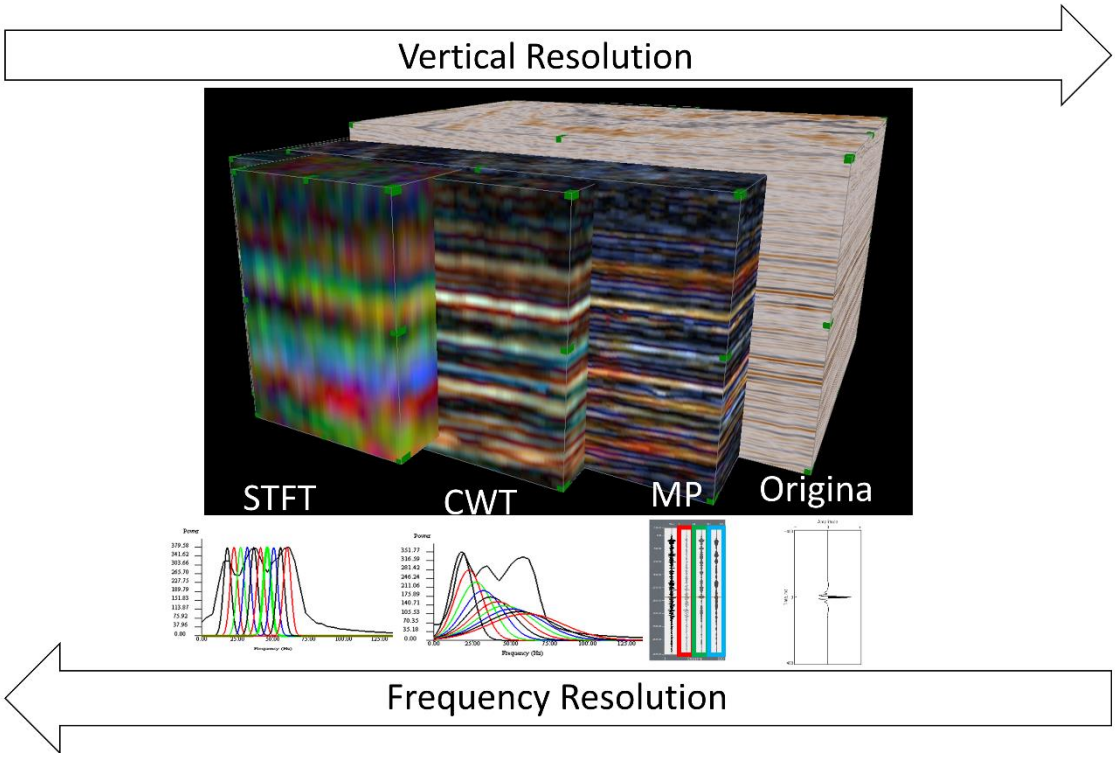

Figure 6.7 Shows the different types of frequency decomposition and the different in vertical and frequency resolutions between the STFT (short time Fourier transforms), CWT (continuous wavelet transforms) and MP (Matching Pursuit) spectral decomposition.

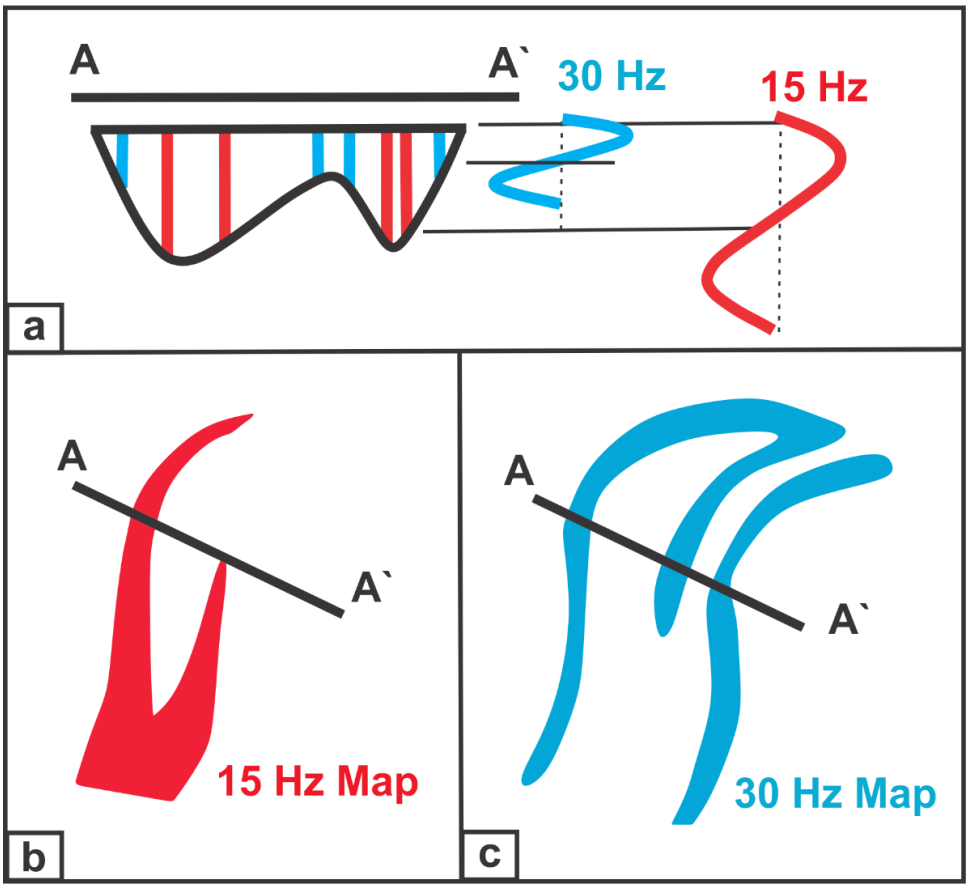

Figure 6.8 Interrelationship between thin-bed tuning and the amplitude of spectral components in thin reservoirs through an idealized channel. (a) A vertical cross section, and (b) spectral components at a lower frequency and (c) spectral components at a high frequency, shown in map view. In the center of the channel, thin-bed tuning occurs at the lower frequencies (in red). On the thinner flanks, thin-bed tuning occurs at the higher-frequency components (in blue) modified from Laughlin et al. (2003).

the animation of spectral components of the seismic volumes, you can pick three dominate frequencies and blend them by RGB.

The traditional problem in frequency decomposition is how to extract the dominant frequencies. By using the Broadband high definition frequency decomposition (HDFD) of GeoTeric® software, you can determine the best frequencies to generate a high definition RGB blend to understand geologic features hidden in the time domain seismic volume. The HDFD Trace Spectrogram allows us to focus on the horizon of interest and adjust the RGB bands to best highlight frequency anomalies, such as channels in the RGB blend. The spectrogram is calculated using Matching Pursuit Algorithm (Mallat and Zhang, 1993).

The dominant frequencies change from one horizon to another through the HDFD Trace Spectrogram. The HDFD Trace Spectrogram shows stacked channels between 3100 ms and 2400 ms. In the Mirador Formation for instance, there are two stacked fluvial channel systems, which we can cover with a frequency spectrum of 18 Hz, 34 Hz, and 51 Hz (Figure 6.9). In contrast, the best dominant frequencies for channel systems in Carbonera C3 are 20 Hz, 45 Hz, and 60 Hz (Figure 6.10)

The dominant frequencies of channel systems in Carbonera C7 are represented by 21 Hz, 42 Hz, and 60 Hz (Figure 6.11). You can compromize dominate frequencies for the whole sequence, but if you need a better result, you have to focus on specific horizons because each channel system reacts differently.

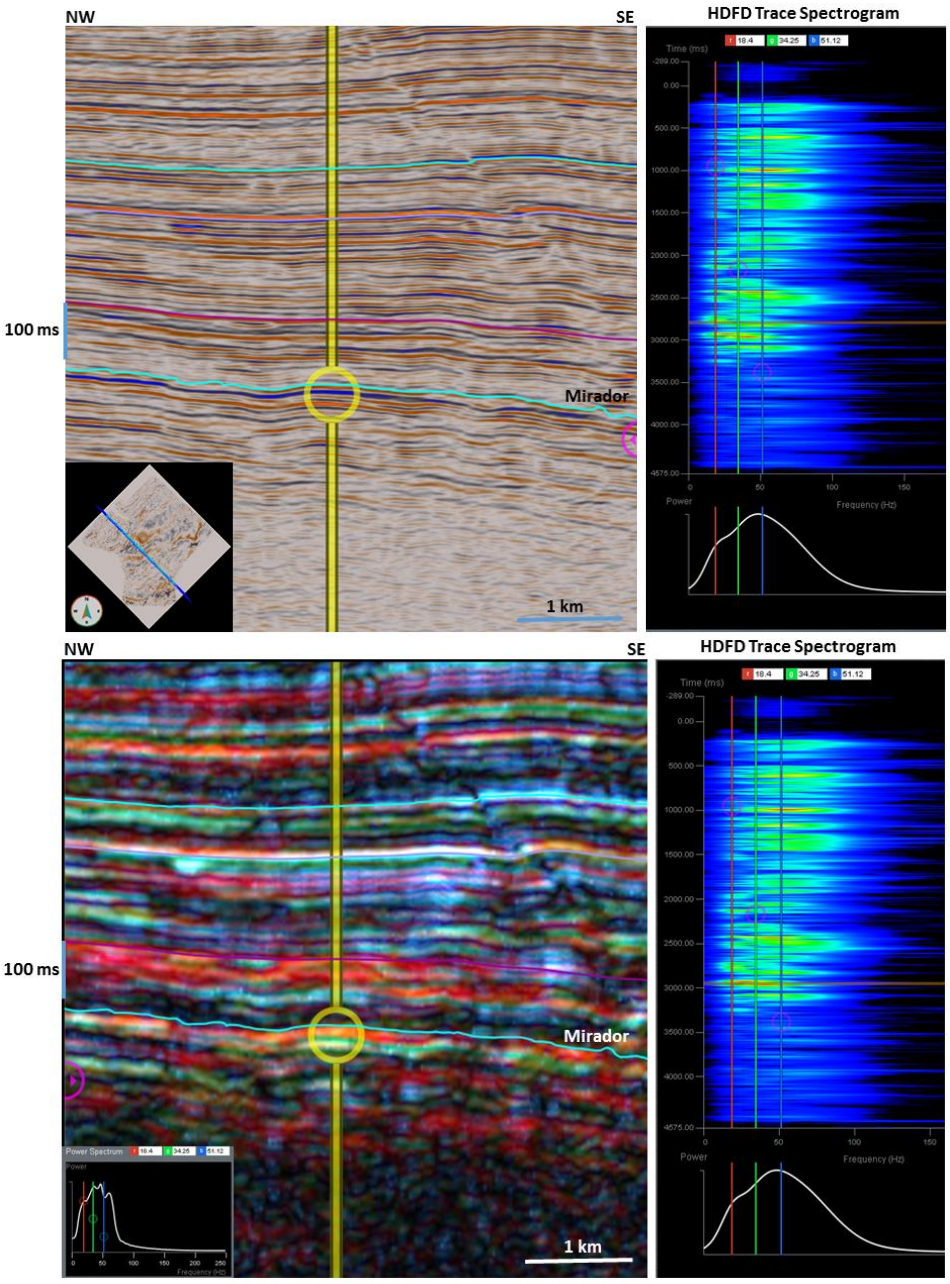

Figure 6.9. Spectral Enhanced (top) seismic data and Matching Pursuit spectral decomposition (bottom) each with HDFD Trace Spectrogram showing stacked channels at 3000 ms in the Mirador Fm., with frequency spectrum 18 Hz, 34 Hz, and 51 Hz.

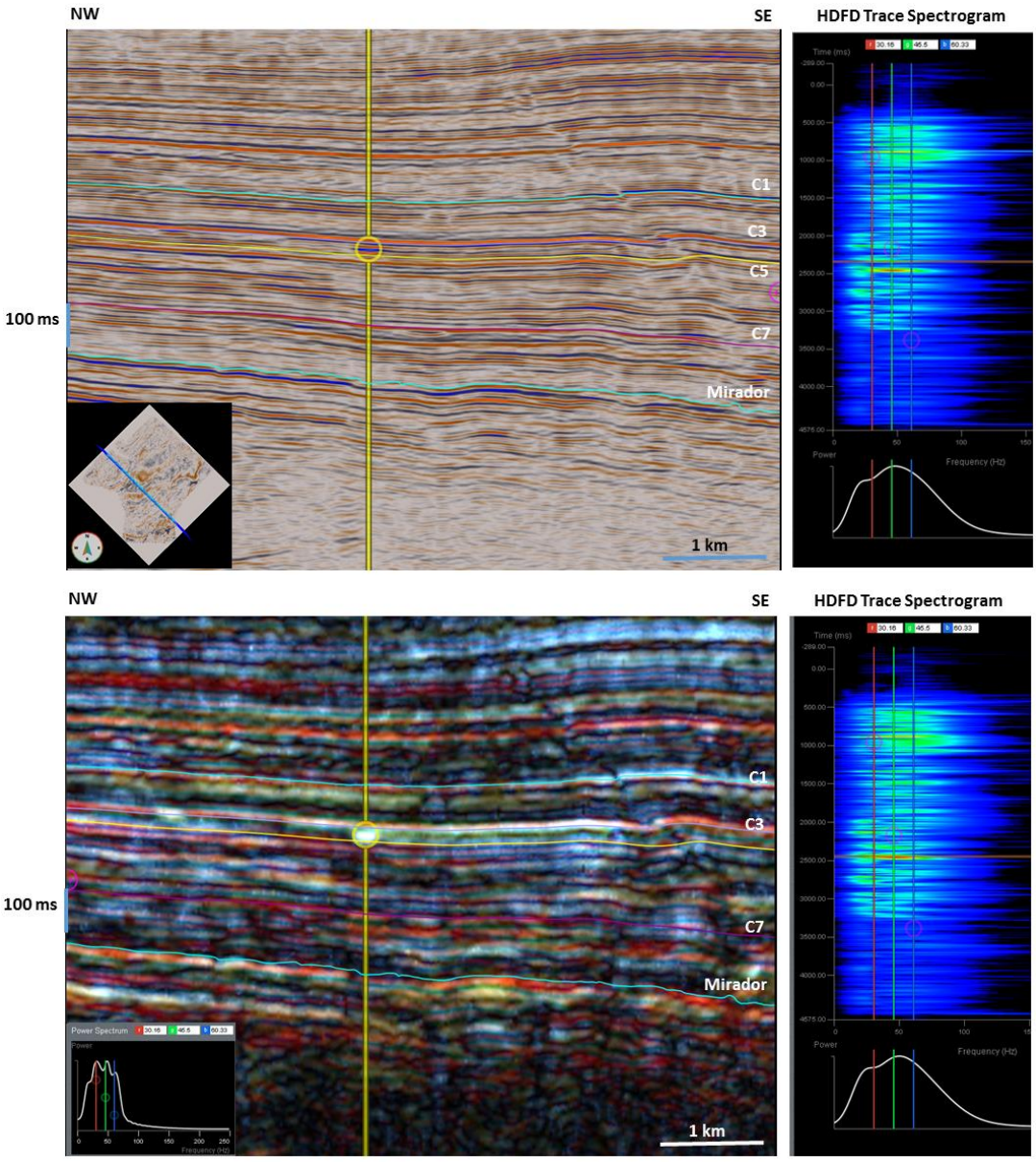

Figure 6.10. Spectral Enhanced (top) seismic data and Matching Pursuit spectral decomposition (bottom) each with HDFD Trace Spectrogram showing a channel at 2500 ms in Carbonera C3, with frequency spectrum 20 Hz, 45 Hz, and 60.

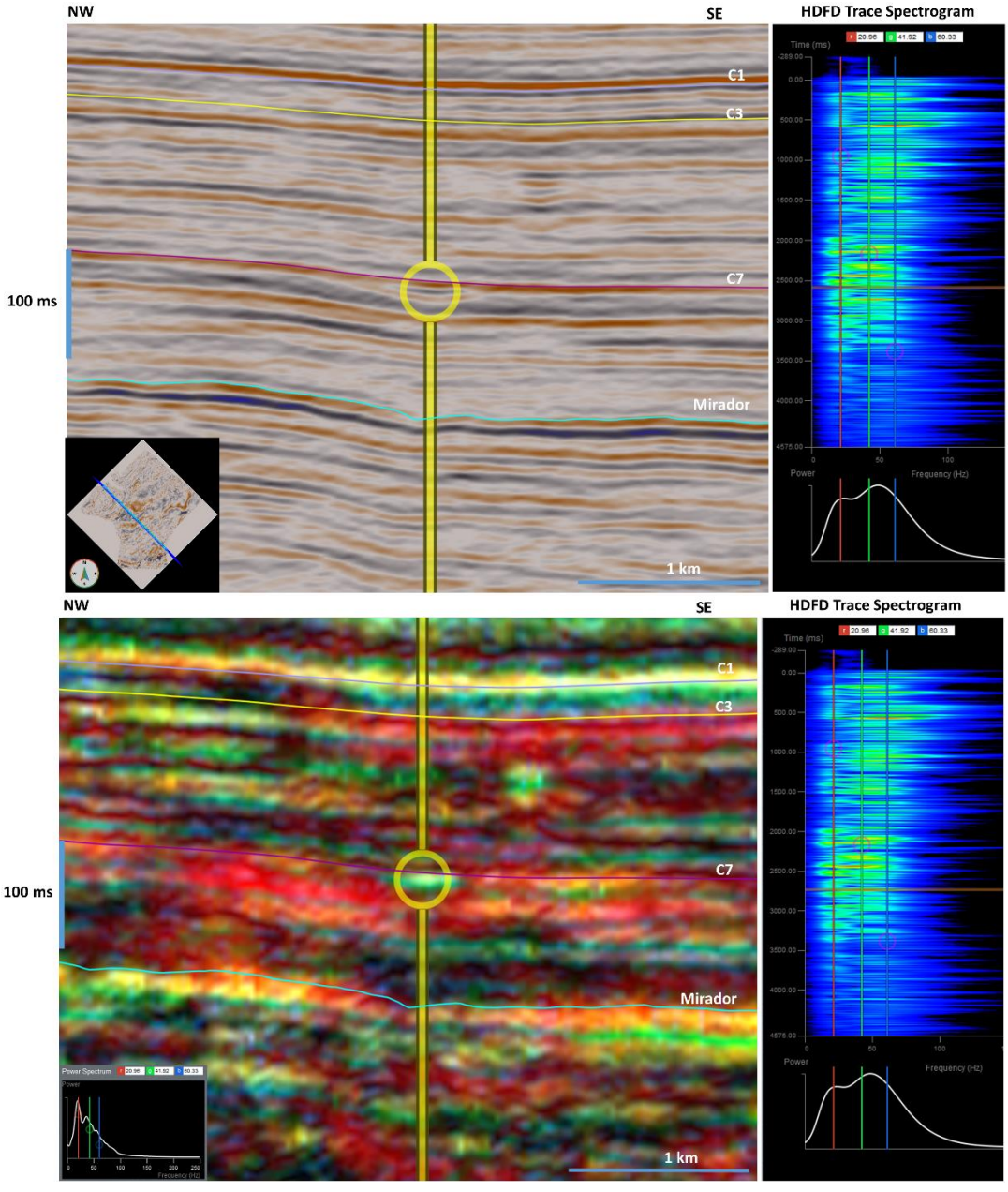

Figure 6.11. Spectral Enhanced (top) seismic data and Matching Pursuit spectral decomposition (bottom) each with HDFD Trace Spectrogram showing a channel at 2700 ms in Carbonera C7., with frequency spectrum 21 Hz, 42 Hz, and 60 Hz.

6.4 RESULTS AND DISCUSSION

Spectral decomposition, especially HDFD, is a powerful tool that was used in this study to map the fluvial systems in the Cenozoic sequences and capture the complicated paleocurrent orientations of the sandier horizons of C7, C5, C3, and Mirador Formation.

Post stack data conditioning can provide volumes with improved signal to noise, allowing interpreters to make better use of automatic pickers and modern voxel detection technology but cannot correct systematic errors introduced through inaccurate velocity analysis and migration.

HDFD Trace Spectrogram solves the dilemma of determining the best frequencies to generate a high definition RGB blend to understand geologic features hidden in the time domain seismic volume. The HDFD Trace Spectrogram allows us to focus on the horizon of interest and adjust the RGB bands to best highlight anomalies such as sand channels in RGB, instead of the animating the seismic volume as described by Partyka et al. (1999).

A modern fluvial analog of the Carbonera Formation is the Ucayali River system of Peru, which shows a complicated fluvial system which shifts enormously in less than 30 yr. as displayed in YouTube films capturing shifts during 5 km/year intervals (Ucayali River Peru, 1985-2013) (https://www.youtube.com/watch?v=izgc3vFimP8). In contrast, the Carbonera Formation accumulated over 35 Ma, and by spectral decomposition techniques we were able to show some of the complicated fluvial systems formed. However, The Cenozoic Carbonera stream size and shape is comparable to that observed in the present-day fluvial settings of North Andes Rivers such as the Ucayali River in Peru and Quebrada La Gritona in northern Colombia and even the Yukon River in Alaska.

The HDFD spectral decomposition of the Carbonera C7 horizon is characterized by high-sinuosity channels oriented NE to SW with widths ranging from 120 m to 200 m. developed parallel to the present Llanos Foothills (Figure 6.12). These channels flowed with the regional drainage of the Oligocene Proto-Orinoco river system (Villamil, 1999).

The HDFD spectral decomposition of C-5 strata shows a low-sinuosity wide channel oriented NNW-SSE with widths ranging from 425 m to 760 m. (Figure 6.12). The channel cuts through the present foothills and the older fluvial system in C7. The channel lacks sharp edges, but it is very clear in almost all the attributes, including Envelop and RMS.

The HDFD spectral decomposition of C3 strata is characterized by high-sinuosity channels incised through the large channel in C5. The channels flow from NW to SE cutting through the edges of the earlier channel with widths ranging from 90 m to 200 m. (Figure 6.12).

The drainage switches from longitudinal channels in Carbonera C7 to transverse channels in Carbonera C5 and C3. In addition, the drainage switches from low sinuosity to high sinuosity channels within the thick fluvial system of the C5-C3 horizons. A key observation related to the C5 horizon is that there is a change in spectral strata that suggests an evolution from braided fluvial accumulation to a meandering fluvial system in the overlying C3 horizon. These changes in geometric character document a change in slope gradient, sediment source, and tectonic activity to that of the present day Eastern Cordillera.

Many authors observed the occurrence of both longitudinal and transverse rivers in mountain belts (e.g., Van der Beek el al., 2002; Ramesy el al., 2008; Babault et al., 2012).

De la Parra et al. (2015) used reworked pollen to establish the intensity of Cenozoic reworking and its relationship to tectonic evolution of the Llanos Foothills and Llanos basin of Colombia. They correlate the peaks of the reworked palynomorphs to Cenozoic tectonic phases of the eastern Andes. Based on these correlations they proposed a tectonic model showing two stages for the evolution of the Eastern Cordillera modified after Babault et al. (2013). A late Eocene-Oligocene stage of shallow detachments was accommodated by longitudinal drainage whereas the late Miocene activation of deep detachments was characterized by a more mature transverse drainage (De la Parra et al., 2015). We used the tectonics model that proposed by De la Parra et al. (2015) but with a context of HDSF spectral decomposition (Figures 6.12 and 6.13). The drainage switches from longitudinal channels in Carbonera C7 to transverse channels in Carbonera C5 and C3.

Using HDSF spectral decomposition identify that the C7 channels flow a regional drainage of the late Oligocene river system (structurally control) which is produced by a thin-skinned tectonics whereas C5-C3 channels cross-cutting the present day of Eastern Cordillera due to Early Miocene thick-skinned (Figure 6.13).

The drainage pattern of the Mirador Formation shows consistency with the overlying Carbonera C7. The Carbonera C7 represented the first fluvial signal of the uplift of the eastern flank of the Eastern Cordillera and marked the change from the marine setting of C8 to the fluvial setting of C7. This coincided with detrital zircon ages from the Carbonera Formation in the eastern foothills of the Eastern Cordillera by Horton et al. (2010b) which concluded that uplift-induced recycling of basin fill was well under way by the latest Oligocene to early Miocene (26-23 Ma). Mora et al. (2013) suggested that the oldest signal of exhumation in the eastern flank of the present-day Eastern Cordillera started between

20 and 30 Ma along faults such as the Servita Fault. However, this Late Oligocene-Early Miocene uplift generated a new drainage system parallel to the eastern flank of the Eastern Cordillera, the "Proto-Orinoco river system" that received sediments from the Guayana Shield to the east and the Eastern Cordillera to the west (Villamil, 1999). Many studies demonstrated that exhumation was ongoing by the Oligocene in the domain of the entire ancestral present Eastern Cordillera (Parra et al. 2009b; Horton et al. 2010b; Mora et al. 2010b, 2011; Mora et al., 2013 and Silva et al., 2013). All of this strengthens our HDFD spectral decomposition of longitudinal channels of Carbonera C7 (Figures 6.12 and 6.13) that accumulated during eastward migration of thin-skinned deformation of the Oligocene C7 as documented by Parra et al. (2009b), Mora et al. (2013) and De la Parra et al. (2013).

The drainage pattern of Carbonera C5-C3 shows a dramatic change in slope gradient, sediment source, and tectonic activity to that of the present day Eastern Cordillera. The HDFD spectral decomposition of Carbonera C5–C3 shows transverse channels that accumulated during deep detachments and topographic growth of the Eastern Foothills in Early Miocene (Figures 6.12 and 6.13). The drainage switches from low sinuosity to high sinuosity channels within the thick fluvial system of the C5-C3 horizons. A key observation related to the C5 horizon is that there is a change in spectral strata that suggests an evolution from braided fluvial accumulation to a meandering fluvial system in the overlying C3 horizon which is reflected in a change in slope gradient, sediment source, and tectonic activity in the early Miocene.

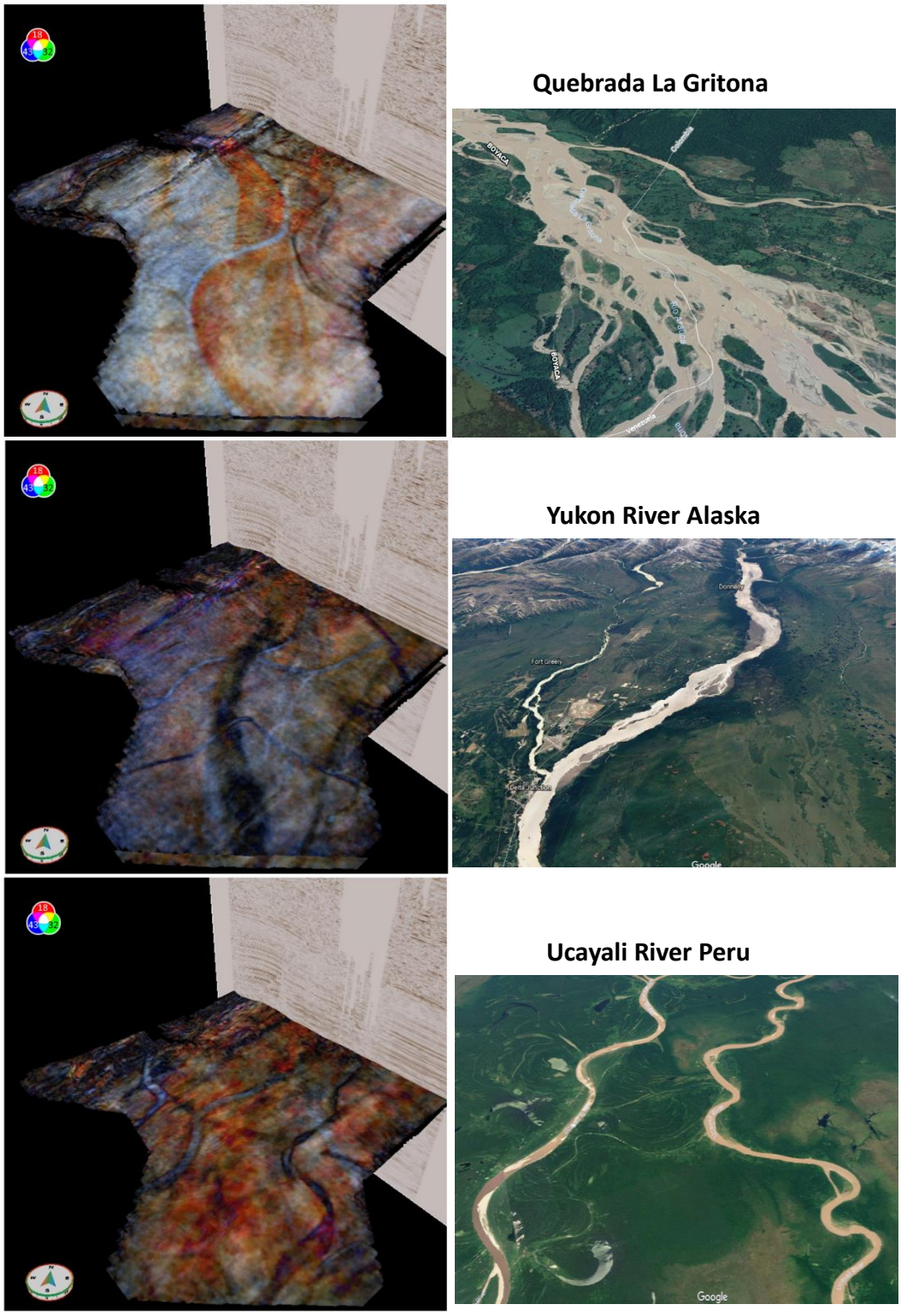

Figure 6.12. HDDF Spectral decomposition (Matching Pursuit) of Carbonera Fm. from bottom C7, C5 (middle), and C3 (top) in narrow frequency bands around 43 Hz as blue, 32 Hz as green and 18 Hz as red. Note the longitudinal channels in C7 and the transverse channels in C5 and C3 crossing the present Eastern Cordillera. The Carbonera stream sizes and shapes are comparable to that observed in the present-day fluvial setting.

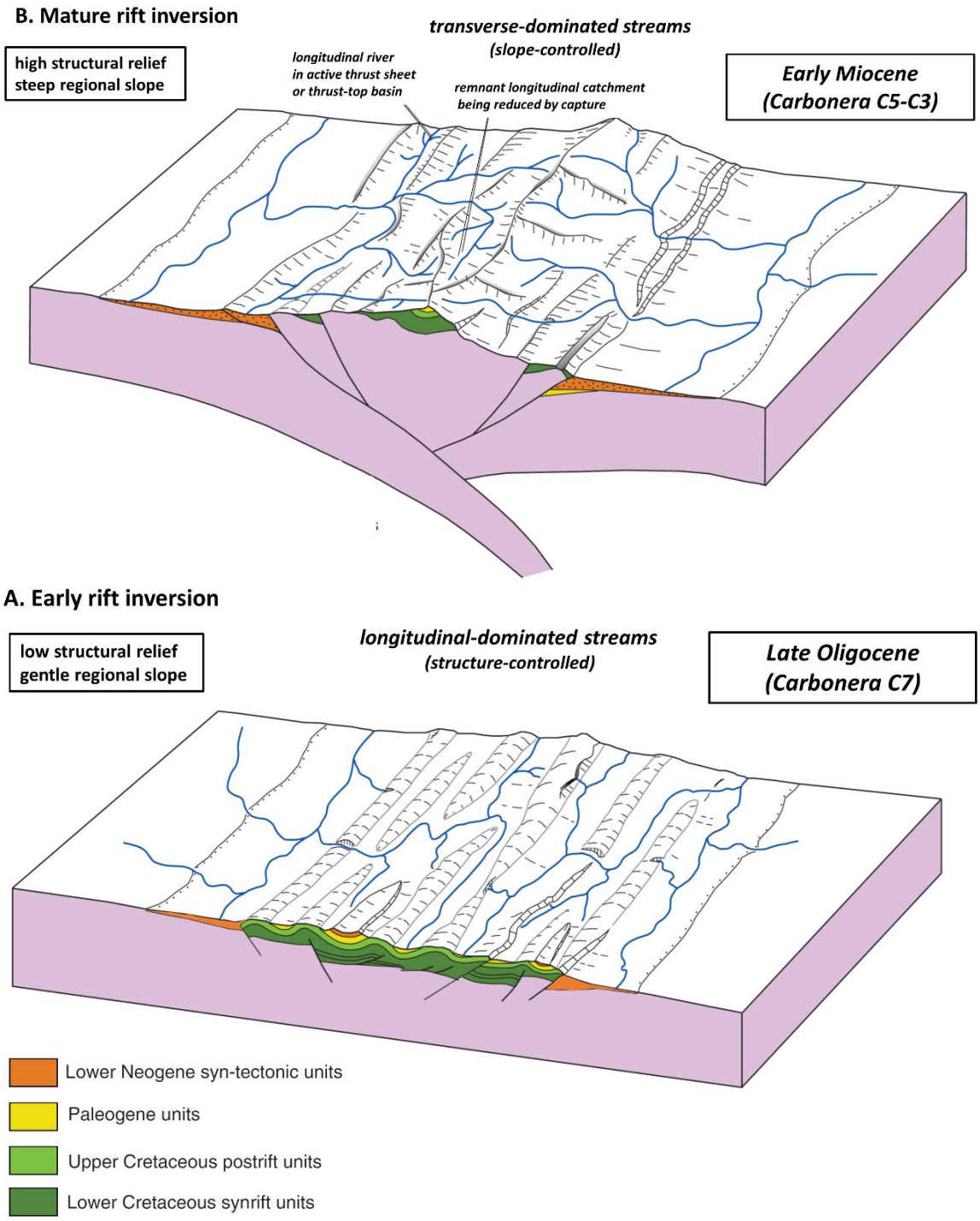

Figure 6.13. Conceptual model of the two stages of fluvial drainage versus tectonic structure and regional slope in the Eastern Cordillera. The evolution from a) longitudinal (late Oligocene Carbonera C7) to b) transverse drainage (early Miocene Carbonera C5-C3) modified after de la Parra et al., (2015).

By late Oligocene to early Miocene, the Farallon plate had broken up into the Nazca and Cocos plates and a new spreading center formed, resulting in increased convergence rates at the plate margins (Wortel and Cloetingh, 1981; Wortel, 1984; Lonsdale, 2005). Farris et al. (2011) suggest that the tectonic collision of the Panama´isthmus actually began by the Late Oligocene which also correlates with recent data on mountain building in the Eastern Cordillera (e.g., Mora et al., 2013; Silva et al., 2013; Reyes-Harkeret al., 2015). The timing, direction, and magnitude of shortening indicate that the Panama arc collision was an important driver for the Andean orogeny in the Eastern Cordillera.

6.5 CONCLUSIONS

In this paper, we describe the tectonic configuration of a segment of the eastern flank of the Eastern Cordillera of the Colombian Andes based on a new frequency decomposition (Matching Pursuit) study of 3D seismic data.

Matching Pursuit decomposition of 3D seismic data helps us understand how regional scale structures and tectonic movement have affected the local geomorphologic history as well as understanding the processes and mechanisms that produced the regional drainage systems. Frequency decomposition techniques identify and detect the first fluvial signal of the Late Oligocene (Carbonera C7) uplift of the eastern flank of the Cordillera with longitudinal drainage. The abrupt change of the regional drainage systems associated with C5-C3 (Early Miocene 22-20 Ma) in the spectral decomposition slices shows transverse drainage cross cutting the present day Eastern Cordillera. Our observations support recent studies showing tectonics events through the Oligocene to Early Miocene along the eastern

flank of the Eastern Cordillera (e.g., Parra et al., 2009b; Horton et al., 2010b; Mora et al., 2010b, 2011; Mora et al., 2013; Silva et al., 2013 and De la Parra et al., 2013).

However, the Cenozoic Carbonera streams size and shape is comparable to that observed in the present-day fluvial setting of North Andes Rivers such as the Ucayali River in Peru and others.

REFERENCES

Agencia Nacional de Hidrocarburos, 2010. Mapa de anomalias de bouguer total de la Republica de Colombia [map]. Bogota, Colombia: Graterol, V.R. (in Spanish).

Aguilera, R., Sotelo V., Burgos, C., Arce, C., Gómez, C., Mojica, J., Castillo, H., Jiménez, D., and Osorno, J. 2010. Organic geochemistry atlas of Colombia, 2nd edition: Earth Sciences Research Journal, Special Edition, v. 14, 174 p.

Allen, P. A., & Allen, J. R., 2005, The petroleum play. Basin Analysis, Blackwell Publishing, second edition, p. 405-474.

Anderson, V.J., Horton, B.K., Saylor, J.E., Mora, A., Tesón, E., Breecker, D.O., and Ketcham, R.A., 2016. Andean topographic growth and basement uplift in southern Colombia: Implications for the evolution of the Magdalena, Orinoco, and Amazon river systems: Geosphere, v. 12, no. 4, p. 1235–1256, doi:10.1130/GES01294.1.

Babault, J., J. Van Den Driessche, and A. Teixell, 2012, Longitudinal to transverse drainage network evolution in the High Atlas (Morocco): The role of tectonics: Tectonics, v. 31, no. 4, TC4020, 15 p., doi:10.1029/2011TC003015.

Bakioglu, B., 2014. Garzón Massif Basement Tectonics: A Geophysical Study, Upper Magdalena Valley, Colombia, Master Thesis, University of south Carolina, 66 p.

Bande, A., Horton, B. K., Ramirez, J. C., Mora, A., Parra, M., and Stockli, D.F., 2012, Clastic deposition, provenance, and sequence of Andean thrusting in the frontal Eastern Cordillera and Llanos foreland basin, Colombia: Geological Society of America Bulletin, v. 124, no. 1-2, p. 59-76, doi:10.1130/B30412.1.

Barrero, D., Pardo, A., Vargas, C. A. and Martínez, J. F., 2007. Colombian Sedimentary Basins: nomenclature, Boundaries and Petroleum Geology, a New Proposal. Agencia Nacional de Hidrocarburos, Bogotá, Colombia. 91.

Bayona, G., Cortés, M., Jaramillo, C., Ojeda, G., Aristizabal, J. J., Reyes-Harker, A., 2008. An integrated analysis of an orogen-sedimentary basin pair: Latest Cretaceous–Cenozoic evolution of the linked Eastern Cordillera orogen and the Llanos foreland basin of Colombia. GSA Bulletin 120, 1171–1197, doi: 10.1130/B26187.1.

Bayona, G., Jaramillo, C., Rueda, M., Reyes-Harker A. & Torres, V., 2007. Paleocene-Middle Miocene flexural-margin migration of the nonmarine Llanos foreland basin of Colombia.CT&F Ciencia, Tecnología y Futuro, v. 3 (3). p. 141-160.

Behar, F., M. Vandenbroucke, Y. Tang, F. Marquis, and J. Espitalie´, 1997, Experimental cracking of kerogen in open and closed systems: determination of kinetic parameters and stoichiometric coefficients for oil and gas generation: Organic Geochemistry, v. 26, p. 321-339.

Blum, M.D. and T.E. Törnqvist, 2000. Fluvial responses to climate and sea-level change: a review and look forward. Sedimentology 47 (Suppl.1): 2-48

Bogota-Ruiz, J., 1988. Contribucion al Conocimiento Estratigrafico de al Cuenca de los Llanos, Colombia: III Simposio Exploracion Petrolera en las Cuencas Sun-Andinas, p.308-346.

Bridge, J.S. and R. S. Tye, 2000. Interpreting the dimensions of ancient fluvial channel bars, channels, and channel belts from wireline-logs and cores. American Association of Petroleum Geologists Bulletin 84: 1205-1228.

Brown, A. R., 2011. Interpretation of three-dimensional seismic data, 7th ed.: AAPG Memoir 42 and SEG Investigations in Geophysics No. 9,

Buitrago, J., 1994. The Petroleum system: From source to trap. In Chapter 30: Part V. Petroleum Systems of the Neiva Area, Upper Magdalena Valley, Colombia. Case Studies--Western Hemisphere (pp.483 – 497). Tulsa: Magoon & Dow.

Bustamante, C., Cardona, A., Bayona, G., Mora, A.R., Valencia, V., Gehrels, G.E., and Vervoort, J., 2010. U-Pb LA-ICP-MS geochronology and regional correlation of Middle Jurassic intrusive rocks from the Garzón Massif, Upper Magdalena Valley and Central Cordillera, southern Colombia: Boletin de Geologia, v. 32, p. 93–109.

Butler, K., & Schamel, S., 1988. Structure along the eastern margin of the Central Cordillera, Upper Magdalena Valley, Colombia. Journal of South America

Cant D. J., 1992. Subsurface facies analysis in Walker R. G., and James N. P., ed., Facies Models, response to sea level change. Geological Association of Canada, p. 27-45.

Castagna, J. P., S. Sun, and R. W. Siegfried, 2003, Instantaneous spectral analysis: Detection of low-frequency shadows associated with hydrocarbons: The Leading Edge, 22, 120–127.

Catuneanu, O. 2002. Sequence stratigraphy of clastic systems: concepts, merits, and pitfalls Journal of African Earth Sciences, Volume 35, Issue 1, Pages 1-43.

Catuneanu, O., Galloway, W.E., Kendall, C.G.St.C., Miall, A.D., Posamentier, H.W., Strasser, A., Tucker, M.E., 2011. Sequence stratigraphy: methodology and nomenclature. Newsletters on Stratigraphy 44 (3), 173e245.

Cazier, E.C., A.B. Hayward, G. Espinosa, J. Velandia, J-F. Mugniot, and W.G. Leel, Jr., 1995. Petroleum geology of the Cusiana Field, Llanos Basin Foothills, Colombia: American Association of Petroleum Geologists Bulletin, v. 79, n. 10, p. 1444-1463.

Chopra, S., and K. J. Marfurt, 2015, Choice of mother wavelets in CWT spectral decomposition: 83rd Annual International Meeting, SEG, Expanded Abstracts, 2957–2961, http://dx.doi.org/10.1190/segam2015-5852193.1.

Chorowicz, J., Chotin, P., and Guillande, R., 1996. The Garzón fault: Active southwestern boundary of the Caribbean plate in Colombia: Geologische Rundschau, v. 85, p. 172–179, doi: 10.1007 /s005310050066.

Coe, A. L., Bosence, W.J, Church, K. D., Flint, S. S., Howell, J. A., and Wilson, R. C. L., 2003. The Sedimentary record of sea-level change. Cambridge, UK: Cambridge University Press and the Open University.

Colletta, B., Hebrard, F., Letouzey, J., Werner, P., Rudkiewicz, J., 1990. Tectonic style and crustal structure of the Eastern Cordillera (Colombia) from balanced cross section. In: Letouzey, J. (Ed.), Petroleum and tectonics in mobile belts. 81-100.

Collinson, J. D., 1996. Alluvial sediments. In: H. G. Reading (Ed.), Sedimentary Environments and Facies, 3rd edition, Elsevier, New York: 37-82.

Cooper, M.A., Addison, F. T., Alvarez, Coral, R. M., Graham, R. H, Hayward, A. B., Howe, S., Martinez, J., Naar, J., Peñ as, R., Pulham, A. J., Taborda, A., 1995. Basin development and tectonic history of the Llanos basin, Eastern Cordillera, and Middle Magdalena Valley, Colombia. AAPG Bulletin 79 (10), 1421-1443.

Csato, I., Granjeon, D., Catuneanu, O. and Baum, G.R., 2012. A three dimensional stratigraphic model for the Messinian crisis in the Pannonian Basin, eastern Hungary. Basin Research, 0, 1-28, doi.org/10.1111/j.1365-2117.2012.00553.x

DATALOG COLOMBIA, 2002. Unpublished end of well report: Iskana 1A, Bogota, Colombia.

De la Parra, F., A. Mora, M. Rueda, and I. Quintero, 2015, Temporal and spatial distribution of tectonic events as deduced from reworked palynomorphs in the eastern northern Andes: AAPG Bulletin, v. 99, no. 8, p. 1455-1472, doi:10.1306/02241511153

De Toni, B., Kellogg, J., 1993. Seismic evidence for blind thrusting of the northwestern flank of the Venezuelan Andes, Tectonics, v. 12, 1,393-1,409.

De'Ath, N., 1997. Discovery history of the giant Cusiana and Cupiagua oil fields, Colombia, Geol. Soc. Malaysia, Bulletin 41, pp. 31-39.

DeCelles, P. G., 2004. Late Jurassic to Eocene evolution of the Cordilleran thrust belt and foreland basin system, Western U.S.A., Am. J. Sci., 304, 105–168.

De Keyser , T., Saeid, E., Kendall, C., Kellogg, J., (in press) Normalized and Color-filled Logarithmic GR Logs to Enhance Subsurface Stratigraphic Interpretation of Carbonates and Siliciclastics. Journal of Petroleum Geology.

Dembicki Jr, H., 2009. Three common source rock evaluation errors made by geologist during prospect or play appraisals: AAPG Bulletin, v. 93, p. 341-356.

Dikey, P., 1992. "La Cira-Infantas Field-Colombia, Middle Magdalena Basin", in Structural Traps VII (Beaumont E. A. and Foster N. H., eds.), AAPG Treatise of Petroleum Geology, Atlas of Oil and Gas Fields: 323 -347

Dueñas, E. G., and Ramirez, C., 2012. Costayaco field, further exploration and production activities in the Putumayo Basin, Colombia: XI Simposio Bolivariano—Exploración Petrolera en las Cuencas Subandinas, Cartagena de Indias, Colombia, July 29–August 1, 2012, Associación Colombiana de Geólogos y Geofisicos del Petróleo, 4 p. Earth Sciences, 1, 109–120.

Echeverry, J. C., Navas, J., Navas, V., Gómez, M. P., 2009. Oil in Colombia: history, regulation and macroeconomic impact, Universidad de los Andes–Facultad de Economía–Cede.

Egbue, O., 2011. Cenozoic tectonic evolution of the Eastern Cordillera and adjacent basins, Ph.D. Dissertation, University of South Carolina, Columbia, 93 pp.

Egbue, O., Kellogg, J., Aguirre, H., Torres, C., 2014. Evolution of the stress and strain fields in the Eastern Cordillera, Colombia, Journal of Structural Geology, V 58 (8-21).

Emery, D. and Myers, K.J., 1996. Sequence Stratigraphy. Blackwell Science, Oxford, 297.

Erslev, E. A., Aydinian, K., Kennedy, L., 2016. Progressive development of basement-involved foreland thrust belts: Results from the NSF/EarthScope Bighorn Project applied to the Laramide orogeny in the Colorado Front Range, in Keller, S.M. and Morgan, M.L., eds, Unfolding the Geology of the West, Geological Society of America Field Guide 44, p. 191-200, doi:10.1130/2016.0044(08).

Fan, M., Carrapa, B., 2014. Late Cretaceous–early Eocene Laramide uplift, exhumation, and basin subsidence in Wyoming: Crustal responses to flat slab subduction, Tectonics, 33, 509-529, doi:10.1002/2012TC003221.

Fuentes, F., Horton, B. K., Starck, D., Boll, A., 2016. Structure and tectonic evolution of hybrid thick- and thin-skinned systems in the Malargüe fold–thrust belt, Neuquén basin, Argentina, Geol. Mag. 153 (5/6), pp. 1066–1084.

Goloshubin, G., Korneev, V., Vindaloo, V., 2002, Seismic low-frequency effects from oil-saturated reservoir zones: 72nd Annual International Meeting of the Society of Exploration Geophysicists, 1813-1816.

Goloshubin, G., Schuyver, C.V., Korneev, V., Silin, D., Vindaloo, V. 2006, Reservoir imaging using low frequencies of seismic reflections'. The Leading Edge, 25 (5):527-531.

Gómez Tapias, J., Nivia Guevara, A., Montes Ramírez, N.E., Jiménez Mejía, D.M., Tejada Avella, M.L., Sepúlveda Ospina, M.J., Osorio Naranjo, J.A., Gaona Narváez, T., Diederix, H., Uribe Peña, H., and Mora Penagos, M., 2007. Mapa Geológico de Colombia (second edition): Bogotá, Ingeominas (Instituto Colombiano de Geología y Minería), scale 1: 1,000,000.

Gómez, A., Jaramillo, C., Parra, M., and Mora, A., 2009, Huesser Horizon: A lake and marine incursion in northwestern South America during the early Miocene: Palaios v. 24, no. 4, p. 199-210.

Gonçalves, F. T. T., Mora, C. A., Cordoba, F., Kairuz, E. C., and B. N. Giraldo, B. N., 2002. "Petroleum generation and migration in the Putumayo Basin, Colombia: insights from an organic geochemistry and basin modeling study in the foothills." Marine and Petroleum Geology 19(6): 711-725.

Gries, R. 1983. Oil and gas prospecting beneath Precambrian of foreland thrust plates in Rocky Mountains. The American Association of Petroleum Geologists Bulletin, 67(1), 1 – 28.

Hamilton, D. S., 1995. Utility of coal seams as genetic stratigraphic sequence boundaries in non marine basins: an example from the Gunnedah Basin, Australia: reply. America Association of Petrolume Geologists Bulletin, v. 79, 1182

Hantschel, T., & Kauerauf, A. I., 2009, Introduction to Basin modelling. In: T. Hantschel & A. I. Kauerauf, (eds) Introduction to Basin and Petroleum System Modelling, Springer, p. 1-30

Haq, B. U., Hardenbol, J., Vail, P. R., 1987. Chronology of fluctuating sea levels since the Triassic. Science 235, 1156–1166.

Head, I. M., Martin Jones, D., Larter, S. R., 2003. Biological activity in the deep subsurface and the origin of heavy oil, Nature, v. 426, 344-352.

Higley, D. K., 2001. The Putumayo-Oriente-Maranon Province of Colombia, Ecuador, and Peru—Mesozoic-Cenozoic and Paleozoic petroleum systems: U.S. Geological Survey Digital Data Series 63, U.S. Department of the Interior, 31 p.

Horton, B.K., Saylor, J.E., Nie, J., Mora, A., Parra, M., Reyes-Harker, A., and Stockli, D.F., 2010a. Linking sedimentation in the northern Andes to basement configuration, Mesozoic extension, and Cenozoic shortening: Evidence from detrital zircon U-Pb ages, Eastern Cordillera, Colombia: Geological Society of America Bulletin, v. 122, p. 1423–1442, doi: 10 .1130 /B30118 .1.

Horton, B.K., Parra, M., Saylor, J.E., Nie, J., Mora, A., Torres, V., Stockli, D., and Strecker, M.R., 2010b, Resolving Andean uplift of the Eastern Cordillera in Colombia using detrital zircon U-Pb age signatures: GSA Today, v. 20, p. doi: 10.1130/GSATG76A.1.

INGEOMINAS, 2003. Geología de las plan planchas 411 La Cruz, 412 San Juan de Villalobos, 430 Mocoa, 431 Piamonte, 448 Monopamba, 449 Orito y 465 Churuyaco, Modificado por Núñez, A. and Colaboración de J. Gómez: Bogotá, Colombia, República de Colombia, Ministerio de Minas y Energía, Instituto de Investigacióne Informacón Geocientífica, Minero-Ambiental y Nublear, INGEOMINAS, Escala 1: 200,000, 1 sheet, 1 p. (in Spanish).

INGEOMINAS-ANH 2008. Mapa preliminar de gradientes geotérmicos (Método BHT). 1:1’500.000. (in Spanish).

Japas, M. S., Héctor Ré, G., Oriolo, S., Vilas, J. F., 2016. Basement-involved deformation overprinting thin-skinned deformation in the Pampean flat-slab segment of the southern Central Andes, Argentina, Geol. Mag. 153 (5/6), pp. 1042–1065, doi:10.1017/S001675681600056X

Jaramillo, C. and Dilcher, D.L. 2000. Microfloral diversity patterns of the late Paleocene-Eocene interval in Colombia, northern South America. Geology 28: 815-818.

Jaramillo, C. and Dilcher, D.L. 2001. Middle Paleogene Palynology of Central Colombia, South America: A Study of Pollen and Spores from Tropical Latitudes. Palaeontographica B 285: 87-213.

Jaramillo, C., Rueda, M., Bayona, G., Santos, C., Florez, P and Parra, F., 2009, Biostratigraphy Breaking Paradigms: Dating the Mirador Formation in the Llanos Basin of Colombia. SEPM Special Publication No. 93, pp. 29–40.

Jimenez, C., 1997. Structural styles of the Andean foothills, Putumayo basin, Colombia. Unpublished Master Thesis. University of Texas at Austin, 73 pp.

Jordan, T.E., Allmendinger, R. W., 1986. The Sierras Pampeanas of Argentina; a modern analogue of Rocky Mountain foreland deformation, American Journal of Science, December 1, 1986 286:737-764, doi: 10.2475/ajs.286.10.737.

Kadar, A.P., T. De Keyser, N. Neog and K.A. Karam (with contributions from Y.M. Le Nindre and R.B. Davies) 2015. Calcareous nannofossil zonation and sequence stratigraphy of the Jurassic System, onshore Kuwait. GeoArabia, v. 20, no. 4, p. 125-180.

Kairuz, E. C., Córdoba, F., Moros, J., Calderón, W., Buchelli, F., 2000. Sistemas petrolíferos del Putumayo, Colombia, Proceedings of the VII Simposio Bolivariano (pp. 525-532), Bogota, Colombia. (in Spanish).

Kellogg, J., Leier, A., and Saeid, E., 2014. Topoyaco Block Technical Report – A stratigraphic and structural framework for Topoyaco Block, Colombia, oil biodegradation and its relation to oil generation and migration vs trap synchronization, Pacific Rubiales Energy. 53 pages.

Kellogg, J.N., and V. Vega, 1995, Tectonic development of Panama, Costa Rica, and the Colombian Andes: Constraints from Global Positioning System geodetic studies and gravity, Geologic and Tectonic Development of the Caribbean plate boundary in southern Central America, GSA Special Paper 295, P. Mann, editor, 75-90.

Kendall C., 2008. Well logs and sequence stratigraphic interpretation, SEPM STRATA SEPM stratigraphy web http://www.sepmstrata.org/page.aspx?&pageid=60&3

Koss, J. E., Ethridge, F. G., and Schumm, S. A., 1994. An experimental study of effects of base-level changes on fluival, coastal plain and shelf systems. Journal of Sedimentary research, v. 64, p. 90-98.

Kroonenberg, S. B., 1982. A Grenvillian Granulite belt in the Colombian Andes and its relation to the Guiana Shield-Geol. Mijnbouw 61:325-333.

Lanson, B., Beaufort, D., Berger, G., Bauer, A., Cassagnabere, A. and Meunier, A. 2002. Authigenic kaolin and illitic minerals during burial diagenesis of sandstones: a review. Clay Minerals, 37, 1-22

Laughlin, K., P. Garossino, and G. Partyka, 2002, Spectral decomposition applied to 3D: AAPG Explorer, 23, 28–31.

Li, F., Lu, W., 2014, Coherence attribute at different spectral scales: Interpretation, 2, SA99–SA10.

Li, F., Qi, J., and Marfurt, K., 2015, Attribute mapping of variable-thickness incised valley-fill systems. The Leading Edge, 34, pp. 48-52.

Linares, R., Aguirre, H., Alzate, J., Galindo, P., 2009. New insights into the Piedemonte license triangle zone in the Llanos foothills- Colombia. Extended Abstracts, X Simposio Bolivariano de Exploración Petrolera en las Cuencas Subandinas, Cartagena Colombia, July 2009.

Liu, L., Spasojevi, S., and Gurnis, M., 2008. Reconstructing Farallon plate subduction beneath North America back to the late Cretaceous, Science, 322, 934–938.

Lunt, I.A., Bridge, J.S., and Tye, R.S., 2004, A quantitative three-dimensional depositional model of gravelly braided rivers: Sedimentology, v. 51, p. 377–414.

Mallat, S., 1999, A wavelet tour of signal processing: Academic Press, 2nd edition.

Mallat, S., 2009. A wavelet tour of signal processing: Academic Press, 3rd edition.

Mallat, S.G. and Zhang, Z., 1993 Matching pursuit with time-frequency dictionaries, IEEE Trans. Signal Processing, vol.41, no. 12, pp. 3397-3415.

Marfurt, K.J., 2015, Techniques and best practices in multiattribute display Interpretation, Vol. 3, No. 1 p. B1–B23. http://dx.doi.org/10.1190/INT-2014-0133.1.

Marfurt, K.J., and R. L. Kirlin, 2001. Narrow-band spectral analysis and thin-bed tuning: Geophysics, 66, 1274-1283.

Martinez, Jaime A., 2006. Structural Evolution of the Llanos foothills, Eastern Cordillera, Colombia. Journal of South American Earth Sciences 21, 510 - 520.

Martínez, M., Márquez, R., Gutiérrez, G., Maya, L., Mora, C., Guzmán, W., Moldowan, J. M., 2014. Is there a pre-Cretaceous source rock in the Colombia Putumayo Basin? Clues from a study of crude oils by conventional and high resolution geochemical methods. Geologica Acta, Vol. 12, 345-350.

McArdle, N.J. and Ackers, M.A. 2012. Understanding seismic thin-bed responses using frequency decomposition and RGB blending. First Break, 30, 57-65.

Miall, A. D. 1984. Variations in fluvial style in the Cenozoic Synorogenic of Lower Cenozoic Synorogenic of the Canadian Arctic Islands. Sedimentary Geology, 38,499-523.

Miall, A. D. 2014. Fluvial depositional systems: Springer-Verlag, Berlin, 316 p.

Miall, A. D., 1996. The Geology of Fluvial Deposits: Sedimentary Facies, Basin Analysis and Petroleum Geology. Berlin: Springer Verlag.

Miall, A.D., 1991. Stratigraphic sequences and their chronostratigraphic correlation. Journal of Sedimentary Petrology 61: 497-505.

Miller, J. and Mitra, S., 2011. Deformation and secondary faulting associated with basement-involved compressional and extensional structures, AAPG Bulletin, v. 95, 675-689.

Mojica, J., & Bayer, K., 1987. Características esenciales del Valle Superior del Magdalena, una cuenca petrolífera Cretácica interandina de Colombia. Memoria 3er Simposio. Cretácico de América Latina, Tucuman, Argentina, Proyecto lnternational Correlation Program, 242, pp. 11–l6.

Montenegro, G., Baragan M., 2011. Petroleum geology of Colombia, Caguan and Putumayo basins, ANH, Vol. 4, pp. 126.

Mora, A., Gaona, T., Kley, J., Montoya, D., Parra, M., Quiroz, L. I., Reyes, G., and Strecker, M. R., 2009. The role of inherited extensional fault segmentation and linkage in contractional orogenesis: A reconstruction of Lower Cretaceous inverted rift basins in the Eastern Cordillera of Colombia: Basin Research, v. 21, no. 1, p. 111–137.

Mora, A., Mantilla, M., De Freitas, M., 2010. Cretaceous paleogeography and sedimentation in the Upper Magdalena and Putumayo basins, southwestern Colombia, Search and Discovery Article #50246, adapted from expanded abstract, AAPG, Rio de Janeiro, nov.15-18, 2009.

Mora, A., Parra, M., Strecker, M.R., Kammer, A., Dimate, C., and Rodriguez, F., 2006. Cenozoic contractional reactivation of Mesozoic extensional structures in the Eastern Cordillera of Colombia. Tectonics, 25, TC2010, doi:10.1029/2005TC001854.

Mora, A., Reyes-Harker, A., Rodriguez, G., Tesón, E., Ramirez-Arias, J.C., Parra, M., Caballero, V., Mora, J.P., Quintero, I., Valencia, V., Ibañez, M., Horton, B. K., and Stockli, D. F., 2013, Inversion tectonics under increasing rates of shortening and sedimentation: Cenozoic example from the Eastern Cordillera of Colombia, in Nemčok, M., Mora, A., and Cosgrove, J.W., eds., Thick-Skin-Dominated Orogens: From Initial Inversion to Full Accretion: Geological Society of London, Special Publication, v. 377. doi: 10.1144/SP377.6.

Narr, W, and Suppe, J., 1994. Kinematics of basement-involved compressive structures, Amer. Journal of Science, v. 294, 802- 860.

Neinast G., S., Knox C., C., 1973 Normalization of well log data, Paper I in 14th annual Logging Symposium Transactions: Society of Professional Well Log Analysts.

North, C.P., 1996. The prediction and modelling of subsurface fluvial stratigraphy. In: P.A. Carling and M.R. Dawson (Eds.), Advances in Fluvial Dynamics and Stratigraphy. John Wiley, Chichester: 395-508.

Núñez, A., and Gómez, J., 2003. Geología de la Plancha 411 La Cruz, 214 San Juan de Villabos, 430 Mocoa, 431 Piamonte, 448 Monopamba, 449 Orito y 465 Churuyaco, Escala 1: 200,000 Instituto Colombiano de Geología y Minería.

Núñez, A., and Gómez, J., 2010. Geología de la Plancha 431 Piamonte, Escala 1: 100.000, Instituto Colombiano de Geología y Minería, INGEOMINAS.

Ojeda, J., 1996. Present day retrodeformed structure of the Eastern Cordillera Cretaceous Basin, Colombia. Master's thesis, University of South Carolina, 57 p.

Parra, M., 2008, Cenozoic foreland-basin evolution in the northern Andes: insights from thermochronology and basin analysis in the Eastern Cordillera, Colombia. PhD. Institutional Repository of the University of Potsdam, 131 p.

Parra, M., Mora, A., Jaramillo, C., Strecker, M. R., Sobel, E. R., Gonzalez, R., 2009a, Episodic orogenic front migration in the northern Andes: Constraints from low-temperature thermochronology in the Eastern Cordillera, Colombia. Tectonics, Vol, 28, TC4004, 1-27.

Parra, M., Mora, A., Jaramillo, C., Strecker, M.R., Sobel, E.R., Quiroz, L., Rueda, M., Torres, V., 2009b, Orogenic wedge advance in the northern Andes: evidence from the Oligocene-Miocene sedimentary record of the Medina Basin, Eastern Cordillera, Colombia. Geological Society of America Bulletin, v. 121, p780-800.

Parra, M., Mora, A., Jaramillo, C., Torres, V., Zeilinger, G., Strecker, M.R., 2010, Tectonic controls on Cenozoic foreland basin development in the north-eastern Andes, Colombia. Basin Research, v. 22, p.874-903.

Partyka, G. A., Bush, M. D., Garossino, P. G. A., and Gutowski, P. R., 2011, Spectral Decomposition. In: Brown, A. R., 2011. Interpretation of three-dimensional seismic data, 7th ed.: AAPG Memoir 42 and SEG Investigations in Geophysics No. 9.

Partyka, G., Gridley, J., and Lopez, J., 1999, Interpretational applications of spectral decomposition in reservoir characterization: The Leading Edge,18, 353-360.

Perez, N. D., Horton, B. K., McQuarrie, N., Stübner, K., Ehlers, T. A., 2016, Andean shortening, inversion, and exhumation associated with thin- and thick-skinned deformation in southern Peru. Geological Magazine, published online 3 June 2016. doi: 10.1017/S0016756816000121.

Person, M., D. Butler, C. W. Gable, T. Villamil, D. Wavrek, and D. Schelling, 2012. Hydrodynamic stagnation zones: A new play concept for the Llanos Basin, Colombia: AAPG Bulletin, v. 96, no. 1, p. 23–41, doi:10.1306/08101111019.

Pindell, J., Tabbutt, K. D., 1995. Mesozoic–Cenozoic Andean Paleogeography and Regional Controls on Hydrocarbon systems. In: Tankard, A.J., Suarez, R., Welsink, J. (Eds.), Petroleum Basins of South America, AAPG Memoir 62, 101–128.

Piper 1944. A graphic procedure in the geochemical interpretation of water analysis, Transactions American Geophysical Union Volume 25, Issue 6, P 914–928.

Portilla, O., 1991. The Putumayo fold belt, Colombia, South America: Structural interpretation and hydrocarbon potential. Unpublished Master of Science thesis, University of South Carolina, 79 p.

Posamentier, H. W., and Vail, P. R., 1988. Eustatic controls on clastic deposition II sequence and systems trct models. In: Wilgus, C. K., Hastings, B. S., Kendall, C. G. St. C., Posamentier, H. W., Ross, C. A. and Van Wagoner, J. C., (eds.) Sea-level changes: an integrated approach. Society of Economic Paleontologisits and Mineralogists Special Publication, v 42, p 125-154.

Posamentier, H. W., and Weimer, P. 1993. Siliciclastic sequence stratigraphy and petroleum geology- where to form here? America Association of Petrolume Geologists Bulletin, v. 77, p. 731-742.

Priem, H.N.A., Boelrijk, N.A.I.M., Hebeda, E.H., Kroonenberg, S.B., 1989. Rb-Sr and K-Ar evidence for the presence of a 1.6 Ga basement underlying the 1.2 Ga Garzón-Santa Marta granulite belt in the Colombian Andes. Precambrian Research, 42(3–4), 315–324.

Ramirez, C., Gutierrez, A., and Solano, F., 2012. El Campo Moqueta, primer descubrimiento en el piedemonte de la Cuenca del Putumayo: XI Simposio Bolivariano— Exploración Petrolera en las Cuencas Subandinas, Cartagena de Indias, Colombia, July 29–August 1, 2012, Asociación Colombiana de Geólogos y Geofisicos del Petróleo, 6 p. (in Spanish). (in Spanish).

Ramón, J. C., 1996, Oil geochemistry of the Putumayo Basin, Ciencia, Tecnología y Futuro, 1, 25-34.

Ramon, J. C., and Fajardo, A., 2006. Sedimentology, sequence stratigraphy, and reservoir architecture of the Eocene Mirador Formation, Cupiagua field, Llanos Foothills, Colombia, in P. M. Harris and L. J. Weber, eds., Giant hydrocarbon reservoirs of the world: From rocks to reservoir characterization and modeling: AAPG Memoir 88/SEPM Special Publication, p. 433-469.

Ramos, V.A., 2010. The Grenville-age basement of the Andes: Journal of South American Earth Sciences, v. 29, p., 77–91.

Ramos, V.A., Cristallini, E. O., Pérez, D. J., 2002. The Pampean flat-slab of the Central Andes, Journal of South American Earth Sciences, 15, 59-78, doi:10.1016/S0895-9811(02)00006-8.

Ramsey, L. A., Walker, R. T. and Jackson, J., 2008 Fold evolution and drainage development in the Zagros Mountains of Fars Province, SE Iran, Basin Res., 20(1), 23–48, doi:10.1111/j.1365-2117.2007.00342. x.

Reid, A.B., Allsop, J. M., Granser, H., Millet, A. J., and Somerton, I. W., 1990. Magnetic interpretation in three dimensions using Euler deconvolution: Geophysics, v. 55, p. 80-91.

Reyes-Harker, A., C. F. Ruiz, A. Mora, J. C. Ramirez-Arias, G. Rodriguez, F. De la Parra, V. Caballero, et al., 2015, Cenozoic paleogeography of the Andean foreland and retroarc hinterland of Colombia: AAPG Bulletin, v. 99, no. 8, p. 1407-1453, doi: 10.1306/06181411110.

Rider, M.H., 1999. Geologic interpretation of well logs. Whittles Publishing Services.

Rider, M.H., 2002. Geologic interpretation of well logs. Whittles Publishing Services

Roberts, D. M., 2011, Visualization and Visual Integration In: In: Brown, A. R., 2011. Interpretation of three-dimensional seismic data, 7th ed.: AAPG Memoir 42 and SEG Investigations in Geophysics No. 9.

Rodriguez, C.J., AVargas Gomez, A., Piragua A., O. Romero Ballén, R. García Delgado, C. Moreno L., R. Pinzón R., 2009. Mapa geológico a escala 1:100,000, Sector del Piedemonte de la Cuenca Caguan-Putumayo, Mapa 3/4, Universidad Pedagógica y Tecnológica de Colombia. (in Spanish).

Rodriguez, G., Zapata, G., Velázquez, M. E., 2003. Geología Plancha 368, San Vicente del Caguán, Bogotá, Ingeominas (Instituto Colombiano de Geología y Minería), escala 1: 100,000.

Saleeby, J., 2003. Segmentation of the Laramide Slab—Evidence from the southern Sierra Nevada region, Geol. Soc. Am. Bull., 115, 665–668.

Sarmiento, L.F., and Rangel, A., 2004. Petroleum systems of the Upper Magdalena Valley, Colombia, Marine and Petroleum Geology 21, 373-391.

Sarmiento-Rojas, L.F., Van Wess, J.D., and Cloetingh, S., 2006. Mesozoic transtensional basin history of the Eastern Cordillera, Colombian Andes: inferences from tectonic models. J. South Am. Earth Sci., 21, 383-411.

Schlumberger, 2013 Log interpretation charts, Schlumberger Ed, Serv., Houston TX/USA

Schlumberger, 2017. Petrel 2017.1 Manual,

Schön, J.H., 2015 Physical properties of rocks: Fundamentals and principles of petrophysics. Developments in petroleum science, V. 65. Elsevier, Amsterdam Netherlands.

Schumm, S.A., 1963. Sinuosity of alluvial channels on the Great Plains. Geological Society of America Bulletin 74: 1089-1100.

Selley, R.C., 1996. Ancient Sedimentary Environments and their Subsurface Diagnosis, 4th ed., Chapman and Hall, London, 300 pp.

Shanley, K. W. and P. J. McCabe, 1993. Alluvial architecture in a sequence stratigraphic framework: a case history from the Upper Cretaceous of southern Utah, USA. In: Flint, S. and Bryant, I.D. (Eds.), The geological modeling of hydrocarbon reservoirs and outcrop analogues. International Association of Sedimentologists Special Publication 15: 21-56.

Shanley, K. W. and P. J. McCabe, 1994. Perspectives on the sequence stratigraphy of continental strata. American Association of Petroleum Geologists Bulletin 78: 544-568

Shanley, K. W., and McCabe, P. J., 1991. Predicting facies architecture through sequence stratigraphy- An example from the Kaiparowits Plateau, Utah, Geology v. 19, p. 742-745.

Shanley, K.W., and McCabe, P.J., 1995, Sequence stratigraphy of Turonian-San- tonian strata, Kaiparowits Plateau, Southern Utah, USA: Implications for regional correlation and foreland basin evolution, In Van Wagoner, J. C., and Bertram, G. T., (eds.) Sequence stratigraphy of foreland basin deposits, outcrop and subsurface examples from the creataceous of north America: America Association of Petrolume Geologists Memoir, v. 64, p. 103-136.

Shier D., E., 2004. Well log Normalization: Methods and Guidelines, PETROPHYSICS 45(3):268-280

Silva, A., Mora, A. et al. 2013. Basin compartmentalization and drainage evolution during rift positive inversion: evidence from multiple techniques in the Eastern Cordillera of Colombia. In: Nemcˇok, M., Mora, A. & Cosgrove, J. W. (eds) Thick-Skin- Dominated Orogens: From Initial Inversion to Full Accretion. Geological Society, London, Special Publications, 377, .doi.org/10.1144/SP377.15.

Sinha, S., P. S. Routh, P. D. Anno, and J. P. Castagna, 2005. Spectral decomposition of seismic data with continuous-wavelet transform: Geophysics, 70, no. 6, P19–P25, doi: 10.1190/1.2127113.

Smithson, S.B., Brewer, J., Kaufman, S., Oliver, J., Hurich, C., 1978. Nature of the Wind River thrust, Wyoming, from COCORP deep-reflection data and from gravity data, Geology, v. 6, p. 648-652.

Stearns, D.W., 1975. Laramide basement deformationin Bighorn Basin-The controlling factor for structures in the layered rocks. Wyo. Geol.Assoc, Guideb., 27th Annu. Filed Conf. PP 149-152.

Suppe, J., 1983. Geometry and kinematics of fault-bend folding: American Journal of Science, v. 283, p. 684-721.

Taboada, A., Rivera, L.A., Fuenzalida, A., Cisternas, A., Hervé, P., Harmen, B., Olaya, J., Rivera, C. (2000). Geodynamics of the northern Andes: subductions and intracontinental deformation (Colombia). Tectonics 19: 787-813.

Tai, S., Puryear, C., Castagna, J. P., 2010, Local frequency as a direct hydrocarbon indicator, SEG Houston 2009 International Exposition and Annual Meeting.

Talukdar, S, C., 2012. Geochemical Evaluation of a crude oil tested from the well Yaraqui-1x, Putumayo Basin, Colombia, unpublished report.

Thomson, D.T., 1982. EULDPH-A new technique for making computer-assisted depth estimates from magnetic data: Geophysics, v. 47, p. 31-37.

Torrado, L., Mann, P., Bhattacharya J., 2014. Application of seismic attributes and spectral decomposition for reservoir characterization of a complex fluvial system: Case study of the Carbonera Formation, Llanos foreland basin, Colombia.

Tye, R. S., 1991. Fluvial-sandstone reservoirs of the Travis Peak Formation, East Texas Basin. In: A. D. Miall and N. Tyler (Eds.), The Three-Dimensional Facies Architecture of Terrigeneous Clastic Sediments and Its Implications for Hydrocarbon Discovery and Recovery. Society of Economic Paleontologists and Mineralogists Concepts in Sedimentology and Paleontology 3: 172-188.

Tyler, N., and R.J. Finley, 1991, Architectural controls on the recovery of hydrocarbons from sandstone reservoirs: Concepts in Sedimentology and Paleontology, v. 3; p. 1-5.

van der Beek, P., B. Champel, and J.-L. Mugnier 2002 Control of detachment dip on drainage development in regions of active faultpropagation folding, Geology, 30(5), 471–474, doi:10.1130/0091-7613 (2002) 030<0471: CODDOD>2.0.CO;2.

Van Der Wiel, A. M. 1991. Uplift and Volcanism of the SE Colombian Andes in Relation to Neogene Sedimentation of the Upper Magdalena Valley. Unpublished doctoral dissertation, University of Utrecth, Utrecht.

Vásquez, M., Altenberger, U., Romer, R., 2009. Neogene magmatism and its possible causal relationship with hydrocarbon generation in SW Colombia, Int. J. Earth Sci (Geol Rundsch) 98: 1053-1062.

Velandia, F., Acosta, J., Terraza, R., and Villegas, H., 2005. The current tectonic motion of the Northern Andes along the Algeciras fault system in SW Colombia: Tectonophysics, v. 399, p. 313–329, doi: 10 .1016 /j. tecto .2004 .12 .028.

Villagómez, D., and Spikings, R., 2013. Thermochronology and tectonics of the Central and Western Cordilleras of Colombia: Early Cretaceous-Tertiary evolution of the northern Andes, Lithos 160-161, 228-249.

Villamil, T., 1999, Campanian–Miocene tectonostratigraphy, depocenter evolution and basin development of Colombia and western Venezuela. Palaeogeography, Palaeoclimatology, Palaeoecology, v. 153 pp. 239–275.

Villegas, M., E., Bachu, S., Ramon, J., and Underschultz, J., 1994. Flow of formation waters in the Cretaceous–Miocene succession of the Llanos Basin, Colombia: AAPG Bulletin, v. 78, p. 1843–1862.

Welsh, A., F. Brouwer, A. Wever, W. Flierman, 2008. Spectral decomposition of seismic reflection data to detect gas related frequency anomalies, EAGE Conference and Exhibition, June.

Wight, V.P., and Marriott, S.B., 1993. The sequence of fluival depositional systems: the role of floodplain sediment storage. Sedimentary Geology, v. 86, p. 203-210.

Witte, J., Westlund, D., Neufeld, C., Duarte, L., 2013. Regional Structural Style of Putumayo Bain: Their effect on trapping style and migration pathways. Abstract, AAPG International Conference & Exhibition, Cartagena, 8-11 September 2013.

Wolaver, B.D., Coogan, J.C., Horton, B.K., Bermudez, L.S., Sun, A.Y., Waerzyniec, T.F., Zhang, T., Shanahan, T.M., Dunlap, D.B., Costley, R.A., de la Rocha, L., 2015. Structural and hydrogeologic evolution of the Putumayo basin and adjacent fold-thrust belt, Colombia, AAPG Bulletin, v. 99, no. 10, 1893-1927.

Yeck, W. L., Sheehan, A. F., Anderson, M. L., Erslev, E. A., Miller K. C., and Siddoway C.S., 2014. Structure of the Bighorn Mountain region, Wyoming, from teleseismic receiver function analysis: Implications for the kinematics of Laramide shortening, J. Geophys. Res. Solid Earth, 119(9), 7028–7042, doi:10.1002/2013JB010769.

Yu, B., Zhou, L. and Wang, X. 2011. Application of the oil-bearing prediction methods based on spectral decomposition. SPG/SEG International Geophysical Conference, Expanded Abstracts, 16631668.

APPENDIX A
SUPPLEMENTAL DATA FOR CHAPTER II

1- Dip angles for 10 exploration wells drilled through Precambrian hanging wall blocks in the Laramide Rocky Mountains and Garzón Massif. (*in 2.4. Garzón thrust fault* and Figur. 2.5)

Table A.1. Well Data of Gries (1983) compared to Iskana – 1 (Garzón Fault, this paper) showing dip angles at TD (Total Depth). Only wells with known dips at TD are included.

Well Name and Operator	**Thrust**	**TD (m)**	**Dip at TD**	**Subthrust fault sliver thickness (m)**
Carter 1 Unit	Emigrant Trail	2009	13.0	268
Shell 1 Govt.	E A	3258	15.0	250
Sinclair 1 Cooper Creek	Emigrant Trail	1997	20.0	none
Mountain Fuel 1 Dickey Springs	Wind River	5212	8.5	none
American Quasar 1 Skinner Fed.	Uinta Mountain	4584	50.0	1189
Champlin Fed. 31 - 19 (Bear Springs)	Uinta Mountain	4209	15.0	none
West Coast Oil 1 Skinner Fed.	Wind River	2468	45.0	unknown
Mobil C – 1 McCormick Fed.	Uncompah gre	5873	27.0	unknown
Supron Energy 1 F - 28 - 30 – 93	Emigrant Trail	2368	10.0	137
ISKANA 1A	***Garzón Fault***	***5247***	***17.0***	***none***

Number of Data	**10.0**
Mean Dip	**22.1**
Standard Deviation	**14.4**

2- Euler deconvolution map (*in 2.4.3 Gravity Magnetic Study of the Garzón Basement Uplift* and Fig. 2.9b)

Euler Deconvolution. The gridded potential field data was inversely modeled in 3D using the Euler deconvolution method. Euler deconvolution estimates the depth and location of a magnetic source by examining the rate of change of the magnetic field as a function of distance (Thompson, 1982; Reid et al., 1990). This technique can be applied to profile or grid data to solve for Euler's Homogeneity Equation:

$$(x-x_0)\, dF/dx + (y-y_0)\, dF/dy + (z-z_0)\, dF/dz = N\,(B-F)$$

Where x0, y0, z0 is the source location whose magnetic field is F, measured at point x, y, z. B is the regional value of the Total Field. N is the Euler's structural index (SI), which characterizes the source's geometry. The SI can be varied from zero to three: 0 (contact of infinite depth), 1 (dike), 2 (pipe), and 3 (sphere). The Euler method also yields estimates of the standard deviation of z0. This quantity $\sigma 0$ is treated as an "error bar" on the depth estimate and forms the basis for an algorithm that determines whether or not a depth estimate is to be retained. This feature permits an uncertainty level in the depth estimate to be set such that all solutions falling below that threshold are discarded. For this study, deconvolution maps were created by varying the structural index from 0-3 and the uncertainty from 5-15 percent.

APPENDIX B
PERMISSION TO REPRINT

oxfordcopyrights (ELS) <oxfordcopyrights@elsevier.com> Tue, Jun 19, 2018 at 6:13 AM
To: "esaeid@geol.sc.edu" <esaeid@geol.sc.edu>
Cc: "Marine and Petroleum Geology (ELS)" <jmpg@elsevier.com>

Dear Mr Saeid,

Thank you for your email.

Please note that, as one of the Authors of this article, you retain the right to reuse it in your thesis/dissertation. You do not require formal permission to do so.

For full details of your rights as a Journal Author, please visit:

https://www.elsevier.com/about/our-business/policies/copyright

Please feel free to contact me if you have any queries.

Kind regards

Laura

Laura Pritchard

Permissions Supervisor | ELSEVIER | The Boulevard| Langford Lane | Kidlington | Oxford OX5 1GB |

Tel: +44 1865 843517 Fax: +44 1865 853333

l.pritchard@elsevier.com

Dear Dr. Adam,

6/23/2018 Department of Earth and Ocean Sciences Mail - RE: Your Submission [180618-006149]

I intend to include " Ms. Ref. No.: JMPG-D-17-00621R1
Title: Garzón Massif basement tectonics: structural control on evolution of petroleum systems in Upper Magdalena and Putumayo basins, Colombia.
Marine and Petroleum Geology" as part of my PhD dissertation and I need a permission to reprint or copyright permission from the JMPG as university request.

Thank you!